

# CHEMIA

2/2017  
Tom I

**STUDIA  
UNIVERSITATIS BABEȘ-BOLYAI  
CHEMIA**

**2/2017  
Tom I**

# EDITORIAL BOARD OF STUDIA UNIVERSITATIS BABEȘ-BOLYAI CHEMIA

## ONORARY EDITOR:

IONEL HAIDUC - Member of the Romanian Academy

## EDITOR-IN-CHIEF:

LUMINIȚA SILAGHI-DUMITRESCU

**EXECUTIVE EDITOR:** CASTELIA CRISTEA

**CO-EDITOR:** SIMONA CODRUȚA COBZAC

## EDITORIAL BOARD:

PAUL ȘERBAN AGACHI, Babeș-Bolyai University, Cluj-Napoca, Romania

LIVAIN BREAU, UQAM University of Quebec, Montreal, Canada

HANS JOACHIM BREUNIG, Institute of Inorganic and Physical Chemistry,  
University of Bremen, Bremen, Germany

MIRCEA DIUDEA, Babeș-Bolyai University, Cluj-Napoca, Romania

JEAN ESCUDIE, HFA, Paul Sabatier University, Toulouse, France

ION GROSU, Babeș-Bolyai University, Cluj-Napoca, Romania

EVAMARIE HEY-HAWKINS, University of Leipzig, Leipzig, Germany

FLORIN DAN IRIMIE, Babeș-Bolyai University, Cluj-Napoca, Romania

FERENC KILAR, University of Pecs, Pecs, Hungary

BRUCE KING, University of Georgia, Athens, Georgia, USA

ANTONIO LAGUNA, Department of Inorganic Chemistry, ICMA, University of  
Zaragoza, Zaragoza, Spain

JURGEN LIEBSCHER, Humboldt University, Berlin, Germany

KIERAN MOLLOY, University of Bath, Bath, UK

IONEL CĂȚĂLIN POPESCU, Babeș-Bolyai University, Cluj-Napoca, Romania

CRISTIAN SILVESTRU, Babeș-Bolyai University, Cluj-Napoca, Romania

<http://chem.ubbcluj.ro/~studiachemia/>; [studiachemia@chem.ubbcluj.ro](mailto:studiachemia@chem.ubbcluj.ro)

[http://www.studia.ubbcluj.ro/serii/chemia/index\\_en.html](http://www.studia.ubbcluj.ro/serii/chemia/index_en.html)

YEAR  
MONTH  
ISSUE  
TOM

Volume 62 (LXII) 2017  
JUNE  
2  
I

# STUDIA UNIVERSITATIS BABEȘ-BOLYAI CHEMIA

2

Tom I

ISSUE DOI:10.24193/subbchem.2017.2

---

STUDIA UBB EDITORIAL OFFICE: B.P. Hasdeu no. 51, 400371 Cluj-Napoca, Romania,  
Phone + 40 264 405352

---

*Dedicated to Professor Costel Sârbu on the Occasion  
of His 65<sup>th</sup> Anniversary*

## CUPRINS – CONTENT – SOMMAIRE – INHALT

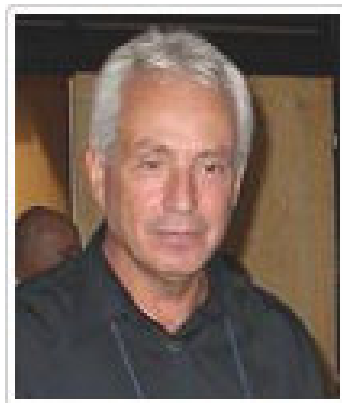
CODRUȚA COBZAC, DORINA CASONI, Professor Costel Sârbu on His 65 <sup>th</sup> Anniversary.....	7
KAITLIN NGUYEN, DANHUI ZHANG, JOSEPH SHERMA, Development of Quantitative HPTLC-Densitometry Methods Following a Model Approach for Transfer of TLC Screening Methods for Pharmaceutical Products of Metformin HCl, Potassium Clavulanate, Caffeine, Fluoxetine HCl, and Gabapentin .....	9
OSSI HOROVITZ, ROXANA-DIANA PAȘCA, Classification of Amino Acids by Multivariate Data Analysis, Based on Thermodynamic and Structural Characteristics .....	19

LORENTZ JÄNTSCHI, Property-Property Relationships for Monosaccharides...	33
GALABA NAUMOVA-LEȚIA, AUGUSTIN C. MOȚ, Probing Reducing Power for Ferryl Phytoglobins of Several Phenolic Compounds Using their Kinetic Profiles Assisted by Chemometric Methods .....	49
MARIA SIMION, SIMONA CODRUTA AURORA COBZAC, DORINA CASONI, Image Analysis Approaches to Improve the Thin Layer Chromatography – Chemometric-Based Investigations of Natural Extracts.....	67
ANDREEA BRASOVAN, RAMONA FLAVIA BURTESCU, NELI-KINGA OLAH, IOAN PETEAN, VLAD CODREA, ANDREI BURTESCU, Algorithm for Assessing Soil Rehabilitation of Sterile Dumps .....	81
AURORA MOCANU, REKA BALINT, CORINA GARBO, LUCIA TIMIS, IOAN PETEAN, OSSY HOROVITZ, MARIA TOMOAI-COTISEL, Low Crystallinity Nanohydroxyapatite Prepared at Room Temperature ...	95
MARIA-LOREDANA SORAN, OVIDIU PANĂ, ALEXANDRINA NAN, CRISTIAN LEOȘTEAN, IOAN BRATU, Synthesis and Spectroscopic Characterization of Hybrid Magnetic Nanoparticles, Based on Fe@Au and Pyrrole .....	105
ASTRID BUICA, JEANNE BRAND, CHRISTINE WILSON, MARIETJIE STANDER, Evaluating South African Chenin Blanc Wine Styles using an Lc-Ms Screening Method .....	113
SZABOLCS VÍGH, ZOLTÁN CZIÁKY, LÁSZLÓ TAMÁS SINKA, CIPRIAN PRIBAC, LIANA MOȘ, VIOLETA TURCUȘ, JUDIT REMENYIK, ENDRE MÁTHÉ, Comparative Chemomapping of Phytoconstituents from Different Extracts of Globe Artichoke - <i>Cynara Scolymus</i> L. ....	125
SZABOLCS VÍGH, ZOLTÁN CZIÁKY, LÁSZLÓ TAMÁS SINKA, CIPRIAN PRIBAC, LIANA MOȘ, VIOLETA TURCUȘ, JUDIT REMENYIK, ENDRE MÁTHÉ, Analysis of Phytoconstituent Profile of Fenugreek – <i>Trigonella Foenuem-Graecum</i> L. - Seed Extracts....	145
JÓZSEF BALÁZSI, CSABA PAIZS, FLORIN-DAN IRIMIE, MONICA IOANA TOȘA, LÁSZLÓ CSABA BENCZE, RÓBERT TÓTÓS, Validated LC-MS/MS Method for the Concomitant Determination of Amoxicillin and Clavulanic Acid from Human Plasma .....	167

Studia Universitatis Babes-Bolyai Chemia has been selected for coverage in Thomson Reuters products and custom information services. Beginning with V. 53 (1) 2008, this publication is indexed and abstracted in the following:

- Science Citation Index Expanded (also known as SciSearch®)
- Chemistry Citation Index®
- Journal Citation Reports/Science Edition





Professor Dr. Habil. Costel Sârbu is one of the pioneers of Chemometrics in Romania. He was born on January 12 1951 in Giurgiuța, Dolj county Romania. He obtained his B.S. degree in 1975 from Babeș-Bolyai University in Cluj-Napoca, followed by his MSc degree in 1976 from the same university. In 1987, he gained the PhD in chemistry with the thesis entitled “Applications of Information Theory in Chromatography with Fluorescence Detection” elaborated under the scientific supervision of illustrious Professor Candin Liteanu. After a short period of engagement in the industry and research, in 1980 he began his academic career as Assistant Professor at Polytechnic Institute Cluj-Napoca. Since 1990 he continued the academic career as Lecturer (1990-1994), Associate Professor (1994-2014) and full Professor (2014-2016) at Babeș-Bolyai University Cluj-Napoca, Faculty of Chemistry and Chemical Engineering. After his retirement in 2016, he was honoured with a Professor Emeritus position.

Professor Sârbu has devoted himself to studying the field of analytical chemistry and chemometrics. He approached a wide variety of fundamental and topical research interests including new applications of chemometric methods in the lipophilicity evaluation, fingerprinting analysis and development of structure-property-activity relationships (QSAR/QSPR/QSRR). Professor Sârbu gained an important international visibility reflected by a Hirsch index 22 founded on scientific papers published in international journals available via ISI Web of Knowledge which gathered more than 1730 citations.



Other publications included monographies and books or book chapters edited by romanian and international specialized publishers. He is the owner of intellectual property rights for 15 patents and he was the scientific coordinator of several national and international projects. His contributions in to the scientific research were rewarded with special honors such as: *Romanian Academy Prize "Nicolae Teclu"* for the papers published in 2008 in the field of Chemometrics and *Special Prize of Patriciu Foundation* for research activity during 2010-2011.

During his scientific activity Professor Sârbu served as editorial member of several international journals and he became a member of prestigious scientific societies including AOAC International, American Chemical Society, Applied Spectroscopy Society and Romanian Society of Chemistry.

Cluj-Napoca, 14.06.2017

In the name of the coworkers,  
Dr. Codruța COBZAC and Dr. Dorina CASONI

*Dedicated to Professor Costel Sârbu on the  
Occasion of His 65<sup>th</sup> Anniversary*

**DEVELOPMENT OF QUANTITATIVE HPTLC-DENSITOMETRY  
METHODS FOLLOWING A MODEL APPROACH FOR TRANSFER  
OF TLC SCREENING METHODS FOR PHARMACEUTICAL  
PRODUCTS OF METFORMIN HCL, POTASSIUM CLAVULANATE,  
CAFFEINE, FLUOXETINE HCL, AND GABAPENTIN**

**KAITLIN NGUYEN<sup>a</sup>, DANHUI ZHANG<sup>b</sup> and JOSEPH SHERMA<sup>a\*</sup>**

**ABSTRACT.** Transfer of thin-layer chromatography Global Pharma Health Fund Minilab kit protocols for detecting counterfeit drugs in pharmaceutical products in the field to quantitative high-performance TLC (HPTLC)-densitometry methods was carried out for potassium clavulanate and metformin HCl using a model process published earlier. HPTLC-densitometry methods were also developed following the model process for caffeine, fluoxetine HCl, and gabapentin, for which methods are not included in the Minilab manual. The model process involves use of EMD Millipore Premium Purity silica gel 60 F<sub>254</sub> plates, automated sample and standard solution application with a CAMAG Linomat 4, and automated densitometry with a CAMAG Scanner 3 for determination of peak purity and identification and for quantification. Detection methods for counterfeit samples of the three drugs not covered in the Minilab manual were also developed and posted online with open access as supplemental methods for the Compendium of Unofficial Methods for Rapid Screening of Pharmaceuticals by Thin Layer Chromatography.

**Keywords:** *thin layer chromatography, drug analysis, metformin HCl, potassium clavulanate, gabapentin, fluoxetine HCl, caffeine*

---

<sup>a</sup> *Department of Chemistry, Lafayette College, Easton, PA, USA*

<sup>b</sup> *Department of Chemical and Biomedical Engineering, Lafayette College, Easton, PA, USA*

\* *Corresponding author: sherma@lafayette.edu*

## INTRODUCTION

A model process was previously described [1-3] for transfer of qualitative/semiquantitative thin-layer chromatography (TLC) screening methods for pharmaceutical products with quality defects contained in the Global Pharma Health Fund E.V. (GPHF) Minilab manual [4] or U.S. Food and Drug Administration Compendium of Unofficial Methods for Rapid Screening of Pharmaceuticals by Thin Layer Chromatography [5] to quantitative high-performance TLC (HPTLC)-densitometry methods. The model process was applied earlier to formulations containing acetylsalicylic acid, acetaminophen, ibuprofen, and chlorpheniramine maleate [1]; mebendazole, diphenhydramine HCl, amodiaquine, and artesunate [2]; amodiaquine and diazepam [3]; lumefantrine + artemether [6]; albendazole, amodiaquine + artesunate [7]; pyrazinamide + ethambutol + isoniazid + rifampicin [8]; quinine sulfate, mefloquine, and dihydroartemisinin + piperazine phosphate [9]; azithromycin, imipramine HCl, and sulfadoxine + pyrimethamine [10]; clarithromycin, azithromycin, and amodiaquine + artesunate [11]; and cefixime, cefuroxime axetil, cephalexin hydrate, ciprofloxacin HCl, levofloxacin, and metronidazole [12].

The model process comprises sample and standard preparation, establishment of a linear or polynomial calibration curve covering 70-130% of the label value, assay of three samples of the pharmaceutical product relative to the label value each in triplicate, evaluation of the accuracy of the method using standard addition analysis at 50, 100, and 150% fortification levels each in triplicate, and peak purity and peak identity tests; only certain relatively nontoxic solvents can be used for standard and sample solution and mobile phase preparation. In this article, we report the use of the model process to transfer TLC Minilab methods to HPTLC-densitometry for pharmaceutical products containing the diabetes medication metformin HCl (CAS No. 1115-70-4) and antibiotic potassium clavulanate (CAS No. 61177-45-5), as well as to develop HPTLC-densitometry methods for the products containing the stimulant caffeine (CAS No. 58-08-2), the nerve pain and anticonvulsant medication gabapentin (CAS No. 60142-96-3), and the antidepressant fluoxetine HCl (CAS No. 56296-78-7) for which there are no Minilab or Compendium methods published.

## RESULTS

Results of the method development for the five pharmaceutical products are displayed in Table 1 for the assay of the three tablets and in Table 2 for the validation analyses. The optimal regression mode for assays and validation of each was chosen based on the best calibration curve r-values,

assay values closer to the label value, accuracy of the standard addition validation, and lower relative standard deviations (RSDs) for the replicated analyses. Calibration curve r-values in our assay and validation experiments were at least 0.99; all validation analysis recoveries at 50, 100, and 150% spike levels were within +/- 5%; and peak purity and identity r-values were 0.99 consistent with the model process requirements. All assays were within 85-115% specification limits of the label value as specified by the U.S. Pharmacopeia (USP) for individual dosage form analysis except for the one high assay result of the potassium clavulanate tablets. RSDs for triplicate assays and validation analyses were within the required 3% except for the 100% spike level for gabapentin.

**Table 1.** Assay results for pharmaceutical products containing caffeine, fluoxetine HCl, gabapentin, metformin HCl, potassium clavulanate respectively

		Tablet 1		Tablet 2		Tablet 3	
Pharmaceutical product	Regression mode	Assay (%)	RSD (%)	Assay (%)	RSD (%)	Assay (%)	RSD (%)
Caffeine	Polynomial	106	0.502	113	1.39	106	0.181
Fluoxetine HCl	Linear	101	1.93	93.2	0.832	97.0	1.13
Gabapentin	Polynomial	89.8	1.98	93.5	0.733	95.5	2.20
Metformin HCl	Linear	100	0.484	106	1.40	105	0.547
Potassium clavulanate	Linear	101	1.74	117	0.914	114	0.751

**Table 2.** Validation results for pharmaceutical products containing caffeine, fluoxetine HCl, gabapentin, metformin HCl, potassium clavulanate respectively

Pharmaceutical product	50% spike		100% spike		150% spike	
	Rec. <sup>a</sup> (%)	RSD (%)	Rec. (%)	RSD (%)	Rec. (%)	RSD (%)
Caffeine	104	1.13	102	2.33	104	2.28
Fluoxetine HCl	100	0.700	101	0.758	96.6	2.76
Gabapentin	104	1.86	103	7.42	101	1.68
Metformin HCl	105	1.88	105	0.0777	105	0.452
Potassium clavulanate	103	1.81	100	0.183	97.5	2.90

<sup>a</sup>Rec.=Recovery

## DISCUSSION

A direct transfer of Minilab TLC methods to HPTLC-densitometry according to the earlier published process involves use of the same solvents in preparing the sample and standard solutions, application of the same weight of sample and standard in 10.00  $\mu\text{L}$  as in 2.00  $\mu\text{L}$ , and use of the same mobile phase and detection method.

The metformin HCl Minilab method for a 250 mg tablet (Volume II, Supplement 2014, Method 6.78, pp. 24-27) could not be transferred directly. The Minilab method involves preparation of stock standard and sample solutions in water followed by dilution with methanol to prepare the 100% standard and sample solutions. The drug was found to precipitate out upon dilution with methanol; therefore dilution was made with water instead. The Minilab mobile phase, methanol-water-glacial acetic acid (15:5:1) did not give tight bands nor symmetrical scan peaks, so the mobile phase methanol-water-1% (w/v) ammonium chloride reported in the literature [13] was adopted. After testing many mobile phases, none without ammonium chloride as a component gave good results, so it was decided that use of this non-hazardous salt was acceptable. When applying sample and standard weights specified in the Minilab unusually high scan areas ( $>10,000$ ) were obtained, but calibration, assay, and validation results were within the model process requirements.

The potassium clavulanate-amoxicillin coformulations Minilab method for a product containing 62.5 mg of clavulanic acid (Volume II, Supplement 2013, Method 6.69, pp.20-23) was directly transferred for our product with a label value of 57 mg of clavulanic acid, equivalent to 67.9 mg of potassium clavulanate except for the detection method. Bands were detected by heating the plate after development at 160°C for 5 min to produce fluorescence quenching bands visible under 254 nm ultraviolet (UV) light rather than using iodine vapor. This reagentless thermochemical activation method involving simple heating of silica gel layers was first reported by our laboratory and has been applied to a variety of drugs and dietary supplements [11]. Assay recovery for one of the three tablets was slightly above the model procedure upper limit of 115%, but the standard addition validation (Table 2) and peak identity and peak purity results meeting requirements indicated the assay was reliable. It was necessary to carefully adjust the integration limits when scanning bands of potassium clavulanate at 254 nm so that streaked amoxicillin bands did not interfere (Figure 1). Potassium clavulanate was also visible as fluorescent bands after heating, but interference of the amoxicillin bands when they were scanned at 366 nm was greater than at 254 nm. The reason for the two high assay results, one greater than the 115% model process limit, is not known, but the good validation results indicate that the assays are accurate and that

the product, which was obtained without a prescription from a shop in China, contains tablets with variable active ingredient amounts. A simultaneous method for assay of the coformulation could not be developed after unsuccessfully testing many different solvents to extract both potassium clavulanate amoxicillin completely from the sample and standard and mobile phases to separate the two compounds without streaked amoxicillin bands. In addition, after weeks of considerable research we have been unable to successfully use any published HPTLC-densitometry method for determination of amoxicillin, or the similar drug ampicillin, in any pharmaceutical product alone or in a coformulation, or to develop and validate a new method.

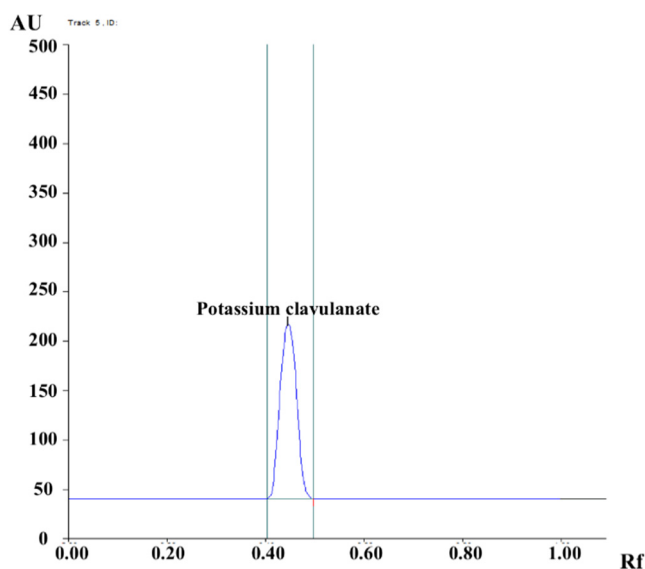


**Figure 1.** Densitogram of 10.0 uL of potassium clavulanate 100% sample solution, representing 3.31 ug of potassium clavulanate when interpolated from the calibration curve based on its area.

The model transfer process has also been used earlier as the basis of development of HPTLC-densitometry methods for drug products covered neither in the Minilab manual nor the Compendium, e.g., naproxen sodium, loperamide HCl, and loratidine [14]. In this paper, methods were similarly developed for caffeine, fluoxetine HCl, and gabapentin. Based on the development of these methods, corresponding TLC screening methods were devised, tested, and published in an open access online supplement to the FDA Compendium [15], from which they could be easily transferred to Minilab

TLC screening methods, if desired, by taking into account the 2.00  $\mu\text{L}$  rather than 3.00  $\mu\text{L}$  spotting volumes and the usual use of an authentic drug product rather than a commercial standard to prepare the standard solutions for Minilab methods.

The caffeine method for a 200 mg tablet was a direct adaptation of a previously published method [16] that used methanol solvent for standard and sample solution preparation, a similar calibration curve weight range, silica gel HPTLC plates, ethyl acetate-methanol (85:15) mobile phase, and fluorescence quenching detection. The fluoxetine HCl method for a 20 mg capsule was directly adapted from a published method for alprazolam and fluoxetine HCl in a tablet formulation [17] with use of methanol solvent for standard and sample solution preparation, acetone-toluene-ammonium hydroxide (6.0:3.5:0.5) mobile phase, and fluorescence quenching detection, but the calibration curve was prepared with weight range about four times greater in order to achieve successful band detection and scanning.

The gabapentin method for an 800 mg tablet was directly transferred from a published method for 200 mg capsules [18] in terms of the use of methanol for standard and sample solution preparation, the same weight range for the calibration curve, and the use of ninhydrin spray reagent for band detection. However, the mobile phase *n*-butanol-water acetic acid (3:3:2) [18] was modified by replacing *n*-butanol with ethanol, which are in the same selectivity group and have a similar solvent strength in Snyder's liquid chromatography solvent classification list [19], because *n*-butanol is not one of the allowed solvents for Minilab or Compendium methods. Unlike potassium clavulanate, heating the plate after development did not produce fluorescence quenching zones to eliminate for the need of a detection reagent, the use of which usually leads to poorer accuracy and precision data in method development.

Depending on the applications of the methods described in this paper, they should be fully validated for parameters such as accuracy, precision (repeatability and intermediate precision), specificity, linearity, range and robustness under relevant guidelines such as those described by the International Conference on Harmonization [20] or subjected to an interlaboratory study [21] to prove that they are suitable for their intended purpose by users.

## CONCLUSIONS

HPTLC-densitometry methods were developed and validated for assay of pharmaceutical formulations of two drugs by transfer of TLC screening methods contained in the Minilab manual, and for formulations of three drugs

not included in the Minilab manual or FDA Compendium. Supplemental Compendium methods that can be easily converted to Minilab methods if desired were devised for these latter drugs and posted on an open access internet site.

## EXPERIMENTAL

### Standard and sample solution preparation

General preparation procedures were carried out as described earlier [1-3] unless otherwise specified. All standards and ground (by mortar and pestle) tablets or capsule contents were dissolved with the aid of 10 min each of magnetic stirring and sonication before syringe filtration to remove undissolved excipients prior to further dilution or direct application. Dilutions were made using appropriate volumetric flasks and transfer and measuring pipets. Solutions were stored in sealed vials wrapped in parafilm in a refrigerator. A description of standards and samples and their sources as well as detailed procedures for stock and 100% working standard and sample solution preparation are shown in Table 3.

**Table 3.** Preparation of 100% standard and 100% sample solutions

Pharmaceutical product	100% standard solution	100% sample solution
Caffeine (200 mg; CVS Pharmacy, Inc., USA)	0.400 µg/ 10.0 µL: dissolve 40.0 mg standard (Sigma-Aldrich, St. Louis, MO, Catalog No. C0750) in 100 mL methanol, then dilute 1.00 mL with 9.00 mL methanol	0.400 µg/ 10.0 µL <sup>a</sup> : dissolve a tablet in 100 mL methanol, then dilute 1.00 mL with 49.0 mL methanol
Fluoxetine HCl (20 mg; Aurobindo Pharma, USA Inc.)	4.01 µg/ 10.0 µL: dissolve 80.1 mg standard (Sigma-Aldrich, No. PHR1394) in 200 mL methanol	4.00 µg/ 10.0 µL: dissolve a capsule in 50.0 mL methanol
Gabapentin (800 mg; Glenmark Pharmaceuticals Inc., USA)	1.60 µg/ 10.0 µL: dissolve 100 mg standard (Sigma-Aldrich, No. PHR1049) in 100 mL methanol, then dissolve 16.0 mL in 84.0 mL methanol	1.60 µg/ 10.0 µL: dissolve a tablet in 100 mL methanol, then dissolve 1.00 mL with 49.0 mL methanol



Pharmaceutical product	100% standard solution	100% sample solution
Metformin HCl (250 mg; Shanghai Xinyi Tianping Pharmaceutical Co., Ltd, Shanghai, China)	8.00 µg/ 10.0 µL: dissolve 40.0 mg standard (Sigma-Aldrich, No. PHR1084) in 50.0 mL deionized water	8.00 µg/ 10.0 µL: dissolve a tablet with 25.0 mL deionized water, then dilute 2.00 mL with 23.0 mL deionized water
Potassium clavulanate (67.9 mg <sup>b</sup> ; Guangzhou Baiyunshuan Pharmaceutical Holdings Co., Ltd, China)	2.72 µg/ 10.0 µL: dissolve 34.0 mg standard (Sigma-Aldrich, No. 33454) in 25.0 mL deionized water, then dilute 1.00 mL with 4.00 mL deionized water	2.72 µg/ 10.0 µL: dissolve a tablet in 50.0 mL deionized water, then dilute 1.00 mL with 4.00 mL deionized water

<sup>a</sup> Concentrations indicated for 100% sample solutions are theoretical concentrations.

<sup>b</sup> The potassium clavulanate sample was a tablet of 57 mg clavulanic acid (or 67.9 mg potassium clavulanate, when adjusted for molecular weight factor) with 400 mg amoxicillin as the other active ingredient.

## HPTLC

Detailed HPTLC-densitometry methods and instruments were described earlier [1-3, 6-12]. Silica gel 60 F<sub>254</sub> Premium Purity HPTLC glass plates (20 x10 cm; EMD Millipore Corp., Billerica, MA, a division of Merck KGaA, Darmstadt, Germany; Part No. 1.05648.0001) were used as received. Application of 7.00, 9.00, 11.0, and 13.0 µL aliquots of the 100% standard solution of each drug [representing 70-130% of the active pharmaceutical ingredient (API) content based on label value] and triplicate 10.0 µL aliquots of 100% sample solution were applied using a CAMAG (Wilmington, NC, USA) Linomat 4 spray on applicator [band length 6 mm, application rate 4 sec/µL (15 sec/µL for solutions containing water), table speed 10 mm/s, distance between bands 4 mm, distance from the left edge of the plate 17 mm, and distance from the bottom of the plate 1 cm). HPTLC-densitometry in the absorption-reflectance mode was performed using a CAMAG Scanner 3 (4.00 x 0.45 mm Micro slit dimensions, 20 mm/s scan rate). The mobile phases used for the five pharmaceutical products and drug R<sub>f</sub> values are shown in Table 4. The fluorescence-quenching bands were scanned with 254 nm UV light, and the colored bands of gabapentin were scanned with 510 nm light. The Scanner 3 winCATS software automatically created calibration curves (linear or 2<sup>nd</sup> order polynomial) based on scan areas versus standard weights applied, interpolated

weights of drugs in bracketed samples based on scan areas, and tested peak purity and identity of the sample based on spectral comparison. Accuracy of the developed methods was validated by using standard addition with a 70-130% calibration curve as described earlier [3].

**Table 4.** Mobile phases selected in our methods for pharmaceutical products containing caffeine, fluoxetine HCl, gabapentin, metformin HCl, potassium clavulanate respectively

Pharmaceutical product	Mobile phase <sup>a</sup>	R <sub>f</sub>
Caffeine	Ethyl acetate-methanol (85:15)	0.36
Fluoxetine HCl	Acetone-toluene-ammonia (6:3.5:0.5)	0.62
Gabapentin	Ethanol-deionized water-glacial acetic acid (3:3:2)	0.75
Metformin HCl	Methanol-water-1% ammonium chloride solution (5:4:1)	0.25
Potassium clavulanate	Ethyl acetate-glacial acetic acid-water (15:5:5)	0.43

<sup>a</sup>All solutions are shown in volume proportions

## ACKNOWLEDGEMENTS

The authors thank Dave Lentz of EMD Millipore Corp. for providing the Premium Purity glass HPTLC plates used in our experiments. Kaitlin Nguyen was supported by the EXCEL Scholars Program. Danhui Zhang was supported by a Camille and Henry Dreyfus Foundation Senior Scientist Mentor Program award to Professor Joseph Sherma and by the Lafayette College EXCEL Scholars Program.

## REFERENCES

1. C. O'Sullivan, J. Sherma, *Acta Chromatographica*, **2012**, 24, 241.
2. K. Lianza, J. Sherma, *Journal of Liquid Chromatography & Related Technologies*, **2013**, 36, 2446.
3. N. Popovic, J. Sherma, *Acta Chromatographica*, **2014**, 26, 615.
4. <http://www.gphf.org>
5. A.S. Kenyon, T.P. Layloff, <http://www.pharmweb.net/pwmirror/library/tlc/tlcall.pdf>
6. M. Nguyen, J. Sherma, *Trends in Chromatography*, **2013**, 8, 131.
7. M. Nguyen, J. Sherma, *Journal of Liquid Chromatography & Related Technologies*, **2014**, 37, 2956.

8. J. Strock, M. Nguyen, J. Sherma, *Journal of Liquid Chromatography & Related Technologies*, **2015**, *38*, 1126.
9. J. Strock, M. Nguyen, J. Sherma, *Acta Chromatographica*, **2016**, *28*, 363.
10. D. Zhang, J. Strock, J. Sherma, *Journal of Liquid Chromatography & Related Technologies*, **2016**, *39*, 277.
11. E. Armour, J. Sherma, *Journal of Liquid Chromatography & Related Technologies*, **2017**, *40*, 282.
12. D. Zhang, E. Armour, J. Sherma, *Acta Chromatographica*, doi:10.1556/1326.2016.29409.
13. H. Mahgoub, R.M. Youssef, M.A. Korany, E.F. Khamis, M.F. Kamal, *Drug Development and Industrial Pharmacy*, **2014**, *40*, 1190.
14. D. Zhang, J. Strock, J. Sherma, *Trends in Chromatography*, **2016**, *10*, 1.
15. Supplement to a Compendium of Unofficial Methods for Rapid Screening of Pharmaceuticals by Thin Layer Chromatography, <http://www.layloff.net>.
16. D. Ruddy, J. Sherma, *Acta Chromatographica*, **2002**, *12*, 143.
17. R.B. Patel, M.R. Patel, M.B. Shankar, K.K. Bhatt, *Journal of AOAC International*, **2009**, *92*, 1082.
18. R.T. Sane, U. Pendse, A. Moghe, S. Khedkar, P. Patil, *Indian Drugs*, **2003**, *40*, 547.
19. T. Tuzimski, Selection of the Type of Mobile Phases for Analysis of Nonionic Analytes: Reversed and Normal Phase HPLC, in *High Performance Liquid Chromatography in Pesticide Residue Analysis*, T. Tuzimski and Joseph Sherma (Editors), CRC Press, Taylor & Francis Group, **2015**, Chapter 7, pp. 174-175.
20. K. Ferenczi-Fodor, Z. Vegh, A. Nagy-Tuak, B. Renger, M. Zeller, *Journal of AOAC International*, **2001**, *84*, 1265.
21. E. Kaale, P. Risha, E. Reich, T. P. Layloff, *Journal of AOAC International*, **2010**, *93*, 1836.

*Dedicated to Professor Costel Sârbu on the  
Occasion of His 65<sup>th</sup> Anniversary*

## **CLASSIFICATION OF AMINO ACIDS BY MULTIVARIATE DATA ANALYSIS, BASED ON THERMODYNAMIC AND STRUCTURAL CHARACTERISTICS**

**OSSI HOROVITZ<sup>a</sup>, ROXANA-DIANA PAȘCA<sup>a\*</sup>**

**ABSTRACT.** Principal component analysis (PCA) and cluster analysis (CA) were applied to classify 20 natural amino acids. We selected 18 characteristics, properties available from literature, as a basis for the classification. The correlations between these characteristics and their classification were investigated, as well as the classification of the amino acids. The results are presented as score plots of the first 3 principal components and as dendrograms obtained by clustering analysis. The resulting classification is consistent with the chemical behavior of amino acids and their mutual substitution possibilities in peptides and proteins.

**Keywords:** *principal component analysis, cluster analysis, amino acids, thermodynamic characteristics, structural characteristics*

### **INTRODUCTION**

Amino acids, as building blocks for peptides and proteins were intensively studied and their importance in human nutrition and in animal feed, in food industry, pharmaceutical and cosmetics industries, as chelating agents, etc. The standard 20 amino acids, implied in the formation of peptides and proteins

---

<sup>a</sup> Babeș-Bolyai University, Faculty of Chemistry and Chemical Engineering, 11 Arany Janos str., RO-400028, Cluj-Napoca, Romania

\* Corresponding author: [rpasca@chem.ubbcluj.ro](mailto:rpasca@chem.ubbcluj.ro)

(proteinogenic amino acids) are enumerated here, together with their 3-letter and 1-letter symbols: glycine (Gly, G); alanine (Ala, A); phenylalanine (Phe, F); valine (Val, V); leucine (Leu, L); isoleucine (Ile, I); aspartic acid (Asp, D); glutamic acid (Glu, Q); asparagine (Asn, N); glutamine (Gln, E); serine (Ser, S); threonine (Thr, T); tyrosine (Tyr, Y); cysteine (Cys, C); methionine (Met, M); lysine (Lys, K); arginine (Arg, R); proline (Pro, P); histidine (His, H); tryptophan (Trp, W).

There are many possibilities to classify amino acids, according to the criteria selected to this aim. Based on their chemical structure [1] we can distinguish monoamino carboxylic acids (Gly, Ala, Val, Leu, Ile, Phe), monoamino dicarboxylic acids and their amides (Asp, Asn, Glu, Gln), hydroxyl amino acids (Ser, Thr, Tyr), thioamino acids (Cys, Met), diamino carboxylic acids and derivatives (Lys, Arg), heterocyclic amino acids (Pro, His, Trp). A classification based on structure and physical and chemical properties [2] groups the amino acids in: acidic (Asp, Glu), basic (Lys, Arg, His), aromatic (Tyr, Trp, Phe), S containing (Cys, Met), uncharged, hydrophilic (Ser, Thr, Asn, Gln), inactive hydrophobic (Gly, Ala, Val, Leu, Ile), special structure (Pro). The same amino acid can be assigned to more different classification groups based on the property considered [3]: polar / hydrophilic (Asn, Gln, Ser, Thr, Lys, Arg, His, Asp, Glu, [Cys, Tyr]); non polar / hydrophobic ([Gly], Ala, Val, Leu, Ile, Pro, Tyr, Phe, Trp, Met, Cys); forming hydrogen bond (Cys, Trp, Asp, Gln, Ser, Thr, Tyr, Lys, Arg, His, Asp, Glu); S containing (Cys, Met); negatively charged at neutral pH / acidic (Asp, Glu [Cys]; positively charged at neutral pH / basic (Lys, Arg, [His]; ionisable (Asp, Glu, His, Cys, Tyr, Lys, Arg); aromatic (Phe, Trp, Tyr, [His]; aliphatic (Gly, Ala, Val, Leu, Ile, Pro); forming covalent cross-bonding (S-S) (Cys); cyclic (Pro).

In view of the overlapping between the different classes, a Venn diagram showing the classification is helpful (Fig. 1) [4-6] This tries to group the amino acids according to their nature (aliphatic, aromatic), to the size of the molecules (small, tiny), to the hydrophobicity and in relation to their polarity (polar, charged - positive or negative).

Since the role of amino acids in the formation of proteins is of prime importance, a classification was proposed according to the interchangeability of different amino acids in the structure of a protein, without interfering with this structure [7]. The diagram in Figure 2 is a graphical representation of this substitutability. Amino acids connected in the diagram can be replaced with 95 % -probability. Marked with red are the solvent-exposed amino acids, with green – those located inside the protein molecule, according to their solvent exposed area (SEA)

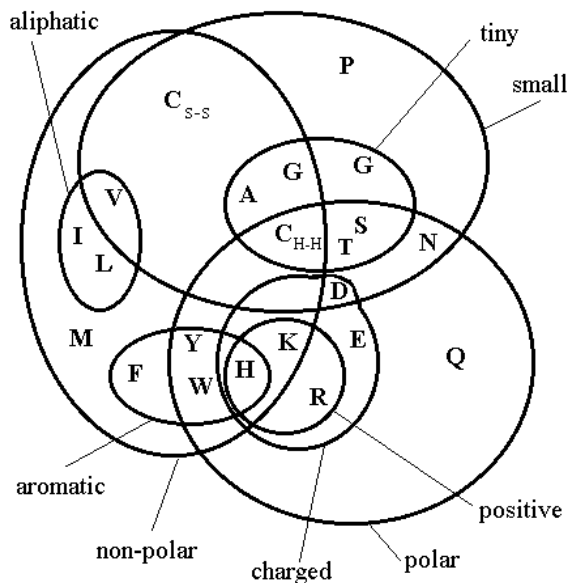


**Figure 1.** Venn diagram grouping the amino acids according to their properties (adapted from [4,5])

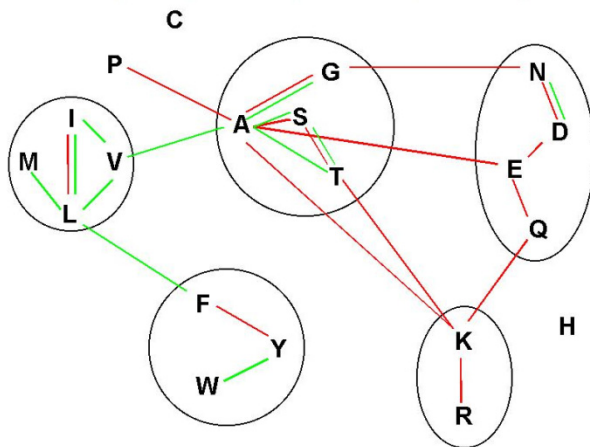


**Figure 2.** Possible substitutions of amino acids (according to [7]); amino acids bounded by lines have a substitution probability of 95%. Red: solvent exposed area (SEA) > 30 Å<sup>2</sup>; green: SEA < 10 Å<sup>2</sup>.

Here we propose a multivariate data analysis [8-14] of the amino acids, by principal components analysis (PCA) and cluster analysis (CA). PCA helps to reduce the number of variables necessary to describe a system, by maintaining the maximum possible information. Using the new variables as coordinates, "similarity maps" can be drawn for the analyzed system. In CA the (dis)similarity between elements is measured as "distances" between points in the space defined by the variables. The elements are then grouped in classes (clusters) by different clustering methods.

## THEORETICAL METHODS

The objects of the classification were the 20 proteinogenic amino acids, enumerated above. As variables (descriptors, characteristics) 18 properties were chosen, as follows:

- Molar mass (MM)
- Acid dissociation constants  $pK = -\lg K_a$  [3, 15, 16], corresponding to the first dissociation step (carboxylic group),  $pK_1$  and the second dissociation (ammonium group),  $pK_2$ . Only seven amino acids present also a third dissociation constant,  $pK_3$ , due to a supplementary group (side chain), which was not considered in the PCA, but used in the calculation of the isoelectric point.
- Isoelectric point (pI), the pH where the molecules have no net electrical charge (zwitterions), and present a minimum solubility in water. The value can be calculated as the mean of the  $pK$  values corresponding to the equilibria which include the uncharged species.

Some descriptors for the elementary composition of the molecules were used:

- Number of carbon atoms (NC), a measure of the length of the carbon chain, and so related to the hydrophobicity of the molecule
- Number of hydrogen atoms (NH)
- Number of nitrogen atoms (NN), a measure of the number of basic functions
- Number of oxygen atoms (NO), a measure of the number of acid groups
- Number of sulphur atoms (NS)

Chou-Fasman Parameters for predicting the secondary structures in proteins [17, 18]

- $P(\alpha)$  – the probability for helix conformations (PA);
- $P(\beta)$  – the probability for  $\beta$ -strands conformations (PB);
- $P(t)$  – the probability for turns (PT)

### Thermodynamic data

• Standard enthalpy of formation,  $H_{298}^0$  (HF) [19]. For 4 amino acids (Phe, Trp, Gln, Arg) no values were found. Therefore, we calculated theoretical values for all aminoacids (except Cys and Met to avoid the complications related to the parametrization for S atoms), on the restricted Hartree-Fock level, by the semi empirical SCF-MO method PM3 [20], using the Hyper Chem 7.5 Software [21]. The molecular geometries for the zwitterionic forms were optimized by the Polak-Ribiere (conjugate gradient) algorithm. Between experimental (exp) and calculated (calc) values the following linear correlation was found:

$$\Delta H_{298}^0(\text{exp}) [\text{kJ/mol}] = (-264 \pm 27) + (1.10 \pm 0.07) \Delta H_{298}^0(\text{calc}), r = 0.979, n = 14$$

This correlation was used to estimate the  $H_{298}^0$  values for the 4 amino acids, where experimental values were not available.

- Standard state accessibility (AS), is defined as the average surface area of the residue X in a tripeptide Gly-X-Gly [22, 23].
  - Average accessible surface area in proteins (AA)
  - Solubility in water (SO) at 25 °C [15, 24]
  - Hydrophobicity index (HP) [3, 25]. There are many different hydrophobicity scales, 46 scales were evaluated [26] and a PCA analysis was made on 40 scales [27]. One of the most used is the KD-scale [28], whose values very similar values with those used here. High positive values denote a strong hydrophobicity, while hydrophilic amino acids present negative values. In proteins, hydrophobic amino acids will be more probably located inside, while hydrophilic ones will be rather in contact with the aqueous environment.
  - Melting points (MP) [29] for amino acids are quite high, an evidence for their zwitterionic character. They are a measure for the intermolecular interactions in solid state and for their stability. Some amino acids are decomposed before melting, for them we used the decomposition temperature.

The values used for the 20 amino acids are given in Table 1.



**Table 1.** Properties of the amino acids (the symbols are given in text)

Amino-acid	M (g/mol)	pK1	pK2	pK3	pI	nC	nH	nN	nO	nS	P(α)	P(β)	P(t)	ΔH <sub>298</sub> <sup>0</sup> (kJ/mol)	AS (Å)	AA (Å)	SO(g/100g)	HP	MP (°C)
GLY,G	75.07	2.21	9.15		5.68	2	5	1	2	0	57	75	156	-527.5	88.1	25.2	24.99	0.67	233
ALA,A	89.09	2.35	9.87		6.11	3	7	1	2	0	142	83	66	-560	118.1	31.5	16.65	1	297
PHE,F	165.19	2.58	9.24		5.91	9	11	1	2	0	113	138	60	-440	222.8	28.7	2.965	2.5	283
LEU,L	131.17	2.36	9.6		6.04	6	13	1	2	0	121	130	59	-646.8	193.1	29	2.426	2.2	294
ILE,I	131.17	2.32	9.76		5.94	6	13	1	2	0	108	160	47	-640.6	181	23	4.117	3.1	284
VAL,V	117.15	2.3	9.6		5.96	5	11	1	2	0	106	170	50	-628.9	164.5	23.5	8.85	2.3	315
SER,S	105.09	2.21	9.15		5.68	3	7	1	3	0	77	75	143	-732.7	129.8	44.2	5.023	-1.1	228
THR,T	119.12	2.15	9.12		5.64	4	9	1	3	0	83	119	96	-776.3	152.5	46	9.7	-0.75	256
TRP,W	204.22	2.38	9.39		5.89	11	12	2	2	0	108	137	98	-350	266.3	41.7	1.136	1.5	289
PRO,P	115.13	1.99	10.6		6.3	5	9	1	2	0	57	55	152	-507.1	146.8	53.7	162.3	-0.29	221
ASP,D	133.1	1.88	9.6	3.65	2.77	4	7	1	4	0	101	54	146	-973.3	158.7	60.9	0.778	-3	270
ASN,N	132.12	2.02	8.8		5.41	4	8	2	3	0	67	89	156	-789	165.5	62.2	3.33	-2.7	234
GLU,E	147.13	2.19	9.67	4.25	3.22	5	9	1	4	0	151	37	74	-1003	186.2	72.3	0.864	-2.6	248
GLN,Q	146.15	2.17	9.13		5.65	5	10	2	3	0	111	110	98	-770	193.2	74	2.5	-2.9	185
TYR,Y	181.19	2.2	9.11	10.07	5.66	9	11	1	3	0	69	147	114	-685.6	236.8	59.1	0.0453	0.08	342
CYS,C	121.16	1.71	8.33	10.78	5.02	3	7	1	2	1	70	119	119	-534.1	146.1	13.9	0.011	0.17	280
MET,M	149.21	2.28	9.21		5.74	5	11	1	2	1	145	105	60	-577.5	203.4	30.5	3.381	1.1	281
ARG,R	174.2	2.18	9.09	13.2	11.15	6	14	4	2	0	98	93	95	-570	256	93.8	15	-7.5	244
LYS,K	146.19	2.2	9.2	10.28	9.59	6	14	2	2	0	114	74	101	-678.7	225.8	110.3	150	-4.6	224
HIS,H	155.16	1.78	8.97	5.97	7.47	6	9	3	2	0	100	87	95	-441.8	202.5	46.7	4.19	-1.7	287

All calculations were executed using the *Statistica* software package on the data matrix (20 objects, 18 variables). After the scaling of variables (to a mean of 0 and a variance of 1), PCA and CA procedures were applied, both for the classification of properties and of amino acids.

## RESULTS AND DISCUSSION

**Table 2.** Table of correlations for the properties of the amino acids (significant correlations at P = 0.95 are bolded)

	MM	PK1	PK2	PI	NC	NH	NN	NO	NS	PA	PB	PT	HF	AS	AA	SO	HP	MP
MM	1.00	0.15	-0.18	0.23	<b>0.88</b>	<b>0.65</b>	<b>0.47</b>	0.03	-0.02	0.23	0.29	-0.24	0.17	<b>0.96</b>	0.37	-0.23	-0.20	0.26
PK1		1.00	0.30	0.12	0.43	0.44	-0.21	-0.24	-0.29	0.44	0.41	<b>-0.57</b>	0.19	0.26	-0.13	-0.38	0.42	0.25
PK2			1.00	-0.12	0.07	0.11	-0.31	-0.02	-0.41	0.23	-0.18	-0.16	<b>-0.04</b>	-0.14	-0.02	-0.09	0.24	0.07
PI				1.00	0.20	<b>0.58</b>	<b>0.73</b>	<b>-0.61</b>	-0.13	-0.05	0.10	-0.13	<b>0.47</b>	0.43	0.44	0.20	-0.42	-0.13
NC					1.00	<b>0.67</b>	0.22	-0.18	-0.21	0.18	<b>0.48</b>	-0.34	0.38	<b>0.87</b>	0.13	-0.24	0.17	0.44
NH						1.00	0.38	-0.35	-0.11	0.37	0.46	<b>-0.58</b>	0.19	<b>0.81</b>	0.34	-0.04	-0.07	0.21
NN							1.00	-0.19	-0.19	-0.01	-0.11	0.06	0.23	<b>0.53</b>	<b>0.57</b>	-0.11	<b>-0.69</b>	-0.23
NO								1.00	-0.22	0.03	-0.42	0.32	<b>-0.88</b>	-0.11	0.36	-0.17	-0.37	-0.19
NS									1.00	0.09	0.08	-0.09	0.18	-0.05	-0.36	0.26	0.16	0.06
PA										1.00	-0.00	-0.14	0.31	0.06	-0.34	0.07	0.22	
PB											1.00	<b>-0.55</b>	0.39	0.33	<b>-0.47</b>	-0.14	<b>0.59</b>	<b>0.58</b>
PT												1.00	-0.16	-0.36	0.24	0.23	-0.40	<b>-0.49</b>
HF													1.00	0.21	-0.39	0.06	0.39	0.25
AS														1.00	0.43	-0.18	-0.22	0.25
AA															1.00	0.14	<b>-0.87</b>	-0.46
SO																1.00	-0.16	-0.32
HP																	1.00	<b>0.55</b>
MP																		1.00

The covariance matrix, identical with the correlation matrix, since data were normalized, is given in Table 2. It confirms that the properties are correlated, and the number of variables can be reduced by PCA.

The eigenvalues (EV) and eigenvectors corresponding to each principal component were calculated. In Table 3, the EV for the first 6 principal components (PC) are given, together with the loadings of the characteristics associated with each PC. The contribution of each PC is given as % from the total variance of the system. The first three PC cumulate about 66% from the total variance, and the first 6 PC over 88%. In Table 3, the values representing the maximum contribution of each property to a PC are bolded.

**Table 3.** Eigenvectors and eigenvalues (EV) for the first 6 principal components (PC). The maximum contribution (loading) of each variable is bolded

Variable	PC1	PC2	PC3	PC4	PC5	PC6
MM	<b>0.732772</b>	-0.418786	0.149100	-0.437709	-0.119962	-0.106764
PK1	<b>0.580684</b>	0.323887	0.318470	0.405112	-0.049469	0.050468
PK2	0.036689	-0.222711	0.402239	<b>0.660723</b>	-0.184703	-0.279568
PI	0.455128	<b>-0.524516</b>	-0.519732	0.409233	-0.084511	0.101819
NC	<b>0.843749</b>	-0.107567	0.132647	-0.205899	-0.346962	-0.207651
NH	<b>0.845821</b>	-0.278541	0.043770	0.149541	0.143806	-0.252191
NN	0.321116	<b>-0.779242</b>	-0.270120	0.029570	-0.005560	0.398847
NO	0.475639	-0.251914	<b>0.735451</b>	-0.363289	-0.075591	-0.074636
NS	-0.068992	0.249191	-0.407097	-0.479635	<b>0.619484</b>	-0.087982
PA	0.422426	0.097598	0.532400	0.150091	<b>0.639621</b>	0.150662
PB	<b>0.646027</b>	0.455109	-0.196461	-0.224951	-0.123477	-0.057888
PT	<b>-0.693531</b>	-0.356646	-0.225276	-0.146697	-0.485925	-0.042470
HF	0.486677	0.233157	<b>-0.707765</b>	0.147943	-0.189069	0.132121
AS	<b>0.830771</b>	-0.454054	0.100198	-0.257977	-0.016263	-0.116410
AA	0.018882	<b>-0.924642</b>	0.237951	0.140003	0.039411	-0.155298
SO	-0.287173	-0.147992	-0.506858	0.090974	0.219967	<b>-0.713778</b>
HP	0.225330	<b>0.942794</b>	-0.044783	-0.001836	-0.142445	-0.093475
MP	0.514421	<b>0.518994</b>	0.105280	-0.285245	-0.121981	0.053338
EV	5.246110	4.066386	2.565046	1.679726	1.370267	0.985620
% total variance	29.14506	22.59103	14.25025	9.33181	7.61260	5.47567
Cumulated (%)	29.1451	51.7361	65.9863	75.3182	82.9308	88.4064

### Classification of properties

Some characteristics with the largest contribution in PC1 are the number of H and C atoms, the AS surface and the molar mass, which are strongly correlated as shown in Table 2. Altogether there are 7 properties with maximum contribution in PC1. In PC2 there are 5 such properties, the most important being hydrophobicity (HP) and accessible surface area (AA), also strongly correlated (negatively). The other PC, 3 to 6, contain each only one or two properties with large contributions. In PC3 there are the number of O atoms (NO) and the enthalpy of formation (HF), also strongly correlated (Table 2): amino acids with more O atoms have actually lower  $H_{298}^0$  values, with Asp and Glu the most stable (Table 1).

Such correlations can be visualized by 2- or 3-D loading plots; as an example, the scatter plot for the first two PC is given in Figure 2. Here related properties are represented by nearby points. But negatively correlated properties appear quite far from one another.

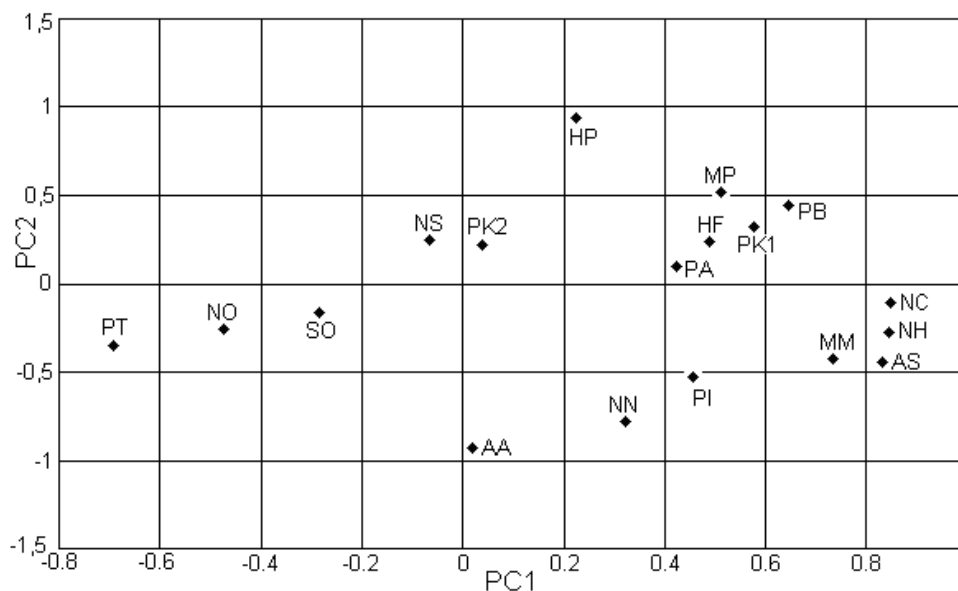


**Figure 3.** PCA loading plot for the two first principal components. The symbols of the characteristics correspond to those in Tables 1-3.

The results of cluster analysis can be presented as dendrograms, grouping the different properties in clusters. In Figure 4 is given such a diagram, obtained by the Complete Linkage method, using Euclidean distances

## Classification of amino acids

In order to apply PCA for the classification of amino acids, we use the scores of each amino acid calculated for the first (more important) PCs. Here the first 3 PCs cumulate 66% of the total variance of data. Therefore, by reducing the number of 18 characteristics (natural variables) to 3 variables (the first 3 PCs) we retain enough information to characterize the system in 2D-representations (in the planes defined by PC1 and PC2, PC1 and PC3 or PC2 and PC3) an 3D- representation (in the space of PC1, PC2 and PC3). As an example, in Figure 5 the representation in the PC1-PC2 plane is given. Some groupings of amino acids are highlighted in the figure.

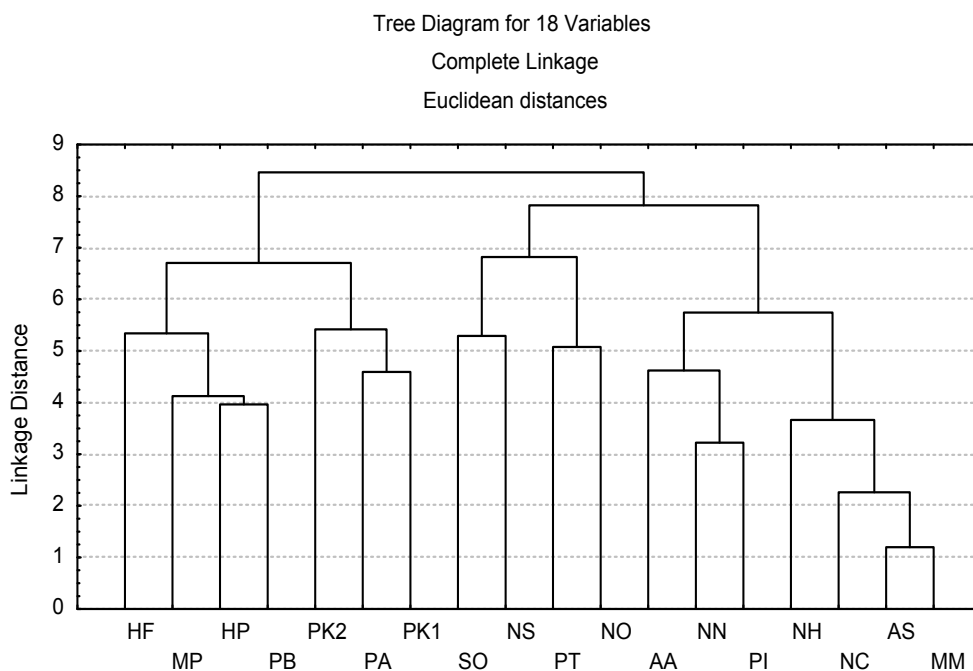


**Figure 4.** Dendrogram for hierarchical clustering for 18 properties

The similarities between amino acids can also be followed on the dendrogram (Figure 6) obtained in CA, using the same Complete Linkage method, with Euclidean distances, as for the properties.

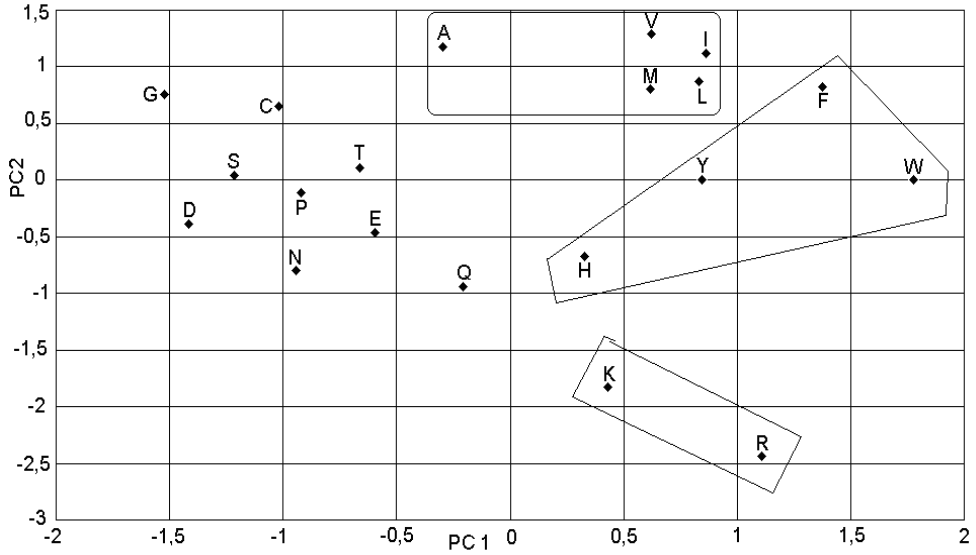


**Figure 5.** PCA score plots for the 20 amino acids in the plane of the two first principal components. 1-letter symbols are used for the amino acids.

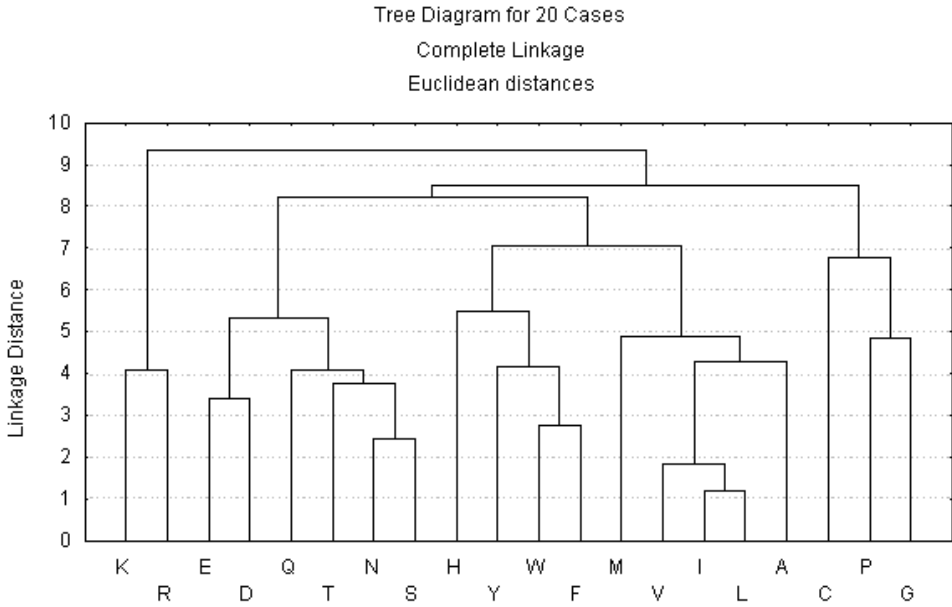


**Figure 6.** Dendrogram for hierarchical clustering by complete linkage method for 20 amino acids. 1-letter symbols are used for the amino acids (see Introduction)

The strongest related amino acids according to CA are leucine (L) and isoleucine (I), isomers with very similar properties. In the dendrogram they are joined by valine (V), methionine (M), and alanine (A). They all are aliphatic hydrophobic amino acids. Another cluster, more loosely connected, contains phenylalanine (F), tryptophan (W), tyrosine (Y), and histidine (H) - all aromatic amino acids, mostly hydrophobic, but also partially hydrophilic, particularly H. These two clusters are then connected (Fig. 6), giving a cluster of mostly hydrophobic amino acids.

Lysine (K) and arginine (R) form a cluster of basic amino acids, positively charged in proteins at physiological pH, histidine, also basic, is near to them in Fig. 5. The two acidic amino acids, negatively charged in proteins: aspartic acid (D), and glutamic acid (E), are also united in a cluster (Fig. 6). Asparagine (N) and serine (S) give a cluster with glutamine (Q), and threonine (T): they are neutral in proteins, but contain polar groups and show hydrophilic properties. Quite loosely interconnected are glycine (G), proline (P), and cysteine (C) – small molecules, rather dissimilar to other amino acids

It is worth noting that though the characteristics used in classification were mostly of physical and stoichiometrical nature, the resulted classification follows quite well the chemical properties and the character of amino acids. It is also interesting to compare the clustering results with the possibilities of mutual interchange of amino acids in proteins [7] (Fig. 2). We find there the same group L, I, M, V as in CA, as well the group F, Y, W, or the group K, R. The other possibilities of substitution in Fig.2 are also quite well reflected in PCA and CA.

## CONCLUSIONS

The use of the methods of multivariate analysis applied for the standard 20 proteinogenic amino acids, based on literature data for 18 structural and physico-chemical characteristics, resulted in a classification able to predict the chemical behavior of these compounds. It demonstrates the possibilities of principal component analysis and cluster analysis in the description of different classes of chemical compounds.

## ACKNOWLEDGMENTS

We thank Prof. Dr. Costel Sârbu, who kindly initiated us in multivariate analysis.

## REFERENCES

1. C.D. Nenițescu, "Chimie organică", Vol. II, 6<sup>th</sup> Edition, EDP București, **1968**.
2. \*\*\*, „Molecular Biology Web Book”, Chap. 2, „Protein Structure and Function”, <http://www.web-books.com/MoBio/Free/Chap2.htm> (accessed September **2016**).
3. U.C. Davis, „Biological Sciences: Amino Acid Structure/Function”, <https://www.mcb.ucdavis.edu/courses/bis102/AAProp.html> (accessed September **2016**).
4. W.R. Taylor, *Journal of Theoretical Biology*, **1986**, 119, 205.
5. M.J. Betts, R.B. Russell. „Amino acid properties and consequences of substitutions“. In „*Bioinformatics for Geneticists*“, M.R. Barnes, I.C. Gray eds., Wiley, Chichester, **2003**.
6. O. Horovitz, A. Mocanu, Gh. Tomoaia, M. Crisan, L.-D. Bobos, Cs. Racz, M. Tomoaia-Cotisel, *Studia UBB Chemia*, **2007**, 52, 53.
7. D. Bordo, P. Argos, *Journal of Molecular Biology*, **1991**, 217, 721.
8. T.P.E. auf der Heyde, *Journal of Chemical Education*, **1990**, 67, 461.
9. H. Pop, C. Sârbu, O. Horovitz, D. Dumitrescu, *Journal of Chemical Information and Computer Sciences*, **1996**, 36, 465.
10. C. Sârbu, O. Horovitz, H.Pop, *Journal of Chemical Information and Computer Sciences*, **1996**, 36, 1098.
11. O. Horovitz, C.Sarbu, H.F.Pop, „Clasificarea rațională a elementelor chimice”, Ed. Dacia, Cluj-Napoca, **2000**.
12. O.Horovitz, C.Sârbu, H.F.Pop, *Revista de Chimie (Bucharest)*, **2000**, 51, 17.
13. O. Horovitz, C. Sârbu, *Journal of Chemical Education*, **2005**, 82, 473.
14. O. Horovitz, C. Sârbu, *Revista de Chimie (Bucharest)*, **2006**, 57, 413.
15. J. Reichert, A. Jabs, P. Slickers, J. Sühnela, *Nucleic Acids Research*, **2000**, 28, 246.
16. D.R. Lide, "Handbook of Chemistry and Physics", 12nd Ed., CRC Press, Boca Raton, **1991**.
17. P.Y. Chou, G.D. Fasman, *Biochemistry*, **1974**, 13, 211.
18. P. Prevelige, Jr., G.D. Fasman, *Chou-Fasman, Prediction of Secondary Structure, in Prediction of Protein Structure and the Principles of Protein Conformation*, ed. G. B. Fasman, Plenum Press, New York, **1989**.
19. \*\*\*, Chemistry WebBook, NIST Standard Reference Database Number 69 - June, <http://webbook.nist.gov/chemistry/> (accessed September **2016**).
20. J.J.P. Stewart, *Journal of Computational Chemistry*, **1989**, 10, 209.
21. \*\*\*, HyperChem7.5 Molecular Modeling System, Hypercube Inc., Gainesville, **2002**.
22. C. Chotia, *J. Mol. Biol.*, **1975**, 105, 1.
23. \*\*\*, CRC Handbook of Chem.& Phys., 58 Ed., Cleveland, Ohio, **1977**.
24. D. Eisner, R.M. Weiss, T.C. Terwilliger, William Wilcox, *Faraday Symp. Chem. Soc.*, **1982**, 17, 109.

25. J.L. Cornette, K.B. Cease, H. Margalit, J.L. Spouge, J.A. Berzofsky, C. DeLisi, *J. Mol. Biol.*, **1987**, 195, 659.
26. A. Neumaier, W. Hoyer, E. Bornberg-Bauer, „Hydrophobicity Analysis of Amino Acids” <http://www.mat.univie.ac.at/~neum/software/protein/aminoacids.html> (accessed September **2016**).
27. J. Kyte, R.F. Doolittle, *Journal of Molecular Biology*, **1982**, 157, 105.
28. R.C Beavis, D. Fenyo, “Amino Acid Properties of Interest in Protein Chemistry”, <http://prowl.rockefeller.edu/aainfo/contents.htm> (accessed September **2016**).





*Dedicated to Professor Costel Sârbu on the  
Occasion of His 65<sup>th</sup> Anniversary*

## PROPERTY-PROPERTY RELATIONSHIPS FOR MONOSACCHARIDES

LORENTZ JÄNTSCHI<sup>a</sup>

**ABSTRACT.** The enormous diversity and complexity of polysaccharides resides in the large number of anomeric positions, diversity in the size of the rings as well as of the large number of the linkage positions of the monosaccharides. By taking this fact into account, in order to provide useful knowledge for insight on polysaccharides, a more comprehensive study of the polymer units, the monosaccharides, is required. A study for relating experimentally measured properties - melting points and solubilities with other properties accessible by calculations was conducted for monosaccharides from trioses to hexoses.

**Keywords:** *Monosaccharides; Property-property relationships; Melting points; Solubilities*

### INTRODUCTION

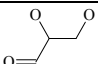
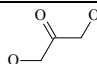
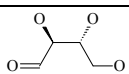
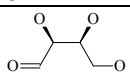
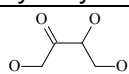
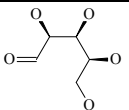
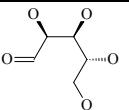
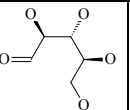
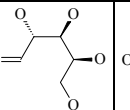
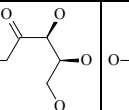
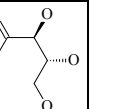
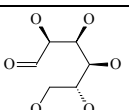
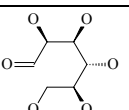
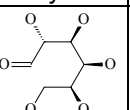
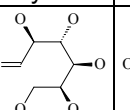
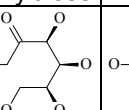
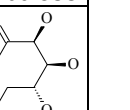
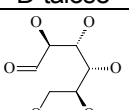
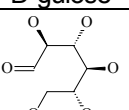
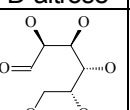
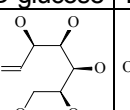
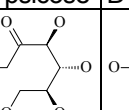
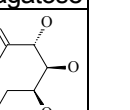
Carbohydrates are structural components of cell walls in plant and algae (cellulose [1]), of DNA - deoxyribonucleic acid (deoxyribose [2]) or RNA - ribonucleic acid (ribose [2]), or of tissues (lyxose [3]). Sugars are short chain carbohydrates, their molecule consisting of carbon (C), hydrogen (H) and oxygen (O) atoms with the general formula  $C_m(H_2O)_n$  where  $2 \leq m$  (and usually  $3 \leq m \leq 7$ ) and  $n \leq m$  (and usually  $n = m$  or  $n = m-1$ ).

---

<sup>a</sup> *Technical University of Cluj-Napoca, Faculty of Materials and Environmental Engineering, Dept. of Physics & Chemistry, 28 Memorandumului str., RO-400114, Cluj-Napoca, Romania; Babeş-Bolyai University, Faculty of Chemistry and Chemical Engineering, Doctoral School of Chemistry, 11 Arany János str., RO-400028, Cluj-Napoca, Romania.  
E-mail: lorentz.jantschi@gmail.com*

The simplest carbohydrate is the monosaccharide with general formula  $(\text{CH}_2\text{O})_n$ , where  $n$  ranges from 2 (diose,  $\text{H}-(\text{C}=\text{O})-(\text{CH}_2)-\text{OH}$ ) to usually 7 ( $n = 3$  for trioses,  $n = 4$  for tetroses,  $n = 5$  for pentoses,  $n = 6$  for hexoses and  $n = 7$  for heptoses). There are 23 monosaccharides (see Table 1) from trioses ( $n = 3$ ) to hexoses ( $n = 6$ ). The monosaccharides with lower number of atoms (e.g.  $n = 3$  and  $n = 4$ ) may cyclize by dimerization leading to cyclic monosaccharides with  $n = 6$  and  $n = 8$ , respectively as the monosaccharides can join together to form disaccharides. A disaccharide is formed whenever two monosaccharides (identical or not) joined. Since two identical monosaccharides can form up to eleven different disaccharides [4], and the number increases even more abruptly when different monosaccharides are connected (in [5] were counted 720 trisaccharides, 34560 tetrasaccharides and 2144640 pentasaccharides) the consequence is an enormous diversity and complexity in carbohydrate structure and chemistry.

**Table 1.** Monosaccharides from trioses to hexoses in open-chain (acyclic) form

n=	Formula	Aldoses				Ketoses	
3	$\text{C}_3\text{H}_6\text{O}_3$	 D-glyceraldehyde				 D-dihydroxyacetone	
4	$\text{C}_4\text{H}_8\text{O}_4$	 D-erythrose	 D-threose	 D-erythrulose			
5	$\text{C}_5\text{H}_{10}\text{O}_5$	 D-ribose	 D-arabinose	 D-xylose	 D-lyxose	 D-xylulose	 D-ribulose
6	$\text{C}_6\text{H}_{12}\text{O}_6$	 D-talose	 D-gulose	 D-altrose	 D-glucose	 D-psicose	 D-tagatose
		 D-galactose	 D-idose	 D-mannose	 D-allose	 D-sorbose	 D-fructose

When applies, the names are \*ose for acyclic and \*opyranose for cyclic forms (e.g. Glucose - acyclic → Glucopyranose - cyclic)

The main problem in studies relating the experimental measurements on carbohydrates is the scarcity of structural information from combined factors (difficulties to crystallize and the limitations in NMR analysis [6]). Another challenge is the fact that usually the researchers studying structural aspects are not the same with the ones conducting the property measurements, and thus the reliability of the data sources being reduced, since very easily during the experimental treatment, monosaccharides may switch from the acyclic to cyclic form as well as the cyclic forms can undergo mutarotation.

The data about melting points and solubilities of 23 monosaccharides were considered in this study to derive property-property relationships.

## RESULTS AND DISCUSSION

The reader would expect to have  $H/T \sim S$  from  $H = E + pV$  and  $G = E + pV - TS$  (for other derived equations, see ref. [7]) but is not the case since here the substances are different.

It should be noted that for all acyclic forms listed in Table 3, the number of conformers is given by the formula  $9^{n-1}$  where  $n$  comes from the molecular formula of monosaccharides,  $(CH_2O)_n$ ; for cyclic forms, there is no general formula, but all hexoses have  $3^6 \cdot 2^2$  conformers (column cf. Table 3).

In order to proceed to assignments (the alternatives from Table 5) between the chemical structures (Table 3) and melting points (Table 2) firstly a relationship between the melting points (column MP (K) in Table 5) and the other properties listed in Table 3, Table 4 and Table 5 inside of the assigned group (the first 13 entries in Table 5) is to be checked.

By keeping in mind that a linear model is significant only when the coefficient of the independent variable is significant enough [8], and aiming to identify at least one principal component [9] in a multiple linear regression [10], the researcher would seek for possible explanation of variables for a given dependent variable (see Table 6).

**Table 6.** Results of simple linear regressions

Dependent variable	Independent variable	p (%)	
MPK	$C_v^{MP}$	≈ 4.82	*
	$S^{MP}$	≈ 4.94	*
	all others	> 5.00	
1/MPK	all	> 5.00	
ln(MPK)	all	> 5.00	
MPK*S <sup>0</sup>	H, E, L, E, DM	> 5.00	
	all others	< 5.00	*

Dependent variable	Independent variable	p (%)	
MPK*S <sup>MP</sup>	H_E, L_E, DM	> 5.00	
	all others <sup>a</sup>	< 5.00	*
MPK*S <sup>OK</sup>	H_E, L_E	> 5.00	
	DM	≈ 4.00	*
	all others <sup>b</sup>	< 5.00	*
H <sup>0</sup> /MPK	H_E, L_E, DM	> 5.00	
	all others	< 5.00	*
G <sup>0</sup> /MPK	H_E, L_E, DM	> 5.00	
	all others <sup>c</sup>	< 5.00	*
H <sup>MP</sup> /MPK	H_E, L_E, DM	> 5.00	
	all others <sup>d</sup>	< 5.00	*
G <sup>MP</sup> /MPK	H_E, L_E, DM	> 5.00	
	all others <sup>e</sup>	< 5.00	*

Notes on data in Table 6:

- ÷ p - Probability to cancel the effect of the independent variable; MPK - melting point in K.
- ÷ The alternatives for independent variables are: Conf(=9<sup>n-1</sup>), L\_E, H\_E, DM, ZPE, Energy, Energy aq., Solv\_E (data in Table 3), n (data in Table 2), ln(n), H<sup>0</sup>, G<sup>0</sup>, S<sup>0</sup>, C<sub>v</sub><sup>0</sup>, S<sup>OK</sup>, C<sub>v</sub><sup>OK</sup>(data in Table 4), S<sup>MP</sup>, C<sub>v</sub><sup>MP</sup>, H<sup>MP</sup>, G<sup>MP</sup> (data in Table 5).
- ÷ The asterisk (\*) indicate statistical significant linear associations.
- ÷ Note <sup>a</sup>: even if all others give linear associations with the dependent variable, however, the associations provided by MPK\*S<sup>0</sup> are stronger than the associations provided by MPK\*S<sup>MP</sup> (in all cases).
- ÷ Note <sup>b</sup>: with two exceptions (Conf and ZPE when the associations given by MPK\*S<sup>0</sup> are stronger than the associations provided by MPK\*S<sup>OK</sup>) the associations given by MPK\*S<sup>OK</sup> are stronger than the associations provided by MPK\*S<sup>0</sup>.
- ÷ Note <sup>c</sup>: associations given by H<sup>0</sup>/MPK are stronger than the associations given by G<sup>0</sup>/MPK.
- ÷ Note <sup>d</sup>: associations provided by H<sup>0</sup>/MPK and G<sup>0</sup>/MPK are stronger than the associations provided by H<sup>MP</sup>/MPK.
- ÷ Note <sup>e</sup>: associations provided by G<sup>MP</sup>/MPK are stronger (in all cases) than the associations provided by H<sup>0</sup>/MPK (and H<sup>MP</sup>/MPK and G<sup>0</sup>/MPK).  
The analysis of simple linear associations (Table 6) revealed that:
- ÷ There is a very little chance to obtain an equation with good estimating capacity when the melting point (either MP or MPK) is used alone as dependent variable. Practically only two predictors barely qualifies to be considered statistically significant: C<sub>v</sub><sup>MP</sup> and S<sup>MP</sup>.
- ÷ Good chances appear when a molar heat quantity (MPK\*S<sup>0</sup>, MPK\*S<sup>MP</sup>, or MPK\*S<sup>OK</sup>) is used in place of the melting temperature. Of course, the convenience is to use one of the MPK\*S<sup>0</sup> and MPK\*S<sup>OK</sup> alternatives, because doesn't require the knowledge on

the melting point and can then be used for predictions. Fortunately,  $MPK \cdot S^{MP}$  performs the worst, but is no a clear indication till this point which of the  $MPK \cdot S^0$  and  $MPK \cdot S^{OK}$  alternatives is the best to be used in building of a property-property relationship.

- ÷ Good chances appear also when a heat transfer quantity ( $H^0/MPK$ ,  $G^0/MPK$ ,  $H^{MP}/MPK$ , or  $G^{MP}/MPK$ ) is used in place of the melting temperature. Again, the convenience is to use one of the  $H^0/MPK$  and  $G^0/MPK$  alternatives, because doesn't require knowing of the melting point and can then be used for predictions. Unfortunately  $G^{MP}/MPK$  performs the best, but also  $H^0/MPK$  comes as the second best alternative.

Even considering the information provided by data in Table 6, to proceed in deriving a property-property relationship is not correct, because the assigned group contains 13 paired determinations (first 13 entries in Table 5) and the pool of possible independent predictors contains 18 variables and is no recipe from which to select a part of them other than trying any possible association [11]; it is still convenient to reduce their number. Of a particular interest is the group formed by  $Conf (=9^{n-1})$ ,  $n$  and  $\ln(n)$  since they provide the shape of the association with  $n$ . By conducting a multiple linear regression with all of them included, the hope is that the survival of the fittest [12] will emerge one or two of them.

Indeed, the multiple regression analysis conducted with  $MPK \cdot S^0$  as dependent variable ( $Y$ ) and  $Conf (=9^{n-1})$ ,  $n$  and  $\ln(n)$  as independent variables ( $X$ 's) when the condition that all coefficients of the model to be statistically significant was imposed, resulted in selection of only one predictor ( $\ln(n)$ , eq.1 below) while analysis conducted with  $MPK \cdot S^{OK}$  as dependent variable selected another one predictor ( $n$ , eq.2 below).

$$MPK \cdot S^0 = Y \sim \hat{Y} = 105337(\pm 4803)_{p=4e-15} \cdot \ln(n), r^2_{adj} = 0.68 \quad (1)$$

$$MPK \cdot S^{OK} = Y \sim \hat{Y} = 6637(\pm 532)_{p=4e-12} \cdot n, r^2_{adj} = 0.67 \quad (2)$$

The results in eq.1 and eq.2 are consistent with the experimental measurements, since the variation of the entropy, at low temperatures, increases its slope (see the data in ref. [13] as an example).

The entropies and the heat capacities at constant volume at 0 K ( $S^{OK}$  and  $C_v^{OK}$  - see the columns in Table 4) are all multipliers of  $R/2$  and  $R$  respectively (where  $R$  is the gas constant). Since  $S = k_B \cdot \log(\Omega)$ , where  $\Omega$  is the number of microscopic configurations [14] and molar  $S$  is  $S_{molar} = N_A \cdot S = R \cdot \log(\Omega)$ , the values obtained for  $S^{OK}$  (Table 4) can be used to obtain the number of microscopic configurations for monosaccharides (by inverting the logarithms:  $\Omega = \log^{-1}(S^{OK}/R)$ ); analogously, for  $C_v^{OK}$  (Table 4), their number of energy components ( $J = 2C_v/R$ , see [15] for derivation of the energy components and [16] as an example of the calculation from  $C_p$  for Hydrogen) at 0 K. Even more, the data in Table 4 reveals a relationship between  $S^{OK}$  and  $C_v^{OK}$  (eq.3).

$$S^{0K} Y \sim \hat{Y} = C_v^{0K} + 4.1561, r^2 = 1.00 \quad (3)$$

It is no big guess that 4.1561 (both  $S^{0K}$  and  $C_v^{0K}$  have  $J \cdot mol^{-1} \cdot K^{-1}$  as measurement unit, the same as the gas constant  $R$  and the same as 4.16212 in eq.3) is actually  $R/2$  ( $R/2 = 4.1572$ ) because the standard error of the difference,  $SE(S^{0K} - C_v^{0K} - R/2)$  is  $7.3 \cdot 10^{-4}$  and the probability to be  $S^{0K} - C_v^{0K} - R/2 \neq 0$  from Student  $t$  distribution is 0.08% ( $< 5.00\%$ ).

There are a series of predictors that are linearly related (Energy, Energy aq., and Solv\_E) in eq.4, ( $S^0$ ,  $H^0$  and  $G^0$ ) in eq.5, (MPK,  $S^{MP}$ ,  $H^{MP}$  and  $G^{MP}$ ) in eq.6.

There are a series of predictors that are linearly related (Energy, Energy aq., and Solv\_E) in eq.4, ( $S^0$ ,  $H^0$  and  $G^0$ ) in eq.5, (MPK,  $S^{MP}$ ,  $H^{MP}$  and  $G^{MP}$ ) and in eq.6.

$$Solv\_E = Y \sim \hat{Y} = 2625 \cdot (\text{Energy aq.} - \text{Energy}), r^2 = 1.00 \quad (4)$$

$$S^0 = Y \sim \hat{Y} = 8806 \cdot (H^0 - G^0), r^2 = 1.00 \quad (5)$$

$$MPK \cdot S^{MP} = Y \sim \hat{Y} = 2625670 \cdot (H^{MP} - G^{MP}), r^2 = 1.00 \quad (6)$$

The eqs.4 to 6 are just expected results, since 1 Hartree = 2625.499 kJ/mol (see the coefficient in eq.4 and Solv\_E is expressed in kJ/mol and Energy aq. and Energy in Hartrees), 1 Hartree/298.15K = 8806 J/mol (see the coefficient in eq.5 and Solv\_E is expressed in J/mol and  $H^0$  and  $G^0$  in Hartrees) and 1 Hartree = 2625499 J/mol (see the coefficient in eq.6 and  $S^{MP}$  is expressed in J/mol/K and  $H^0$  and  $G^0$  in Hartrees).

Even more, eq.6 is nothing else than a well known relation among the state parameters,  $G = H - TS$ , rewritten now as  $TS = H - G$ . Somebody may say that this is wonderful, but it is not. It cannot be used for predictions of the melting points (MP), because in order to obtain  $H^{MP}$  and  $G^{MP}$  first MP should be known.

Other two predictors proved to be highly correlated with other relations among quantities:  $C_v^0$  with Energy -  $H^0$ , and  $C_v^{MP}$  with Energy -  $H^{MP}$ .

After removal of the dependent predictors from the pool of potential descriptors, 11 still remained:  $n$ ,  $\ln(n)$ , ZPE, DM,  $H^0$ ,  $G^0$ ,  $H^{MP}$ ,  $G^{MP}$ ,  $C_v^{0K}$ , Energy, and Energy aq. At this point, a step-by-step strategy of removal for the not statistically significant predictors was applied based on the likelihood of their coefficients.

For  $MPK \cdot S^{0K}$  as dependent variable, Energy was first to be removed,  $G^0$  the second,  $H^{MP}$  the third, DM the fourth, Energy aq. the fifth. At this point two variables ( $n$  and ZPE) had a probability of non-null effect between 5% and 1% (2.4% for ZPE and 1.1% for  $n$ ). It was decided to continue the removal by removing ZPE. After this removal, other two were eliminated at 5% risk being in error:  $n$  and  $\ln(n)$ . The obtained equation is eq.7.

$$\text{MPK} \cdot \text{S}^{\text{OK}} = Y \sim \hat{Y} = -14804(\pm 1495) + 589191(\pm 46615) \cdot \text{H}^0 - 589157(\pm 46610) \cdot \text{G}^{\text{MP}} + 383(\pm 21) \cdot \text{C}_v^{\text{OK}} \quad (7)$$

with  $r_{\text{adj}}^2 = 0.999$

The same procedure was applied to  $\text{MPK} \cdot \text{S}^{\text{MPK}}$ , excepting in this case  $\text{H}^{\text{MP}}$  was removed implicitly (see eq.6 and its comments for the reason). ZPE was the first removed,  $\text{C}_v^{\text{OK}}$  the second,  $\text{G}^0$  the third,  $n$  the fourth, Energy aq. the fifth. At this point one variable (DM) had a very little probability of non-null effect when compared to the rest of the variables in the model ( $10^{-2}$  vs.  $10^{-6}$ ). It was decided to continue the removal with DM. The obtained model contained two variables with high contribution to the explained variance ( $\text{H}^0$  and  $\text{G}^{\text{MP}}$ ) and other two with much less ( $\ln(n)$  and Energy). It was decided to keep only first two variables. The obtained equation is eq.8.

$$\text{MPK} \cdot \text{S}^{\text{OK}} = Y \sim \hat{Y} = -38044(\pm 4736) + 3950677(\pm 144780) \cdot \text{H}^0 - 3950629(\pm 144769) \cdot \text{G}^{\text{MP}} \quad (8)$$

with  $r_{\text{adj}}^2 = 0.999$

Analogously was proceeded for  $\text{H}^0/\text{MPK}$ , and the resulted equation is eq.9.

$$\text{H}^0/\text{MPK} = Y \sim \hat{Y} = 48.7319(\pm 2.6944) \cdot \text{H}^{\text{MP}} - 48.7288(\pm 2.6944) \cdot \text{H}^0 \quad (9)$$

with  $r_{\text{adj}}^2 = 0.998$

The model eq.9 was used to do the assignments in relation: measured melting points and chemical structures. The entries in Table 5 from 'Alternate assignments: first option' and 'Alternate assignments: second option' were one by one alternatively joined with the main group (of first 13 entries). The decision which assignment to be kept is based on the standard error (SE) since it is an unbiased estimator of the population variance [17]. The step-by-step results of this analysis are given in Table 7.

**Table 7.** Assignments between chemical structures and melting points

Sample size	Added CID	MPK (MP in K)	Standard error (SE)	MPK (MP in K)	Standard error (SE)	Selected
		first option		second option		option
13	-	-	0.011047	-	0.011047	Eq.9
14	751	405.15	0.011408	418.15	0.011339	second
14	751	-	0.011339	-	0.011339	-
15	79014	418.15	0.011707	405.15	0.011846	none
14	-	-	0.011339	-	0.011339	-
15	66308	436.15	0.055598	429.15	0.010967	second



Sample size	Added CID	MPK (MP in K)	Standard error (SE)	MPK (MP in K)	Standard error (SE)	Selected
15	66308	-	0.010967	-	0.010967	-
16	65550	379.65	0.010797	352.65	0.011143	first
16	65550	-	0.010797	-	0.010797	-
17	5311110	368.15	0.010497	355.15	0.010649	first
17	5311110	-	0.010497	-	0.010497	-
18	644160	416.15	0.116208	363.65	0.122194	none
17	-	-	0.010497	-	0.010497	-
18	5289590	343.65	0.012235	324.15	0.017894	first
18	5289590	-	0.012235	-	0.012235	-
19	102288	414.15	0.011956	401.15	0.012163	first
19	102288	-	0.011956	-	0.011956	-
20	167792	424.15	0.011620	333.15	0.015747	first
20	167792	-	0.011620	-	0.011620	-
21	92092	407.65	0.011487	404.15	0.011526	first
21	92092	-	0.011487	-	0.011487	-

As can be seen in Table 7, the difference between the initial (from 13 paired values) estimation of the standard error (0.11047) and the final (from 21 paired values) estimation of the standard error (0.11487) is negligible – less than 5%, which indicates that the sample of 13 paired data and the sample of 21 paired data belongs to the same population (see for further details of this type of analysis [18] and [19]). Based on the results from Table 7, the following assignments have been made: MP(CID\_751) = 145 °C (418.15 K), MP(CID\_66308) = 156 °C (429.15 K), MP(CID\_65550) = 106.5 °C (379.65 K), MP(CID\_5311110) = 95 °C (368.15 K), MP(CID\_5289590) = 70.5 °C (343.65 K), MP(CID\_102288) = 141 °C (414.15 K), MP(CID\_167792) = 151 °C (424.15 K), MP(CID\_92092) = 134.5 °C (407.65 K).

Due to the lack of assignment between the structural data and the solubilities, it is even more difficult to derive a relationship able to express the solubility as a function of other properties. Actually, by using all data in Table 2 combined with the data in Table 3 and Table 4, no linear relationship can be derived to express the solubility. The main reason is the fact that actually the same solubility is assigned to two cyclic forms in three out of eight cases. Actually these forms are in slow equilibrium with each other and with the acyclic form in aqueous solution [20]. By using the square root transformation [21] applied to the solubility, a relationship were derived and in eq.10.

$$\sqrt{\text{Solubility}} = Y \sim \hat{Y} = -37(\pm 35) - 4.4(\pm 4.2) \cdot \ln(\text{Conf}) + 0.079(\pm 0.072) \cdot S^0 + 0.076(\pm 0.075) \cdot \text{ZPE} \quad (10)$$

with  $r_{\text{adj}}^2 = 0.3$

Unfortunately, even if all the coefficients of eq.10 are statistically significant, qualifying all predictors ( $\ln(\text{Conf})$ ,  $S^0$  and ZPE) to belong to the model, due to the small number of measurements (11 paired data from which only 8 distinct) the eq.10 failed to provide a reliable model (probability to reject the model from Fisher's distribution is 15%).

## CONCLUSIONS

The study revealed that is very difficult to derive reliable property-property relationships when the structural determinations of the substances subjected to property measurements are scarce. Therefore more structural and property determinations are essential for the advance of the knowledge in this field.

By involving statistical analysis, in this study were assigned the melting points for a number of eight monosaccharides to the corresponding deposited PubChem structure information files by constructing property-property relationships on their pool of chemical structures.

## EXPERIMENTAL SECTION

The available data about melting points and solubilities of 23 monosaccharides (listed in Table 1) were collected from the literature.

The structural information as 3D geometries was taken from PubChem database. As can be seen in Table 2 the assignments between a certain monosaccharide conformation and its measured properties were not guaranteed by the source of the data. Thus excepting D-glucose of which melting points are available in all three listed conformations, when the literature provided more than one melting point was necessary to conduct an assignment (alternatives listed in Table 5).

For the 23 monosaccharides 45 different geometries (3D) were available in the PubChem database. For one monosaccharide (CID 111123 corresponding to D-idose) the 3D geometry was build from its 2D geometry. On the 46 files containing different geometries of monosaccharides, a series of properties were calculated (listed in Table 3) using Spartan'14 software in the following configuration: energy calculation with Hartree-Fock (HF) method, 6-31G\* dual basis, with computing of infra-red (IR) parameters and deriving of thermodynamic entities (listed in Table 4).

**Table 2.** Monosaccharides experimental data

Name	(CH <sub>2</sub> O) <sub>n</sub>	n	MP/ref	Solubility/ref		
D-dihydroxyacetone			90   1			
D-glyceraldehyde	C <sub>3</sub> H <sub>6</sub> O <sub>3</sub>	3	132   11			
D-glyceraldehyde			145   2			
D-erythrose	C <sub>4</sub> H <sub>8</sub> O <sub>4</sub>	4	129   2			
D-erythrulose						
D-threose			115   6			
D-arabinose	C <sub>5</sub> H <sub>10</sub> O <sub>5</sub>	5	163   5	0.0816   12		
D-arabinose			156   2			
D-lyxose			106.5   4			
D-lyxose			79.5   1			
D-ribose			95   1			
D-ribose			82   2			
D-ribulose			85   4			
D-xylose			143   4	0.12953   12		
D-xylose			90.5   1			
D-xylulose			70.5   4			
D-xylulose			51   4			
D-allose			C <sub>6</sub> H <sub>12</sub> O <sub>6</sub>	6	141   8	0.04489   14
D-allose					128   8	
D-altrose					104   1	
D-fructose	103   10	0.0735   15				
D-galactose	164   8	0.0432   12				
D-glucose	83   1					
D-glucose	146   5	0.09447   12				
D-glucose	149   5					
D-gulose	151   5					
D-gulose	60   7					
D-idose	168.5   11					
D-mannose	132   3	0.25884   12				
D-psicose	165   3	0.2266   13				
D-sorbose	165   9					
D-tagatose	134.5   1					
D-tagatose	131   8					
D-talose	126.5   8					

Notes on data in Table 2:

- ÷ MP: melting points, in °C;
- ÷ MP/refs: 1: Chem.nlm.nih.gov; 2: ChemSpider.com; 3: CompTox CompTox.epa.gov; 4: [22]; 5: SigmaAldrich.com; 6: [23]; 7: [24]; 8: [25]; 9: [26]; 10: [27]; 11: <http://drugfuture.com/chemdata/>;
- ÷ Solubility: in mole fraction (mol/mol), at 25°C;
- ÷ Solubility/refs: 12: [28]; 13: converted from [29], 2.93g/g; 14: converted from [30], 47%wt; 15: extrapolated from [31] at 79.3%wt.

## PROPERTY-PROPERTY RELATIONSHIPS FOR MONOSACCHARIDES

**Table 3.** Calculated molecular properties

	CID	Name (D-...)	F	Conf	L_E	H_E	DM	ZPE	Energy	Energy aq.	Solv_E
1	670	dihydroxyacetone	A	81	2.67	-12.25	3.28	244.43	-341.62377	-341.64382	-52.645
2	751	glyceraldehyde	A	81	2.62	-12.23	3.14	244.26	-341.61839	-341.63820	-52.017
3	79014	glyceraldehyde	A	81	2.72	-12.39	3.88	246.46	-341.62398	-341.63983	-41.617
4	94176	erythrose	A	729	2.37	-12.57	2.85	325.24	-455.49945	-455.51811	-48.998
5	5460177	erythulose	A	729	2.43	-12.06	5.55	322.53	-455.49497	-455.52238	-71.961
6	439665	threose	A	729	2.07	-12.49	3.37	325.25	-455.49416	-455.51614	-57.712
7	66308	arabinose	A	6561	2.13	-12.53	2.28	401.87	-569.37840	-569.40304	-64.690
8	7044039	arabinose	C	324	4.31	-12.56	4.91	390.66	-569.38571	-569.41441	-75.327
9	65550	lyxose	A	6561	2.57	-12.32	2.65	401.39	-569.38046	-569.40478	-63.846
10	439240	lyxose	C	324	4.63	-12.38	3.93	402.92	-569.39170	-569.41829	-69.811
11	5311110	ribose	A	6561	2.47	-12.41	1.81	405.34	-569.38097	-569.40334	-58.726
12	10975657	ribose	C	324	4.21	-12.07	3.30	402.93	-569.39333	-569.41408	-54.473
13	151261	ribulose	A	6561	2.28	-12.48	2.00	400.21	-569.37434	-569.40118	-70.455
14	439203	ribulose	C	1944	3.83	-12.63	4.34	384.39	-569.38383	-569.41247	-75.173
15	644160	xylose	A	6561	2.41	-12.62	4.19	401.19	-569.37312	-569.39904	-68.046
16	89398913	xylose	C	324	4.62	-12.26	3.4	403.45	-569.38100	-569.41096	-78.662
17	444173	xylose	C	324	4.04	-12.43	3.81	393.20	-569.39701	-569.42139	-63.999
18	6027	xylose	C	324	4.68	-12.46	0.98	401.23	-569.39506	-569.41926	-63.537
19	5289590	xylulose	A	6561	2.64	-12.20	5.54	401.61	-569.38225	-569.40690	-64.704
20	439204	xylulose	C	1944	4.20	-12.69	5.53	381.81	-569.38713	-569.41472	-72.455
21	102288	allose	A	59049	2.29	-12.30	5.05	475.89	-683.23768	-683.26573	-73.659
22	439507	allose	C	2916	3.96	-12.65	2.43	456.74	-683.26202	-683.29304	-81.437
23	94780	altrose	A	59049	1.93	-12.16	5.53	474.85	-683.22915	-683.26127	-84.332
24	441032	altrose	C	2916	4.32	-11.94	2.36	477.72	-683.26918	-683.29816	-76.073
25	5984	fructose	A	59049	2.46	-12.36	7.42	470.36	-683.24467	-683.28345	-101.82
26	2723872	fructose	C	2916	4.48	-12.55	2.11	465.13	-683.27403	-683.30156	-72.267
27	3037556	galactose	A	59049	2.34	-12.53	2.62	476.41	-683.24712	-683.27771	-80.301
28	439357	galactose	C	2916	4.03	-12.44	4.35	468.31	-683.26896	-683.29681	-73.121
29	6036	galactose	C	2916	4.35	-12.51	3.65	466.37	-683.27512	-683.30107	-68.126
30	107526	glucose	A	59049	2.24	-12.46	3.06	472.20	-683.23648	-683.27206	-93.406
31	79025	glucose	C	2916	3.62	-12.58	3.04	460.59	-683.26300	-683.29710	-89.536
32	64689	glucose	C	2916	4.04	-12.54	2.29	459.19	-683.26572	-683.29809	-84.990
33	167792	gulose	A	59049	2.13	-12.74	2.77	473.93	-683.24025	-683.27051	-79.442
34	441033	gulose	C	2916	4.52	-12.25	0.54	467.88	-683.27228	-683.30047	-74.005

	CID	Name (D-...)	F	Conf	L_E	H_E	DM	ZPE	Energy	Energy aq.	Solv_E
35	111123	idose	A	59049	2.24	-12.56	4.37	484.82	-683.25735	-683.28439	-70.993
36	441034	idose	C	2916	4.21	-12.04	2.69	471.29	-683.27792	-683.30248	-64.465
37	12305800	mannose	A	59049	2.27	-12.39	4.74	473.14	-683.24174	-683.27724	-93.210
38	18950	mannose	C	2916	4.14	-12.62	2.26	458.14	-683.27324	-683.30087	-72.558
39	90008	psicose	A	59049	2.43	-12.15	5.56	472.52	-683.24826	-683.28337	-92.166
40	441036	psicose	C	2916	4.43	-12.34	2.01	463.92	-683.29092	-683.30944	-48.621
41	107428	sorbose	A	59049	2.37	-12.40	5.76	471.30	-683.24880	-683.28402	-92.456
42	439192	sorbose	C	2916	4.39	-12.32	4.86	466.68	-683.26798	-683.29185	-79.204
43	92092	tagatose	A	59049	2.20	-12.37	5.61	467.84	-683.24604	-683.28039	-90.195
44	439312	tagatose	C	2916	4.61	-12.39	4.43	463.69	-683.26650	-683.29556	-76.297
45	99459	talose	A	59049	2.21	-12.3	4.86	474.96	-683.23829	-683.26867	-79.783
46	441035	talose	C	2916	4.11	-12.27	6.09	466.81	-683.26205	-683.29147	-77.247

Notes on data in Table 3:

- ÷ CID - compound identifier from PubChem; F - form (A: acyclic, C - cyclic); L\_E: LUMO energy (in eV); H\_E: HOMO energy (in eV); DM: Dipole moment (in Debye); ZPE: Zero point energy (in kJ/mol); Energy: total energy (in a.u.; a.u. = Hartrees); Energy aq.: total energy in solvated form at infinite dilution (in a.u.; a.u. = Hartrees); Solv\_E: solvation energy (in kJ/mol).

**Table 4.** Calculated molecular thermodynamic properties

	H <sup>0</sup> (a.u.)	G <sup>0</sup> (a.u.)	S <sup>0</sup> (J·mol <sup>-1</sup> ·K <sup>-1</sup> )	C <sub>v</sub> <sup>0</sup> (J·mol <sup>-1</sup> ·K <sup>-1</sup> )	S <sup>0K</sup> (J·mol <sup>-1</sup> ·K <sup>-1</sup> )	C <sub>v</sub> <sup>0K</sup> (J·mol <sup>-1</sup> ·K <sup>-1</sup> )
1	-341.52336	-341.56082	329.83	101.2	45.73	41.57
2	-341.51804	-341.55559	330.66	100.2	45.73	41.57
3	-341.52291	-341.56019	328.23	98.60	37.41	33.26
4	-455.36621	-455.40860	373.31	142.3	62.36	58.20
5	-455.36255	-455.40540	377.30	145.8	70.67	66.52
6	-455.36090	-455.40336	373.82	142.5	54.04	49.89
7	-569.21371	-569.26121	418.31	188.0	78.99	74.83
8	-569.22494	-569.27270	420.52	195.2	78.99	74.83
9	-569.21592	-569.26352	419.12	188.3	78.99	74.83
10	-569.22690	-569.27333	408.87	184.2	78.99	74.83
11	-569.21506	-569.26235	416.42	185.1	78.99	74.83
12	-569.22854	-569.27490	408.17	184.5	70.67	66.52
13	-569.20997	-569.25802	423.13	191.4	95.62	91.46
14	-569.22476	-569.27392	432.88	204.2	103.9	99.77

## PROPERTY-PROPERTY RELATIONSHIPS FOR MONOSACCHARIDES

	$H^0$ (a.u.)	$G^0$ (a.u.)	$S^0$ (J·mol <sup>-1</sup> ·K <sup>-1</sup> )	$C_v^0$ (J·mol <sup>-1</sup> ·K <sup>-1</sup> )	$S^{0K}$ (J·mol <sup>-1</sup> ·K <sup>-1</sup> )	$C_v^{0K}$ (J·mol <sup>-1</sup> ·K <sup>-1</sup> )
15	-569.28865	-569.25624	419.08	188.2	78.99	74.83
16	-569.21608	-569.26216	405.82	183.5	70.67	66.52
17	-569.23537	-569.28291	418.65	193.2	87.30	83.14
18	-569.23080	-569.27752	411.47	185.6	70.67	66.52
19	-569.21749	-569.26524	420.54	189.9	87.30	83.14
20	-569.22899	-569.27818	433.18	206.0	112.2	108.1
21	-683.04234	-683.09508	464.50	236.5	95.62	91.46
22	-683.07285	-683.12749	481.15	253.3	112.2	108.1
23	-683.03418	-683.08687	464.02	237.3	95.62	91.46
24	-683.07345	-683.12530	456.59	232.1	95.62	91.46
25	-683.05095	-683.10463	472.74	242.8	112.2	108.1
26	-683.08219	-683.13587	472.70	246.2	112.2	108.1
27	-683.05159	-683.10428	463.96	236.3	87.30	83.14
28	-683.07611	-683.12922	467.70	242.4	112.2	108.1
29	-683.08298	-683.13636	470.08	243.2	112.2	108.1
30	-683.04232	-683.09538	467.29	240.0	103.9	99.77
31	-683.07265	-683.12685	477.27	249.8	112.2	108.1
32	-683.07587	-683.13011	477.65	249.9	112.2	108.1
33	-683.04548	-683.09850	466.87	238.3	103.9	99.77
34	-683.07967	-683.13273	467.31	241.9	103.9	99.77
35	-683.05924	-683.11040	450.51	224.9	78.99	74.83
36	-683.08423	-683.13684	463.34	238.9	103.9	99.77
37	-683.04731	-683.10033	466.88	238.6	95.62	91.46
38	-683.08370	-683.13821	479.99	250.8	120.6	116.4
39	-683.05385	-683.10740	471.59	241.0	112.2	108.1
40	-683.09941	-683.15337	475.09	247.8	120.6	116.4
41	-683.05475	-683.10841	472.61	242.0	112.2	108.1
42	-683.07571	-683.12909	470.13	244.0	112.2	108.1
43	-683.05310	-683.10723	476.66	245.3	120.6	116.4
44	-683.07505	-683.12875	472.97	248.1	112.2	108.1
45	-683.04323	-683.09607	465.35	237.4	95.62	91.46
46	-683.06980	-683.12283	467.00	242.8	103.9	99.77

Notes on data in Table 4:

- ÷ The thermodynamic quantities from Table 4 are given for standard conditions ( $T_0 = 298.15$  K):  $H^0$ ,  $G^0$ ,  $S^0$ ,  $C_v^0$  and at 0K:  $S^{0K}$ ,  $C_v^{0K}$ .

**Table 5.** Calculated molecular thermodynamic properties for acyclic forms at their melting points

	Name	CID	F	MP (K)	S <sup>MP</sup>	C <sub>v</sub> <sup>MP</sup>	H <sup>MP</sup>	G <sup>MP</sup>
3	D-dihydroxyacetone	670	A	363.15	346.47	116.72	-341.520858	-341.568781
4	D-erythrose	94176	A	402.15	407.12	176.02	-455.360734	-455.423093
5	D-threose	439665	A	388.15	402.46	171.90	-455.356251	-455.415750
19	D-ribulose	151261	A	358.15	447.69	215.97	-569.206107	-569.267187
25	D-altrose	94780	A	377.15	501.43	277.25	-683.027889	-683.099919
45	D-fructose	5984	A	376.15	509.55	281.01	-683.044734	-683.117736
34	D-galactose	3037556	A	437.15	527.01	303.34	-683.039957	-683.127706
27	D-glucose	107526	A	356.15	495.00	269.52	-683.037758	-683.104905
37	D-idose	111123	A	441.65	517.27	295.25	-683.047430	-683.134443
39	D-mannose	12305800	A	405.15	516.81	291.30	-683.038595	-683.118346
30	D-psicose	90008	A	438.15	533.21	306.21	-683.042179	-683.131162
43	D-sorbose	107428	A	438.15	536.19	307.44	-683.043023	-683.132504
21	D-talose	99459	A	399.65	512.83	287.75	-683.035010	-683.113071
Alternate assignments: first option								
1	D-glyceraldehyde	751	A	405.15	357.24	125.28	-341.513873	-341.569000
2	D-glyceraldehyde	79014	A	418.15	357.24	126.72	-341.518231	-341.575127
9	D-arabinose	66308	A	436.15	449.85	221.91	-569.208455	-569.273418
15	D-lyxose	65550	A	379.65	450.95	222.72	-569.210598	-569.275806
7	D-ribose	5311110	A	368.15	444.24	214.67	-569.210632	-569.272924
11	D-xylose	644160	A	416.15	464.37	236.51	-569.200737	-569.274341
17	D-xylulose	5289590	A	343.65	439.48	209.07	-569.214618	-569.272142
41	D-allose	102288	A	414.15	517.60	293.47	-683.032798	-683.114444
23	D-gulose	167792	A	424.15	525.01	299.42	-683.035059	-683.119874
32	D-tagatose	92092	A	407.65	525.84	297.25	-683.044164	-683.125809
Alternate assignments: second option								
1	D-glyceraldehyde	751	A	418.15	360.22	128.12	-341.513322	-341.570673
2	D-glyceraldehyde	79014	A	405.15	354.30	123.86	-341.518795	-341.573468
9	D-arabinose	66308	A	429.15	468.38	240.79	-569.204757	-569.281317
15	D-lyxose	65550	A	352.65	440.36	211.75	-569.212468	-569.271616
7	D-ribose	5311110	A	355.15	439.26	209.36	-569.211508	-569.270926
11	D-xylose	644160	A	363.65	444.85	216.08	-569.204485	-569.266100
17	D-xylulose	5289590	A	324.15	431.37	200.99	-569.215879	-569.269137
41	D-allose	102288	A	401.15	511.86	287.66	-683.033978	-683.112185
23	D-gulose	167792	A	333.15	484.19	256.56	-683.042845	-683.104284
32	D-tagatose	92092	A	404.15	524.34	295.74	-683.044475	-683.125189

Notes on data in Table 5:

- ÷ Not for all monosaccharides are available the melting points; were included in Table 5 only the ones with available data.
- ÷ It is known that in the absence of the water monosaccharides have the tendency to take the acyclic form, while in water exists mainly in the cyclic form (see pentoses and hexoses as typical examples); therefore, the melting points were assigned to the acyclic forms (F='A' in Table 5).

- ÷ The melting points were converted to Kelvin scale (MP (K) in Table 5) and were used to obtain the thermodynamic quantities at the melting point  $S^{\text{MP}}$  (in  $\text{J}\cdot\text{mol}^{-1}\cdot\text{K}^{-1}$ ),  $C_V^{\text{MP}}$  (in  $\text{J}\cdot\text{mol}^{-1}\cdot\text{K}^{-1}$ ),  $H^{\text{MP}}$  (in a.u.), and  $G^{\text{MP}}$  (in a.u.).

## ACKNOWLEDGMENTS

This paper is dedicated to Prof. Costel SÂRBU with the occasion of his 65<sup>th</sup> birthday (on January 12, 2016).

## REFERENCES

1. D.M. Updegraff, *Analytical Biochemistry*, **1969**, 32(3), 420.
2. C.M. Hogan, "Deoxyribonucleic acid". In: Encyclopedia of Earth. National Council for Science and the Environment (Eds.: S. Draggan and C. Cleveland). Washington DC, **2010**.
3. D.B. Dickinson, *Phytochemistry*, **1982**, 21(4), 843.
4. A. Paulus, A. Klockow-Beck, "Structures and properties of carbohydrates". In: Analysis of Carbohydrates by Capillary Electrophoresis (Eds.: A. Paulus, A. Klockow-Beck), Vieweg Teubner Verlag, Wiesbaden, **1999**, p. 28.
5. R.R. Schmidt, *Angewandte Chemie International Edition in English*, **1986**, 25, 212.
6. C. Zwahlen, S.J.F. Vincent, *Journal of the American Chemical Society*, **2002**, 124(24), 7235.
7. L. Jäntschi, S. D. Bolboacă, *Journal of Computational Science*, **2014**, 5, 597.
8. L. Jäntschi, *Leonardo Journal of Sciences*, **2002**, 1(1), 31.
9. C. Sârbu, H.F. Pop, *Talanta*, **2005**, 65(5), 1215.
10. L. Jäntschi, *Applied Medical Informatics*, **2004**, 15(3-4), 48.
11. L. Jäntschi, S.D. Bolboacă, *Leonardo Electronic Journal of Practices and Technologies*, **2007**, 6(11), 163.
12. L. Jäntschi, *Genetic algorithms and their applications*, PhD Thesis in Horticulture (PhD Advisor: R. E. Sestraş), University of Agricultural Sciences and Veterinary Medicine Cluj-Napoca, Cluj-Napoca, 2010.
13. E.F. Jr. Westrum, J.B. Hatcher, D.W. Osborne, *The Journal of Chemical Physics*, **1953**, 21(3), 419.
14. L. Boltzmann, *Wiener Berichte*, **1868**, 58, 517.
15. L. Jäntschi, *Physical chemistry - theory, applications and problems*, Academic Direct, Cluj-Napoca, **2013**, p. 24.
16. M.P. Fodor, S.D. Bolboacă, L. Jäntschi, *Bulletin UASVMCN. Horticulture*, **2013**, 70(1), 10.
17. R.A. Fisher, *Metron*, **1925**, 5, 90.
18. L. Jäntschi, S.D. Bolboacă, *The Scientific World Journal*, **2010**, 10, 865.



19. L. Jäntschi, S.D. Bolboacă, M. V. Diudea, R. E. Sestraş, *Bulletin UASVMCN. Agriculture*, **2010**, 67(1), 169.
20. F.W. Lichtenhaler, S. Ronninger, *Journal of the Chemical Society, Perkin Transactions 2*, **1990**, 8, 1489.
21. S.A. Alber, D.W. Schaffner, *Applied and Environmental Microbiology*, **1992**, 58(10), 3337.
22. P.A. Levene, R. Stuart Tipson, *The Journal of Biological Chemistry*, **1936**, 115, 731.
23. G.G.S. Dutton, K.N. Slessor, *Canadian Journal of Chemistry*, **1964**, 42(3), 614.
24. R. Kosler, P. Idelmann, W.F. Dahlhof, *Angewandte Chemie International Edition in English*, **1980**, 19(7), 547.
25. M.L. Wolfrom, J.N. Schumacher, H.S. Isbell, F.L. Humoller, *Journal of the American Chemical Society*, **1954**, 76(22), 5816.
26. J.V. Karabinos, *Advances in Carbohydrate Chemistry*, **1952**, 7, 99.
27. C.S. Hudson, D.H. Brauns, *Journal of the American Chemical Society*, **1916**, 38(6), 1216.
28. M.C. Gray, A.O. Converse, C.E. Wyman, *Applied Biochemistry and Biotechnology*, **2003**, 105-108, 179.
29. K. Fukada, T. Ishii, K. Tanaka, M. Yamaji, Y. Yamaoka, K.-I. Kobashi, K. Izumori, *Bulletin of the Chemical Society of Japan*, **2010**, 83(10), 1193.
30. T. Kozakai, K. Fukada, R. Kuwatori, T. Ishii, T. Senoo, K. Izumori, *Bulletin of the Chemical Society of Japan*, **2015**, 88(3), 465.
31. A.E. Flood, J. Addai-Mensah, M. R. Johns, E. T. White, *Journal of Chemical & Engineering Data*, **1996**, 41(3), 418.

*Dedicated to Professor Costel Sârbu on the  
Occasion of His 65<sup>th</sup> Anniversary*

## PROBING REDUCING POWER FOR FERRYL PHYTOGLOBINS OF SEVERAL PHENOLIC COMPOUNDS USING THEIR KINETIC PROFILES ASSISTED BY CHEMOMETRIC METHODS

GALABA NAUMOVA-LEȚIA<sup>a</sup>, AUGUSTIN C. MOȚ<sup>a\*</sup>

**ABSTRACT.** Several phenolic compounds belonging to different classes were comparatively analyzed for their ability to reduce ferryl forms of three non-symbiotic phytooglobins which were generated *in situ* by hydrogen peroxide and thus acting as enzymes. The kinetic profiles of the substrates oxidation were evaluated using principal component analysis and cluster analysis. The three globins were different not only in terms of rate but also in mechanism and the electron donor ability of the studied phenolics were strongly enzyme specific and did not depend only upon their chemical structure but also upon assumptive binding pocket environment.

**Keywords:** phenolics, flavonoids, phytoglobin, reducing power

### INTRODUCTION

Natural phenolic compounds constitute a broad group of phytochemicals with various physiological and biochemical activity. They form one of the largest classes of secondary plant metabolites which act effectively against different abiotic and biotic stresses in plants. Phenolic compounds are produced within two metabolic pathways: acetate/malonate pathway in which

---

<sup>a</sup> Babeș-Bolyai University, Faculty of Chemistry and Chemical Engineering, 11 Arany Janos str., RO-400028, Cluj-Napoca, Romania

\* Corresponding author: [augustinmot@chem.ubbcluj.ro](mailto:augustinmot@chem.ubbcluj.ro)

simple phenols are produced and shikimate/phenylpropanoid pathway that leads to phenylpropanoids or combination of the both pathways, resulting in formation of flavonoids, one of the most abundant phenolic classes in nature. Some phenolic compounds are widely distributed in the plant kingdom while others can be found in specific plant families, specific plant organelles or only at certain phase of the plant developing tissues [1-3].

Phenolic compounds can be classified in different ways: distribution in nature, form and location in plants (insoluble - bound into stable complexes with biomolecules of the cell wall or soluble – free, not bound fractions). One of the most accepted and general classification is based on the basic carbon skeleton which categorized them in couple main classes such as simple phenols, phenolic acids and analogs, chalcones, coumarins, stilbenes, flavonoids, lignans, lignins and others [1,4]. Due to the large diversity of structures and properties, phenolic compounds possess variety of different functions in the plants starting with involvement in the growth of the plant to plant reproduction and participation in defense mechanisms. Phenolic compounds can act as visual signals for attracting pollinating insects, phytoalexins, photoreceptors, detoxifying agents, scavenger of reactive oxygen species (ROS) such as H<sub>2</sub>O<sub>2</sub>, hydroxyl, peroxy or alkoxy radical; they also, contribute to different flavours and colour shades in flowers, leaves, fruits and vegetables, protect the plant cells against UV radiation, fungal, bacterium or virus pathogens, parasites and herbivores, etc. [5-12].

Phenolic acids include two subclasses: *hydroxybenzoic acids* (e.g. vanillic acid, gallic acid, protocatechuic acid etc.) with C<sub>6</sub>-C<sub>1</sub> structure and *hydroxycinnamic acids* (e.g. caffeic acid, *p*-coumaric acid, ferulic acid etc.) with C<sub>6</sub>-C<sub>3</sub> structure. Phenolic acids naturally occur in free form or conjugate esters or amides [13]. Stilbenoids (stilbenes) are phenylpropanoids belonging to the family of phenolic compounds with C<sub>6</sub>-C<sub>2</sub>-C<sub>6</sub> structure (two aromatic rings connected with ethane bridge). Stilbenoids are hydroxylated derivatives of stilbene and they are not present in all plant species, due to limited stilbene synthase genes expression, but their distribution is rather heterogenous through the plant kingdom. The natural stilbenoids exist in monomeric or oligomeric form (e.g. *trans*-resveratrol) or frequently as glycosylated form with different substitution [13,14]. Coumarins (2*H*-chromen-2-one) are natural compounds belonging to the group of lactones with C<sub>6</sub>-C<sub>3</sub> rich electron conjugated system with a charge transport properties. Coumarins are synthesised with hydroxylation, isomerization, glycolysis and cyclization of cinnamic acid and naturally in plants are present in free form, but most often as glycosides (e.g. aesculetin) [1,13,15,16].

Flavonoids (or bioflavonoids) are extensively distributed in green plant kingdom. Flavonoids are present in all part of the plants, especially the photosynthesising plant cells of a wide range of vascular plants; up to date

over 8000 flavonoid compounds have been identified and the number is still increasing. Chemically, they all have characteristic C<sub>6</sub>-C<sub>3</sub>-C<sub>6</sub> benzo- $\gamma$ -pyrone skeleton consists of two benzene rings (A and B, Table 1) connected through heterocyclic pyran ring (C) [5,6,8,17]. Flavonoids generally, occur in plants as glycosides (O-glycoside or C-glycoside) with a monosaccharide or disaccharide attached, but also as aglycones or methylated and sulfated derivatives [9,11]. Flavonoids can be divided into several classes based on the structure of the carbon skeleton, substitution, conjugation, degree of hydroxylation and degree of polymerization such as, flavones, flavonols, flavanones, flavanols, isoflavones, flavanonols and anthocyanidins [5,8,18]. UV-Vis spectral features of flavonoids display two major absorption bands in the region from 200-400 nm, which are known as band I (300-385 nm) and band II (250-285 nm) [9,19,20]. The substitution of functional groups in the flavonoid skeleton can cause shift in absorption maximum. The radical scavenging activity of the flavonoids is in connected with the chemical structure and type of substituents of the B and C rings; meaning that the greater the number of hydroxyl groups in ring B, the lower the redox potential and the stronger the reducing power [21]. In general, flavonoids with catechol moiety on ring B ( $0.23 < E_{p,a} < 0.75$  V) will be highly active and better antioxidant agents, than non-catechol derivatives ( $E_{p,a} > 0.8$  V) [5,12,22].

Hemoglobins (Hbs) are a large family of globular proteins found in all kingdoms of life with various biological functions such as oxygen transport and storage, electron transfer, O<sub>2</sub>, NO and CO sensing and redox catalysis [23-26]. Nonsymbiotic plant hemoglobins (nsHbs) are divided in three different classes (class 1, class 2 and class 3 or truncated Hb) based on oxygen affinity and structural features [27-29]. Similar to all Hbs, nsHbs are involved in ROS and RNS involving pathways, exhibiting nitrite reductase activity, peroxidases activity and are capable of NO scavenging under hypoxic stress [24,26,30-32]. The highly reactive ferryl species  $[\text{Fe}^{4+}=\text{O}^{2-}]^{2+}$  can be formed due to abiotic or biotic stresses under different physiological conditions in reaction of the hemoglobins with hydrogen peroxide (H<sub>2</sub>O<sub>2</sub>) [33,34]. The phenolic compounds, especially flavonoids have ability to scavenge ferryl hemoglobin [35]. Both ferryl heme and the protein radical are very reactive species, which can induce oxidation of the biomolecules and cause tissue damage [33,36].

Phenolic compounds under some stress conditions can exhibit pro-oxidant activity, which was previously reported [37]. The effects on some flavonoids (rutin, quercetin, (+)-catechin, luteolin, kaempferol, apigenin, genistein, (-)-epigallocatechin gallate, hesperetin) on the redox reaction, reducing ability, mechanisms, transportation, distribution, binding sites to human or bovine hemoglobin at physiological pH or acidic pH were investigated using different

techniques like fluorescence spectroscopy, circular dichroism (CD), UV–Vis absorption spectroscopy, molecular modelling and Western blotting [34,38-42]. In general, phytophenolic compounds are well known for their antioxidant activity and act protective towards the oxidative damage *in vitro* and *in vivo*. Transportation, distribution, physiological and biochemical action of phenolic compounds is connected with important globular proteins [39] and lipid bilayer [43] interactions which makes them important besides their antioxidant capacity.

## RESULTS AND DISCUSSION

Thirteen phenolic compounds were used in our study and their reducing powers towards the three different classes ferryl phytoglobins from *Arabidopsis thaliana* were investigated. Their chemical structures of the studied compounds, together with their classification are shown in Table 1. The ferryl species of the studied Hbs were generated *in situ* by hydrogen peroxide oxidation of the ferric form. These species are thought to be responsible electron subtraction from the phenolic compounds, oxidizing them while the ferryl is reduced back to the ferric form and reenters the catalytic cycle. Therefore, the studied Hbs served as enzymes (used in catalytic amounts) that oxidized the phenolic compounds coupled with peroxide reduction to water. The kinetic profiles of the phenolic compounds oxidation were monitored and a comparative analysis of their ferryl reducing power was employed using two chemometric methods, principal component analysis (PCA) and cluster analysis.

The studied phenolic compounds belong to two large classes (flavonoids and phenolic acids) including one representative from coumarins (aesculetin) and stilbenes (resveratrol) classes. In this study, the *flavone* (luteolin and apigenin), *flavonol* (quercetin, rutin and isoquercitrin) and *flavanols* (catechin and epicatechin) subclasses were part of the flavonoid class. Phenolic acids, as mentioned above are categorized here into two major subclasses, hydroxybenzoic acids and hydroxycinnamic acids; in our study we used vanillic acid, belonging to the first subclass and caffeic, ferulic and *p*-coumaric acids representatives from the second subclass (Table 1).

**Table 1.** Chemical structural details of the studied phenolic compounds and their classification based on them, together with the working wavelength in their UV-vis spectrum (maximum peak). Color codes are kept the same during the study.

	Code name	Compound name	$\lambda_{max}$ (nm)	Subclass	General structure	No. of carbon atoms in the flavonoid skeleton								
						C3	C5	C6	C7	C8	C3'	C4'		
<b>FLAVONOIDS</b>														
1	FLV-ON1	Luteolin	356	flavone		H	OH	H	OH	H	OH	OH	OH	
2	FLV-ON2	Apigenin	348	flavone		H	OH	H	OH	H	H	H	OH	
3	FLV-OL1	Quercetin	374	flavonol		OH	OH	H	OH	H	OH	OH	OH	
4	GLY1	Rutin	362	flavonol (glycoside)		O-Rut <sup>a</sup>	OH	H	OH	H	OH	OH	OH	
5	GLY2	Isoquercitrin	360	flavone (glycoside)		O-Glc <sup>b</sup>	OH	H	OH	H	OH	OH	OH	
6	FLV-3-OL1	(+)-Catechin (2R,3S)	412 <sup>c</sup>	flavan-3-ol		$\beta$ -OH	OH	H	OH	H	OH	OH	OH	
7	FLV-3-OL2	(-)-Epicatechin (2R,3R)	412 <sup>c</sup>	flavan-3-ol		$\alpha$ -OH	OH	H	OH	H	OH	OH	OH	
<b>PHENOLIC ACIDS</b>						No. of the carbon atoms in the cinnamic acid structure								
8	VAL	Vanillic acid	284	benzoic ac		C3	C4	C5	C6					
9	HYDCN1	Caffeic acid	312	hydroxy-cinnamic		OH	OH	H	H	cinnamic acid				
10	HYDCN2	Ferulic acid	311	hydroxy-cinnamic ac		OCH3	OH	H	H					
11	HYDCN3	p-Coumaric acid	284	hydroxy-cinnamic ac		H	OH	H	H					
<b>OTHERS</b>														
12	COUM1	Aesculetin <sup>d</sup>	364	hydroxy-coumarin										
13	STB1	Resveratrol <sup>e</sup>	317	stilbenoid										

<sup>a</sup>Rut-disaccharide *Rutinose* ( $\alpha$ -L-rhamnopyranosyl-(1 $\rightarrow$ 6)- $\beta$ -D-glucopyranose);

<sup>b</sup>Glc-monosaccharide D-Glucose ( $\beta$ -D-glucopyranose); <sup>c</sup>wavelength of the maximum peak of reaction product. <sup>d</sup>Aesculetin (6,7-dihydroxycoumarin) <sup>e</sup>Resveratrol (3,5,4'-trihydroxystilbe

The typical spectral changes of four phenolic compounds (luteolin, quercetin, resveratrol and epicatechin), belonging to different classes and subclasses, in the presence of H<sub>2</sub>O<sub>2</sub> and one of the three phytooglobins are shown on Figure 1. The UV-vis spectra features, including the extinction coefficients and position of maxima of the spectra are specific for each compound with more or less similarities, depending of their chemical structures. In the case of luteolin and quercetin (Figure 1A, B) the starting spectra have two salient absorption bands, as previously described, band I and band II. The absence of a 3-hydroxyl group in flavones differentiate them from flavonols, so the band I is always absorbing at a lower wavelength by 20-40 nm in contrast to the absorption maximum of flavonols [9,44]. In our case the flavonol quercetin displays a maximum absorbance at 374 nm in contrast to the flavone luteolin with maximum absorbance at 356 nm, (all the maximum absorbances are given in Table 1). In the case of quercetin the reaction could be tracked by shifting of the maximum absorbance and appearing

of new maximum absorbance at 334 nm, characteristic for generating oxidized form of quercetin (quinone form), while in the case of luteolin the reaction could be tracked by the decrease of the typical band I (356 nm), due to the consumption of the luteolin during the reaction with the ferryl Hb. The stilbenoid resveratrol (Figure 1C) is having three maximum absorbances, one below 220 nm and two very close to each other (307 nm and 317 nm). The reaction is followed by the decrease of these bands, but appearing of a new band at 252 nm and a shoulder around 375 nm, probably with some interferences of the Hb contribution around 405 nm.

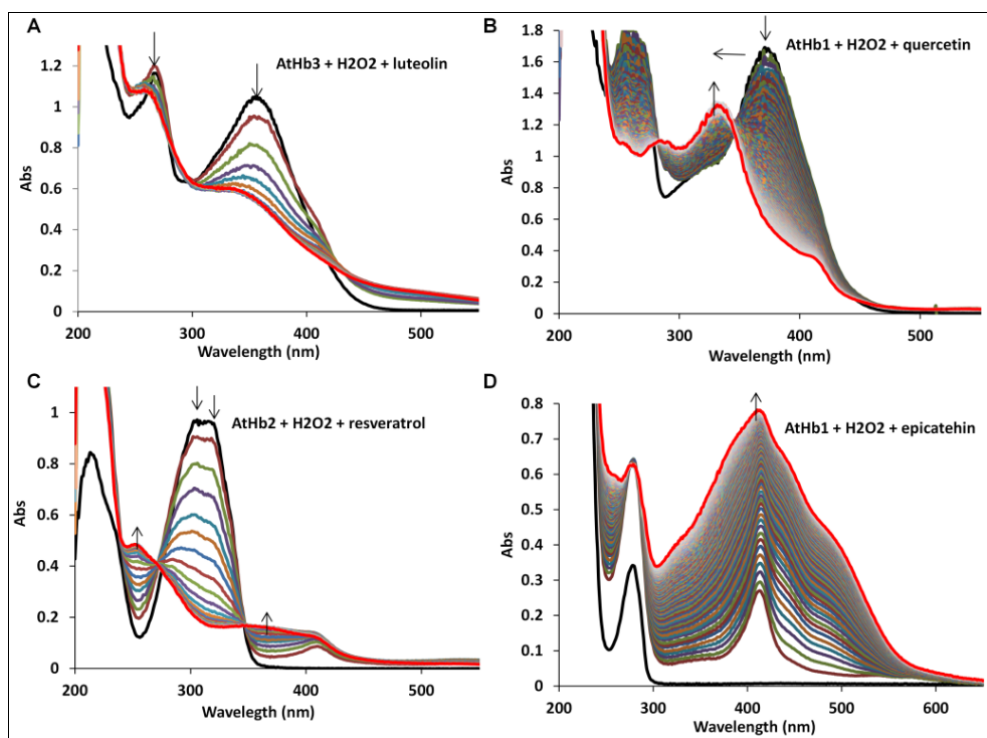


**Figure 1.** Reaction between the phenolic compounds and *A. thaliana* non-symbiotic hemoglobins in the presence of hydrogen peroxide ( $\text{H}_2\text{O}_2$ ). UV-Vis spectra changes of phytophenolic substrates oxidation in 50 mM phosphate buffer pH 7 and 25°C. (A) 0.1 mM luteolin, 0.5 mM  $\text{H}_2\text{O}_2$  and 1  $\mu\text{M}$  metAtHb3; (B) 0.1 mM quercetin, 1 mM  $\text{H}_2\text{O}_2$  and 2  $\mu\text{M}$  metAtHb1; (C) 0.1 mM resveratrol, 1 mM  $\text{H}_2\text{O}_2$  and 2  $\mu\text{M}$  metAtHb2; (D) 0.1 mM epicatechin, 1 mM  $\text{H}_2\text{O}_2$  and 2  $\mu\text{M}$  metAtHb1;

The flavanols epicatechin (Figure 1D) and the catechin (spectra not shown) from our investigation are the only phenolic compounds in which the product of the reaction is characterized with formation and appearing of band with maximum absorbance in the visible region, at 412 nm, instead of the typical decay of the starting bands which was the case for the others investigated phenolic compounds. The reason for this may be the formation of a more stable epicatechin/catechin based radical generated during the reaction or a dimer/trimer oxidized form that have an extended aromatic structure which leads to absorbances at higher wavelengths, but further investigation and employing of other techniques (such as EPR, NMR, chromatography) would be necessary. In addition, other tested compounds exhibit no reaction such as vanilic and gallic acid, most probably due to too high redox potential compared to the ferryl redox potential.

One may expect that the ferryl abstracts one electron from the phenolic compound, generating an unstable transient radical-based species that may further be oxidized either enzymatically or by interacting with other radicals leading to stable quinone forms or dimers or multimeric species, however, little influence is expected from Hb to another since they are expected to behave similarly. However, in some cases, the fact that the product/s of the reaction may be different from the type of used Hb appears very interesting (catechin and epicatechin, Figure 2 AB).

A further comparison between the starting and the end point spectra in the reaction of some compounds with the three phytooglobins (AtHb1, AtHb2 and AtHb3) in the presence of  $H_2O_2$  is shown on Figure 2. In all cases (shown in Figure 2) the oxidation of the phenolic compounds in the presence of AtHb3 is the least completed, probably due to the high sensitivity of this truncated hemoglobin towards  $H_2O_2$ , in which case the highly reactive ferryl species are generated very fast with far smaller peroxide amounts (data not shown), so in the presence of higher peroxide concentration degradation of the hemoglobin occurs. Besides other aspect that may influence the end reaction spectrum (the intensity rather than the profile) is the completion of the reaction (the Hbs have different stability in the working condition and high peroxide concentration), the small different features may be explained by the rate of the monoelectronic abstraction, shape and size of the binding pocket which could lead to slight different transient species with different fate.



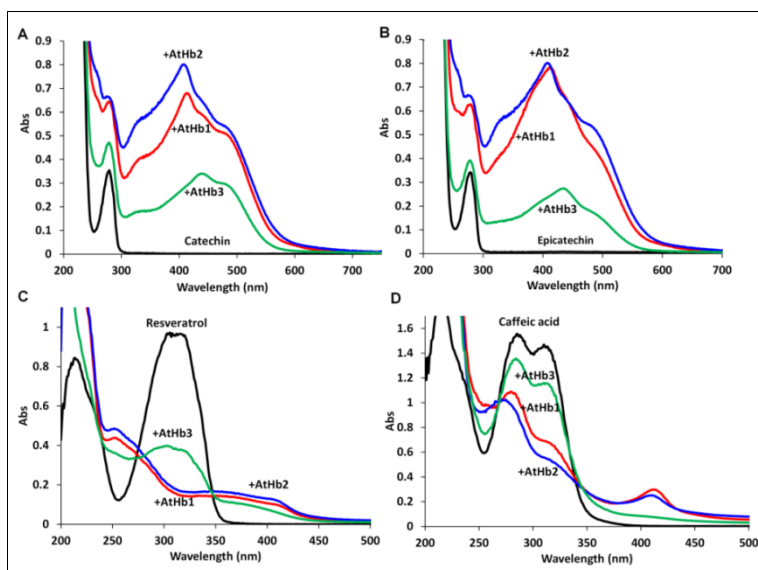


**Figure 2.** Characteristic UV-Vis spectra (A) 0.1 mM catechin; (B) 0.1 mM epicatechin; (C) 0.1 mM resveratrol; (D) 0.1 mM caffeic acid in the presence and absence of the AtHb1, AtHb2 and AtHb3

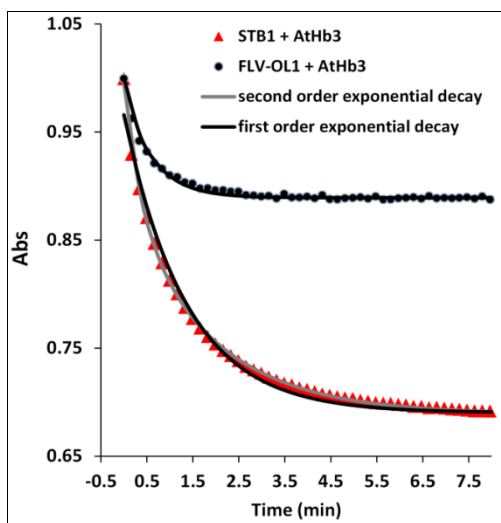


**Figure 3.** Kinetic traces for the oxidation of resveratrol (STB1) and quercetin (FLV-OL1), both in presence of AtHb3 and peroxide exhibiting different decay profiles, resveratrol requiring second order exponential decay model ( $R^2=0.999$ ) while for quercetin first order exponential decay being sufficed ( $R^2=0.995$ ).

The kinetic profiles of the phenolics oxidation (absorbance change in time) follow either a first order or second order exponential decay described by the equation 1 (where  $t$  refers to time,  $t_1$  and  $t_2$  are the time constants and  $A_{1,2}$  are amplitude relating constants) and are compound specific, in a similar fashion with the reaction between the artificial radical DPPH and phenolic compounds (Figure 3) [45]. This could be a good indication for the complexity of the reaction; reactions that follow a first order exponential decay profile suggest a direct oxidation of the substrate to a single oxidized product. Second order exponential decay trend may indicate either two types of generated radicals with similar but different end products or enzymatic independent generation of secondary radicals that might at their turn lead to different oxidized products. Furthermore, this is not only substrate specific but also globin specific, for example the two studied glycosides follow a second order exponential decay profile for AtHb1 and AtHb3 but a monoexponential curve for AtHb2 while the opposite is valid for caffeic acid (HYDCN1) (see Table 2 for all data regarding this aspect).

**Table 2.** Time constants  $t_1$  and  $t_2$  and the half-life  $t_{1/2}$  for the oxidation of the studied compounds in presence of peroxide and the three Hbs. The slash in the  $t_2$  columns indicates that first order decay suffice to fit the data.

	Code Name	AtHb1			AtHb2			AtHb3		
		$t_1$	$t_2$	$t_{1/2}$	$t_1$	$t_2$	$t_{1/2}$	$t_1$	$t_2$	$t_{1/2}$
1	FLV-ON1	0.52± 0.04	3.80± 0.03	0.46± 0.003	0.71± 0.08	12.52± 0.35	0.67± 0.06	0.32± 0.007	/	0.22± 0.005
2	FLV-ON2	9.19± 0.51	/	6.37± 0.35	2.67± 0.35	10.46± 0.83	2.13± 0.24	0.8±0 .17	23.27 ±7.47	0.77± 0.17
3	FLV-OL1	1.34± 0.02	15.45 ±0.08	1.23± 0.019	1.29± 0.17	21.16± 0.50	1.22± 0.13	0.43± 0.004	/	0.30± 0.003
4	GLY1	2.35± 0.05	9.10± 0.25	1.87± 0.04	10.73 ±0.04	/	7.44± 0.03	0.43± 0.02	2.89± 0.28	0.38± 0.017
5	GLY2	2.53± 0.11	9.51± 0.33	1.99± 0.08	11.85 ±0.05	/	8.12± 0.03	0.53± 0.05	1.34± 0.12	0.38± 0.03
6	FLV-3-OL1	1.03± 0.016	4.66± 0.09	0.84± 0.14	3.18± 0.04	13.85± 0.13	2.58± 0.03	0.197 ±0.00 1	0.98± 0.013	0.16± 0.001
7	FLV-3-OL2	1.10± 0.016	4.74± 0.1	0.89± 0.014	3.49± 0.13	10.28± 0.21	2.61± 0.08	0.33± 0.004	1.27± 0.03	0.27± 0.003
8	VAL	No reaction in the present conditions								
9	HYDCN1	2.01± 0.02	/	1.39± 0.016	6.85± 0.22	22.72± 1.6	5.27± 0.19	1.27± 0.02	/	0.88± 0.014
10	HYDCN2	0.62± 0.02	6.80± 0.06	0.57± 0.018	12.87 ±0.22	/	8.92± 0.15	0.77± 0.15	2.97± 0.22	0.61± 0.09
11	HYDCN3	0.26± 0.01	7.21± 0.15	0.25± 0.009	6.75± 0.13	/	4.68± 0.09	1.63± 0.05	/	1.13± 0.035
12	COUM1	5.88± 0.12	/	4.08± 0.008	67.91 ±0.95	/	47.07 ±0.66	0.38± 0.013	/	0.27± 0.09
13	STB1	1.82± 0.007	/	1.26± 0.005	1.65± 0.05	/	1.15± 0.04	0.37± 0.017	1.84± 0.03	0.31± 0.01

This data further supports the fact that these enzymes do not only influence the rate of the reaction but also the enzymatic mechanism.

$$Abs_t = Abs_0 + A1e^{\frac{-t}{t_1}} + A2e^{\frac{-t}{t_2}} \quad (\text{Equation 1})$$

Regarding the rate of the reaction, the time constants  $t_1$  and  $t_2$  and the half-lives  $t_{1/2}$  for the investigated phenolic compounds are presented in Table 2. The calculated values for the  $t_{1/2}$  in the case of AtHb3 are lowest, ranging in the interval of 0.16-1.13 min for catechin and *p*-coumaric acid, respectively, indicating very fast reactions. The highest are in the case of AtHb2 in the interval of 0.67-8.92 min; for luteolin and ferulic acid, respectively with exception of aesculetin with value of 47.07 min, thus this globin is a poor catalyst for type of reaction while the AtHb1 sets in between the two.

In order to easily evaluate simultaneously the profile, rate and the yield of the reaction (also influenced by enzyme stability), graphical representation of the reaction product percentage, at three stages are shown in Figure 4.

PCA based mapping allows evaluation of the similarities or lack thereof between the studied compounds, based on their kinetic profiles using the three different globins as enzymes (Figure 5). Poor grouping based on structural similarities is observed (especially for AtHb1) but notably again highly different mapping exists from enzyme to enzyme. In case of AtHb2 and AtHb3, a weak but visible grouping of the compounds, based on their structural similarities, is noticed.

A better grouping of the compounds, in good agreement with their structural details (Table 1) is observed if cluster analysis is employed upon the kinetic parameters (Figure 6). Once more, the compound grouping was enzyme specific. In case of Athb1, two major clusters were obtained, one consisting of the flavonoids (with the exception of flavan-3-ols) and another including all the others while in the case of the other two enzymes, one compound was very different from the rest (aesculetin in case of AtHb2, very poor reaction and apigenin for AtHb3, very fast reaction with AtHb3); all the others were grouping in three small groups with more or less structural similarities (Figure 6). In addition, the correlation circle of the variables obtained after PCA application upon the kinetic parameters suggests that the  $t_{1/2}$  is mainly determined by the  $t_1$  component and the rates were in the following order: AtHb2, AtHb1 and AtHb3, in good agreement with their peroxidase activity while the amplitude of the percentage of the oxidized reaction product is in reverse order as expected from the data presented in Figure 4.

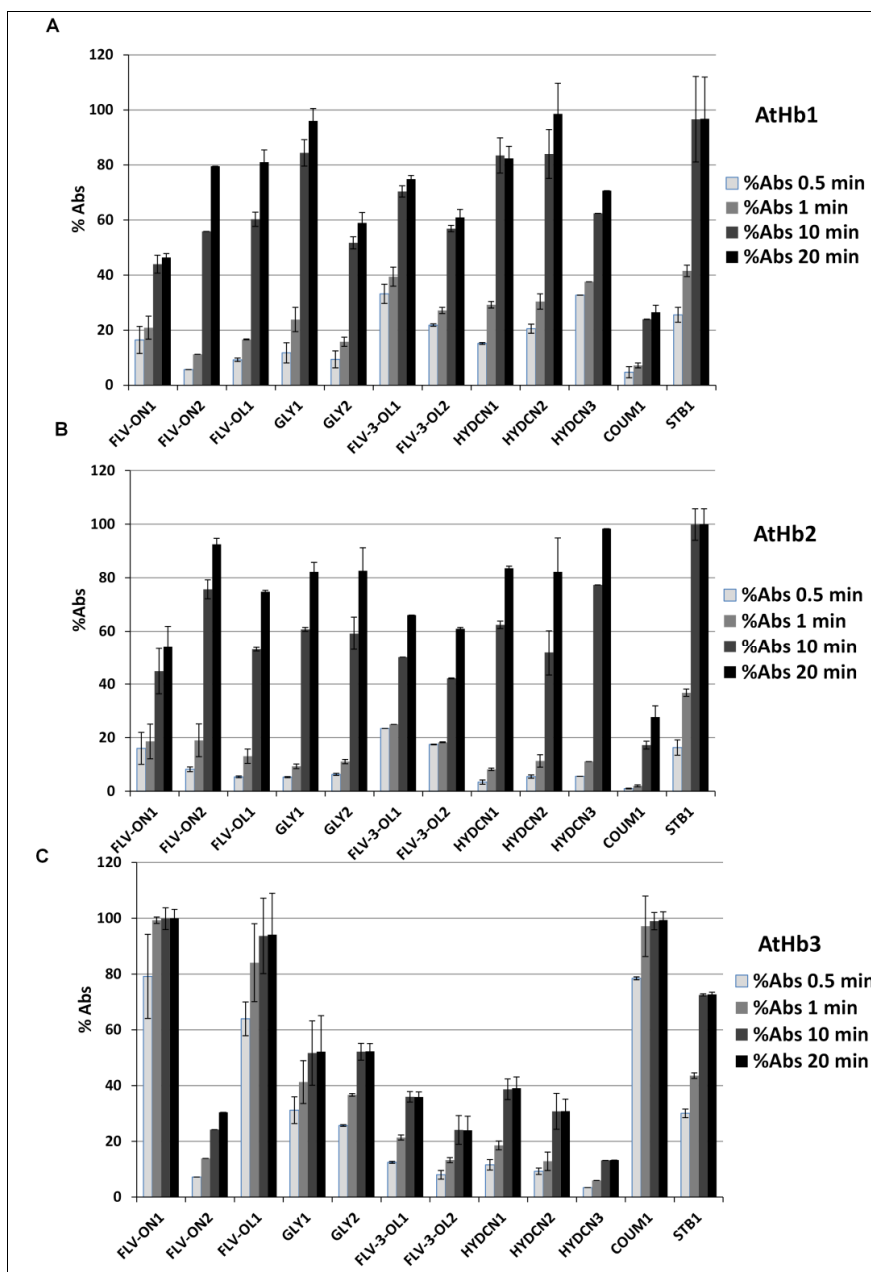


**Figure 4.** Percentage of oxidized phenolics monitored at the  $\lambda_{max}$  in presence of (A) metAtHb1 (B) metAtHb2 and (C) metAtHb3 after 0.5 min, 1 min, 10 min and 20 min reaction time (error bars represent standard deviations of the mean).

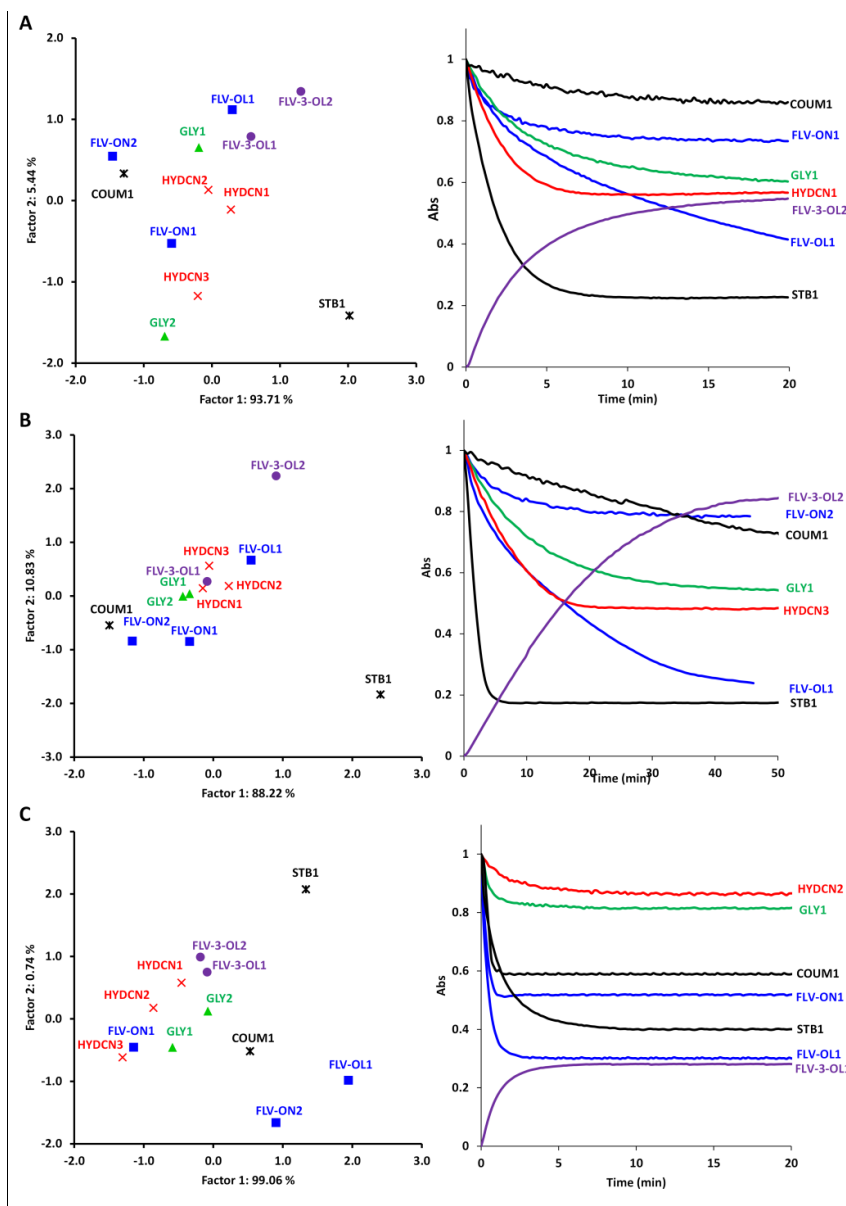


**Figure 5.** PCA based mapping of the studied compounds using the entire kinetic profiles for the reactions between 0.1 mM phenolic compound in presence of peroxide and (A) metAtHb1, (B) metAtHb2, (C) metAtHb3. On the right, the kinetic profiles of some representatives from different classes are shown. Color codes are consistent with Tables 1 and 2.

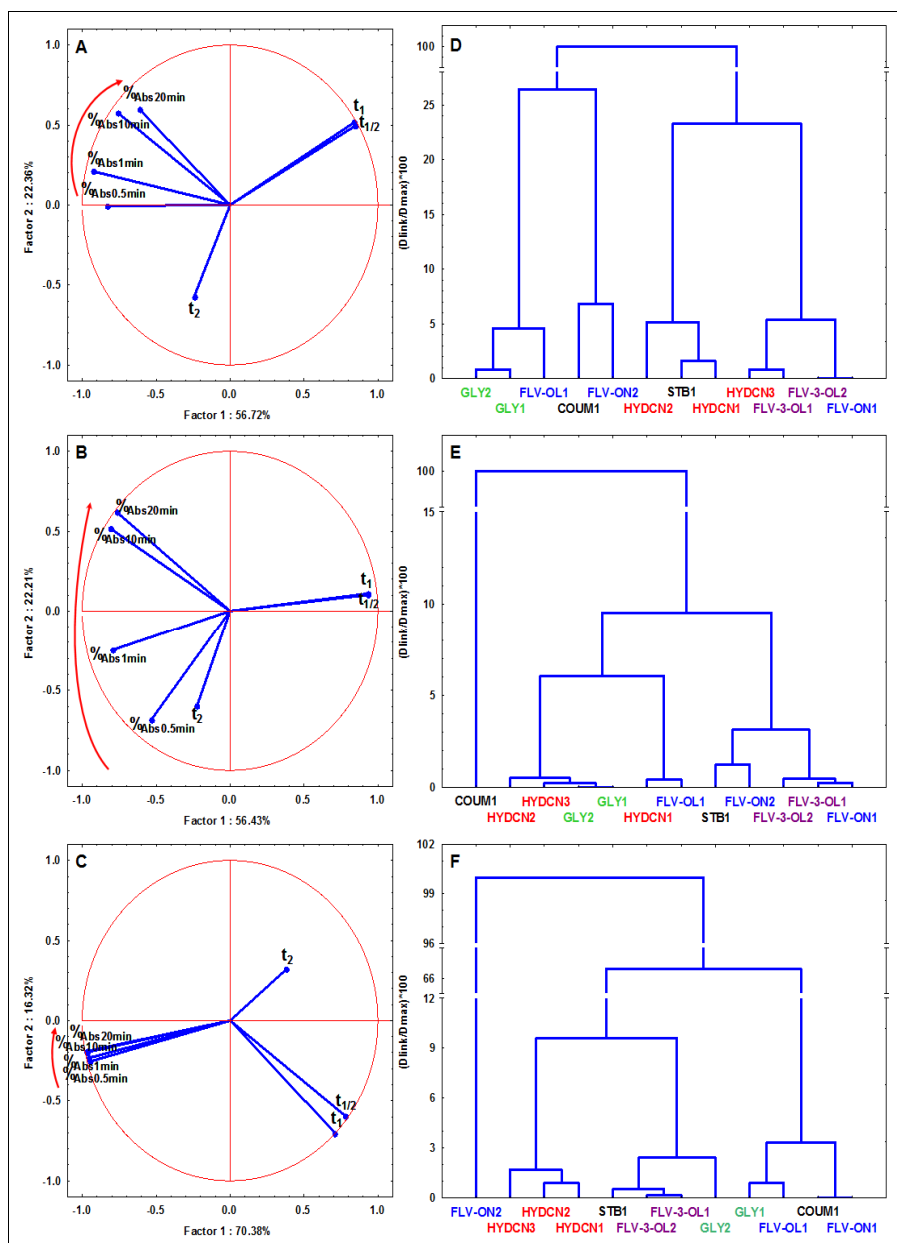


**Figure 6.** Correlation circle of the variables after PCA applying upon the kinetic and yields of the reactions for the three enzymes A. AtHb1, B. AtHb2, C. AtHb3 and the clustering results obtained through cluster analysis on the same data (Ward's method, distance measure: 1-Pearson r), D. AtHb1, E. AtHb2, F. AtHb3.

Coupling the profiles analysis, their PCA mapping and cluster analysis, one may observe that the presence of a 3-hydroxyl group in the heterocyclic C ring at flavonoids (quercetin) increases the reducing power of the compounds, while the substitution with additional hydroxyl or methoxyl groups at positions 3, 5 and 7 of rings A and C seem to be less important. Glycosylation of 3-hydroxyl group in ring C, such as at rutin, quercitrin or isoquercitrin, reduces significantly the reducing power, most probably due to steric hindrance. This is in good agreement with other biochemical or the electrochemical activity of the flavonoids that they depend on the chemical structure and the moieties orientation in the molecule [44].

## CONCLUSIONS

To conclude, a set of thirteen phenolic compounds were comparatively analysed for their reducing power for ferryl forms of the three *A. thaliana* non symbiotic hemoglobins. The kinetic profiles of their oxidation processes were analysed using PCA and cluster analysis and it was found that the three globins are different not only in terms of rate but also in terms of mechanism, thus, the reducing power of the studied compounds is strongly enzyme specific with weak accuracy to be predicted solely from their chemical structure.

## EXPERIMENTAL SECTION

### Materials and methods

Quercetin, rutin, quercetin, isoquercitrin, caffeic acid, ferulic acid, *p*-coumaric acid, vanillic acid, hydrogen peroxide (H<sub>2</sub>O<sub>2</sub>) and methanol were purchased from Sigma–Aldrich (Steinheim, Germany). Luteolin, apigenin, (+)-catechin, (-)-epicatechin, aesculetin, and resveratrol were obtained from Fluka (Buchs, Switzerland). The stock solutions of the phenolic compounds were prepared by dissolving the compound in methanol.

The three recombinant *Arabidopsis thaliana* non-symbiotic plant hemoglobins (AtHb1, AtHb2 and AtHb3), each belonging to a different class of phytohemoglobins were expressed in *E. coli* BL21 (DE3) as follows: *E. coli* cells containing the expression vector were grown at 37°C and 190 rpm in LB medium and 100 mg/L ampicillin until the OD<sub>600</sub> reached 0.6-0.8 (for AtHb1 and AtHb2) followed by temperature decreasing to 25°C, then 0.3 mM hemin and 0.25 mM isopropyl β-d-1-thiogalactopyranoside (IPTG) were

added. For AtHb3, the cells were grown at 37°C and 190 rpm in LB medium supplemented with 100 mg/L ampicillin until the OD<sub>600</sub> reached 1.1 - 1.2, then, the temperature was reduced to 28°C and 0.1 mM ferrous ammonium sulfate, 0.25 mM 5-aminolevulinic acid and 0.3 mM IPTG was added to the culture flask. Additionally, 40 mL LB medium saturated with CO by purging CO gas directly into the LB medium for approximately 20 min, was added before the flask was sealed. [46] The cells were incubated overnight at 25°C (for AtHb1 and AtHb2) and 28°C for AtHb3 at 110 rpm. Cells were harvested by centrifugation (4000 rpm for 20 min at 4°C), resuspended in 100 mL lysis buffer pH 7.8 (300 mM NaCl, 50 mM Na<sub>2</sub>HPO<sub>4</sub>), previously purged with CO gas for 15 min in case of AtHb3. The cells were sonicated on ice, in the presence of 1mM phenylmethanesulfonyl fluoride. The lysate was centrifuged (16000 rpm for 45 min at 4°C) and the hemoglobin containing supernatant was purified using Ni-NTA-agarose affinity resin (GE Healthcare), MBPTrap HP columns (GE Healthcare) and size exclusion chromatography.

The spectrophotometric data were acquired using Varian Cary® 50 UV-Vis Spectrophotometer equipped with temperature - controlled multi cell holder using 1 cm quartz cuvette.

The reducing power of thirteen phenolic compounds towards the three plant hemoglobins (ferric Hb, Fe<sup>3+</sup>-Hb) in 50 mM phosphate buffer (Na<sub>2</sub>HPO<sub>4</sub>), pH 7.4 and temperature of 25°C was investigated. For this purpose 0.1 mM of each phenolic substrate was transferred into a 1 mL quartz cuvette, followed by addition of 2 µM AtHb1; shortly after 1 mM H<sub>2</sub>O<sub>2</sub> was added and the reaction was monitored by continuously acquiring UV-Vis spectra between 200 and 800 nm. The same procedure, under the same conditions, was done for each phenolic substrate, only using 2 µM AtHb2; while in the case of AtHb3 0.1 mM of each phenolic substrate was mixed with 1 µM AtHb3, followed by addition of 0.5 mM H<sub>2</sub>O<sub>2</sub>. All experiments were done in duplicates. The traces extracted at the maximum absorption wavelength in time were fitted in Origin 6.1 using the function for exponential decay with first or second order, with exception of FLV-3-OL1 and 2 which showed hyperbolic increasing of the absorbance in time, so the values of the absorption were transformed into exponential decay. Following the kinetic profile of the reactions,  $\tau$  (time constant of the decay quantity) was estimated and using the following equation, accordingly:  $t_{1/2} = \tau \times \ln 2$  (reactions following exponential decay with first order) and  $t_{1/2} = \frac{\tau_1 \times \tau_2}{\tau_1 + \tau_2}$  (reactions following exponential decay with second order),  $t_{1/2}$  (the total half-life) was calculated; the results are shown in Table2. *For statistical evaluation, principal component analysis and cluster analysis, Statistica 8 (Stat. Soft Inc., USA) was used.*



## ACKNOWLEDGMENTS

Financial support from the Romanian National Authority for Scientific Research and Innovation (CNCS – UEFISCDI, project PN-II-RU-TE-2014-4-2555) is gratefully acknowledged.

## REFERENCES

1. M. De L. R. Giada, "Oxidative Stress and Chronic Degenerative Diseases – A Role for Antioxidants", InTech, Rijeka, Croatia, **2013**, chapter 4.
2. K.G. Ramawat, J.M. Mérillon, "Natural Products : Phytochemistry, Botany and Metabolism of Alkaloids, Phenolics and Terpenes", Springer, **2013**, chapter 6.
3. D. Lin, M.Xiao, J. Zhao, Z.Li, B. Xing, X. Li, Q. Zhang, Y. Liu, H. Chen, W. Qin, H. Wu, S. Chen, *Molecules*, **2016**, *21*, 1374.
4. N. Balasundram, K. Sundram, S. Samman, *Food Chemistry*, **2006**, *99*, 131-203.
5. P.G. Pietta, *Journal of Natural Products*, **2000**, *63*, 1035-1042.
6. S. Amallesh, G. Das, K.S. Das, *International Journal of Pharmacy Sci Tech*, **2011**, *6*, 12-35.
7. V. Cheynier, *Phytochemistry Reviews*, **2012**, *11*, 153-177.
8. J. Treml, K. Šmejkal, *Comprehensive Reviews in Food Science and Food Safety*, **2016**, *15*, 720-738.
9. S. Kumar, A.K. Pandey, *The ScientificWorld Journal*, **2013**, *2013*, 16.
10. G. Agati, M. Tattini, *New Phytologist*, **2010**, *186*, 786-793.
11. G. Agati, E. Azzarello, S. Pollastri, M. Tattini, *Plant Science*, **2012**, *196*, 67-76.
12. R.J. Nijveldt, E.V. Nood, D. EC. V. Hoorn, K.V. Norren, P. AM. V. Leewen, *The American Journal of Clinical Nutrition*, **2001**, *74*, 418-425.
13. W.Y. Huang, Y.Z. Cai, Y. Zhang, *Nutrition and Cancer*, **2010**, *62*, 1-20.
14. C. Rivière, A.D. Pawlus, J. M. Mérillon, *Natural Product Reports*, **2012**, *29*, 1317-1333.
15. K.N. Venugopala, V. Rashmi, B. Odhav, *BioMed Research International*, **2013**, *2013*, 14-19.
16. A.V. Rao, L.G. Rao, "Phytochemicals Isolation, Characterisation and Role in Human Health", AvE4EvA, InTech, **2015**, chapter 5.
17. K.E. Heim, A.R. Tagliaferro, D.J. Bobilya, *The Journal of Nutritional Biochemistry*, **2002**, *13*, 572-584
18. B. Sciences, B.G.- Hospital, *Biochemical Pharmacology*, **1992**, *43*, 1167–1179,
19. J. Xi R. Guo, *International Journal of Biological Macromolecules*, **2007**, *40*, 305–311.
20. K. Weng, S. Mat-junit, A. Ismail, N. Aminudin, A. Abdul-aziz, *Food Chemistry*, **2014**, *146*, 85–93.

21. M.F. V.N. Arroyo-Currás, *ECS transactions*, **2010**, 29, 349–359.
22. E.S. Gil, R.O. Couto, *Revista Brasileira de Farmacognosia, Brazilian Journal of Pharmacognosy*, **2013**, 23, 542-558.
23. N. Wijayanti, N. Katz, S. Immenschuh, *Current Medicinal Chemistry*, **2004**, 11, 981-986.
24. A. Sakamotoa, S. Sakuraob, K. Fukunagab, T. Matsubarac, M. Ueda-Hashimotoa, S. Tsukamotoa, M. Takahashia, H. Morikawa, *FEBS Letters*, **2004**, 572, 27-32.
25. M. Delledonne, Y. Xia, R.A. Dixon, C. Lamb, *Nature*, **1998**, 394, 585–588.
26. M. Tiso, J. Tejero, C. Kenney, S. Frizzell, M.T. Gladwin, *Biochemistry*, **2012**, 51, 5285-5292.
27. Gautam Sarath,<sup>3</sup> Jean-Louis Hilbert,<sup>4</sup> Richard A. Watts,<sup>5,6</sup> Elizabeth S. Dennis,<sup>5</sup> W. James Peacock, B. J. Smagghe, J.A. Hoy, R. Percifield, S. Kundu, M.S. Hargrove, G. Sarath, J. Hilbert, R.A. Watts, E.S. Dennis, W.J. Peacock, S. Dewilde, L. Moens, G.C. Blouin, J.S. Olson, C.A. Appleby, *Biopolymers*, **2009**, 91, 1083–1096.
28. V.G. Villegas, S.K. Gopalasubramaniam, R.A. Peter, *Gene*, **2007**, 398, 78–85.
29. J.A. Hoy, H. Robinson, J.T. Trent, S. Kakar, B.J. Smagghe, M.S. Hargrove, *Journal of Molecular Biology*, **2007**, 371, 168–179.
30. J. Tejero, M.T. Gladwin, *Biological Chemistry*, **2014**, 395, 631–639.
31. Y. Wang, X. Barbeau, A. Bilimoria, P. Lagüe, M. Couture, J.K.H. Tang, *PLoS One*, **2015**, 10, 1–30.
32. A. Lama, S. Pawaria, K.L. Dikshit, *FEBS Letters*, **2006**, 580, 4031–4041.
33. R. Silaghi-Dumitrescu, B.J. Reeder, P. Nicholls, C.E. Cooper, M.T. Wilson, *Biochemical Journal*, **2007**, 395, 391–395.
34. N. Lu, Y. Ding, Z. Yang, P. Gao, *International Journal of Biological Macromolecules*, **2016**, 89, 175–180.
35. L. Gebicka, E. Banasiak, *Acta Biochimica Polonica*, **2009**, 56, 509–513.
36. A.I. Alayash, R.P. Patel, R.E. Cashon, *Antioxidants & Redox Signaling*, **2001**, 3, 313-327.
37. A.C. Moț, C. Coman, C. Miron, G. Damian, C. Sarbu, R. Silaghi-Dumitrescu, *Food Chemistry*, **2014**, 143, 214–222.
38. N. Lu, P. Chen, Q. Yang, Y. Peng, *Toxicology in Vitro*, **2011**, 25, 833–838.
39. J. Yuan, H. Liu, X. Kang, Z. Lv, G. Zou, *Journal of Molecular Structure*, **2008**, 891, 333–339.
40. Y. Jia, A. I. Alayash, *Free Radical Biology & Medicine*, **2008**, 45, 659-666.
41. S. Chakrabortya, S. Chaudhurib, B. Paharib, J. Taylorc, P. K. Senguptab, B. Senguptac, *Journal of Luminescence*, **2013**, 132, 1522–1528.
42. R. Gabbianelli, M. Santroni, D. Fedeli, Kantar, G. Falcioni, *Biochemical and Biophysical Research Communications*, **1998**, 242, 560–564.
43. Y.S. Tarahovsky, Y.A. Kim, E.A. Yagolnik, E.N. Muzafarov, *BBA Biomembranes*, **2014**, 1838, 1235–1246.
44. L.H. Yao, Y.M. Jiang, J. Sji, F.A. Tomás-Barberán, N. Datta, R. Singanusong, S.S. Chen, *Plant Foods for Human Nutrition*, **2004**, 59, 113–122.

45. A.C. Moț, R. Silaghi-Dumitrescu, C. Sârbu, *Journal of Food Composition and Analysis*, **2011**, 24, 516–522.
46. B.J. Reeder and M.A. Hough, *Acta Crystallographica Section D*, **2014**, D70, 1411–1418.

*Dedicated to Professor Costel Sârbu on the  
Occasion of His 65<sup>th</sup> Anniversary*

## **IMAGE ANALYSIS APPROACHES TO IMPROVE THE THIN LAYER CHROMATOGRAPHY – CHEMOMETRIC-BASED INVESTIGATIONS OF NATURAL EXTRACTS**

**MARIA SIMION<sup>a</sup>, SIMONA CODRUTA AURORA COBZAC<sup>a\*</sup>,  
DORINA CASONI<sup>a</sup>**

**ABSTRACT** The combination of high-performance thin-layer chromatography (HPTLC) with image analysis (IA) and chemometrics becomes an attractive tool for natural extracts investigations. The large variability of these samples requires powerful image acquisition devices, multivariate image processing techniques and advanced chemometric methods to facilitate the interpretation of the chromatographic data. In the current study, two image acquisition devices and different image processing procedures were investigated using the HPTLC chromatograms of hydroalcoholic extracts of *Gallium verum*. Different sets of chromatographic data were generated for both UV chromatograms (obtained at 254 nm and at 366 nm) using images acquired with a digital camera and an UV-Vis TLC scanner. In all cases the Principal Component Analysis (PCA) technique was used in order to extract the information from chromatographic profiles. Variables of gray and pure colour red, green and blue intensities of pixels from start to front were used as input data in all cases. The results obtained by PCA investigations of HPTLC data from UV chromatograms at 254 nm and 366 nm respectively, provided complementary information related to the characteristics of the investigated extracts. Moreover, important steps as appropriate color scale selection and image processing/analysis procedures were pointed out based on the obtained results.

**Keywords:** *Thin-Layer Chromatography, Image Analysis, Principal Component Analysis, Gallium verum extracts*

---

<sup>a</sup> Babeş-Bolyai University, Faculty of Chemistry and Chemical Engineering, 11 Arany Janos, RO-400028, Cluj-Napoca, Romania.

\* Corresponding author: csimona@chem.ubbcluj.ro

## INTRODUCTION

Thin layer chromatography (TLC) is a very popular analytical technique currently used to investigate the number of components in a mixture, verify the identity of substances, quantify numerous compounds in various foods, pharmaceuticals and biological samples and monitor the progress of reactions. Nowadays, due to the advantages offered by the improvements regarding sample application technique, image acquisition systems, computer controlled scanning instrument and image analysis software, high performance TLC combined with image analysis (HPTLC-IA) is feasible to analyze the compounds with overlapping chromatograms [1], quantify the fluorescent compounds [2], investigate the antiradical activity of plant materials [3], screening the compounds from natural extracts [4, 5] and fingerprinting analysis of various plants material [6, 7]. Among the numerous application of HPTLC, the fingerprint analysis is of special interest. In this area, chemometric techniques for HPTLC data evaluation were recently employed [8, 9]. Chromatographic data can be obtained from the chromatograms by the means of classical densitometry, or by processing the image obtained with flatbed scanner or different digital cameras [10-12]. Several software packages such as ImageJ, Just TLC, Sorbfil TLC Videodensitometer and others can be used for image processing [13-17]. Once the chromatographic data are properly recorded, extracted, and pre-treated, multivariate data analysis methods such as principal component analysis (PCA), hierarchical cluster analysis (HCA) or linear discriminant analysis (LDA) can be applied to extract the most important chemical information which lead to samples classification or to detect the classification patterns [18-21]. The increasing scientific interest to combine HPTLC with multivariate data analysis is a promising research field in herbal analysis. In this area, more investigations related to the image acquisition and image processing techniques are necessary in order to extract the meaningful information from obtained chromatograms.

In this context, the present paper focused on transformation of HPTLC chromatogram of *Galium verum* extracts into numerical data appropriate to chemometric analysis using various image analysis procedures of images acquired with two different systems. In our investigation, extracts of *Galium verum* (Lady's Bedstraw) were used as test model. The plant, currently involved in traditional folk medicine, can be easily recognized by its distinct sunny yellow color and tiny little flowers [22-24]. As a remedy, Lady's Bedstraw is used for skin problems (burns, psoriasis), kidney and bladder stones and epilepsy (due to its sedative effect). Also it is used to curd milk and as a yellow food dye. The beneficial effects of *Galium verum* extracts are generally attributed to the biological active compounds as iridoides, flavonoids, antrakinnone, alkane and

essential oils which are present in the plant [25, 26]. Due to this large variety of compounds, the hydroalcoholic extracts of *Gallium verum* were considered as a good input data for image processing and multivariate analysis investigations.

The aim of the study is to highlight the most appropriate steps in image processing prior to application of multivariate data analysis in order to differentiate various *Gallium verum* hydroalcoholic extracts based on their HPTLC fingerprints. For a better understanding of extracts classification, the available red, blue, green and gray channels will be used for chromatograms digitization. Also the study aims to identify the factors that lead to extracts classification according to their provenience and extraction system.

## RESULTS AND DISCUSSION

Extracts from natural products are complex mixtures that contain a large number of compounds. Usually thin-layer chromatographic profiles are taken into consideration for quality evaluation or authenticity assays. In most of the cases different chemometric approaches are used in order to extract the valuable information from chromatographic profile. In the current study, the Principal Component Analysis (PCA) technique was used as an alternative way to differentiate various *Gallium verum* hydroalcoholic extracts based on image analysis (IA) of their HPTLC fingerprints. Different aspects related to the image acquisition and processing techniques of chromatograms obtained with two different detection approaches (fluorescence quenching under 254 nm and fluorescence at 366 nm respectively) were employed in order to provide complementary information on hydroalcoholic extracts characteristics.

### HPTLC fingerprint of *Gallium Verum* extracts

The HPTLC fingerprint analysis based on images obtained under UV light investigation at 254 nm and 366 nm after spraying with NTS was used to seek for characteristic patterns of *Gallium verum* extracts of different origin using the advantages of multivariate image processing and principal component analysis (PCA) tool.

Hydroalcoholic extracts of *Gallium verum* vegetal material commercialized by Plafar (P) and Dacia (D) manufacturers (Romania), obtained with different composition of extracting system (60% - 100% ethanol) were investigated. A normal-phase chromatographic system, using a HPTLC Silica gel 60 F<sub>254</sub> plates and the developing solvent mixture composed of ethyl acetate: toluene: formic acid: water (30:1.5:4:3 v/v), was employed to separate highly and medium polar phenolics and obtain chromatographic bands with improved shapes.

The HPTLC chromatograms (Fig.1) obtained under 254 nm and respectively 366 nm (images acquired with digital camera) revealed differences between D and P samples especially in upper area. Moreover, the investigation under 366 nm revealed that the extracts are rich in some phenolic compounds with a pattern dominated by blue and red color bands.

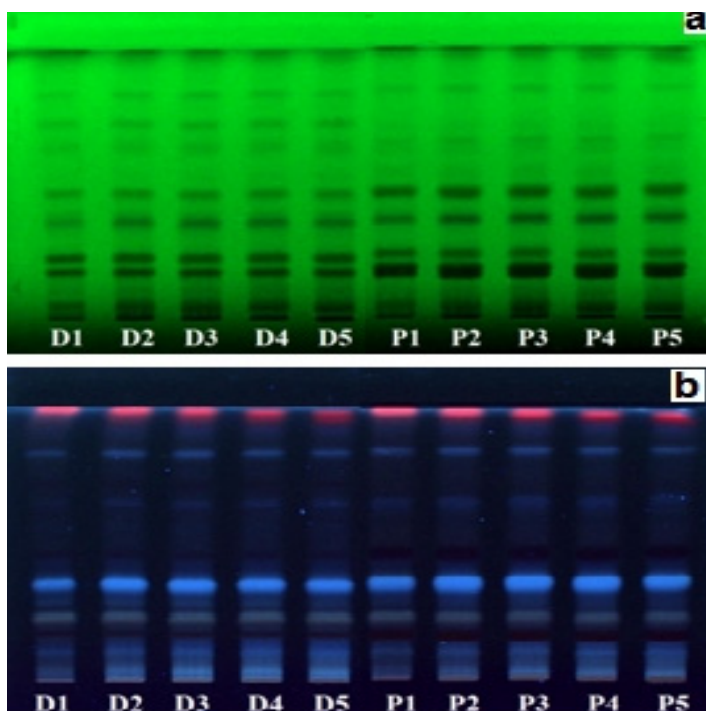


**Figure 1.** HPTLC chromatograms of *Gallium verum* extracts obtained using HPTLC Silica gel 60 F<sub>254</sub> chromatographic plates and mixture of ethyl acetate - toluene - formic acid - water (30:1.5:4:3, v/v) as mobile phase: (a) detection at  $\lambda = 254$  nm; (b) detection at  $\lambda = 366$  nm after spraying with NTS (D1-D5 extracts of *Gallium verum* vegetal powder commercialized by Dacia manufacturer using 100%, 90%, 80% 70% and 60% ethanol solutions; P1-P5 extracts from *Gallium verum* vegetal powder commercialized by Plafar manufacturer using 100%, 90%, 80% 70% and 60% ethanol solutions)

Based on these observations, different image processing approaches have been applied for a complete evaluation of the chromatographic profile of analyzed samples. Image processing through the gray (Gy), red (R), green (Gn) and blue (B) scales were used in order to increase the detection selectivity and differentiate between compounds according to their fluorescent colors and quantity found in the investigated extracts.

## Data acquisition and chemometric analysis

Different sets of chromatographic data were generated for both UV chromatograms (obtained at 254 nm and at 366 nm) using images acquired by a digital camera and an UV-Vis TLC scanner device. In all cases, the HPTLC chromatograms were digitized using the TLC Analyser software and selection of the gray, red, green and blue scales respectively. According to the different colour channels used for digitizing the HPTLC chromatograms, the obtained profiles show different maximum and minimum values at the same  $R_f$  values (Fig. 2). This finding revealed that all of the scales contribute with important complementary information related to characteristic aspects of investigated extracts. Moreover, it could be observed that in case of fluorescence quenching, green and gray scales seems to provide the most significant quantity of information related to the investigated extracts.

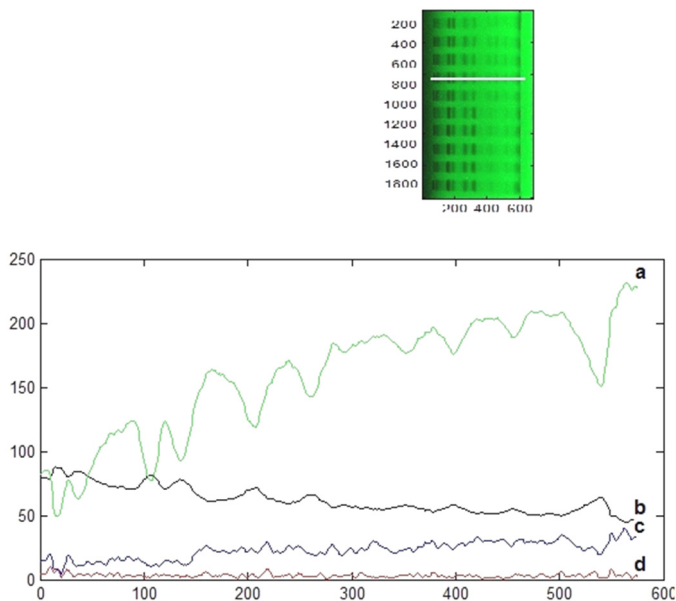


**Figure 2.** Digitized HPTLC chromatograms obtained by processing the UV image (fluorescence quenching) of chromatographic plate using TLC Analyser software on different colour scale: (a) green (Gn); (b) gray (Gy); (c) blue (B); (d) red (R) scale

For more insights, the PCA technique was applied on data matrices represented by numerical values of gray and pure RGB color intensity (as independent variables) corresponding to the associated  $R_f$  values. Based on the PCA investigations, the most significant results are discussed as follows.



Using the image acquired under UV light at  $\lambda = 254$  nm by digital camera, the first principal component (PC1, representing 93.89 % of the total variance in the data set) was associated with the upper edge of the plate ( $R_f = 0.975$ ) while the second PC (PC2, accounting 5.96% from the data variability) was associated with the bottom area of the plate ( $R_f = 0.02$ ). Considering also the third PC (PC3, accounting only 0.100% of data variability) the area associated to the middle of the plate ( $R_f = 0.44$ ) could be investigated. By a graphical representation of the first two PCs (Fig. 3) no significant differences were revealed between information provided by red and blue scale selection while each of the gray and green scales account for supplementary information on the investigated extracts. Moreover, by using the green scale for investigation, a good separation of the extracts according to the provenience (commercial manufacturers) could be observed.

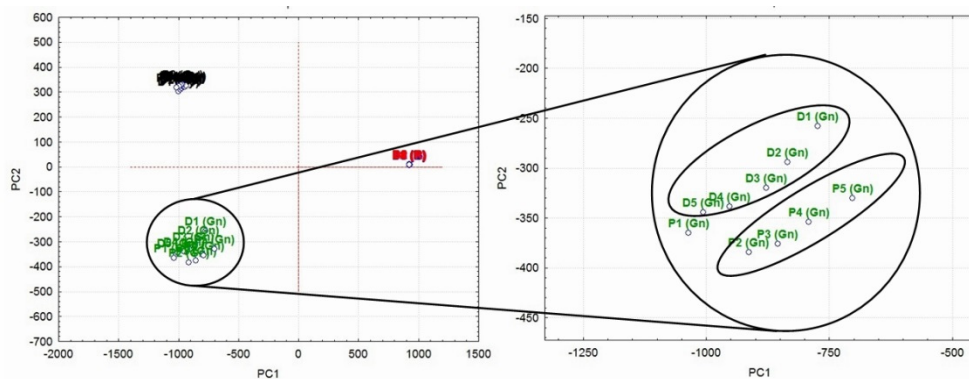


**Figure 3.** PCA classification of the investigated extracts (according to PC1 vs. PC2 representation) based on chromatographic fingerprints provided by UV254 image (acquired with digital camera) digitized through the gray (Gy) and red (R), blue (B), green (Gn) color scale selection

Considering the contribution of the PC3, the representation PC1 vs. PC3 (Fig. 4) shows, on green and gray scale, a good separation of the investigated samples according to their provenience.

The PCA investigations of the data matrices, provided by TLC image (fluorescence quenching) acquired with the scanner device revealed that the first three PCs explain 99.82% of the total variability. The PC1 variable (accounting for 96.22% of data variability) was associated with the upper area of the plate ( $R_f = 0.97$ ) while the PC2 (accounting for 3.43% of data variability) was associated with the bottom area of the plate ( $R_f = 0.03$ ).

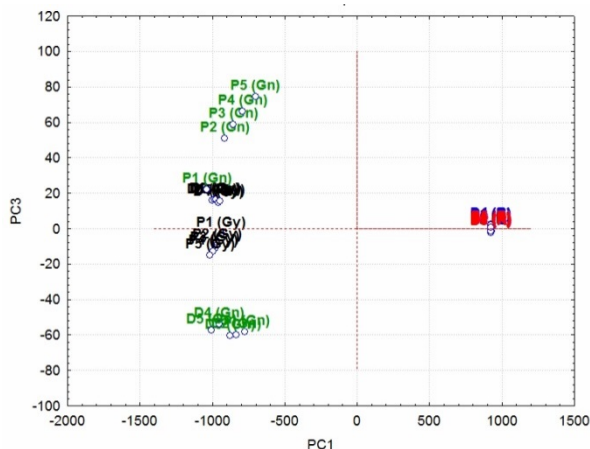


**Figure 4.** PCA classification of the investigated extracts (according to PC1 vs. PC3 representation) based on chromatographic fingerprints provided by UV<sub>254</sub> image acquired using Nikon digital camera and green (Gn), gray (Gy), blue (B) and red (R) scale selection for image processing.

According to the PC1 vs. PC2 representation (Fig. 5), it could be observed a differentiation of information provided by red and blue scales and also an improved quantity of information provided by green and gray scales respectively. As previously observed, on the green scale the samples are classified according to their provenience (commercially manufacturers).

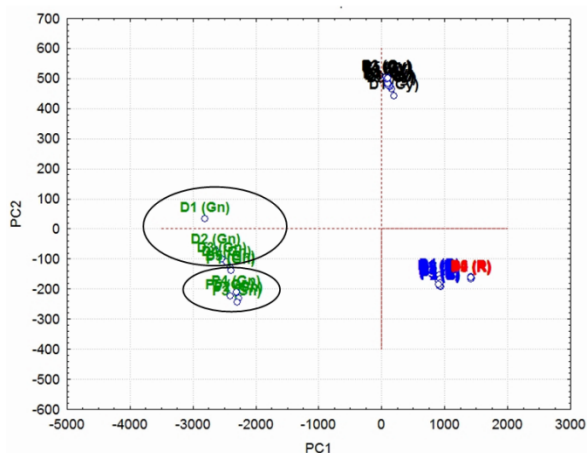


**Figure 5.** PCA classification of the investigated extracts (according to PC1 vs. PC2 representation) based on chromatographic fingerprints provided by UV<sub>254</sub> image acquired using TLC scanner device and green, gray, blue and red scale selection for image processing.

In case of the plate documented under UV at  $\lambda = 366$  nm both images acquired using digital camera and UV-Vis TLC scanner device respectively provided significant information related to the investigated samples.

The PCA investigations on the data matrices provided by digital camera images revealed that the first eight PCs explain more than 99.48% of the data variability. The PC1 variable (accounting for 82.26% of data variability) was associated with the area of the plate corresponding to  $R_f=0.37$  while the PC2 and PC3 variables (accounting for 13.35% of data variability and 1.75% respectively) were associated with the areas that correspond to a  $R_f$  values of 0.39 and 0.93 respectively. In this case, the PC1 vs. PC2 representation shows a good separation between information provided by each scale (Fig. 6).

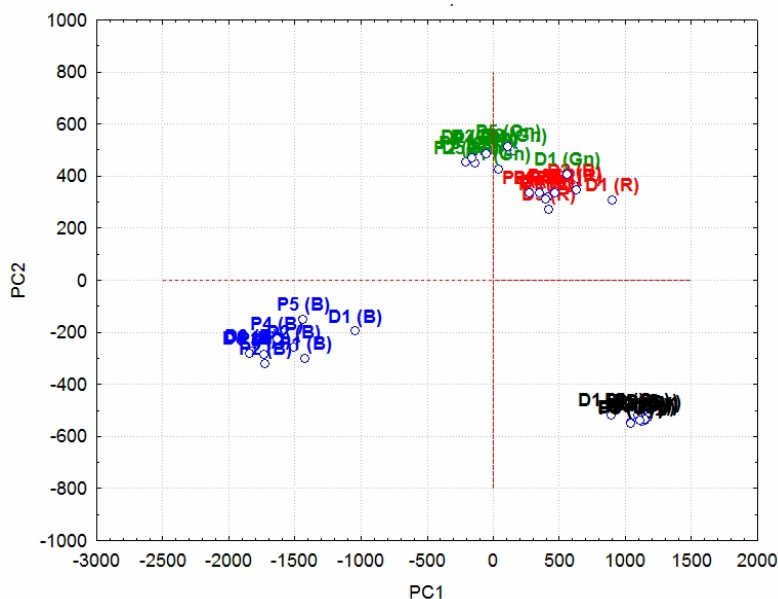


**Figure 6.** PCA classification of the investigated extracts (according to PC1 vs. PC2 representation) based on chromatographic fingerprints provided by UV<sub>366</sub> image acquired using Nikon digital camera and green (Gn), gray (Gy), blue (B) and red (R) scale selection for image processing.

Moreover, according to the PC4 contribution (accounting for 0.66% of data variability) a good differentiation of the investigated samples based on the extraction system composition was achieved when grey and green scale were used (Fig. 7)

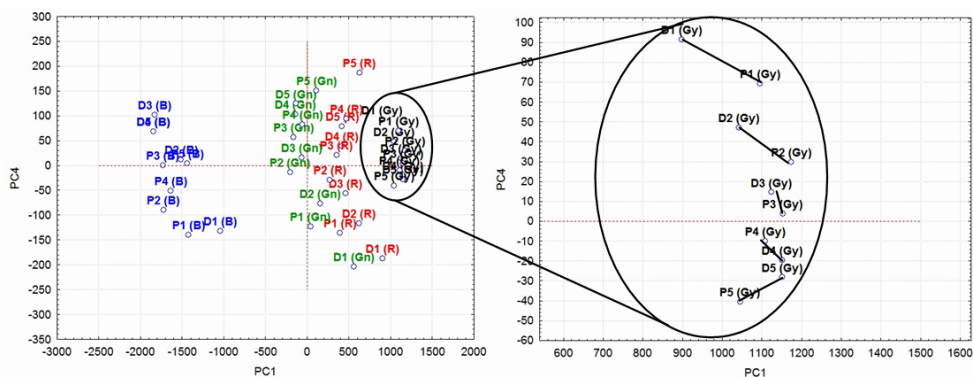


**Figure 7.** PCA classification of the investigated extracts (according to PC1 vs. PC4 representation) based on chromatographic fingerprints provided by UV<sub>366</sub> image acquired using Nikon digital camera and green (Gn), gray (Gy), blue (B) and red (R) scale selection for image processing.

Similar results were obtained based on PCA investigations on data matrices provided by images acquired using UV-Vis TLC scanner device and UV light at  $\lambda = 366$  nm for chromatographic plate documentation (Fig. 8). In this case the PC1 variable (accounting for 60.55% of data variability) was associated with the area of the plate corresponding to  $R_f$  values 0.36 while the PC2 variables (accounting for 32.45%) was associated with the area of the plate corresponding to  $R_f$  values of 0.94.

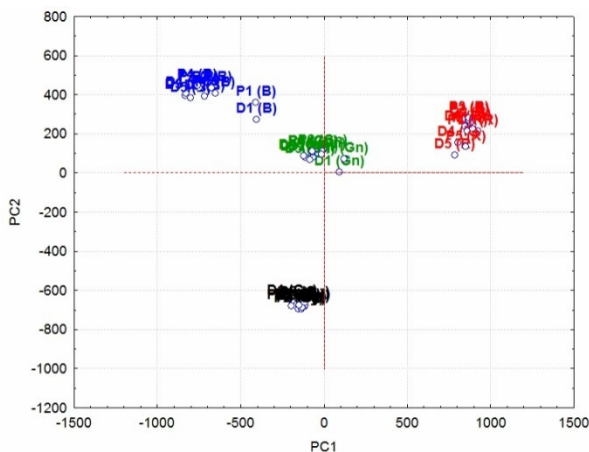


**Figure 8.** PCA classification of the investigated extracts (according to PC1 vs. PC2 representation) based on chromatographic fingerprints provided by UV<sub>366</sub> image acquired using TLC scanner device and green (Gn), gray (Gy), blue (B) and red (R) scale selection for image processing.

Considering PC3 which represents 2.48% of data variability, the graphical representation of PC1 vs. PC3 revealed the tendency of samples differentiating based on the composition of the extraction system (Fig. 9).

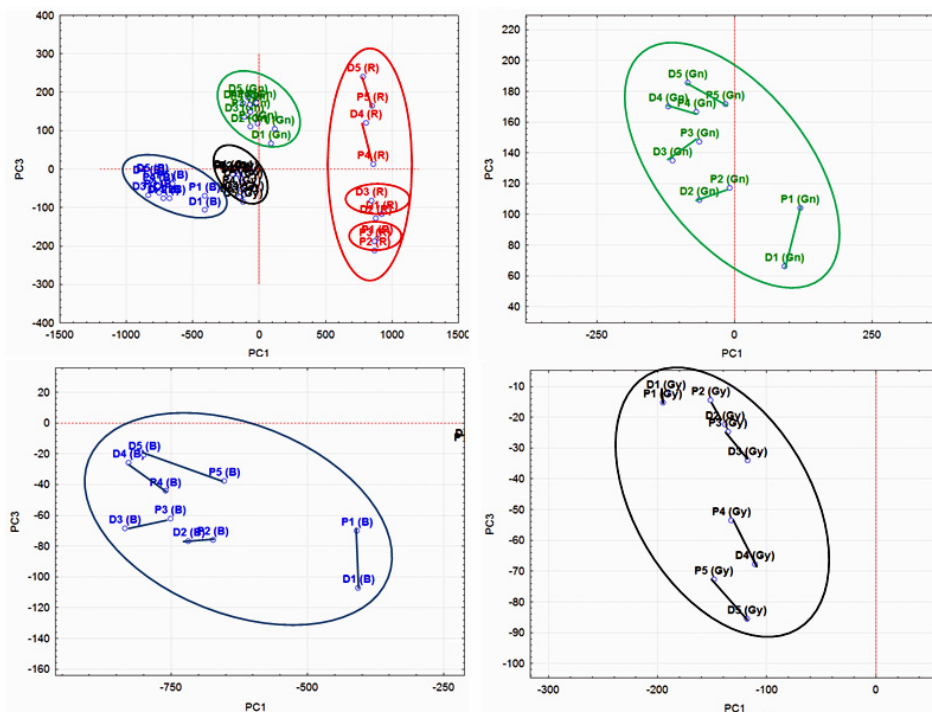


**Figure 9.** PCA classification of the investigated extracts (according to PC1 vs. PC3 representation) based on chromatographic fingerprints provided by UV<sub>366</sub> image acquired using TLC scanner device and green (Gn), gray (Gy), blue (B) and red (R) scale selection for image processing.

Apart of gray, green and blue scale, the red one provides a mixed classification of the extracts: by producer for extract 1-3 (D1-D2-D3 and P1-P2-P3) and by extraction solvent composition for extracts 4 and 5 (D4-P4; D5-P5).

Based on the above observations it can be concluded that the information provided by images acquired under UV light at  $\lambda = 254$  nm processed on green and gray scale are suitable for samples differentiation by their origin while the information provided by images acquired under UV light at  $\lambda = 366$  nm and processed on green, gray and blue scale are appropriate for samples classification according to the composition of the system used for extraction procedure.

## CONCLUSIONS

Using various hydroalcoholic extracts from dry vegetal material of *Gallium verum* plant as test samples for investigations, important aspects related to the HPTLC-IA technique combined with PCA were highlighted.

Based on the obtained results it could be concluded that for image acquisition procedure each of the investigated systems (advanced digital camera and UV-Vis TLC scanner device) were able to provide sufficient information for fingerprint investigation.

The images acquired under UV light at both  $\lambda = 254$  nm and respectively at  $\lambda = 366$  nm provides complementary information which are necessary for a complete characterization of complex matrices such as those of extracts from natural plants.

Good differentiation of vegetal samples having different origin (different manufacturers) was obtained by PCA analysis of the chromatographic data provided by fingerprints on UV254 images using green and gray scale selection for chromatograms processing. Classification of extracts according to the composition of extraction system can be achieved using UV<sub>366</sub> image processing on green, gray and blue scale selection.

HPTLC-IA methodology combined with the PCA technique can be considered a powerful tool in the characterization, authentication, and quality evaluation of extracts from natural plants.

## EXPERIMENTAL SECTION

### Material and methods

#### *Reagents and chemicals*

Analytical grade organic solvents ethanol, ethyl acetate, formic acid and toluene were purchased from Merck (Darmstadt, Germany). Chromatographic separations were carried out on HPTLC Silca gel G 60 F<sub>254</sub> (20x10) plates purchased from Merck (Darmstadt, Germany). NTS reagent (2-aminoethyl diphenylborinate, 98%) was from Alfa Aesar (Karlsruhe, Germany).

#### *Sample preparation and HPTLC developments*

*Gallium verum* dry plant for infusion, from Dacia and respectively Plafar manufacturers (Romania), was milled and sieved. The fine powder fractions, with particle size  $d_p < 250$   $\mu\text{m}$ , were used for extraction procedure. The extracts were obtained by 15 days maceration at room temperature using 0.5 g of powder material and 25 mL hydroalcoholic mixtures of ethanol - water in different ratio

(100:0; 90:10; 80:20; 70:30; 60:40, v/v). All the obtained extracts were separated from the vegetal material by filtration and stored protected from light at 4 °C temperature. Volumes of 20 µL from each extract were applied on HPTLC Silica gel 60 F<sub>254</sub> plate (20 × 10 cm) as 10 mm band using the Linomat 5 TLC applicator (Camag, Muttenz, Switzerland) with an application rate of 60 nL/s. The chromatographic separation was performed in the normal chamber 20 × 10 cm (CAMAG, Muttenz, Switzerland) with a mixture of ethyl acetate – toluene - formic acid - water (30:1.5:4:3, v/v/v/v) up to a migration distance of 8 cm (from the lower plate edge). After the plate was dried their documentation was first performed under UV light at 254 nm (fluorescence quenching) and then sprayed with NTS solution and documented under UV light at 366 nm.

### **Image acquisition and processing**

In both cases of visualising, the plate image was captured in two ways; using an advanced digital camera (Nikon D3100, Nikon Corp., Japan, image size of 1922 × 952 pixel) and a specialized UV-Vis TLC scanner device (the second-generation instrument for quantitative measurements in TLC, equipped with high qualified Micortek 3-linear color CCD camera with a resolution of 300DPI, BioDit Technology, Co.) respectively. For the multivariate analysis of HPTLC data, the RGB images of chromatograms visualized by fluorescence quenching (UV<sub>254</sub> image) and under 366 UV light after spraying with NTS (UV<sub>366</sub> image) were converted into gray (Gy), green (Gn), blue (B) and red (R) pure color scales. The obtained images were further processed with the TLC Analyser software ([http://www.sciencebuddies.org/science-research-papers/tlc\\_analyzer.shtml](http://www.sciencebuddies.org/science-research-papers/tlc_analyzer.shtml)) and transformed into numerical data.

### **Multivariate data analysis**

Among various computational chemometric methods, especially those classified as multivariate exploratory techniques are used to extract systematic information often dispersed over large sets of data. The principal component analysis (PCA), a linear dimensionality reduction technique is the most employed in many chromatographic investigations [27–29]. This is because of its capacity to reduce the dimensionality of the original dataset by retaining the maximum variability of a large number of variables by few underlying factors (principal components - PCs) which explain most of the data variability without losing the important information. In this case the data matrix was composed of numerical values (as independent variables) related to intensities on separated chromatographic bands corresponding to well defined R<sub>F</sub> values calculated according to the total units considered from the start to front of the plate. For PCA investigation developed on the obtained HPTLC data the Statistica 8.0 (StatSoft, Inc. 1984–2007, Tulsa, USA) software package was used.

## ACKNOWLEDGMENTS

This work was possible with the financial support offered by Romanian Ministry of Education, Research, Youth and Sports through research project PN-II-ID-PCE-2011-3-0366.

## REFERENCES

1. B. Hemmateenejad, N. Mobaraki, F. Shakerizadeh-Shirazi, R. Miri, *Analyst*, **2010**, *135*, 1747.
2. L.A. Fazakas, R.D. Nascu-Briciu, C. Sârbu, *Journal of Liquid Chromatography & Related Technologies*, **2011**, *34*, 2315.
3. M. Olech, Ł. Komsta, R. Nowak, Ł. Cieśla, M. Waksmundzka-Hajnos, *Food Chemistry*, **2012**, *132*, 549.
4. C. Tistaert, B. Dejaegher, Y.V. Heyden, *Analytica Chimica Acta*, **2011**, *690*, 148.
5. K. Misra, R. Tulsawani, R. Shyam, D.K. Meena, G. Morlock, *Journal of Liquid Chromatography & Related Technologies*, **2012**, *35*, 1364.
6. M. Gupta, M. Singh, H.M. Mukhatr, S. Ahmad, *Pharmacognosy Journal*, **2010**, *2*, 381.
7. H. Wagner, R. Bauer, D. Melchart, P.-Gen Xiao, A. Staudinger, Chromatographic fingerprint analysis of herbal medicines. Thin-layer and High Performance Liquid Chromatography of chinese drugs, Vol. 1, Second Revised and Enlarged Edition, Springer, Wien, New York, **2011**.
8. R. Tian, P. Xie, H. Liu, *Journal of Chromatography A*, **2009**, *1216*, 2150.
9. D. Milojković-Opsenica, P. Ristivojević, F. Andric, J. Trifković, *Chromatographia*, **2013**, *76*, 1239.
10. I.A. Sima (Tuhuțiu), D. Casoni, C. Sârbu, *Talanta*, **2013**, *114*, 117.
11. P. Ristivojević, J. Trifković, I. Vovk, D. Milojković-Opsenica, *Talanta*, **2017**, *162*, 72.
12. A. Bansal, V. Chhabra, R.K. Rawal, S. Sharma, *Journal of Pharmaceutical Analysis*, **2014**, *4*, 223.
13. N. Popović, J. Sherma, *Trends in Chromatography*, **2014**, *9*, 21.
14. R.T. Tian, P.S. Xie, H.P. Liu, *Journal of Chromatography A*, **2009**, *1216*, 2150.
15. G.E. Morlock, P. Ristivojevic, E.S. Chernetsova, *Journal of Chromatography A*, **2014**, *1328*, 104.
16. K.H. Wong, V. Razmovski-Naumovski, K.M. Li, G.Q. Li, K. Chan, *Journal of Pharmaceutical and Biomedical Analysis*, **2014**, *95*, 11.
17. P.S. Xie, S. Sun, S. Xu, L. Guo, *Journal of Chromatography & Separation Techniques*, **2014**, *5*, 249.
18. T. Tang, W. Guo, Y. Xu, S. Zhang, X. Xu, D. Wang, Z. Zhao, L. Zhua, D. Yang, *Phytochemical Analysis*, **2014**, *25*, 266.



19. P. Ristivojević, F.Lj Andrić, J.Đ. Trifković, I. Vovk, L.Ž. Stanisavljević, Ž.Lj Tešić, D.M. Milojković-Opsenica, *Journal of Chemometrics*, **2014**, *28*, 301.
20. G.E. Morlock, P. Ristivojevic, E.S. Chernetsova, *Journal of Chromatography A*, **2014**, *1328*, 104.
21. J.M. Bosque-Sendra, L. Cuadros-Rodriguez, C. Ruiz-Samblas, A. Paulina de la Mata, *Analytica Chimica Acta*, **2012**, *724*, 1.
22. H. Atmaca, E. Bozkurt, M. Cittan, H.D. Tepe, *Journal of Ethnopharmacology*, **2016**, *186*, 305.
23. N. Chaher, S. Krisa, J.C. Delaunay, S. Bernillon, E. Pedrot, J.M. Mérillon, D. Atmani, T. Richard, *Journal of Pharmaceutical and Biomedical Analysis*, **2016**, *117*, 79.
24. M. Tamas, D. Stana, S. Timis, *Notulae Botanicae Horti Agrobotanici Cluj-Napoca*, **2006**, *34*, 1842.
25. L.O. Demirezer, F. Urbuz, Z. Guvenalp, K. Stroch, A. Zeeck, *Turkish Journal of Chemistry*, **2006**, *30*, 525.
26. A. Chevallier, *Enciclopedia of Herbal Medicine*, Ed. DK Penguin Random House, **2016**, 214.
27. D. Casoni, C. Sârbu, *Spectrochimica Acta Part A: Molecular and Biomolecular Spectroscopy*, **2014**, *118*, 343.
28. A. Kume, S. Kawai, R. Kato, S. Iwata, K. Shimizu, H. Honda, *Journal of Bioscience and Bioengineering*, **2016**, *20*, 1.
29. K.K. Vasani, B. Surendiran, *Perspectives in Science*, **2016**, *8*, 510.

*Dedicated to Professor Costel Sârbu on the  
Occasion of His 65<sup>th</sup> Anniversary*

## ALGORITHM FOR ASSESING SOIL REHABILITATION OF STERILE DUMPS

**ANDREEA BRASOVAN<sup>a</sup>, RAMONA FLAVIA BURTESCU<sup>b</sup>,  
NELI-KINGA OLAH<sup>b,c,\*</sup>, IOAN PETEAN<sup>d</sup>, VLAD CODREA<sup>a</sup>,  
ANDREI BURTESCU<sup>e</sup>**

**ABSTRACT.** Ileana Veche is the most representative waste rock (sterile) dump formed by the coal mining activities in Lupeni (Petroșani Basin). We developed an algorithm based on the computational engineering concepts in order to establish the connection between the waste rock soil particles composition and the dump rehabilitation by Scots Pine (*Pinus sylvestris*). The results show that the Ileana Veche pit coal dump features minerals suitable for plants growth like: calcite, biotite, potassium feldspar and chemically inert one as quartz. The quantitative measurements prove that the soil minerals are enough to allow a fair growing of the *P. sylvestris* population able to start the soil type conversion from the entantrosoil type to a more fertile one. The measurements found that the upper soil presents humus formation and features nitrogen and phosphorous while in the deeper layer are missing.

**Keywords:** coal mining, coal dump, rehabilitation, mineralogy, Petroșani Basin, Romania.

---

<sup>a</sup> Babeș-Bolyai University of Cluj-Napoca, 1 Kogălniceanu Str., 400084, Cluj-Napoca, Romania

<sup>b</sup> SC PlantExtrakt SRL, 407059 Rădaia. Cluj, Romania

<sup>c</sup> "Vasile Goldis" Western University of Arad, Faculty of Pharmacy, 86 Rebreanu Street, Arad, Romania

<sup>d</sup> Technical University of Cluj-Napoca, Faculty of Materials Science and Engineering, Muncii Ave. No.103-105, Cluj-Napoca, Romania

<sup>e</sup> Technical University of Cluj-Napoca, Faculty of Mechanical Engineering and Mechatronics, Muncii Ave. No.103-105, Cluj-Napoca, Romania

\* Correspondent author: nelolah@yahoo.com

## INTRODUCTION

Petroșani is one of the main post-tectonic sedimentary basins of the Southern Carpathians. The sedimentary fillings are composed of Paleogene and Miocene deposits [1]. Several Paleogene coal beds were and still are exploited. The main coal deposits occur in the so-called “second (middle) horizon” or “lower productive”, part of the Dâlja-Uricani Formation (early Eggerian) [2]. This formation bears 22 coal beds, but only 11 are thick enough to have economic value. The sedimentary succession includes repetitive interleaving of lacustrine (bituminous shale, coal), brackish (clay, marl, dysodyle shale) and subordinate marine deposits [1-3]. The bituminous coal was under the influence of the tectonic metamorphism, i.e. pressure and temperature due to the basin compression after its filling with sediments [4]. Such mining exploitation involved coal and sterile rocks (waste rock), which is stored in sterile dumps.

Ileana Veche was the first dump resulted from Lupeni mining processes. It was built up by sterile discharging directly from the trolleys on a suspended railway system. It is oriented on east-western direction as a particularly consequence of sterile depositing. The dumping ceased in 1980. Nowadays it is fully covered by pines (*P. sylvestris*) that seem to record a healthy growth. Planting trees is a proper solution to fix and greening the coal dumps as reported in literature [5, 6]. *P. sylvestris* was also used abroad in cases of settling [7] and for plant-rehabilitation of the coal dumps [5, 6].

However, the dump was rebuilt in the last years in terraces and platforms, with low slope angles [8, 9, 34, 35]. To reduce the out-flow from the dump, two drainage systems were built, one on the northern side of the dump, which was connected to second drainage system on the western side.

According to the actual soil taxonomy, the soil covering this coal dump belongs to entantrosols [10, 28]. Studies on these soils issued from industrial works, in terms of composition and morphology can yield important data for dump rehabilitation [11, 12]. The landfills and dumps rehabilitation are very important works during environment ecology processing [5, 6]. Some recent studies are following this trend also in Romania [13, 11, 12].

The environmental analysis and prediction tendency are to use modern computational algorithms [14, 15]. Even the environmental rehabilitation supported computational treatment and monitoring [16]. Recently, the computational and engineering algorithms are employed to modeling physical phenomena such as thermodynamic processes [17]. Such approach could be extended to other processes such as landfill and dumps rehabilitation. Further, we develop an algorithm to evaluate the rehabilitation process of Ileana Veche sterile dump.

The measure of the dump rehabilitation is related to the satisfactory response to the critical questions raised by the designed algorithm. The specific analyses performed on the soil samples leads to an answer to the algorithm questions. Further, the algorithm shows whether the rehabilitation process is well developed or not.

## RESULTS AND DISCUSSION

The sterile resulting from the technological flow of coal exploitation is deposited in waste dumps. This constitutes the dumps entiantrosoil. In this case appear certain critical questions affecting the dump rehabilitation, ie the entiantrosoil transformation into a more fertile soil [18, 19, 36]. As mentioned before [17], some operational steps could be modeled by a general logic cycle instruction as presented in Eq. (1):

$$\left[ \begin{array}{l} \text{DO WHILE (CONDITIONS)} \\ \text{BEGIN} \\ \text{Cycling instructions} \\ \text{END} \end{array} \right. = LC \quad (1)$$

The algorithm could use such cycled instructions (LC) for each critical questions regarding the dump rehabilitation. Furthermore, the final algorithm will have a form like Eq. (2):

$$\left[ \begin{array}{l} \text{REHABILITATION ALGORITHM} \\ \text{BEGIN} \\ LC_1 \rightarrow LC_2 \rightarrow LC_n \\ \text{END} \end{array} \right. \quad (2)$$

We designed the algorithm suitable for any pit coal sterile dump rehabilitation considering the critical questions and presented cycling instruction. The logical scheme for the designed algorithm is presented in Fig.1. and it is suitable for any programming environment. It features all elements necessary for a proper computational program; each critical question “Q” represents the cycling condition for each step meanwhile the remedy “R” represents the cycling instruction. The “remedy” is cycled while the answer to the critical condition “Q” is proper. Once a step is passed, the following step is cycled until the FINISH instruction occurs.

Our research has been made for two soil samples, one from the surface (AS<sub>1</sub>) and another from a depth of 1 m (AS<sub>2</sub>).

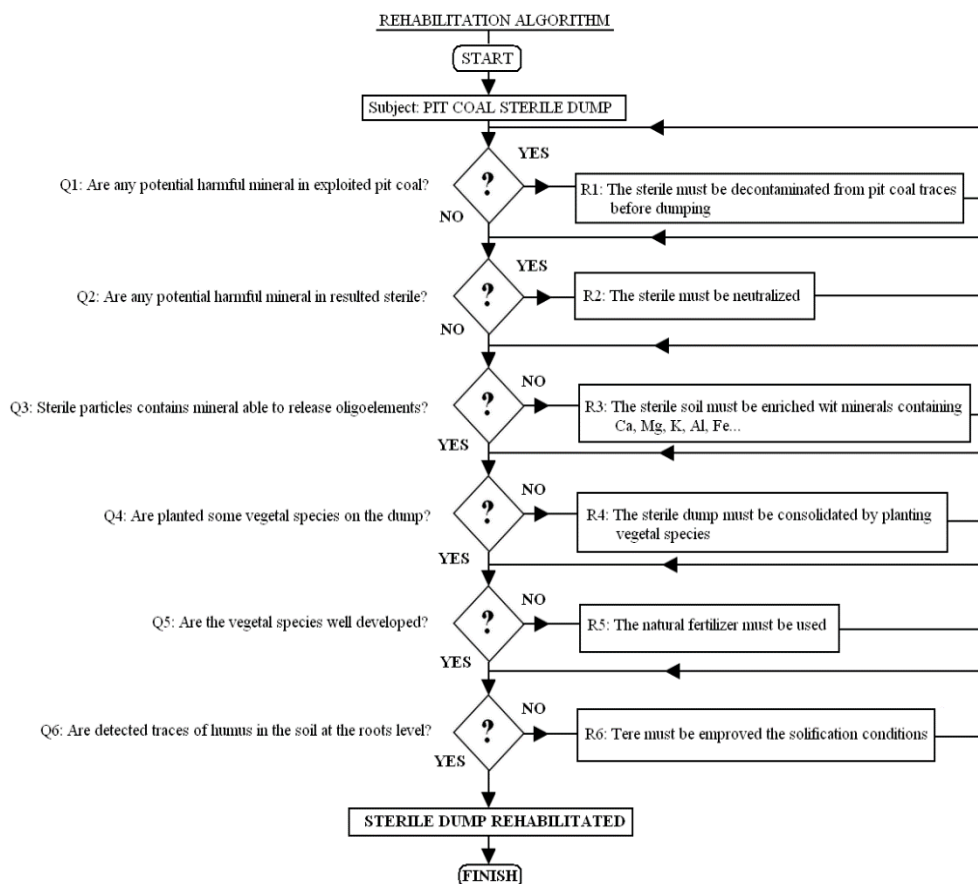


**Figure 1.** The sterile dump rehabilitation algorithm

$Q_1$  question refers to the mineralogical composition of exploited coal and the possible/potentially harmful effect to the environment. The answer to this question has been elaborated in mineralogy and crystallography analyzes achieved by average coal sample. The diffraction results are shown in Figure 2.

The general appearance of the diffractogram (fig 2.a) shows an amorphous mass base conferring a specific allure with a „hump”. We observe that the overlapping variation identified distinct diffraction peaks which exceed the neutral background radiation. They are the result of the presence of accompanying minerals. Following the standard procedures has been identified these components.

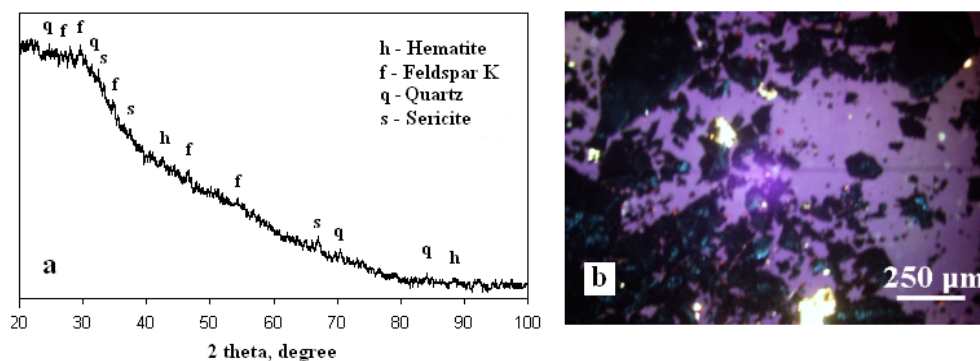


**Figure 2.** The pit coal from Lupeni average representative sample APCS: a) X-ray diffraction pattern and b) optical cross polarized light microphotograph

In the coal from E.M. Lupeni have been identified the following minerals as crystalline constituents in coal sample: -  $\text{SiO}_2$  quartz, -  $\text{Fe}_2\text{O}_3$  hematite, sericite,  $\text{KAl}_2(\text{Si}_3\text{Al})\text{O}_{10}(\text{OH},\text{F})_2$ , -  $\text{K}(\text{AlSi}_3\text{O}_8)$  potassium feldspar.

Minerals found in the average coal sample correspond to the chemical composition reported in previous studies [20, 21, 22]. Low mineral content is proven by small peaks present in the diffractogram (fig. 2.a). Optical microscopy in polarized light confirmed the results obtained by X-ray diffraction, (fig. 2.b). Are observed quartz particles with gray-green color, with a diameter of 25 μm, potassium feldspar particles which appear bright white with a diameter of 200 μm, hematite particles which color vary from dark blue to gray and then to brown-red, depending on the particle position toward the optical microscope axis.

The diffractogram allure is specific to an amorphous material, represented by the carbon mass specific to the coal. There were identified diffraction peaks specific to quartz, potassium feldspar, sericite and hematite, but with a very low relative intensity in relation to the diffractogram background. The minimum concentration of the crystalline compound identifiable with DRON 3 diffractometer is between 1-3% depending on the specificity and sample preparation. Diffraction peaks identified in diffractogram (fig 2.a) are very close to the detection limit, because it comes from a crystalline material content a little over 3%. The fact itself indicates a very low content of crystalline material in the composition of investigated coal.

The information from literature indicates the ash content of the burning coal between 5-40% [4], that means between 5 and 40% sterile inclusions, which are usually present in crystalline form. Consequently by X-ray diffraction we

can appreciate the content of crystalline material accompanying the investigated coal samples, to be around the 5%, value for the summe of crystalline compounds. Therefore the investigated coal samples from Lupeni are of the highest quality. All minerals found in the average coal sample are commonly found in the natural environment and does not generates pollution risk.

The results of elementary analyzes performed for sample are consistent with the results obtained by Rebrişoreanu 2002 [22]. The major component is the silicon from quartz. Silicon, aluminum and potassium oxides are found in potassium feldspar and sericite.  $Fe_2O_3$  iron oxide crystallized in the rhombohedral system is present in hematite.

Crystalline inclusions from coal sample can be found in sterile dump only in certain circumstances, but their dominant effect is found in ash from burnt coal. Recent studies show that potassium feldspar and sericite is converted to mullite, while hematite is dried and becomes goetia [23]. The sterile dump is not normally exposed to intense combustion, therefore it is expected that some crystalline phases to maintain a long period of time. In addition, it is possible that some crystalline inclusions from the carbon not to be found in sterile dump due to different petrogenesis.

The answer to the critical question  $Q_1$  is negative, which can be observed from the results of average coal sample measurements. This means that we could pass to the evaluation of critical question  $Q_2$ . This item refers to the mineralogical composition of the soil samples  $AS_1$ ,  $AS_2$ , for the sterile dump Ileana Veche from Lupeni.

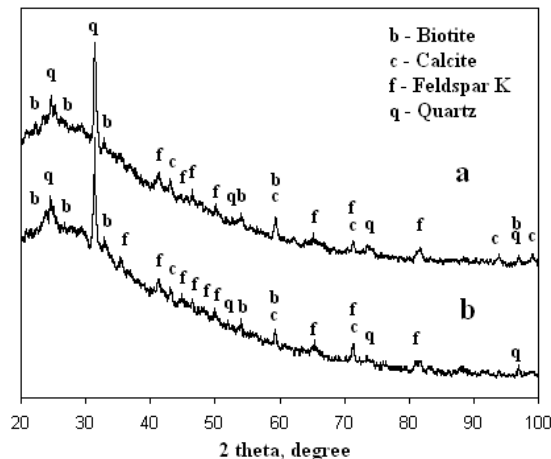


**Figure 3.** X-ray diffraction patterns for the soil samples collected from Ileana Veche – Lupeni sterile dump: a)  $AS_1$  and b)  $AS_2$

The two soil samples AS<sub>1</sub> and AS<sub>2</sub> collected from the sterile dump were investigated by X-ray diffraction and the obtained patterns are shown in Figure 3. In both samples are observed diffraction peaks well defined and different stages of crystallization.

AS<sub>1</sub> collected from the roots level of *P. sylvestris* is rich in quartz and potassium feldspar (minerals encountered in average coal sample). We also found significant amounts of CaCO<sub>3</sub> - calcite and H<sub>4</sub>K<sub>2</sub>Mg<sub>6</sub>Al<sub>2</sub>Si<sub>6</sub>O<sub>24</sub> - biotite. The minerals found in AS<sub>1</sub> are very similar to those found in soil samples from the sea buckthorn level roots of the West Well 7 from Vulcan sterile dump [24]. These minerals come from sterile intercalations of coal layers of sedimentary formation Dâlja-Uricani represented by sandstones and marl.

Therefore, quartz is the major component of sterile dump, about 50%, as evidenced by the diffractogram (fig. 3), in which the diffraction peaks are 100%. Diffraction peaks for other minerals not exceed 50% and are represented in AS<sub>1</sub> by potassium feldspar, calcite and biotite. Elemental analysis provides a more precise distribution of the elements from AS<sub>1</sub>. Lack of hematites and sericites from AS<sub>1</sub> and AS<sub>2</sub> shows that coal is well sorted / separate from sterile.

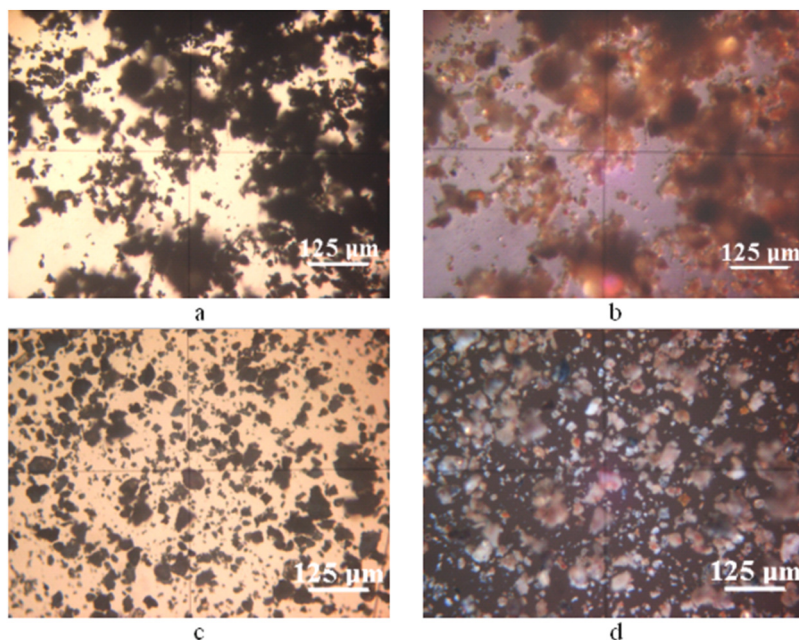


**Figure 4.** Optical microscopy inspection of AS<sub>1</sub> and AS<sub>2</sub> samples:  
 a) AS<sub>1</sub> transmitted light; b) AS<sub>1</sub> cross polarized light;  
 c) AS<sub>2</sub> transmitted light; d) AS<sub>2</sub> cross polarized light.



X-ray diffraction pattern for AS<sub>2</sub> (fig. 3) reveals similar mineralogical aspects as AS<sub>1</sub>, because also in this sample we find quartz, potassium feldspar, biotite and calcite particles. This proves that both samples were collected from the same sterile dump and come from sediments present between coal layers from Lupeni. This gives a negative answer the critical question Q<sub>2</sub>.

Critical question Q<sub>3</sub> refers to the ability of soil to release oligoelements as Ca, Mg, K, Fe, Al, useful for vegetation development. The answer depends on the resulting data from X-ray diffraction reported to the microstructure sample.

AS<sub>1</sub> sample provides information about the particle size between 20 and 150 µm as shown in Figure 4.a. The distribution of particles is unusual as an aspect for industrially processed particles [23]. Further data was obtained by optical microscopy in crossed polarized light (fig. 4.b). In this figure it can be observed the quartz minerals such as grain, yellowish-brown calcite, potassium feldspar and biotite (the reddish-brown due to the presence of Fe and Mg), in diameter around 20 µm related to the organic material. The organic material is expected to be humus formed by *P. sylvestris* roots that populate the sterile dump.

AS<sub>2</sub> microstructure (fig. 4.c) reveals a totally different particle distribution than AS<sub>1</sub>. The particles are well dispersed, individually disposed, without any binder. The crossed polarized light (fig. 4.d) reveals a large amount of quartz and calcite minerals, similar to spherical grains with average diameter around 20 µm, while the potassium feldspar and biotite has a lamellar - tabulated form with an average plan diameter of 15 µm. In terms of the microstructural investigations AS<sub>2</sub> is an initial entiantro-soil while AS<sub>1</sub> is a rehabilitated soil.

The quartz particles are stable physically and chemically, representing the foundation soil. Calcite particles are very sensitive to interaction with water, being able to release Ca<sup>2+</sup>. Recent studies have revealed that the clay minerals are capable of releasing ions under conditions of high humidity [25, 26]. Considering this hypothesis, the AS<sub>1</sub> and AS<sub>2</sub> soils are able to provide the most important oligoelements required to develop vegetation. The potassium feldspar is able to release K<sup>+</sup> and Al<sup>3+</sup>, while the biotite is able to release Mg<sup>2+</sup> and Fe<sup>3+</sup>. This is supported by X-ray fluorescence analysis for AS<sub>1</sub> and AS<sub>2</sub>, the data are presented in Table 1.

**Table 1.** The XRF elemental analysis results for the soil samples

Compound	Si <sup>4+</sup>	Al <sup>3+</sup>	Fe <sup>3+</sup>	Ca <sup>2+</sup>	K <sup>+</sup>	Mg <sup>2+</sup>
AS <sub>1</sub> , wt%	45.5	8.83	4.37	4.09	1.65	1.03
AS <sub>2</sub> , wt%	49.5	8.65	4.69	3.90	1.43	0.82

The data from the Table 1 show that the sample AS<sub>1</sub> is able to supply enough Ca, Mg, K, Fe to sustain a vegetation development. The answers to the Q<sub>3</sub> critical question is definitely affirmative, and the evaluating of the rehabilitation process could move forward to the following critical questions. The visual investigations performed on the sterile dump during the samples collection, answer affirmative to the critical questions Q<sub>4</sub> and Q<sub>5</sub>, which prove that the minerals from the sterile particles are to ensure the good development of the population of *P. sylvestris*. The covering the sterile dump with pine plantations proves to be a good method of rehabilitation. The results are in accordance with previously published data [7].

A critical question to the designed algorithm remains the Q<sub>6</sub> question. Answering this question is beside the soil analysis, much improved and presented in Table 2 with the standards values [27].

**Table 2.** Results of soil formation parameters

Soil formation parameter	Sterile dump Ileana Veche			
	AS <sub>1</sub>	AS <sub>2</sub>	Standard values	Evaluation
pH	7.20	7.08	0-14	Neutral
Humus, %	9	0.32	2.57-15	Good content at roots level
Total nitrogen, %	0.46	0.05	0.02-0.77	Moderate content
Phosphorus, ppm	0.11	0.06	Max. 11	Low content
Potassium, ppm	60.00	20.00	Max. 96	Moderate content

The pH of the AS<sub>1</sub> sample is very close to neutral value, which proves the balance between the acid behavior of the feldspar and biotite particles in contact with water, than the calcite particles, which proves an excellent basic behavior. Humus value is 9% for AS<sub>1</sub> while as for AS<sub>2</sub> is almost absent. The lack of humus in depth, in AS<sub>2</sub> sample shows that the soil-forming agent is the life cycle of *P. sylvestris* population.

The transition from the AS<sub>2</sub> entiantrosoil to the fertile soil of the AS<sub>1</sub> sample is also evidenced by the absorption of nitrogen and phosphorus from AS<sub>1</sub> particles, which is closely related to pine roots action. The measured value for potassium is significant and corresponds to a common fertile soil with moderate potassium. This can be explained by the stable chemical bonds achieved of K<sup>+</sup> in the structure of potassium feldspar which influences the release of the K<sup>+</sup> ion in the aqueous solution. Finally, the answer to the critical question Q<sub>6</sub> is affirmative, and we can conclude that Ileana Veche dump rehabilitation is well done.

## CONCLUSIONS

The designed algorithm proves to be suitable for assessing of the sterile dump rehabilitation through critical questions which refer to the influence of the soil mineralogical composition on the vegetation growth. This clearly shows that the successful rehabilitation of the sterile dump depends on the soil mineralogical composition. The designed algorithm could be developed into a proper programming environment with a better standard parameters database. It could be made in such a way to evaluate the state of sterile dump rehabilitation and to anticipate the needed measures to achieve a good level of rehabilitation. This algorithm can be applied as in the case of sterile dump West Well 7 from Vulcan which is rehabilitated with sea buckthorn or for the sterile dump from Câmpu lui Neag where we find more tree species and wild rose.

We employed a new modeling concept based on computational engineering in order to establish the relationship between the sterile soil particles composition and the dump rehabilitation by *P. sylvestris*. Our measurements established the mineralogical composition of Ileana Veche pit coal dump soils, with quartz, calcite, biotite and potassium feldspar. The minerals found in soil are also found as inclusion minerals into the pit coal, along with few traces of hematite and sericite. However, we observe that the pit coal composition do not affect the mineral composition of the sterile dump soil, organic matter being less than 1% in initial state. The quartz particles are a very good support for a proper soil formation. Calcite, biotite, and potassium feldspar represent proper vegetation source with oligoelements such Ca, Mg, K, Fe and Al in the presence of water.

The increasing value tendency of oligoelements in upper soil AS<sub>1</sub> was observed. Considering each modeling step evaluation, it results that the Ileana Veche pit coal dump has minerals suitable for vegetation growth (quartz, calcite, biotite and potash feldspar). The quantity of oligoelements provided by the soil minerals is enough to support the growing of the *P. sylvestris* population. According to this proposed computational model, the humus presence and the adsorption of phosphorous and nitrogen at the soil level confirms that the *P. sylvestris* population induce the transition from the entantrosoil category to fertile one. Finally, we may conclude that the rehabilitation of Ileana Veche pit coal dump achieve a good level of rehabilitation.

## EXPERIMENTAL SECTION

### Soil sampling

The soil samples were collected from the top surface and from a 1 m depth (beneath the *P. silvestris* roots), in ten representative collecting locations over the dump's surface. The average representative soil samples were obtained by mixing equal amounts from each sampling point. It result the top surface average sample (AS<sub>1</sub>) and depth average representative sample (AS<sub>2</sub>). The pit coal samples from Lupeni exploitation were collected from at least five different sorts. Each pit coal sample was grinded and equal quantities of resulted powder were mixed into an average pit coal sample (APCS).

### Mineralogical analysis

Mineralogical analysis was performed on the average samples by X-ray diffraction (XRD) analyses, using DRON 3 diffractometer with data acquisition module and Matmec VI.0 software, the X-ray characteristic being for cobalt Co  $\alpha$ . The diffraction peaks were identified using Standard X-Ray Diffraction Data Base – MATCH 1.0 from Crystal impact Co. The results obtained by X-ray diffraction were certified by the optical microscopy analysis, using a Karl Zeiss Jena mineralogical optical microscope.

The elemental analysis was performed according to the standard sampling and operating procedures using a Rigaku ZSX100 X-ray fluorescence spectrometer (XRF) in order to measure the main elements corresponding to the minerals identified by XRD. There was used a WDXRF wavelength detector for a wide range of atomic species. The samples were dried at 80 °C for 12 h, powdered (325 mesh) and mixed with boric acid in a 1:4 ratio (100 mg of sample and 400 mg of H<sub>3</sub>BO<sub>4</sub>). The mixture was pressed at 203 MPa for 10 minutes, obtaining 2,5 cm diameter pellets of 100 mg/cm<sup>2</sup> surface density. The results are read with the Spectra Plus software and the determination of elements is done using Dyna Match international database. The measurements and readings were made according to EN ISO 9001:2000. The final value represents the average of reading for 3 similar samples for both AS<sub>1</sub> and AS<sub>2</sub>.

The pH determination was performed on a potentiometer device INULAB®. The humus content in the AS<sub>1</sub> sample was measured by titration using Walkley-Black method [29, 30].

The nitrogen measurements were performed on a Panas-Wagner device according to the Kjeldahl method [31].

The phosphorus and potassium determinations were measured by Nikolov and Egner, Riehm, Domingo methods [32, 33] using a METERTECH SP 830 PLUS spectrometer.

## REFERENCES

1. E. Pop, "Monografia geologică a Bazinului Petroșani", Ed. Academiei Române, București, **1993**, 303.
2. V. Moiescu, *Revue Roumaine de Géologie, Géophysique et Géographie*, **1983**, 27, 53.
3. V. Moiescu, "Contributions à la connaissance de la faune de mollusques eggeriens prélevée du forage 19-Hobiceni (Bassin de Petroșani). In: The Oligocene from the Transylvanian Basin Romania", Cluj-Napoca, **1989**, 275.
4. I. Petrescu, M. Ionescu, "Zăcăminte de huile din Oligocenul Superior-Miocenul Inferior. Zăcămintele din Bazinul Petroșani. In: Petrescu, I, Bițoiianu, C, Nicorici, M, Mărgărit, Gh., Nicorici, E, Pătruțoiu, I, Todros, C, Popescu, D, Ionescu, M, Dușa, A, Munteanu, A, Buda, A., *Geologia zăcămintelor de cărbuni*", Ed. Tehnică, București, **1987**, 315, vol. 1, 387, vol. 2.
5. A.G. Khan, C. Kuek, T.M. Chaudhry, C.S. Khoo, W.J. Hayes, *Chemosphere*, **2000**, 41, 197.
6. Z. Stêpniewska, A. Wolińska, W. Pióro, *Polish Journal of Ecology*, **2007**, 55 (2), 139.
7. G. Szarek-Łukaszevska, K. Grodzińska, *Polish Journal of Ecology*, **2007**, 55 (2), 261.
8. C. Biro, "Reabilitarea terenurilor degradate de activitățile antropice din Bazinul minier Petroșani" Ph.D. Thesis, Universitatea Petrosani, **2005**.
9. I. Rotunjanu, "Asecarea și stabilitatea lucrărilor miniere în cariere", Ed. Litografică a Institutului de mine, Petroșani, **1984**.
10. C.V. Secu, C. Patriche, I. Vasiliu, *Aspects Regarding Correlation of the Romanian Soil Taxonomy System (2003) with WRB (2006)*. *Грунтознавство*, **2008**, Т. 9, 3–4, 56.
11. F. Damian, Gh. Damian, R. Lacatusu, Gh. Macovei, Gh. Iepure, I. Napradean, R. Chira, L. Kollar, L. Rata, D.C. Zaharia, *Carpathian Journal of Earth and Environmental Sciences*, **2008**, 3, 1, 85.
12. Gh. Damian, F. Damian, D. Nasui, C. Pop, C. Pricop, *Carpathian Journal of Earth and Environmental Sciences*, **2010**, 5, 1, 139.
13. C. Zaharia, D. Șuteu, *Environmental Engineering and Management Journal*, **2011**, 10, 11, 1693.
14. E. Petraitis, M. Pranskevičius, L.R. Izdelis, P. Vaitiekūnas, *Environmental Engineering and Management Journal*, **2011**, 10, 12, 1935.
15. V. Petrescu, G.O. Sumbasacu, N. Sîrbu, *Environmental Engineering and Management Journal*, **2011**, 10, 11, 1779.
16. M.E. Fortuna, I.M. Simion, M. Gavrilă, *Environmental Engineering and Management Journal*, **2011**, 10, 12, 1987.
17. G.R. Mocanu, A.D. Pop, G. Arghir, *Acta Technica Napocensis, Applied Mathematics and Mechanics Series*, **2011**, 54, 1, 179.

18. M. Cresser, K. Killham, T. Edwards, "Soil chemistry and its application", Cambridge University Press, Great Britain, **1993**.
19. J. Hassink, A.P. Whitmore, J. Kubat, *European Journal of Agronomy, Montrouge Cedex-France*, **1997**, 7, 189.
20. H.E. Belkin, S.J. Tewalt, J.C. Hower, J.D. Stucker, J.M.K. O'Keefe, C.A. Tatu, G. Buia, *International Journal of Coal Geolog*, **2010**, 60.
21. C. Panaitescu, "Petrologia cărbunilor, cocsurilor și produselor carbonice", Ed. Enciclopedica, București, **1991**, 324.
22. M. Rebrîșoreanu, E. Traistă, A. Matei, O. Barbu, V. Codrea, *The impact of the bituminous coal combustion from the thermoelectric power plant from Paroșeni on the environment of Jiu Valley*. Studia Universitatis Babeș-Bolyai, Geologia, Cluj-Napoca, **2002**, XLVII, 1: 117-126.
23. A. Brașovan, R.F. Câmpean, G. Arghir, V. Codrea, *Metalurgia International*, **2010**, XV, 7, 40.
24. A. Brașovan, V. Codrea, G. Arghir, R.F. Câmpean, I. Petean, *Carpatian Journal of Earth and Environmental Sciences*, **2011**, 6, 1, 221.
25. F. Tateo, V. Summa, M.L. Giannossi, G. Ferraro, *Applied Clay Science*, **2006**, 33, 181.
26. F. Tateo, V. Summa, *Applied Clay Science*, **2007**, 36, 64.
27. M. Dumitru, S. Dumitru, V. Tănase, V. Mocanu, A. Manea, N. Vrânceanu, M. Preda, M. Eftene, C. Ciobanu, I. Calciu, I. Rînovceanu, "Monitoringul stării de calitate a solurilor din România. Institutul național de cercetare-dezvoltare pentru pedologie agrochimie și protecția mediului IPCA București", Ed. Sitech Craiova, **2011**, 82.
28. I. Rotunjeanu, "Stabilitatea versanților și taluzurilor", Ed. Infomin, Deva, **2005**, 351.
29. V.J. Kurth, M.D. MacKenzie, T.H. DeLuca, *Geoderma* **2006**, 137, 135.
30. F. Gelman, R. Binstock, L. Halicz, *Fuel*, **2012**, 96, 608.
31. F.V.M. Pontes, M.C. Carneiro, D.S. Vaitsman, G.P. Rocha, L.I.D. Silva, A.A. Neto, M.I.C. Monteiro, *Analytica Chimica Acta*, **2009**, 632, 284.
32. H. Egnér, H. Riehm, W.R. Domingo, „Untersuchungen über die chemische Bodenanalyse als Grundlage für die Beurteilung de Nährstoffzustandes der Böden. II. Kungl Lantbrukshögskolans Annaler 26”, **1960**, 199.
33. K. Ivanov, P. Zapryanova, M. Petkova, V. Stefanova, V. Kmetov, D. Georgieva, V. Angelova, *Spectrochimica Acta*, **2012**, Part B 71-72, 117.
34. O. Brandula, M. Lazăr, F. Faur, *Research Journal of Agricultural Sciences*, **2015**, 47, 4, 19.
35. M. Dumitru, D. Cărăbiș, L. Pârvan, C. Sârbu, *Agriculture and Agricultural Science Procedia*, **2016**, 10, 3-9.
36. R. Erdogan, Z. Zaimoglu, *Environmental Engineering, Advances in bioremediation of wastewater and polluted soil*, **2015**, chapter 10.



*Dedicated to Professor Costel Sârbu on the  
Occasion of His 65<sup>th</sup> Anniversary*

## LOW CRYSTALLINITY NANOHYDROXYAPATITE PREPARED AT ROOM TEMPERATURE

AURORA MOCANU<sup>a</sup>, REKA BALINT<sup>a</sup>, CORINA GARBO<sup>a</sup>, LUCIA TIMIS<sup>a</sup>,  
IOAN PETEAN<sup>a</sup>, OSSI HOROVITZ<sup>a</sup>, MARIA TOMOAI-COTISEL<sup>a\*</sup>

**ABSTRACT.** In order to obtain a low crystalline nanohydroxyapatite (HAP), suitable for biomedical application, a new synthesis procedure was developed, based on the aqueous precipitation method, at room temperature, without any additives. Accordingly, lyophilized HAP powders, both calcined and non calcined, were prepared, and characterized by XRD, TEM and AFM imaging, FTIR spectroscopy, zeta potential and BET measurements. The results confirmed HAP as the only phase present. The high porosity of this nanomaterial is attained. The nanoparticle size and shape as well as the crystallinity degree of the obtained HAP samples were also determined.

**Keywords:** *nanohydroxyapatite, chemical synthesis, XRD, TEM, AFM, FTIR, BET*

## INTRODUCTION

Hydroxyapatite,  $\text{Ca}_{10}(\text{PO}_4)_6(\text{OH})_2$ , (HAP) is a preferred material for hard tissue replacement, due primarily to its bioactivity and biocompatibility. Most physical and chemical properties of synthetic hydroxyapatite are largely influenced by the preparation conditions. Wet chemical methods are considered as most capable to achieve controlled shapes and sizes of HAP particles, by

---

<sup>a</sup> Babeş-Bolyai University, Faculty of Chemistry and Chemical Engineering, 11 Arany Janos str., RO-400028, Cluj-Napoca, Romania,

\* Corresponding author: [mcotisel@gmail.com](mailto:mcotisel@gmail.com)



the variation of synthesis parameters [1]. In the precipitation method, based on the reaction of calcium nitrate and diammonium hydrogen phosphate in aqueous solutions at basic pH (over 10), a rather long maturation stage is needed for their full conversion to the less soluble and thermodynamically most stable product, HAP, with a high crystallinity degree [2]. But here we are interested in a small size of nanoparticles and low crystallinity, which jointly with a high porosity of the material should assure a good biological activity, for potential biomedical use. Following our syntheses of different calcium phosphates, more or less substituted [3-5], we designed a preparation procedure for pure HAP, without the addition of other substances, at room temperature, and without maturation at higher temperatures.

## RESULTS AND DISCUSSION

*X-ray diffraction patterns* were obtained for the noncalcined (sample A) and calcined (sample B) lyophilized HAP powders. In Figure 1 the spectra for sample A and sample B are compared with the PDF 74-0565 for stoichiometric hydroxyapatite. For both samples, hydroxyapatite is the only crystalline phase present. The calcination at 300°C could not bring about a conversion to  $\beta$ -tricalcium phosphate, which might be possible only at much higher temperatures. The highest peak occurs at a  $2\theta$  value about 32°, and corresponds to the (211) peak of HAP [6]. Rather broad peaks are observed in Fig. 1.

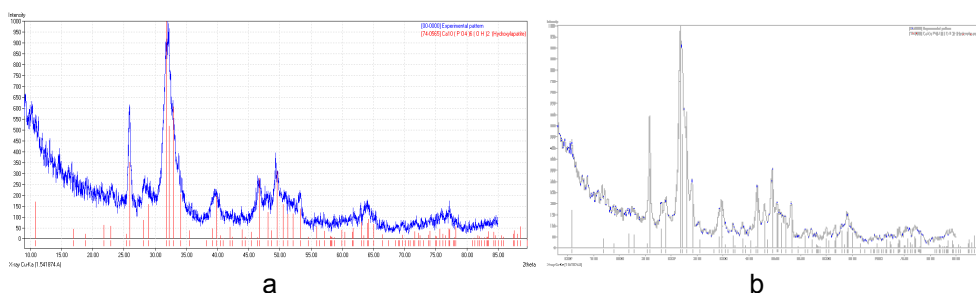


**Figure 1.** XRD patterns for sample A (a) and sample B (b), compared with PDF 74-0565 for stoichiometric hydroxyapatite

Such peaks can result from either a poor crystallinity or a very small crystal size [7], and for small crystallites it is difficult to discriminate between these two factors [8]. The crystallite domain is estimated as 13.8 nm (sample A), and 15.1 nm (after calcination, sample B), while the crystallinity degree is 21.3%

(A), respectively 23.1% (B), so here both causes apply. For a fast mixing of reactants, as in our experiments, the decreased HAP crystallinity was also observed [9], as an outcome of the supersaturation and local inhomogeneity resulted from the rapid mixing of the phosphate and the calcium containing solutions. Calcination brings about a slight increase, both in crystallite size and crystallinity degree, as found also for related situations [10].

TEM images for the aqueous dispersion of sample A (an example in Fig. 2) show acicular (rod-like) formations, which at higher resolution prove to be filiform assemblies of small nanoparticles. Most of these needles have a length in the range of 50 – 70 nm, while a few attain even over 100 nm; their diameter is the diameter of a nanoparticle, namely about 10 nm. These observations are similar to those found in the state of the art for related systems. Rod-shaped crystals with diameters 10–60 nm and lengths 200–500 nm were observed for HAP obtained at a temperature of 37 °C, aged overnight, and air dried [11]. Rods formed by smaller particles with sizes around 5 nm were also observed [7].

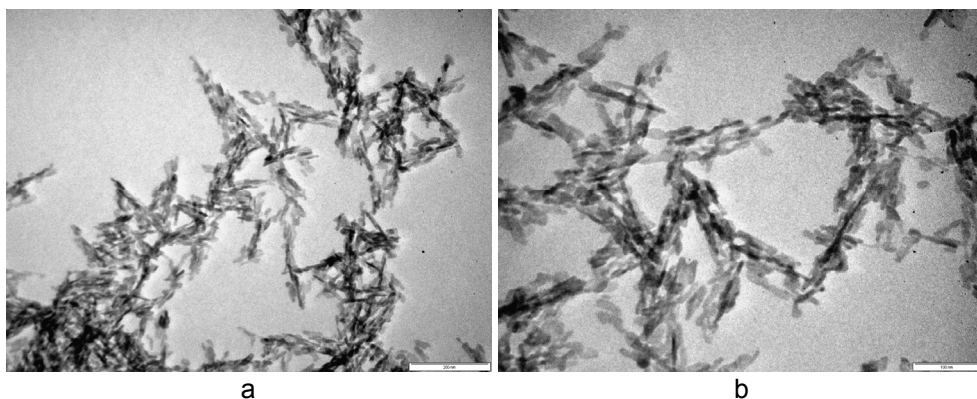


**Figure 2.** TEM images of sample A dispersed in water; the bars in the images are 200 nm (a), and 100 nm (b)

The FTIR spectra are compared in Figure 3 for lyophilized samples without calcination (A) and after calcination at 300 °C for 1 h (B). The spectra were normalized to 1 for the highest absorption peak and shifted along the y axis for comparison. The characteristic absorption bands corresponding to the vibrations of the PO<sub>4</sub> and OH groups of hydroxyapatite are present.

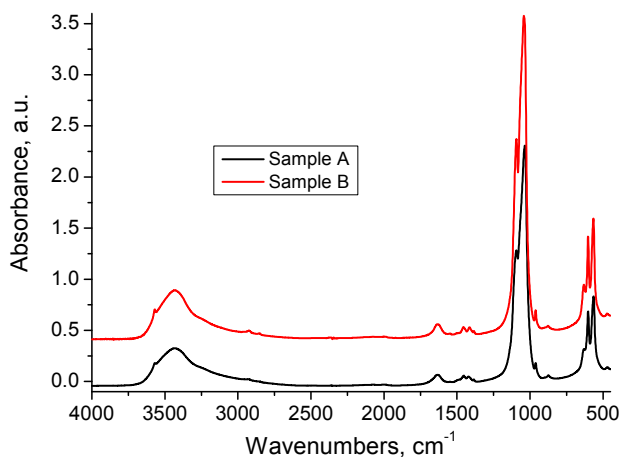


**Figure 3.** FTIR spectra of lyophilized samples without calcination (A) and after calcination (B); the spectra are normalized

The most intense band is that corresponding to the asymmetric  $\text{PO}_4$  stretching mode  $\nu_3$ ; it has two peaks: the highest at 1036 (A), and 1043  $\text{cm}^{-1}$  (B), the lower at 1093-1094  $\text{cm}^{-1}$ . They are characteristic for stoichiometric HAP, but the presence of type B carbonate substitution (wave number 1045  $\text{cm}^{-1}$ ) could contribute to the shift of one of the main peak to higher wave numbers [12]. The symmetric  $\text{PO}_4$  stretching mode  $\nu_1$  is IR-inactive for the ideal tetrahedral symmetry ( $T_d$ ) of the group, but the deformation of the  $\text{PO}_4$  tetrahedron in the apatite lattice lowers its symmetry [13, 14], so an absorption peak appears with low intensity at 962  $\text{cm}^{-1}$ . The bending modes of  $\text{PO}_4$  appear at lower wave numbers. The asymmetric bending  $\nu_4$  (triply degenerate for  $T_d$  symmetry) [15] generates a band with two peaks, at 565-567 and 603-604  $\text{cm}^{-1}$ . The symmetric bending mode  $\nu_2$  gives only a low intensity maximum at 472-473  $\text{cm}^{-1}$ .

The characteristic OH peaks appear at 3569-3570 and 632-633  $\text{cm}^{-1}$  and are an indication for the appropriate stoichiometric ratios in the synthesis of HAP [16,17]. The first peak is due to a stretching OH vibration [18,19] and is superposed on the broad band with maximum at 3431-3433  $\text{cm}^{-1}$  due to O-H stretching vibrations in absorbed water molecules [20] with hydrogen bonding O-H...O in the samples. The HAP OH band appears more distinct in the calcined sample (B), probably because of a partial loss of absorbed water by calcination, and a corresponding diminution of its broad absorption band. The peak at 632  $\text{cm}^{-1}$  corresponds to the OH libration band. The band at 1633-1635  $\text{cm}^{-1}$  originates from absorbed water.

The bands at 1455-1457, 1415-1421 and 875-878  $\text{cm}^{-1}$  are assigned to  $\text{CO}_3^{2-}$  (asymmetric stretching  $\nu_3$  and out of plane bending  $\nu_2$  the last) [21], originated from the interactions of HAP with  $\text{CO}_2$  absorbed by the samples from the atmospheric air. In the samples calcined at 300°C these bands are attenuated.

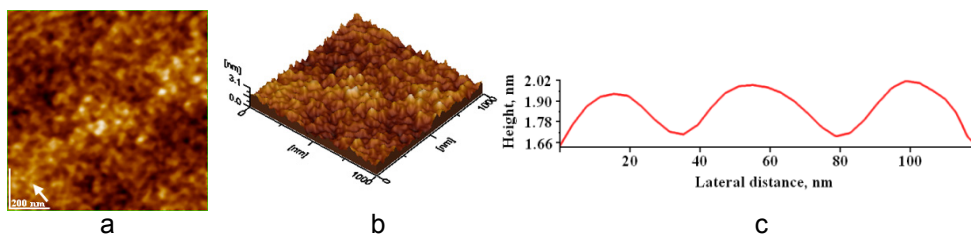


**Figure 4.** AFM images for sample B adsorbed on glass support for 10 s: 2D-topography (a), 3D-topography (b) and cross section profile (c) along the arrow in panel (a); scanned area of  $1\ \mu\text{m} \times 1\ \mu\text{m}$ .

Carbonated HAP can contain  $\text{CO}_3^{2-}$  ions substituting for  $\text{OH}^-$  (type A) or for  $\text{PO}_4^{3-}$  (type B). While biological apatites are mostly type B, synthetic HAPs are of mixed type (AB) [22]. The bands ca. 1415 and 1450  $\text{cm}^{-1}$  are characteristic for type B or AB [23]. The presence of  $\text{CO}_3^{2-}$  may improve the bioactivity of HAP rather than being a cause of concern [24].

In the spectra of our samples are missing the bands assigned to vibrations of non-apatitic  $\text{HPO}_4^{2-}$  ion, at 530-540  $\text{cm}^{-1}$  [12, 25] or 1125 and 1145  $\text{cm}^{-1}$  [12], as well as maxima characteristic for non-stoichiometric apatites (1018  $\text{cm}^{-1}$ ) [12]. This confirms the phase purity of the obtained HAP samples, as evident also from the XRD patterns.

Some typical AFM images are given in Figure 4 for the calcined HAP sample (B). They include 2D and 3D topographical images, and cross section profiles along selected directions in the 2D topography. The images are consistent with the results of TEM and XRD investigations regarding the shape and size of nanoparticles.

The samples presented low positive *zeta potential* values. For instance the lyophilized not calcined sample A had  $\zeta = 6.71$  mV. This positive potential could be a consequence of ionization (release of  $\text{OH}^-$  ions in the solution).

The BET measurements revealed a rather high specific surface area: 144  $\text{m}^2/\text{g}$  for the not calcined sample. By calcination the specific surface area is diminished to 91  $\text{m}^2/\text{g}$ , as an effect of nanoparticles sintering, while the pores specific volume is rather unchanged (0.332, respectively, 0.361  $\text{cm}^3/\text{g}$ ). The values are comparable with reported data for related circumstances [26];

for instance “as precipitated” HAP made at room temperature was reported to possess a surface area of 90 m<sup>2</sup>/g, after oven drying, and 113 m<sup>2</sup>/g after freeze-drying [27]. The adsorption-desorption isotherms are of type IV. The most probable pore radius was 7.7 nm, so the samples can be classified as mesoporous materials, according to the IUPAC notation [28], with pore diameters between 2 and 50 nm. Since the nanoparticles themselves (TEM images) are not porous, this porosity results mainly from the agglomerations of nanoparticles.

## CONCLUSIONS

The proposed chemical preparation method, by precipitation in aqueous phase, without any organic and inorganic additives (surfactants, templates), at room temperature and without a long maturation stage resulted in a low crystallinity nanostructured hydroxyapatite. Together with its high porosity, these properties should assure a good biological activity, which recommend this material for biomedical applications, along with substituted hydroxyapatites, containing silicon [29], zinc [26], strontium [30], magnesium [5] or silver [31].

## EXPERIMENTAL SECTION

Nanostructured hydroxyapatite was prepared by a simple method, starting with two solutions: (a) a 0.25 M calcium nitrate solution, obtained from Ca(NO<sub>3</sub>)<sub>2</sub>·4H<sub>2</sub>O (pure p.a., Merck) dissolved in ultrapure water, with 25% ammonia solution, in order to assure a pH value of 8.5, and (b) a 0.15 M diammonium hydrogen phosphate solution, prepared from (NH<sub>4</sub>)<sub>2</sub>HPO<sub>4</sub> (pure p.a., Sigma-Aldrich) dissolved in ultrapure water, with 25% ammonia solution added to assure a pH value of 11. The two solutions, at room temperature (22°C), were quickly mixed, using a peristaltic pump and an impact reactor type Y for the two fluid streams, containing the reactants in stoichiometric ratio.

The obtained dispersion, without any subsequent treatment, in the presence of the mother liquor, was filtered (Filter Disks Munktell, grade: 382), and washed with ultrapure water (until no nitrate ions were detected). A wet precipitate (paste) was obtained. *Sample A* (lyophilized powder) was prepared by further processing of the precipitate: it was dried by lyophilization (freeze drying) at -50°C at a pressure of 0.040 mbar (0.03 torr), and the obtained material was dispersed by grinding in an agate mortar. *Sample B* (calcined lyophilized powder) was obtained by calcination of sample A at 300 °C (for 1 h).

The samples were characterized by *X-Ray Diffraction* (XRD) investigations used a DRON-3 diffractometer, in Bragg-Brentano geometry, equipped with a X-ray tube with Co K $\alpha$  radiation (wavelength 1.79026 Å), 25 kV/20 mA. Phases were identified by comparing the peak positions of the diffraction patterns with PDF files such as PDF 74-0566 for stoichiometrical HAP. The average crystallite size for these samples was evaluated by the Scherrer method, from the width of the most intense diffraction peaks, measured at half-maximum. The crystallinity degree of the samples was also estimated.

The samples were observed with a *transmission electron microscope* (TEM, JEOL – JEM 1010). The HAP aqueous dispersion of sample A (paste), needed for TEM imaging, was prepared by ultrasonification, using a high intensity ultrasonic processor Sonics Vibra-Cell, model VCX 750, for 5 minutes, at room temperature. From their aqueous dispersion, the particles were adsorbed on the specimen grids, while the excess solution was removed with filter paper and the samples were air dried. TEM images have been recorded with JEOL standard software. *Atomic force microscopy* (AFM) images were obtained using the AFM JEOL 4210 equipment, operated in tapping mode [32-41], with standard cantilevers having silicon nitride tips (resonant frequency in the range of 200-300 kHz, spring constant 17.5 N/m). The particles were adsorbed (horizontal adsorption) from their aqueous dispersion for 10 s on glass. Different areas from 10  $\mu\text{m}$  x 10  $\mu\text{m}$  to 0.5  $\mu\text{m}$  x 0.5  $\mu\text{m}$  were scanned on the same film. The images (2D- topographies, phase and amplitude images, and cross-section profiles for the adsorbed HAPs layer, along a selected direction) were processed by the standard AFM JEOL procedures.

*FTIR spectra* were measured on KBr pellets, containing the sample powder with a FTIR spectrometer JASCO 6100 in the 4000-400  $\text{cm}^{-1}$  range of wave numbers, with a 4  $\text{cm}^{-1}$  resolution. *Zeta potential* measurements were performed using the Malvern Zetasizer Nano-ZS90, on the aqueous dispersions of lyophilized non calcined and calcined samples. *BET analysis* was achieved with an automated Sorptomatic 1990 instrument, with nitrogen adsorption at 77 K. The calculation of surface area was made in the P/P $_0$  range between 0.03 and 0.3, and the total pore volume was determined at P/P $_0$  = 0.95. Before the analysis the samples were outgassed for 6 h at 70 °C.

## ACKNOWLEDGMENTS

This work was supported by the Romanian Executive Agency for Higher Education, Research, Development and Innovation Funding (UEFISCDI) through grant 241/2014.

## REFERENCES

1. K. Lin, C. Wu, J. Chang, *Acta Biomaterialia*, **2014**, *10*, 4071.
2. H.E. Lundager Madsen, F. Christensson, *Journal of Crystal Growth*, **1991**, *114*, 613.
3. C. Garbo, *PhD Thesis*, Babes-Bolyai University of Cluj-Napoca, Cluj-Napoca, 2016.
4. G. Tomoaia, M. Tomoaia-Cotisel, L. B. Pop, A. Pop, O. Horovitz, A. Mocanu, N. Jumate, L.-D. Bobos, *Revue Roumaine de Chimie*, **2011**, *56*, 1039.
5. G. Tomoaia, O. Soritau, M. Tomoaia-Cotisel, L.-B. Pop, A. Pop, A. Mocanu, O. Horovitz, L.-D. Bobos, *Powder Technology*, **2013**, *238*, 99.
6. S. Manocha, P. Joshi, B. Patel, L.M. Manocha, *Eurasian Chemico-Technological Journal*, **2011**, *13*, 85.
7. G.A. Martínez-Castañón, J.P. Loyola-Rodríguez, N.V. Zavala-Alonso, S.E. Hernández-Martínez, N. Niño-Martínez, G. Ortega-Zarzosa, F. Ruiz, *Superficies y Vacío*, **2012**, *25* (2), 101.
8. S.V. Dorozhkin, *Acta Biomaterialia*, **2010**, *6*, 715.
9. E. Kramer, J. Podurgiel, M. Wei, *Materials Letters*, **2014**, *131*, 145.
10. Y.X. Pang, X. Bao, *Journal of the European Ceramic Society*, **2003**, *23*, 1697.
11. V. Dhand, K.Y. Rhee, S.J. Park. *Materials Science and Engineering: C*, **2014**, *36*, 152.
12. H. Ou-Yang, E.P. Paschalis, A.L. Boskey, R. Mendelsohn, *Biopolymers, Biospectroscopy*, **2000**, *57*, 129.
13. N. Pleshko, A. Boskey, Mendelsohn, *Biophysical Journal*, **1991**, *60*, 786.
14. R.N. Panda, M.F. Hsieh, R.J. Chung, T.S. Chin, *Journal of Physics and Chemistry of Solids*, **2003**, *64*, 193.
15. C.B. Baddiel, E.E. Berry, *Spectrochimica Acta*, **1966**, *22*, 1407.
16. F. Bakan, O. Laçin, H. Sarac, *Powder Technology*, **2013**, *233*, 295.
17. W.L. Suchanek, P. Shuk, K. Byrappa, R.E. Riman, K.S. Ten Huisen, V.F. Janes, *Biomaterials*, **2002**, *23*, 699.
18. K. Nakata, T. Kubo, C. Numako, T. Onoki, A. Nakahira, *Materials Transactions*, **2009**, *50*, 1046.
19. A.Y. Pataquiva Mateus, C.C. Barrias, C. Ribeiro, M.P. Ferraz, F.J. Monteiro, *Journal of Biomedical Materials Research Part A*, **2008**, *86A*, 483.
20. A. Sionkowska, Kozłowska, *International Journal of Biological Macromolecules*, **2010**, *47*, 483.
21. D. Gopi, S. Nithiya, E. Shinyjoy, L. Kavitha, *Spectrochimica Acta Part A: Molecular and Biomolecular Spectroscopy*, **2012**, *92*, 194.
22. A. Slosarczyk, Z. Paskiewicz, C. Paluszkiwicz, *Journal of Molecular Structure*, **2005**, *744-747*, 657.
23. J.C. Merry, J.R. Gibson, S.M. Best, W. Bonfield, *Journal of Material Science: Materials in Medicine*, **1998**, *9*, 779.
24. K.P. Sanosh, M.C. Chu, A. Balakrishnan, T.N. Kim, S.J. Cho, *Bulletin of Materials Science*, **2009**, *32*, 465.

25. C. Drouet, F. Bosc, M. Banu, C. Largeot, C. Combes, G. Dechambre, C. Estournès, G. Raimbeaux, C. Rey, *Powder Technology*, **2009**, 190, 118.
26. C. Garbo, M. Sindilaru, A. Carlea, G. Tomoaia, V. Almasan, I. Petean, A. Mocanu, O. Horovitz, M. Tomoaia-Cotisel, *Particulate Science and Technology*, **2017**, 35, 29.
27. E. Bouyer, F. Gitzhofer, M.I. Boulos, *Journal of Material Science: Materials in Medicine*, **2000**, 11, 523.
28. J. Rouquerol, D. Avnir, C.W. Fairbridge, D.H. Everett, J.M. Haynes, N. Pernicone, J.D.F. Ramsay, K.S.W. Sing, K.K. Unger, *Pure and Applied Chemistry*, **1994**, 66, 1739.
29. Gh. Tomoaia, A. Mocanu, I. Vida-Simiti, N. Jumate, L.D. Bobos, O. Soritau, M. Tomoaia-Cotisel, *Materials Science and Engineering C*, **2014**, 37, 37.
30. P.T. Frangopol, A. Mocanu, V. Almasan, C. Garbo, R. Balint, G. Borodi, I. Bratu, O. Horovitz, M. Tomoaia-Cotisel, *Revue Roumaine de Chimie*, **2016**, 61 337.
31. A. Mocanu, G. Furtos, S. Rapuntean, O. Horovitz, C. Flore, C. Garbo, A. Danisteanu, Gh. Rapuntean, C. Prejmerean, M. Tomoaia-Cotisel, *Applied Surface Science*, **2014**, 298, 225.
32. M.A. Naghiu, M. Gorea, E. Mutch, F. Kristaly, M. Tomoaia-Cotisel, *Journal of Material Science and Technology*, **2013**, 29(7), 628.
33. O. Horovitz, Gh. Tomoaia, A. Mocanu, T. Yupsanis, M. Tomoaia-Cotisel, *Gold Bulletin*, **2007**, 40 (4), 295.
34. M. Tomoaia-Cotisel, A. Tomoaia-Cotisel, T. Yupsanis, Gh. Tomoaia, I. Balea, A. Mocanu, Cs. Racz, *Revue Roumaine de Chimie*, **2006**, 51 (12),1181.
35. A. Danistean, M. Gorea, A. Avram, S. Rapuntean, Gh. Tomoaia, A. Mocanu, C. Garbo, O. Horovitz, M. Tomoaia-Cotisel, *Studia UBB Chemia*, **2016**, 61 (3), 275.
36. Gh. Tomoaia, O. Horovitz, A. Mocanu, A. Nita, A. Avram, C.P. Racz, O. Soritau, M. Cenariu, M. Tomoaia-Cotisel, *Colloids and Surfaces B: Biointerfaces*, **2015**, 135, 726.
37. P.T. Frangopol, D.A. Cadenhead, Gh. Tomoaia, A. Mocanu, M. Tomoaia-Cotisel, *Revue Roumaine de Chimie*, **2015**, 60(2-3), 265.
38. G. Furtos, M. A. Naghiu, H. Declercq, M. Gorea, C. Prejmerean, O. Pana, M. Tomoaia-Cotisel, *Journal of Biomedical Materials Research Part B. Applied Biomaterials*, **2016**, 104 (7), 1290.
39. M. Tomoaia-Cotisel, A. Mocanu, *Revista de Chimie (Bucharest)*, **2008**, 59(11), 1230.
40. R.D. Pasca, G. Tomoaia, A. Mocanu, I. Petean, G.A. Paltinean, O. Soritau, M. Tomoaia-Cotisel, *Studia UBB Chemia*, **2015**, 60(3), 257.
41. G. Tomoaia, A. Mocanu, L.D. Bobos, L.B. Pop, O. Horovitz, M. Tomoaia-Cotisel, *Studia UBB Chemia*, **2015**, 60 (3), 265.





*Dedicated to Professor Costel Sârbu on the  
Occasion of His 65<sup>th</sup> Anniversary*

## **SYNTHESIS AND SPECTROSCOPIC CHARACTERIZATION OF HYBRID MAGNETIC NANOPARTICLES, BASED ON FE@AU AND PYRROLE**

**MARIA-LOREDANA SORAN<sup>a\*</sup>, OVIDIU PANĂ<sup>a</sup>, ALEXANDRINA NAN<sup>a</sup>,  
CRISTIAN LEOȘTEAN<sup>a</sup>, IOAN BRATU<sup>a</sup>**

**ABSTRACT.** The synthesis and characterization of Fe@Au and Fe@Au covered with pyrrole and pyrrole functionalized with N-succinimide is presented. The synthesis of Fe@Au nanoparticles, with diameters between 5 -7 nm was performed by the reverse micelles method. The hybrid composites Fe@Au nanoparticles covered by the pyrrole copolymer were obtained by chemical oxidative polymerization of a mixture of pyrrole and substituted pyrrole with N-succinimide monomers in water. The properties of these composites were investigated by transmission electron microscopy and FTIR spectroscopy.

**Keywords:** *Nanoparticles; Iron; Gold; Polypyrrole; N-succinimide*

### **INTRODUCTION**

Various types of magnetic nanoparticle systems have been subject to a considerable interest in the last few years from both fundamental and applicative point of view [1-3]. Generally, when the sizes of the magnetic particles are decreased to the nanometric scale, a transition occurs from polydomain magnetism to monodomain magnetic systems [4-5]. A system of non-interacting nanoparticles displays the superparamagnetism phenomenon [6].

---

<sup>a</sup> *National Institute for Research & Development of Isotopic and Molecular Technologies, 65-103 Donath Street, Cluj-Napoca, Romania*

\* *Corresponding author: loredana.soran@itim-cj.ro*

Besides the adjustment of dimensions, additional control and design of magnetic nanoparticles could be achieved by developing core-shell structured nanosystems. This type of particles has drawn the attention since they allow the tailoring of the combined surface and core properties providing also an increased number of applications [7-9]. Among the core shell nanoparticles those formed with magnetic core and having the outer shell formed by noble metals have drawn interest since one obtains an enhancement of the thermal and chemical stability of nanoparticles, an improvement of the solubility [10-14]. For instance, an outer Au shell makes them less cytotoxic and allows the functionalization by attaching other molecules to the surface of the particles. In certain cases, the shell also prevents the oxidation of the core material [7]. The coating of the magnetic nanoparticles with polymers represents a new route for tailoring the properties. It could be achieved by controlling the polymer composition and structure [15]. In the present study we report the synthesis, characterization (mainly spectroscopic) and possible applications of the iron-core and gold – shell (Fe@Au) nanoparticles covered with copolymer between pyrrole and pyrrole functionalized with N-succinimide (PPy-NHS).

## RESULTS AND DISCUSSION

As an example, the TEM image of an ensemble of Fe@Au core-shell nanoparticles is shown in Fig. 1a. It corresponds to the FA1 sample from Table 1. In the Fig. 1b it is presented the TEM image of the hybrid composite formed by Fe@Au nanoparticles and the Py/Py-NHS copolymer. One can see that also the copolymer surrounds the Fe@Au nanoparticles in a core-shell like arrangement forming globular structures.

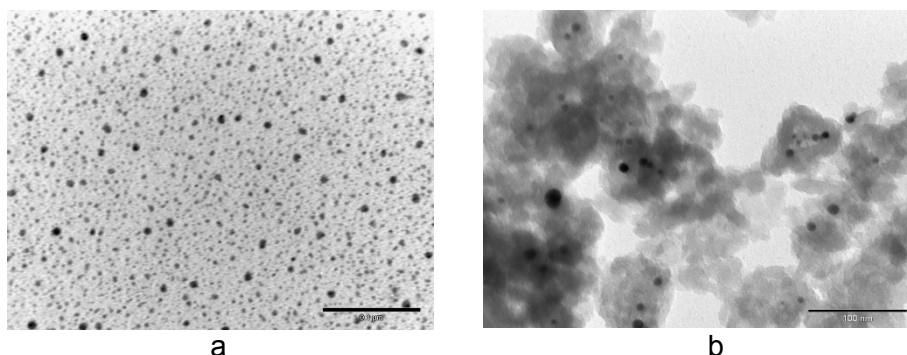


**Figure 1.** TEM characterization of the Fe@Au nanoparticles and Fe@Au hybrid composites: (a) image of FA1 sample and (b) TEM image of the FA1 covered with PPy-NHS copolymer.

The TEM images of the Fe@Au nanoparticles were used to determinate the size distributions of the diameters. At least 400 nanoparticles were considered for each sample.

The normalized size distributions of the Fe@Au samples are presented in Fig. 2. One can observe that the mean diameters of the Fe@Au nanoparticles are around 5-7 nm. Due to the superparamagnetic behavior of these systems the size distributions of nanoparticles play an important role for the adjustment of their magnetic properties.

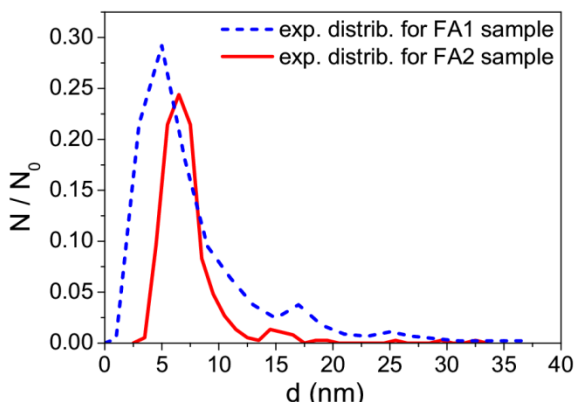


**Figure 2.** The distributions of the diameters of the nanoparticles for FA1 and FA2 samples.

In Fig. 3 it is presented the UV-Vis spectrum of Fe@Au nanoparticles (FA2 sample for instance). It can be observed the characteristic peak at 553.8 nm which represents the extinction of the plasmonic mode at the gold surface of nanoparticles. This value appears red shifted as compared to the pure gold nanoparticles (526 nm) and proves that the “core-shell” structure for Fe@Au nanoparticles is formed [1].

Further, the FTIR technique was used to determine whether or not the PPy-NHS copolymer is formed around the Fe@Au nanoparticles. In Fig. 4 it is presented the FTIR spectra of FA1-PPy-NHS and FA2-PPy-NHS. For comparison, the spectrum of the Py-NHS monomer it is also shown. The spectra of the hybrid composites contain the characteristic absorption bands due to pyrrole ring vibrations located at 914, 1190, 1465  $\text{cm}^{-1}$  and the band located around 1700  $\text{cm}^{-1}$ , ascribed to C=O group from the functionalized pyrrole. The presence of the mentioned above bands into the hybrid composites spectra demonstrates the formation of the copolymer between pyrrole and pyrrole functionalized with N-succinimide covering the Fe@Au nanoparticles. A

frequency shift of the C=O band ( $1737\text{ cm}^{-1}$ ) to lower wave numbers ( $1707\text{ cm}^{-1}$ ) is observed in the spectra of the composites samples as compared with that one of the N-succinimide substituted monomer. Possible hydrogen bonding between pyrrole rings and N-succinimide radicals can appeared.

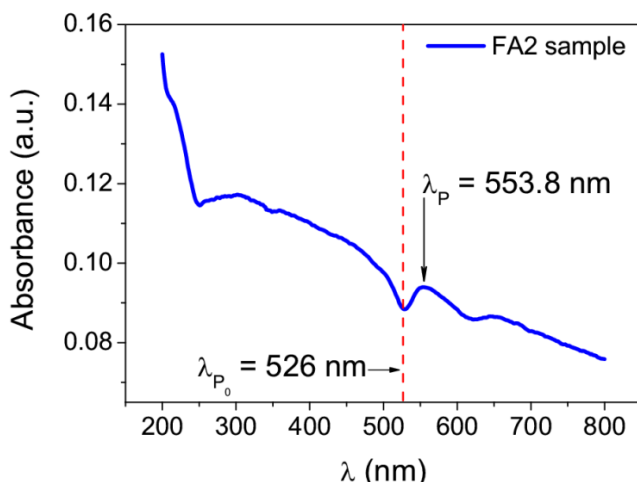


**Figure 3.** UV-Vis spectrum of FA2 sample.

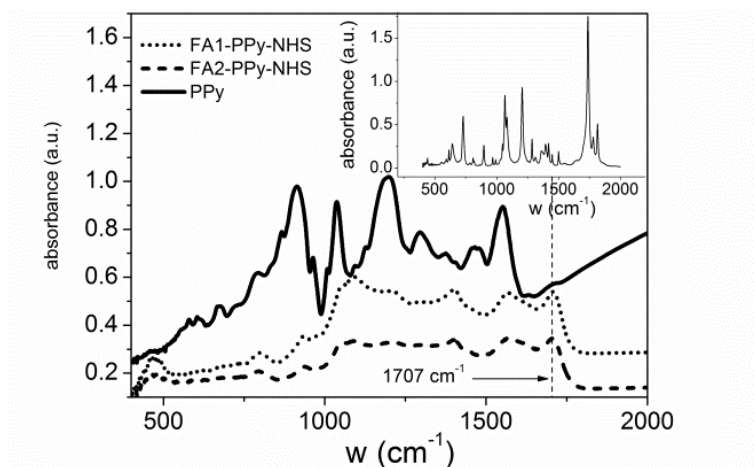


**Figure 4.** FTIR spectra of hybrid nanocomposites Fe@Au-PPy-NHS compared with the FTIR spectrum of polypyrrole. The inset shows FTIR absorption spectra of Py-NHS monomer.

On the other hand, the spectra of the two hybrid nanocomposites containing functionalized polypyrroles show significant changes concerning the relative peak intensities and the peak positions as compared to the typical polypyrrole. Therefore, the pyrrole ring vibrations bands located at 914, 1190, 1465  $\text{cm}^{-1}$  in PPy are shifted to higher wave numbers in the PPy-NHS functionalized cases.

Furthermore, the absorption bands ascribed to the collective vibration mode of intra-ring and inter-ring C=C/C-C are shifted from 1550  $\text{cm}^{-1}$  in PPy to 1569  $\text{cm}^{-1}$  in magnetic nanoparticles FA1-NHS and 1574  $\text{cm}^{-1}$  for FA2-NHS, respectively. The ring charge distribution modification can be responsible for this effect.

Further, the hybrid nanostructures Fe@Au covered with copolymer functionalized with N-succinimide could be used for the attachment of various bioentities (such as: proteins) that contains NH- or SH- groups by a substitution reaction of N-succinimide. Therefore, this property makes this material suitable for *in vitro* applications like magnetic separation of biomolecules and cells, or *in vivo* applications as magnetically driven drug delivery.

## CONCLUSIONS

The Fe@Au nanoparticles were obtained by reversed micelles method and these were introduced in copolymer pyrrole and pyrrole functionalized with N-succinimide.

The distribution of the Fe@Au particle sizes was determined from TEM images; the mean diameter is around 5-7 nm.

The characteristic red shift observed for the plasmonic extinction, as indicated in the UV-Vis spectrum of Fe@Au nanoparticles (526 to 553 nm), also proves that the “core-shell” structure for Fe@Au nanoparticles is formed.

By using the FTIR spectroscopy it was shown that the N-succinimide functionalized copolymer was attached to the Fe@Au nanoparticles; this conclusion is also sustained by the TEM images of the hybride nanocomposite material. The magnetic behaviour of these samples is under investigation.

## EXPERIMENTAL SECTION

### Materials

The used substances were purchased from different companies:  $\text{FeSO}_4$  from Chimopar (Romania),  $\text{HAuCl}_4$  (“Raluca Ripan” Institute for Research in Chemistry, Romania),  $\text{NaBH}_4$  (12% aq. sol. in 14M NaOH, Aldrich),

cetyltrimethylammonium bromide (Sigma), pyrrole (97%, Merck), ammonium persulfate ( $\geq 98\%$ , Sigma-Aldrich), N-hydroxysuccinimide (98%, Sigma-Aldrich). All the solvents were from Chimopar (Bucharest, Romania). All chemicals were of analytical grade.

## Methods

The iron-gold core-shell nanoparticles (Fe@Au) were prepared by reverse micelle method using cetyltrimethylammonium bromide (CTAB) as surfactant and 1-butanol as co-surfactant. The oil phase was octane.

An amount of 2.4 mL 0.8M FeSO<sub>4</sub>(aq.) and 2.4 mL NaBH<sub>4</sub> 1M were mixed together under magnetic stirring and inert atmosphere, for 1 h. In this reaction was obtained Fe<sup>0</sup> (core material). A gold shell was added in aim to protect the iron core. In this goal, the micelles were obtained by adding a solution of 1.5 mL NaBH<sub>4</sub> 1.6M, followed by corresponding quantity of 0.44 M HAuCl<sub>4</sub> (Table 1), in 1-butanol and octane. The mixture obtained was stirred at room temperature under inert atmosphere for 5 h. After synthesis, the remaining surfactant was removed by washing with a 1 : 1 (v/v) chloroform/methanol mixture. The powder obtained was dried at 60°C, in an oven. Further the resulting Fe@Au nanoparticles were covered by copolymer between pyrrole and pyrrole functionalized with N-succinimide.

**Table 1.** The conditions of Fe@Au nanoparticles synthesis.

Sample	Molar ratios		
	surfactant : HAuCl <sub>4</sub>	surfactant : FeSO <sub>4</sub>	FeSO <sub>4</sub> : HAuCl <sub>4</sub>
FA <sup>a)</sup> 1	10.4	14	1.5
FA2	12.5	14	1.8

<sup>a)</sup>FA = Fe@Au

The hybrid composites with Fe@Au nanoparticles covered by the pyrrole copolymer were obtained by chemical oxidative polymerization of a mixture of pyrrole (Py) and substituted pyrrole with N-succinimide (Py-NHS) monomers in water. The oxidation agent used in this reaction was ammonium persulfate (APS). Two weight ratios between the monomers (Py, Py-NHS) and Fe@Au nanoparticles were used, namely 1.6 and 0.16 for the synthesis of the sample named FA1-NHS1, and sample FA1-NHS2 respectively. The

molar ratio between APS and Py-NHS was 0.5. The reaction time was 10 hours and during this time the solution was kept under sonication. Finally, the co-polymerization reaction was stopped with methanol. The as resulted black precipitate was washed with water. It was separated from the solution by centrifuging and by drying at 100°C in an oven.

The samples obtained (Fe@Au-NHS) were analyzed by transmission electron microscopy (TEM) and optical spectroscopic methods (UV-Vis, FTIR).

TEM analysis was performed on 1010 JEOL transmission electron microscope, and UV-Vis analysis on an ABL&E Jasco V550 spectrophotometer. FTIR measurements were done with a 6100 JASCO spectrometer in the 4000 to 400  $\text{cm}^{-1}$  spectral range with a resolution of 2  $\text{cm}^{-1}$  using the well-known KBr pellet technique.

## ACKNOWLEDGMENTS

Financial assistance provided through the Ministry of Education and Research of Romania (Research Programs, Projects: ID-76, ID-119) is gratefully acknowledged.

## REFERENCES

1. M. Li, H. Schnablegger, S. Mann, *Nature*, **1999**, 402, 393.
2. J. Chatterjee, Y. Haik, C.J. Chen, *Journal of Magnetism and Magnetic Materials*, **2002**, 246, 382.
3. J.M. Vargas, L. M. Socolovsky, M. Knobel, D. Zanchet, *Nanotechnology*, **2005**, 16, S285.
4. F.M. Mulder, R.C. Thiel, K.H.J. Buschow, *Journal of Alloys and Compounds*, **1995**, 223, 127.
5. E. Carpenter, C.T. Seip, C.J.O'Connor, *Journal of Applied Physics*, **1999**, 85, 5184.
6. L. Néel, *Comptes Rendus de l'Académie des Sciences Paris*, **1949**, 228, 664.
7. N. Sounderya, Y. Zhang, *Recent Patents on Biomedical Engineering*, **2008**, 1, 34.
8. Y.H. Huang, C.H. Yan, Z.M. Wang, C.S. Liao, G.X. Xu, *Solid State Communications*, **2001**, 118, 541.
9. W.F. Jr. Brown, *Physical Review*, **1963**, 130, 1677.
10. J. Lin, W. Zhou, A. Kumbhar, J. Wiemann, J. Fang, E.E. Carpenter, C.J. O'Connor, *Journal of Solid State Chemistry*, **2001**, 159, 26.
11. E.E. Carpenter, C. Sangregorio, C.J. O'Connor, *IEEE Transaction on magnetic*, **1999**, 35, 3496.



12. Y. Bao, K.M. Krishnan, *Journal of Magnetism and Magnetic Materials*, **2005**, 293, 15.
13. W.L. Zhou, E.E. Carpenter, J. Lin, A. Kumbhar, J. Sims, C.J. O'Connorl, *European Physical Journal D*, **2001**, 16, 289.
14. T.T.H. Pham, C. Cao, S.J. Sim, *Journal of Magnetism and Magnetic Materials*, **2008**, 320, 2049.
15. P. Jeffrey, *Polymer Reviews*, **2007**, 47, 231.

*Dedicated to Professor Costel Sârbu on the  
Occasion of His 65<sup>th</sup> Anniversary*

## EVALUATING SOUTH AFRICAN CHENIN BLANC WINE STYLES USING AN LC-MS SCREENING METHOD

**ASTRID BUICA<sup>a\*</sup>, JEANNE BRAND<sup>a</sup>, CHRISTINE WILSON<sup>a</sup>,  
MARIETJIE STANDER<sup>b</sup>**

**ABSTRACT.** Sensory evaluation is the approach currently used when evaluating the style of a South African Chenin Blanc wine. Using an untargeted LC-HRMS approach, a number of wine samples previously attributed to the three recognized styles were used to build a statistical model which was further used to predict to which style group additional samples belonged. This application can be considered proof of principle.

**Keywords:** *Chenin Blanc wine styles; LC-MS; screening; sorting*

### INTRODUCTION

With the help of chemometrics, large amounts of data generated for wine analyses can be used for statistical modelling. Classification and discrimination of samples, quantification of certain classes of compounds, and prediction was successfully achieved in wine research using chemometrics [1–4]. Sensory evaluation is also a field that makes use of statistics, in experimental design, panel performance testing, and, of course, data handling

---

<sup>a</sup> *Department of Viticulture and Oenology, Stellenbosch University, Private Bag X1, Matieland 7602, South Africa*

<sup>b</sup> *Mass Spectrometry Unit, Central Analytical Facility, Stellenbosch University, Private Bag X1, Matieland 7602, South Africa*

\* *Corresponding author: [abuica@sun.ac.za](mailto:abuica@sun.ac.za)*

[5–7]. Various sensory methods have been developed hand in hand with their own data handling approach [8]. The results are generally used for discrimination and classification between samples, but not for prediction. The question is – with the appropriate analysis technique, can sensory behaviour be predicted?

Chemical analysis and sensory evaluation are the two means through which wines are assessed, but linking the two has usually met with limited success. This is maybe counterintuitive, since the chemical composition will dictate the flavour, taste, and mouth-feel of a wine through the various compounds present in the sample.

The issue resides rather in the approach. Sensory evaluation has a holistic and comprehensive approach, in the sense that the entire product is evaluated at once and it is seen as a whole and not the sum of parts. However, looking into the chemical composition of a wine using targeted separation techniques reduces the whole to the sum of parts. In that case, sensory and chemistry results seldom correlate well. On the other hand, an untargeted approach has more chances of succeeding. Some analytical techniques, such as UV/Vis and IR spectroscopy, have been utilised successfully in the classification, discrimination, and quantification of certain classes of compounds present in wine [4,9–11]. Similarly, untargeted or comprehensive chromatographic approaches coupled with chemometrics have a better chance of succeeding because they are information-rich. The use of untargeted analytical techniques to profile, model, and predict sensory behaviour is an expanding area of research. The applications are at the moment relatively few and some are heavily chemistry-based while the sensory aspects are more informal [12–15].

Chenin Blanc is one of the most important white wine cultivars in South Africa. It has received a lot of attention and accolades in the past years and more research than ever is dedicated to this versatile cultivar. According to the Chenin Blanc Association of South Africa, there are three recognized dry wine styles, Fresh and Fruity (FF), Rich and Ripe Unwooded (RRU), and Rich and Ripe Wooded (RRW) [16]. They are traditionally established with the aid of expert sensory evaluation, but the cost and the (subjective) human factor are aspects to be taken into account. Also, the number of samples that can be judged in one tasting session is limited [17].

A more objective and robust way of assessing and attributing these styles can be the use of chemical analysis. Chemical composition can be a better way for discriminating between style groups using an untargeted approach such as LC-MS. This approach is information-rich and offers numerous possibilities for statistical data modelling (PCA, PLS, HCA, *etc.*). Creating

prediction models to include additional samples possibly without the need for sensory evaluation is a powerful tool for future applications. As always, there are some possible drawbacks to this approach, too, such as the need for data pre-processing that doesn't remove relevant information but helps build strong and reliable models. Additionally, creating a reliable model depends on the choice of training set (done by sensory evaluation) so the choice of appropriate (representative) samples for the training set still falls on the sensory assessment.

In this work, a sample set representative of the three Chenin Blanc wine styles was evaluated sensorially by a panel of expert judges. These wines and additional samples were analysed by LC-HRMS. The data obtained was used to create a statistical model used to predict to which of the styles the additional samples belonged, thus avoiding the need for sensorial evaluation for the additional samples.

## RESULTS AND DISCUSSION

The sensory and chemistry data sets were treated separately and groupings of samples around the predefined styles were found for both sets.

### Sensory evaluation

Sample repeats are close to each other, indicating good repeatability of the expert panel. Similar to previous findings, the sensory evaluation of Chenin Blanc wines leads to the formation of 2 rather than 3 defined groups. At first glance, RRW group is set apart from the FF and RRU wines which form a continuum rather than two distinct groups (Fig 1). Even though there is a trend for the FF-RRU wines to have FF wines on one side and RRU wine to the other, they do not make distinct groups. This is illustrated by the two wines that have been placed with equal frequency in the FF and RRU groups, LKAP and WGHV.

Moreover, looking at the dendrogram representation of the results, it becomes apparent that there are in fact four groups, and not only two (Fig 2). The dendrogram (Fig 2) shows that the grouping is not as clear as suggested by the configuration plot (Fig 1). The two samples that were placed by the judges equally in the FF and RRU groups, LKAP and WGHV, are indeed placed with two other samples that belong to those groups, SVP to FF and BCG to RRU, respectively. On the other hand, one of the RRW samples, WGHV, is positioned with two samples that belong in the RRU group, REM and MP. This is not unusual, as often the wines described as rich and ripe unwooded are the most challenging to ascribe to a well-defined group.

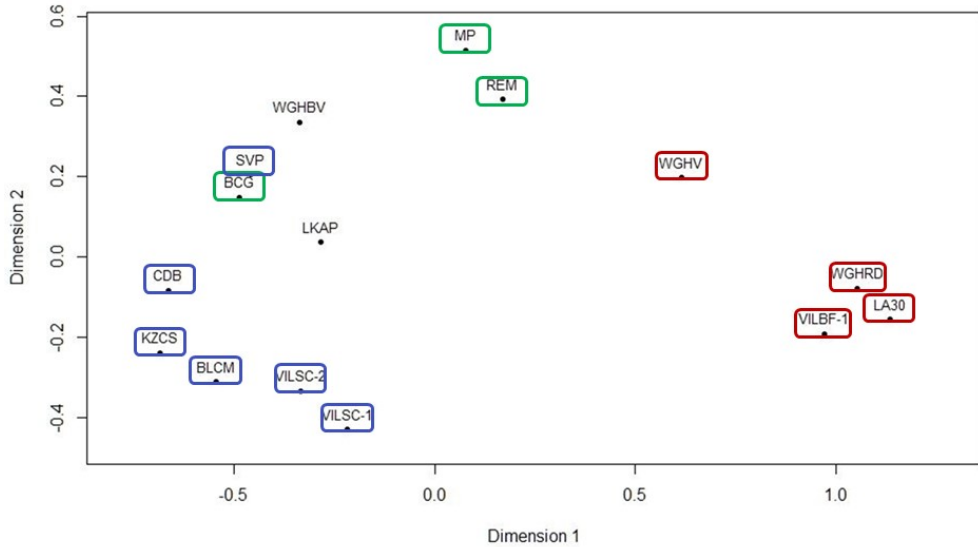


**Figure 1.** Configuration plot after directed sorting task. The styles are attributed as FF (blue), RRU (green), and RRW (red). The codes without frames are from samples that were attributed to two groups equally (FF and RRU).

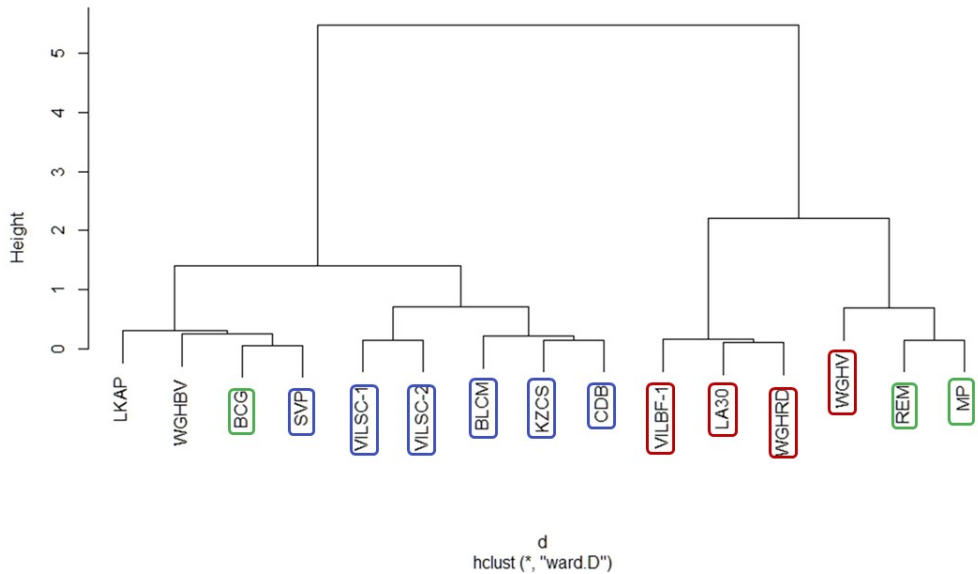


**Figure 2.** Dendrogram for the directed sorting task results. The styles are attributed as FF (blue), RRU (green), and RRW (red). The codes without frames are from samples that were attributed to two groups equally (FF and RRU).

### LC-MS analysis

The representation of all data, combining the results for positive and negative ionization modes, is shown in Fig 3a and 3b. The PCA model for all samples, including the wines not classified during the sensory evaluation, shows some grouping that is more obvious in the representation of PC1 and 3 (Fig 3b). In that case, the separation of wines from the RRW group seems more apparent than for PC1 and 2 (Fig 3a). The configuration is similar for chemistry and sensory data (Fig 1 vs Fig 3b) with a continuum between the FF and RRU groups and in opposite quadrants from RRW. The additional 'no class' samples are more difficult to ascribe to a style group when inspecting the PCAs.

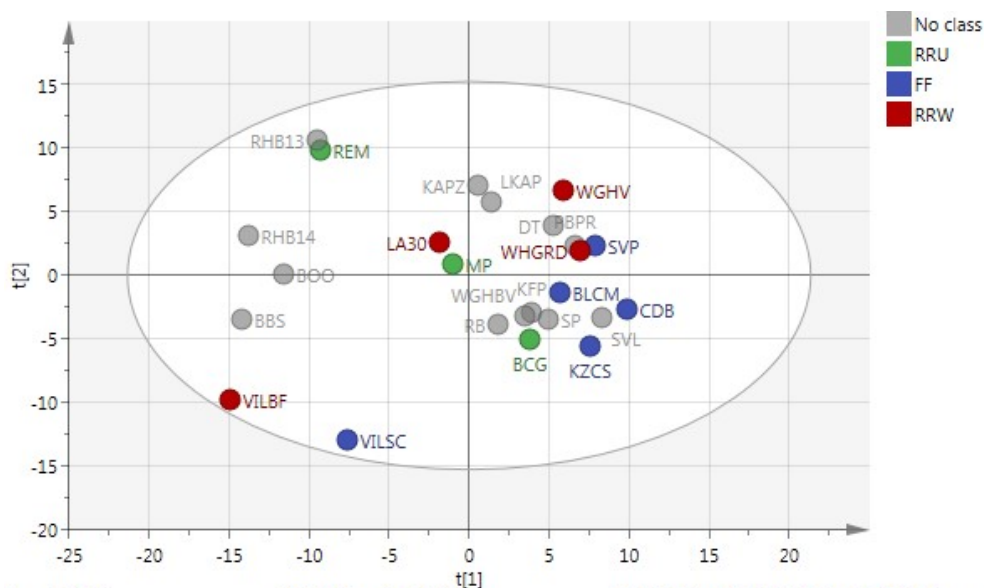


**Figure 3a.** Component 1 and 2 of the PCA-X model for the combined LC-HRMS results, no sample pre-processing (n=25). Styles attributed by the sensory task. 'No class' samples were not included in the sensory task.

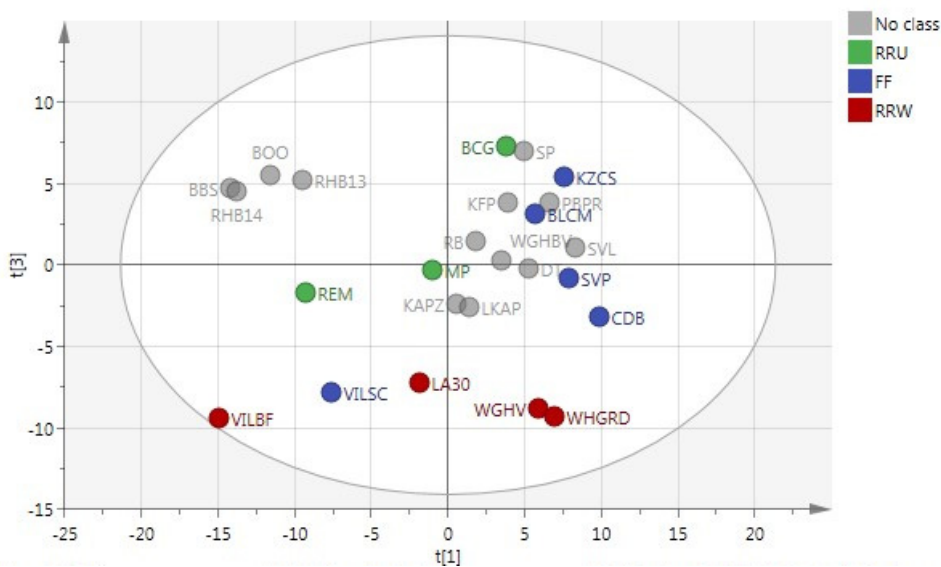


**Figure 3b.** Component 1 and 3 of the PCA-X model for the combined LC-HRMS results, no sample pre-processing (n=25). Styles attributed by the sensory task. 'No class' samples were not included in the sensory task.

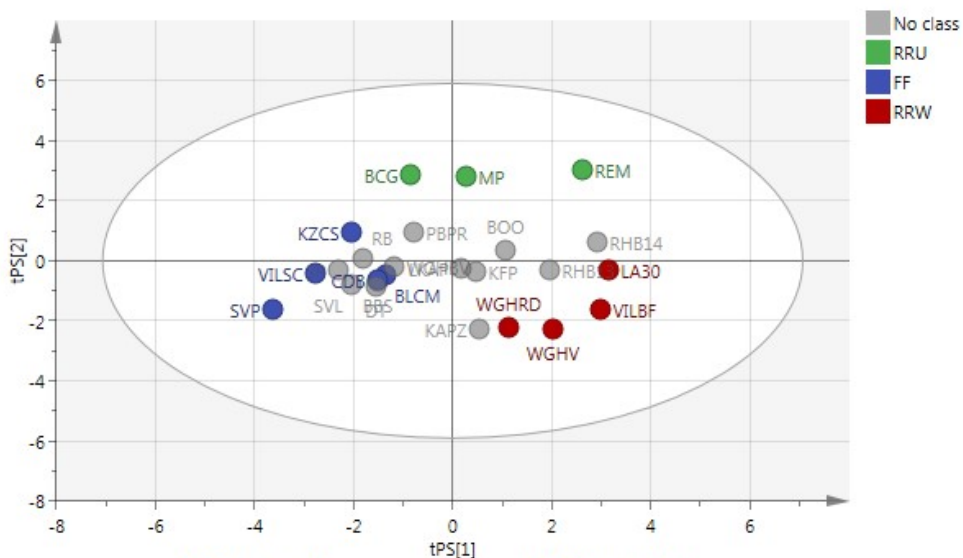


**Figure 4a.** PLS-DA model for positive ionization LCHRMS results, no sample pre-processing (n=25). Styles attributed by the sensory task. 'No class' samples constitute the prediction set.





As expected, the DA representation for the samples attributed to styles shows good grouping, which is promising for future work. In order to try and predict to which group the 'no class' samples belong, a PLS-DA model was created, using the wines subjected to sensory analysis as training set. The drawback is in this case the number of samples used to create the model. There were more samples included in the negative ionization mode experiment (39 vs 25), which resulted in a larger prediction set for this MS mode, while the working set remained the same size. A prediction certainty of 50% resulted in 2 samples being unclassified in positive MS mode (n=25), 3 in negative (n=39), and 1 in combined data sets (n=25). Increasing the level of certainty to 75% resulted in 7, 15, and 8 unclassified samples, respectively.

The wines that were not attributed clearly to a style group had to be excluded from the training set, too. Interestingly, the chemical analysis places these two sample, LKAP and WGHBV, in the middle of the plot, between the FF and RRU groups (Fig 4 and 5). When looking at the predicted scores for these wines, they fall below 50% certainty for assigning to a style group. This can possibly explain the difficulty that the judges had in placing these particular samples in either of the styles.

The general configuration is similar when considering the LC-HRMS results from the two ionization modes separately and combined (Fig 4 and 5). Even though the general configurations obtained from separate and combined MS ionization mode data appear similar, the prediction scores change depending on the set used, therefore there is merit in using a more complete set of results. For example, for the samples REM (RRU, training set), and RHB13 and RHB14 (prediction set), their positions change depending on the MS data considered. They are not closely associated in the representation of the positive mode (Fig 4a) but situated together in the representation of the negative and combined data sets (Fig 4b and 5). The prediction scores indicate the same. For positive MS mode, RHB13 and RHB14 can be attributed to both RRU and RRW groups with a certainty of around or less than 50%. In negative mode and combined sets, both samples are attributed to the RRU group with a confidence higher than 90%. Some insight into the samples reveals that they are all from the same estate, made in similar conditions, the differences between the two samples in the prediction set is the vintage (therefore, the age at the time of analysis) and that, often, these wines are sensorially characterized as RRU. This particular situation makes the case for combining the ionization mode results to avoid loss of information.

Up to this point, the work presented here can be considered more proof of principle rather than definitive evidence that Chenin Blanc styles can be predicted using LC-MS data. More in-depth data analysis will possibly

reveal the compounds correlated with styles. The presence of such markers should eliminate the need for insight or sensory information in the case of samples that fall in-between groups. At the same time, removing superfluous MS information would result in decreasing the statistical noise and make predictions more reliable.

## CONCLUSIONS

Results indicate that even though the traditional evaluation of Chenin Blanc styles has its merits, a more objective way of attributing the style is also possible with the help of chemical analysis coupled with integrated statistical tools. Even though models based on chemical data can designate a wine as fitting in a specific group, sensory evaluation has in some cases more relevance, as it deals with human perception, be it for experts or consumers. In the field of sensory research, this translates into a need for a sensory method that can evaluate more wines to increase the training set and create a more reliable model.

The issue of choice for representative samples for the training set could be avoided in the future with the help of marker molecules. Identification of markers for styles would make the discrimination between groups easier, avoiding the issue of wines that fall “in between” the groups in both sensory and chemical evaluation.

## EXPERIMENTAL SECTION

### **Sensory evaluation: Directed sorting**

A sample set of 15 wines (including 2 repeats) were subjected to sensory evaluation in duplicate by 15 experts using a directed sorting task, taking into account both aroma and taste. The judges were asked to divide the samples into three groups according to the Chenin Blanc wine style. The data has been analysed using DISTATIS to assess individual differences between samples as well as to build a multivariate map of the data using multidimensional scaling (MDS).

### **Chemical analysis: LC-HRMS**

Wine samples (n=39, including the ones used for sensory evaluation) were analysed by UPLC (Waters Corporation) equipped with a Synapt G2 quadrupole time-of-flight mass spectrometer (Waters Corporation). The

separation was done on an Acquity UPLC HSS T3 column (1.8  $\mu\text{m}$  internal diameter, 2.1 mm x 100 mm, Waters Corporation) using 0.1% formic acid (mobile phase A) and acetonitrile (mobile phase B) and a scouting gradient. Flow rate was 0.3 mL/min and the column temperature 55 °C. The injection volume was 2  $\mu\text{L}$ .

Data was acquired in MS<sup>e</sup> mode which consisted of a low collision energy scan (6V) from m/z 150 to 600 and a high collision energy scan from m/z 40 to 600. The high collision energy scan was done using a collision energy ramp of 30-60 V. The mass spectrometer was optimized for best sensitivity, cone voltage 15 V, nitrogen desolvation gas at 650 L/hr and desolvation temperature 275°C. The instrument was operated with an electrospray ionization probe in both positive and negative mode.

Chromatographic data was extracted as (RT\_m/z, intensity) matrix by the application manager used. The MS data generated from both ionization modes (separate and combined sets) was analysed using MarkerLynx XS (Waters Corporation), an application manager that performs 3D peak integration, data set alignment and incorporates multivariate statistical tools. The software is directly integrated with SIMCA-P (Umetrics) and the statistical algorithms are directly applied to the processed data sets.

## ACKNOWLEDGMENTS

The authors would like to thank THRIP and Winetech for the financial support.

## REFERENCES

1. A. De Villiers, P. Majek, F. Lynen, A. Crouch, H. Lauer, P. Sandra, *European Food and Research Technology*, **2005**, 221, 520.
2. A. Tredoux, A. De Villiers, P. Majek, F. Lynen, A. Crouch, P. Sandra, *Journal of Agricultural and Food Chemistry*, **2008**, 56, 4286.
3. L. Jaitz, K. Siegl, R. Eder, G. Rak, L. Abranko, G. Koellensperger, S. Hann, *Food Chemistry*, **2010**, 122, 366.
4. J.L. Aleixandre-Tudo, H. Nieuwoudt, J.L. Aleixandre, W.J. Du Toit, *Journal of Agricultural and Food Chemistry*, **2015**, 53, 1088.
5. O. Tomic, A. Nilsen, M. Martens, T. Næs, *LWT - Food Science and Technology*, **2007**, 40, 262.
6. T. Dahl, O. Tomic, J.P. Wold, T. Næs, *Food Quality and Preference*, **2008**, 19, 103.

7. O. Tomic, G. Luciano, A. Nilsen, G. Hyldig, K. Lorensen, T. Næs, *European Food and Research Technology*, **2009**, 230, 497.
8. M. Hoffmann, P. Varela, G. Ares, "Novel Techniques in Sensory Characterization Profiling and Consumer", CRC Press, Taylor & Francis Group, Boca Raton, **2014**.
9. D. Cozzolino, W. Cynkar, N. Shah, P. Smith, *Analytical and Bioanalytical Chemistry*, **2011**, 401, 1497.
10. A. Edelmann, J. Diewok, K.C. Schuster, B. Lendl, *Journal of Agricultural and Food Chemistry*, **2001**, 49, 1139.
11. M. Urbano, M.D. Luque De Castro, P.M. Pérez, J. García-Olmo, M.A. Gómez-Nieto, *Food Chemistry*, **2006**, 97, 166.
12. M. Le Moigne, C. Maury, D. Bertrand, F. Jourjon, *Food Quality and Preference*, **2008**, 19, 220.
13. L.M. Schmidtke, A. Rudnitskaya, A.J. Saliba, J.W. Blackman, G.R. Scollary, A.C. Clark, D.N. Rutledge, I. Delgadillo, A. Legin, *Journal of Agricultural and Food Chemistry*, **2010**, 58, 5026.
14. A.L. Fudge, K.L. Wilkinson, R. Ristic, D. Cozzolino, *Journal of Agricultural and Food Chemistry*, **2012**, 60, 52.
15. J.L. Aleixandre-Tudo, I. Alvarez, M.J. Garcia, V. Lizama, J.L. Aleixandre, *Czech Journal of Food Science*, **2015**, 33, 217.
16. CBA. 2016. Chenin Blanc Styles. Available from: <http://www.chenin.co.za/styles.html> accessed 16 Dec 2016
17. D. Valentin, S. Chollet, M. Lelievre, H. Abdi, *International Journal of Food Science and Technology*, **2012**, 47, 1563.



*Dedicated to Professor Costel Sârbu on the  
Occasion of His 65<sup>th</sup> Anniversary*

## COMPARATIVE CHEMOMAPPING OF PHYTOCONSTITUENTS FROM DIFFERENT EXTRACTS OF GLOBE ARTICHOKE - *CYNARA SCOLYMUS* L.

SZABOLCS VÍGH<sup>a,b</sup>, ZOLTÁN CZIÁKY<sup>b</sup>, LÁSZLÓ TAMÁS SINKA<sup>b</sup>,  
CIPRIAN PRIBAC<sup>c</sup>, LIANA MOȘ<sup>c</sup>, VIOLETA TURCUȘ<sup>c</sup>,  
JUDIT REMENYIK<sup>d</sup> and ENDRE MÁTHÉ<sup>b,c,d,\*</sup>

**ABSTRACT.** Artichoke (*Cynara scolymus* L.) is a well-known herb for its efficiency in the prevention/treatment of liver injuries, among other human chronic diseases. The aim of present study was to analyse the phytoconstituents content of aqueous and hydro-alcoholic extracts obtained from the leaves of artichoke. The chemomapping was carried out using UHPLC-ESI-MS. Several new and some known phytoconstituents were identified in the two type of extracts that have slightly different composition profiles. The newly found phytoconstituents in artichoke, plead for multiple health promoting effects that have presumably more stochastic than determinative features. Therefore, further experiments are needed using such extracts, and based on a system biology approach to clarify the complexity of beneficial effects of artichoke.

**Keywords:** globe artichoke, *Cynara scolymus*, phytoconstituents, bioactive compound, LC-ESI-MS

---

<sup>a</sup> University of Nyíregyháza, Institute of Agricultural Sciences, Sostói str. 31/B, H-4432, Nyíregyháza, Hungary (present address)

<sup>b</sup> University of Nyíregyháza, Agricultural and Molecular Research Institute, Sostói str. 31/B, H-4432, Nyíregyháza, Hungary

<sup>c</sup> “Vasile Goldiș” Western University of Arad, Faculty of Medicine, Liviu Rebreanu Str.91-93, RO-310414, Arad, Romania

<sup>d</sup> University of Debrecen, Faculty of Agriculture and Food Sciences and Environmental Management, Böszörményi str. 138, H-4032 Debrecen, Hungary

\* Corresponding author: endre.mathe64@gmail.com

## INTRODUCTION

Globe artichoke (*Cynara scolymus* L.) has been cultivated since the ancient times in the Mediterranean and North African regions. In the middle ages, its cultivation spread across Western Europe from Italy to Spain, France, The Netherlands, England, and later on, in the 1800s reaches the Southern parts of USA. Moreover, Northern African countries like Egypt, Algeria and Tunisia together with South American countries like Argentina and Peru did become important artichoke producers in recent times.

Globe artichoke is considered a healthy food due to its nutritive and phytoconstituent content. It contains proteins, minerals, a low amount of lipids, dietary fibre and a high proportion of phenolics [1-2]. Among phenolics there were identified compounds like cynarin (1,3-di-O-caffeoylquinic acid), luteolin, cynaroside (luteolin-7-O-glucoside), scolymoside (luteolin-7-rutinoside); phenolic acids such as caffeic, coumaric, hydroxycinnamic, ferulic, caffeoylquinic acid derivatives; mono- and dicaffeoylquinic acids, including chlorogenic; acid alcohols; flavonoid glycosides [2-3]. The content of phytoconstituents was shown to vary among different cultivars and conditions related to cultivation, harvest, post-harvest and cooking [4-5].

Globe artichoke features a relatively high antioxidant capacity [6-7], its hepatoprotective, bile-enhancing and lipid-lowering effects have been demonstrated [8], while its implications in preventing cardiovascular disease by its lipidic and glycemic-reducing action has also been confirmed [9-10]. Moreover, its putative anticancer effect has been studied, and some experimental data suggests that artichoke extracts could be applied as a nonconventional, adjuvant therapy for cancer chemoprevention and/or treatment [11-13].

In the present paper we are describing the comparative UHPLC-ESI-MS chemomapping of aqueous and hydro-alcoholic artichoke extracts that were found to inhibit significantly the proliferation of several human cancer cell lines [14]. Our study was meant to identify all possible phytoconstituents with the used experimental setup, and as a consequence 49 and 51 molecules were described in the aqueous and hydro-alcoholic artichoke extracts, respectively. Some of the newly identified compounds were confirmed by standards, while other compounds have already been reported by others [15-26].

## RESULTS AND DISCUSSION

In this paper, we are describing the qualitative analysis performed for artichoke (*Cynara scolymus* L.) extracts by applying reversed phase UHPLC-ESI-MS using a gradient mobile phase consisting of acetonitrile and water. The

aqueous and the hydro-alcoholic extracts of artichoke leaves were investigated in positive and negative ionisation modes as described in Materials and Methods.

There have been 49 phytoconstituents identified in the aqueous artichoke extract as shown on the corresponding chromatograms (Figure 1-2.) and in Table 1.

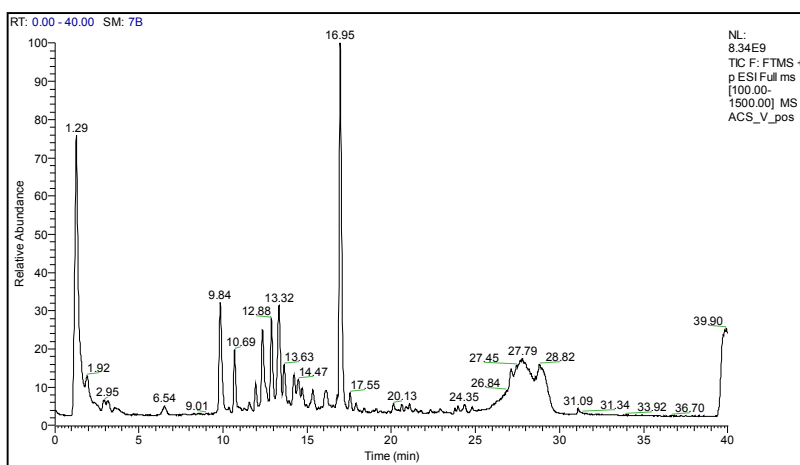


**Figure 1.** Total ion chromatogram of aqueous extract of artichoke in positive ionisation mode.

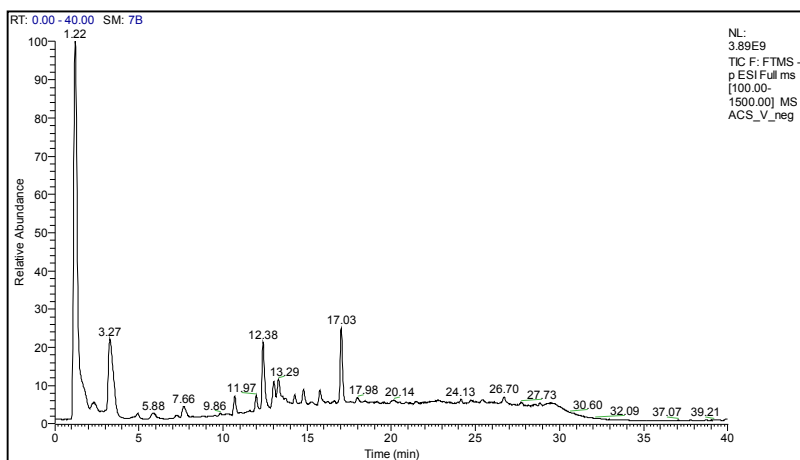


**Figure 2.** Total ion chromatogram of aqueous extract of artichoke in negative ionisation mode.



**Table 1.** Phytoconstituents identified in the aqueous artichoke extract. Rt –retention time; [M+H]<sup>+</sup> - molecular ion masses; [M+H]<sup>-</sup> - the found fragment ion mass; Ref- references; (\*) [M]<sup>+</sup>; (\*\*) confirmed by standards. The difference between measured and calculated molecular ion masses were always below 5 ppm.

Peak	R <sub>t</sub>	[M+H] <sup>+</sup>	[M-H] <sup>-</sup>	Formula	Fragments found	Assignment	Ref.
1	1.22	104.10754 <sup>*</sup>		C <sub>5</sub> H <sub>14</sub> NO	60.0814, 59.0736	Choline	
2	1.27	175.11951		C <sub>6</sub> H <sub>14</sub> N <sub>4</sub> O <sub>2</sub>	158.0922, 130.0975	Arginine <sup>**</sup>	
3	1.27		179.05557	C <sub>6</sub> H <sub>12</sub> O <sub>6</sub>	113.0229, 101.0229	Glucose or galactose	
4	1.29	138.05550 <sup>*</sup>		C <sub>7</sub> H <sub>8</sub> NO <sub>2</sub>	110.0602, 96.0447	Trigonelline	
5	1.32	133.06132		C <sub>4</sub> H <sub>8</sub> N <sub>2</sub> O <sub>3</sub>	116.0344, 88.0397	Asparagine <sup>**</sup>	
6	1.43	324.05968		C <sub>9</sub> H <sub>13</sub> N <sub>3</sub> O <sub>5</sub>	112.0507, 95.0240	Cytidine <sup>**</sup>	
7	1.48	146.09296		C <sub>5</sub> H <sub>11</sub> N <sub>3</sub> O <sub>2</sub>	128.0817, 111.0555	4-Guanidinobutyric acid	
8	1.51	136.06233		C <sub>5</sub> H <sub>5</sub> N <sub>5</sub>	119.0352, 94.0402	Adenine	
9	1.52		362.05018	C <sub>10</sub> H <sub>14</sub> N <sub>5</sub> O <sub>8</sub> P	211.0005, 150.0408	Guanosine 5'-monophosphate	
10	1.53	168.06607		C <sub>8</sub> H <sub>9</sub> NO <sub>3</sub>	150.0548, 140.0705	Pyridoxal <sup>**</sup>	
11	1.57	124.03986		C <sub>6</sub> H <sub>5</sub> NO <sub>2</sub>	96.0448, 80.0499	Nicotinic acid <sup>**</sup>	
12	1.59	144.10245 <sup>*</sup>		C <sub>7</sub> H <sub>14</sub> NO <sub>2</sub>	102.0554, 98.0968	Stachydrine	
13	1.71	170.08172		C <sub>8</sub> H <sub>11</sub> NO <sub>3</sub>	152.0704, 134.0600	Pyridoxine <sup>**</sup>	
14	1.74		243.06171	C <sub>9</sub> H <sub>12</sub> N <sub>2</sub> O <sub>6</sub>	200.0557, 153.0291	Uridine	
15	1.76	113.03511		C <sub>4</sub> H <sub>4</sub> N <sub>2</sub> O <sub>2</sub>	96.0084, 95.0245	Uracil <sup>**</sup>	
16	1.78	182.08172		C <sub>9</sub> H <sub>11</sub> NO <sub>3</sub>	165.0544, 147.0439	2-Hydroxyphenyl-alanine	
17	1.92	123.05584		C <sub>6</sub> H <sub>6</sub> N <sub>2</sub> O	106.0291, 96.0447	Nicotinamide <sup>**</sup>	
18	2.34		346.05526	C <sub>10</sub> H <sub>14</sub> N <sub>5</sub> O <sub>7</sub> P	211.0006, 192.9902	Adenosine 5'-monophosphate	
19	2.62		282.08385	C <sub>10</sub> H <sub>13</sub> N <sub>5</sub> O <sub>5</sub>	150.0408, 133.0143	Guanosine	
20	2.94	268.10458		C <sub>10</sub> H <sub>13</sub> N <sub>5</sub> O <sub>4</sub>	136.0617, 119.0350	Adenosine <sup>**</sup>	

## COMPARATIVE CHEMOMAPPING OF PHYTOCONSTITUENTS FROM DIFFERENT EXTRACTS OF ...

Peak	R <sub>t</sub>	[M+H] <sup>+</sup>	[M-H] <sup>-</sup>	Formula	Fragments found	Assignment	Ref.
21	3.18	166.08681		C <sub>9</sub> H <sub>11</sub> NO <sub>2</sub>	149.0602, 131.0492	Phenylalanine**	
22	3.27		353.08726	C <sub>16</sub> H <sub>18</sub> O <sub>9</sub>	191.0552, 179.0342	Caffeoylquinic acid I	16
23	4,78	122.09698		C <sub>8</sub> H <sub>11</sub> NO <sub>2</sub>	105.0702, 103.0546	Phenethylamine	
24	4.83	220.11850		C <sub>9</sub> H <sub>17</sub> NO <sub>5</sub>	202.1073, 184.0967	Pantothenic acid**	
25	5.90		337.09234	C <sub>16</sub> H <sub>18</sub> O <sub>8</sub>	191.0552, 163.0388	Coumaroylquinic acid I	17
26	6.52	205.09771		C <sub>11</sub> H <sub>12</sub> N <sub>2</sub> O <sub>2</sub>	188.0705, 170.0599	Tryptophan**	
27	7.66		353.08726	C <sub>16</sub> H <sub>18</sub> O <sub>9</sub>	191.0552, 179.0338	Caffeoylquinic acid II	16
28	8.31	190.05042		C <sub>10</sub> H <sub>7</sub> NO <sub>3</sub>	162.0547, 144.0442	Kynurenic acid	
29	8.84	341.08726		C <sub>15</sub> H <sub>16</sub> O <sub>9</sub>	179.0338, 151.0388	Esculin	
30	8.86		335.07669	C <sub>16</sub> H <sub>16</sub> O <sub>8</sub>	179.0339, 161.0231	Caffeoylshikimic acid I	
31	9.57	295.12940		C <sub>14</sub> H <sub>18</sub> N <sub>2</sub> O <sub>5</sub>	278.1119, 232.0961	γ-Glutamylphenylalanine	
32	9.97	298.09739		C <sub>11</sub> H <sub>15</sub> N <sub>5</sub> O <sub>3</sub> S	163.0422, 145.0313	5'-S-Methyl-5'-thioadenosine	
33	10.19		337.09234	C <sub>16</sub> H <sub>18</sub> O <sub>8</sub>	191.0552, 163.0389	Coumaroylquinic acid II	17
34	11.53	191.07082		C <sub>11</sub> H <sub>10</sub> O <sub>3</sub>	176.0466, 148.0518	7-Methoxy-4-methylcoumarin	
35	12.78		593.15065	C <sub>21</sub> H <sub>18</sub> O <sub>11</sub>	473.1093, 383.0772	Vicenin-2	
36	13.02		335.07669	C <sub>16</sub> H <sub>16</sub> O <sub>8</sub>	179.0339, 161.0232	Caffeoylshikimic acid III	
37	13.02		515.11896	C <sub>25</sub> H <sub>24</sub> O <sub>12</sub>	335.0776, 191.0552	1,3-Di-O-caffeoylquinic acid (Cynarin)	
38	13.27	283.15455		C <sub>15</sub> H <sub>22</sub> O <sub>5</sub>	265.1429, 247.1324	Cynaratriol	
39	13.54		461.07201	C <sub>21</sub> H <sub>18</sub> O <sub>12</sub>	285.0404, 217.0501	Luteolin-7-O-glucuronide	18
40	13.54	146.06059		C <sub>9</sub> H <sub>7</sub> NO	118.0652,1 17.0573	Indole-4-carbaldehyde	
41	13.81	179.07082		C <sub>10</sub> H <sub>10</sub> O <sub>3</sub>	161.0594, 147.0438	4-Hydroxy-3-methoxy-cinnamaldehyde	
42	14.60		445.07709	C <sub>21</sub> H <sub>18</sub> O <sub>11</sub>	269.0454, 225.0546	Apigenin-7-O-glucuronide	19

Peak	R <sub>t</sub>	[M+H] <sup>+</sup>	[M-H] <sup>-</sup>	Formula	Fragments found	Assignment	Ref.
43	14.74		593.15065	C <sub>27</sub> H <sub>30</sub> O <sub>15</sub>	285.0404, 133.0275	Luteolin-7-O-rutinoside (Scolymoside)	20
44	14.79		447.09274	C <sub>21</sub> H <sub>20</sub> O <sub>11</sub>	327.0509, 285.0403	Luteolin-7-O-glucoside (Cynaroside)	18, 19, 21
45	15.20		193.05009	C <sub>10</sub> H <sub>10</sub> O <sub>4</sub>	178.0262, 149.0596	Ferulic acid	
46	15.67	433.11347		C <sub>21</sub> H <sub>20</sub> O <sub>10</sub>	271.0600, 153.0180	Cosmosiin (Apigenin-7-O-glucoside)**	22, 23
47	17.98		285.03991	C <sub>15</sub> H <sub>10</sub> O <sub>6</sub>	217.0499, 199.0393	Luteolin	
48	20.34		809.43235	C <sub>42</sub> H <sub>66</sub> O <sub>15</sub>	647.3814, 603.3902	Cynarasaponin E	26
49	21.86		793.43744	C <sub>42</sub> H <sub>66</sub> O <sub>14</sub>	631.3859, 587.3961	Cynarasaponin C	26

There have been 51 phytoconstituents identified in the hydro-alcoholic artichoke extract as shown on Fig.3-4 and in Table 2.

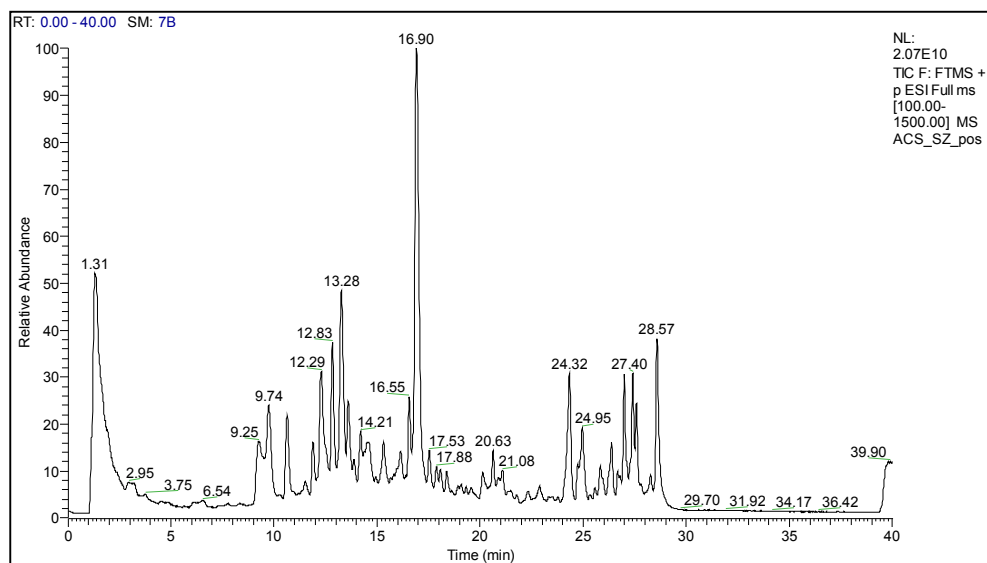


**Figure 3.** Total ion chromatogram of hydro-alcoholic extract of artichoke in positive ionisation mode.

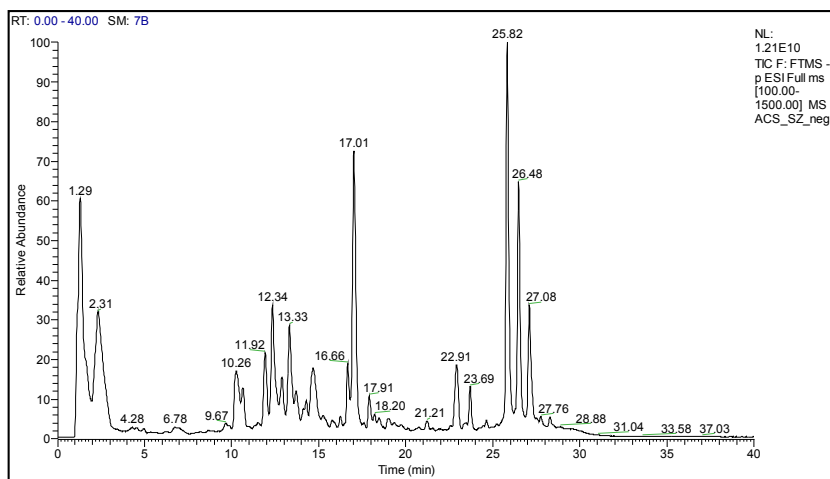


**Figure 4.** Total ion chromatogram of hydro-alcoholic extract of artichoke in negative ionisation mode.

**Table 2.** Phytoconstituents identified in the hydro-alcoholic artichoke extract. Rt –retention time; [M+H]<sup>+</sup> - molecular ion masses; [M+H]<sup>-</sup> - the found fragment ion mass; Ref- references; (\*) [M]<sup>+</sup>; (\*\*) confirmed by standards. The difference between measured and calculated molecular ion masses were always below 5 ppm.

Peak	R <sub>t</sub>	[M+H] <sup>+</sup>	[M-H] <sup>-</sup>	Formula	Fragments found	Assignment	Ref.
1	1.26	138.05550*		C <sub>7</sub> H <sub>8</sub> NO <sub>2</sub>	110.0603, 96.0449	Trigonelline	
2	1.28	104.10754*		C <sub>5</sub> H <sub>14</sub> NO	60.0814, 59.0736	Choline	
3	1.30	175.11951		C <sub>6</sub> H <sub>14</sub> N <sub>4</sub> O <sub>2</sub>	158.0923, 130.0976	Arginine**	
4	1.35	133.06132		C <sub>4</sub> H <sub>8</sub> N <sub>2</sub> O <sub>3</sub>	116.0343, 88.0397	Asparagine**	
5	1.38		179.05557	C <sub>6</sub> H <sub>12</sub> O <sub>6</sub>	113.0229, 101.0230	Glucose or galactose	
6	1.50	324.05968		C <sub>9</sub> H <sub>13</sub> N <sub>3</sub> O <sub>5</sub>	112.0507, 95.0243	Cytidine**	
7	1.52	146.09296		C <sub>5</sub> H <sub>11</sub> N <sub>3</sub> O <sub>2</sub>	128.0815, 111.0554	4-Guanidinobutyric acid	
8	1.53	136.06233		C <sub>5</sub> H <sub>5</sub> N <sub>5</sub>	119.0353, 94.0403	Adenine	
9	1.62	124.03986		C <sub>6</sub> H <sub>5</sub> NO <sub>2</sub>	96.0448, 80.0500	Nicotinic acid**	

Peak	R <sub>t</sub>	[M+H] <sup>+</sup>	[M-H] <sup>-</sup>	Formula	Fragments found	Assignment	Ref.
10	1.75	170.08172		C <sub>8</sub> H <sub>11</sub> NO <sub>3</sub>	152.0704, 134.0601	Pyridoxine**	
11	1.83	113.03511		C <sub>4</sub> H <sub>4</sub> N <sub>2</sub> O <sub>2</sub>	96.0084, 95.0245	Uracil**	
12	1.84	182.08172		C <sub>9</sub> H <sub>11</sub> NO <sub>3</sub>	165.0542, 147.0439	2-Hydroxyphenyl-alanine	
13	1.94	123.05584		C <sub>6</sub> H <sub>6</sub> N <sub>2</sub> O	106.0290, 96.0448	Nicotinamide**	
14	2.68		282.08385	C <sub>10</sub> H <sub>13</sub> N <sub>5</sub> O <sub>5</sub>	150.0408, 133.0142	Guanosine	
15	2.99	268.10458		C <sub>10</sub> H <sub>13</sub> N <sub>5</sub> O <sub>4</sub>	136.0617, 119.0347	Adenosine**	
16	3.23	166.08681		C <sub>9</sub> H <sub>11</sub> NO <sub>2</sub>	149.0601, 131.0493	Phenylalanine**	
17	4.85	122.09698		C <sub>8</sub> H <sub>11</sub> N	105.0702, 103.0546	Phenethylamine	
18	4.87	220.11850		C <sub>9</sub> H <sub>17</sub> NO <sub>5</sub>	202.1070, 184.0967	Pantothenic acid**	
19	6.54	205.09771		C <sub>11</sub> H <sub>12</sub> N <sub>2</sub> O <sub>2</sub>	188.0705, 170.0598	Tryptophan**	
20	8.26	190.05042		C <sub>10</sub> H <sub>7</sub> NO <sub>3</sub>	162.0547, 144.0442	Kynurenic acid	
21	8.79	341.08726		C <sub>15</sub> H <sub>16</sub> O <sub>9</sub>	179.0337, 151.0389	Esculin	
22	9.55	295.12940		C <sub>14</sub> H <sub>18</sub> N <sub>2</sub> O <sub>5</sub>	278.1121, 232.0964	γ-Glutamylphenyl-alanine	
23	9.95	298.09739		C <sub>11</sub> H <sub>15</sub> N <sub>5</sub> O <sub>3</sub> S	163.0422, 145.0318	5'-S-Methyl-5'-thioadenosine	
24	11.49	174.11302		C <sub>8</sub> H <sub>15</sub> NO <sub>3</sub>	156.1010, 132.1019	N-Acetylisoleucine	
25	11.51	191.07082		C <sub>11</sub> H <sub>10</sub> O <sub>3</sub>	176.0462, 148.0517	7-Methoxy-4-methylcoumarin	
26	12.03	174.11302		C <sub>8</sub> H <sub>15</sub> NO <sub>3</sub>	156.1012, 132.1019	N-Acetylleucine	
27	12.52		593.15065	C <sub>21</sub> H <sub>18</sub> O <sub>11</sub>	473.1084, 383.0770	Vicenin-2	
28	12.57		461.07201	C <sub>21</sub> H <sub>18</sub> O <sub>12</sub>	285.0403, 217.0499	Luteolin-7-O-glucuronide	18
29	12.86	193.05009		C <sub>10</sub> H <sub>8</sub> O <sub>4</sub>	178.0258, 165.0544	Scopoletin	
30	13.05		515.11896	C <sub>25</sub> H <sub>24</sub> O <sub>12</sub>	335.0770, 191.0552	1,3-Di-O-caffeoylquinic acid (Cynarin)	
31	13.27	283.15455		C <sub>15</sub> H <sub>22</sub> O <sub>5</sub>	265.1429, 247.1324	Cynaratriol	

## COMPARATIVE CHEMOMAPPING OF PHYTOCONSTITUENTS FROM DIFFERENT EXTRACTS OF ...

Peak	R <sub>t</sub>	[M+H] <sup>+</sup>	[M-H] <sup>-</sup>	Formula	Fragments found	Assignment	Ref.
32	13.32	163.07591		C <sub>10</sub> H <sub>10</sub> O <sub>2</sub>	131.0492, 103.0545	Methyl cinnamate	
33	13.38		581.18703	C <sub>27</sub> H <sub>34</sub> O <sub>14</sub>	297.1768, 167.0337	Naringin dihydrochalcone	
34	13.52	146.06059		C <sub>9</sub> H <sub>7</sub> NO	118.0652,1 17.0572	Indole-4-carbaldehyde	
35	13.65		445.07709	C <sub>21</sub> H <sub>18</sub> O <sub>11</sub>	269.0454, 225.0550	Apigenin-7-O-glucuronide	19
36	13.80	179.07082		C <sub>10</sub> H <sub>10</sub> O <sub>3</sub>	161.0595, 147.0439	4-Hydroxy-3-methoxy-cinnamaldehyde	
37	14.71		593.15065	C <sub>27</sub> H <sub>30</sub> O <sub>15</sub>	285.0404, 133.0279	Luteolin-7-O-rutinoside (Scolymoside)	20
38	14.73		447.09274	C <sub>21</sub> H <sub>20</sub> O <sub>11</sub>	327.0507, 285.0400	Luteolin-7-O-glucoside (Cynaroside)	18, 19, 21
39	15.19		193.05009	C <sub>10</sub> H <sub>10</sub> O <sub>4</sub>	178.0259, 149.0595	Ferulic acid	
40	15.22		269.04500	C <sub>15</sub> H <sub>10</sub> O <sub>5</sub>	225.0550, 201.0550	Apigenin**	21, 24
41	15.54	579.17139		C <sub>27</sub> H <sub>30</sub> O <sub>14</sub>	271.0595, 153.0176	Isorhoifolin (Apigenin 7-O-rutinoside)	25
42	15.66	433.11347		C <sub>21</sub> H <sub>20</sub> O <sub>10</sub>	271.0594, 153.0179	Cosmosiin (Apigenin-7-O-glucoside)**	22, 23
43	17.89		285.03991	C <sub>15</sub> H <sub>10</sub> O <sub>6</sub>	217.0498, 199.0391	Luteolin	
44	18.94		539.04618	C <sub>25</sub> H <sub>16</sub> O <sub>14</sub>	269.0453, 201.0548	Unknown Apigenin derivative	
45	19.03	301.07121		C <sub>16</sub> H <sub>12</sub> O <sub>6</sub>	286.0466, 258.0515	Diosmetin	
46	21.76	329.10251		C <sub>18</sub> H <sub>16</sub> O <sub>6</sub>	314.0781, 313.0697	Salvigenin	
47	25.38	291.23241		C <sub>19</sub> H <sub>30</sub> O <sub>2</sub>	259.2035, 241.1949	Stearidonic acid methyl ester	
48	25.85	305.24806		C <sub>20</sub> H <sub>32</sub> O <sub>2</sub>	259.2058, 241.1939	Stearidonic acid ethyl ester	
49	27.20	457.36818		C <sub>30</sub> H <sub>48</sub> O <sub>3</sub>	439.3553, 411.3619	Ursolic acid	
50	19.43		809.43235	C <sub>42</sub> H <sub>66</sub> O <sub>15</sub>	647.3806, 603.3903	Cynarasaponin E	26
51	21.20		793.43744	C <sub>42</sub> H <sub>66</sub> O <sub>14</sub>	631.3851, 587.3955	Cynarasaponin C	26

The identification of the phytoconstituents was achieved by comparing individually the retention time, accurate mass, isotopic distribution and fragmentation pattern of every single newly detected molecule with artichoke compounds already reported in literature, and by screening MS databases like Metlin, mzCloud and Massbank. The identified molecules belong to twelve classes of phytoconstituents, and besides similarities, there are some striking differences among the aqueous and hydro-alcoholic artichoke extracts regarding their content as summarized in Table 3.

**Table 3.** Phytoconstituents identified in the aqueous and hydro-alcoholic artichoke extracts.

Phytoconstituents		Aqueous artichoke	Hydro-alcoholic artichoke
<b>Alkaloids</b>	Kynurenic acid	+	+
	Trigonelline	+	+
	Stachydrine <sup>a</sup>	+	
<b>Aminoacids</b>	2-Hydroxyphenylalanine	+	+
	4-Guanidinobutyric acid	+	+
	Arginine	+	+
	Asparagine	+	+
	L-Phenylalanine	+	+
	γ-Glutamilphenylalanin	+	+
	Tryptophan	+	+
	N-Acetylisoleucine <sup>b</sup>		+
	N-Acetylleucin <sup>b</sup>		+
<b>Coumarins</b>	7-Methoxy-4-methylcoumarin	+	+
	4-hidroxy-3-methoxy-cinnamaldehyde	+	+
	Scopoletin <sup>b</sup>		+
<b>Flavonoids</b>	Unknown Apigenin derivative <sup>b</sup>		+
	Apigenin <sup>b</sup>		+
	Cosmosiin (Apigenin-7-O-glucoside)	+	+
	Diosmetin <sup>b</sup>		+
	Luteolin	+	+
	Luteolin-7-O-glucoside (cynaroside)	+	+
	Luteolin-7-O-glucuronide	+	+
	Apigenin-7-O-glucuronide	+	+
	Luteolin-7-O-rutinoside (scolymoside)	+	+
	Isorhoifolin (Apigenin-7-O-rutinoside) <sup>b</sup>		+
	Salvigenin <sup>b</sup>		+
	Naringin dihydrochalcone <sup>b</sup>		+
	Vicenin-2 (6,8-Di-C-glucosylapigenin)	+	+

Phytoconstituents		Aqueous artichoke	Hydro-alcoholic artichoke
<b>Polyphenols</b>	1,3-Di-O-caffeoylquinic acid (Cynarin)	+	+
	5-O-Caffeoylshikimic acid I <sup>a</sup>	+	
	5-O-Caffeoylshikimic acid II <sup>a</sup>	+	
	Esculin	+	+
	Ferulic acid	+	+
	Caffeoylquinic acid I <sup>a</sup>	+	
	Caffeoylquinic acid II <sup>a</sup>	+	
	Coumaroylquinic acid I <sup>a</sup>	+	
Coumaroylquinic acid II <sup>a</sup>	+		
<b>Other metabolites</b>	Indole-4-carbaldehyde	+	+
	Choline	+	+
	Methyl cinnamate <sup>b</sup>		+
	Phenethylamine	+	+
<b>Purines and pyrimidines</b>	5'-S-Methyl-5'-thioadenosine	+	+
	Adenine	+	+
	Adenosine	+	+
	Adenosine 5'-monophosphate (AMP) <sup>a</sup>	+	
	Cytidine	+	+
	Guanosine	+	+
	Guanosine 5'-monophosphate (GMP) <sup>a</sup>	+	
	Uracil	+	+
	Uridine <sup>a</sup>	+	
<b>Saponins</b>	Cynarasaponin E	+	+
	Cynarasaponin C	+	+
<b>Terpenoid</b>	Cynaratriol	+	+
	Ursolic acid <sup>b</sup>		+
<b>Sugars</b>	Glucose or Galactose	+	+
<b>Steroids</b>	Stearidonic acid methyl ester <sup>b</sup>		+
	Stearidonic acid ethyl ester <sup>b</sup>		+
<b>Vitamines</b>	Nicotinamide	+	+
	Nicotinic acid (B3)	+	+
	Pantothenic acid (B5)	+	+
	Pyridoxal <sup>a</sup>	+	
	Pyridoxine (B6)	+	+

<sup>a</sup> Compounds to be found only in aqueous extract

<sup>b</sup> Compounds found only in hydro-alcoholic extracts

According to our current knowledge, we were the first to identify the kynurenic acid, trigonelline and stachydrine as the major alkaloids present in both artichoke extracts. The neuroprotective role of kynurenic acid has been already



demonstrated, and is achieved via the kynurenine pathway by metabolizing the tryptophan amino acid that is also present in both of our artichoke extracts [27]. The presence of trigonelline in plant extracts like coffee and fenugreek was demonstrated, and some experimental data did indicate its Nrf2 inhibitory effect together with the blocking of Nrf2-dependent expression of proteasomal genes, and reduced proteasome activity in some pancreatic carcinoma cell lines [28]. Stachydrine is a prolinebetaine type of alkaloid that was suggested to play an important role in prevention of cardiovascular diseases by inhibiting the deleterious effect of high-glucose on endothelial cells through the modulation of SIRT1 pathway [29].

With the exception of phenylalanine and asparagine, all the other amino acids listed in Table 3. are reported for the first time in the case of artichoke extracts [30].

In this paper we are describing also for the first time the presence of some coumarins in artichoke extracts. The newly identified 7-methoxy-4-methylcoumarin was shown by others to behave like the multidrug resistant modulator verapamil that was more cytotoxic against tumor cells than normal cells [31]. Cinnamaldehyde is found in both of our artichoke extracts, and it was shown by others to ameliorate the induced cardiac dysfunction in rats by inhibiting ROS production and autophagy through TLR4-NOX4 pathway and exhibits anti-inflammatory activity [32]. Similarly to others [33], we were able to identify the scopoletin in artichoke leaves hydro-alcoholic extracts, and it was suggested to have an important anti-inflammatory activity by inhibiting the phosphorylation of NF- $\kappa$ B and p38 MAPK in mice [34].

Flavonoids like apigenin, apigenin-7-O-glucoside, apigenin-7-O-glucuronide, luteolin-7-O-glucuronide, luteolin-7-O-glucoside and apigenin-7-rutinoside had been already reported [35-38]. However, flavonoids like diosmetin, salvigenin, naringin dihydrochalcone and vicenin-2 have been for the first time identified, and are mostly present in the hydro-alcoholic artichoke extract (see Table 3.). Diosmetin was shown by others to inhibit the metastasis of hepatocellular carcinoma cells [39,40], while salvigenin antitumor and immunomodulatory effects on tumor bearing mice had been demonstrated [41]. The naringin dihydrochalcone biological effects were not analysed to present days, however its major constituent the naringin was suggested to be the main component of Ganshuang granule that plays an anti-fibrotic role through deactivation of hepatic stellate cells in cirrhotic mouse model [42], and through the attenuation of EGFR/ERK signalling could suppress cancer cell growth [43]. In the case of vicenin-2 has been recently shown that can suppress high-glucose induced vascular inflammatory processes in human umbilical vein endothelial cells and mice, thereby suggesting its effectiveness as a therapeutic agent for vascular inflammatory diseases [44, 45].

The polyphenol content of artichoke was extensively analysed, and several papers were published comparing mature and baby plants in raw or cooked forms with the a relevant phytoconstituent like cynarin -1,3-Di-O-caffeoylquinic acid [46]. Our aqueous artichoke extract contained much more polyphenols than the hydro-alcoholic extract, and several bioactive constituents were identified for the first time in artichoke, including 5-O-caffeoylshikimic acid, esculin and coumaroylquinic acids (see Table 3.). At present, no data are available regarding the biological effects of 5-O-caffeoylshikimic acid. Esculin has been found to feature gastroprotective effect in mice presumably through the inhibition of NF- $\kappa$ B activation [47], and its protective role against the genotoxicity induced by mitomycin C on liver and kidney mice cells was also described [48]. Ferulic acid is considered the methylated derivate of caffeic acid, and it was suggested that together with other flavonoids and polyphenols to contribute to the antioxidant, anti-inflammatory and anti-septic potential of *Lolium multiflorum* extracts [49].

Among metabolites we could identify indole-4-carbaldehyde that has not been described in previously by others, while the incidence of choline, methyl cinnamate and phenethylamine are shown for the first time in the case of artichoke extracts. Methionine- and choline-deficient diet leads to nonhydro-alcoholic fatty liver diseases in mouse, rat and swine model systems, therefore, it is expected that the administration of choline would contribute to the prevention of nonhydro-alcoholic steatohepatitis and fibrosis. Methyl cinnamate is a safe antibacterial and flavouring agent used in food industry, and was shown to inhibit the gastrointestinal contractility [50], PPAR $\gamma$  activity and adipocyte differentiation in part, by the CaMKK2-AMPK signalling pathway [51]. Phenethylamine is widely used in weight-loss type of dietary supplements [52].

We were able to confirm the finding of others with respect to the presence of saponins like cynarasaponin C, E, B and K in artichoke extracts [26, 53], while their biological effects remained totally elusive.

Among terpenoids the cynaratriol was already reported in artichoke extracts, while the ursolic acid is a newly identified phytoconstituent. The cynaratriol biological effects are not elucidated, while for ursolic acid has been demonstrated to exert anti-oxidative and anti-inflammatory effects on mouse brain injury model by activating the Nrf2-ARE pathway [54], moreover its anti-cancer and anti-metastatic effects were also proven [55,56].

We were also able to identify carbohydrates in artichoke extracts, though the applied method did not allow us to distinguish between glucose and galactose.

According to our current knowledge, steroids like stearidonic acid methyl ester and stearidonic acid ethyl ester were not reported in the case of previously studied artichoke extracts. However, the steroids detected by us

are derivatives of the stearidonic acid (18:4n-3), a plant-derived dietary n-3 PUFA, whose impact on tissue n-3 PUFA content are lacking.

The identification of vitamin C and some vitamins belonging to the B group (thiamine, riboflavine, nicotinamide and nicotinic acid) in artichoke extracts was already reported [57]. It has been demonstrated that the nicotinic acid can inhibit lipolysis, acutely reducing plasma free fatty acid concentrations, and may act in much the same manner as cynarin [58]. We are describing for the first time the incidence of pantothenic acid, pyridoxal and pyridoxine in artichoke extracts, while the above mentioned B5 and B6 vitamins were suggested to act as cancer risk reduction agents [59], and having anti-inflammatory effects associated with atherosclerosis and autoimmunity [60].

During our study, we also came across other phytoconstituents like vitamin C, thiamine, rutin, luteolin and quercetin. The molecular peaks have been identified for the above mentioned phytoconstituents, and the corresponding specific isotopic patterns confirm their molecular structure, but their fragmentation profiles do not corroborate with the values previously reported in scientific literature.

## CONCLUSIONS

In the current paper, we are describing the comparative chemomapping of aqueous and hydro-alcoholic extracts of artichoke leaves. Some previously reported phytoconstituents presence was confirmed, while many other newly identified compounds are reported for the first time to be specific to artichoke. The currently described phytoconstituent profile strongly supports the liver and gallbladder tonic effect of artichoke by interfering with lipid metabolism. Moreover, some kind of anti-cancerous effect could also be expected based on some phytoconstituents. Indeed we were able to demonstrate that the aqueous and hydro-alcoholic extracts of artichoke presented in this paper possess anti-cancerous effects [14]. Based on individual effects of the identified phytoconstituents, multiple mechanisms could be evoked to explain the artichoke health promoting effects like the inhibition of cholesterol synthesis and lipolysis, together with the activation of anti-inflammatory, anti-tumour growth cellular pathways. It seems therefore likely that due to the plethora of phytoconstituents found in artichoke, the health promoting effect of the analysed extracts, might have a more stochastic than determinative nature. Further experiments are needed based on a system biology type of approach to clarify the complexity of the beneficial effects including the correlations with chemical composition.

## EXPERIMENTAL SECTION

### x. Materials and methods

#### x.1. Chemicals and reagents

HPLC-MS grade acetonitrile, water and formic acid were purchased from Fisher Scientific (Geel, Belgium). HPLC grade ammonium acetate and ammonium formate were purchased from Sigma-Aldrich (Munich, Germany).

#### x.2. Plant material

The artichoke dried leaves were obtained from TTDR 2000 Ltd., Hungary.

#### x.3. Sample preparation

Aqueous (AE) extract: Artichoke dried leaves (5 g) were cooked (5 min) in boiling water (100 ml). After cooling at room temperature, the extract was centrifuged (10 min, 4000 rpm) and filtered through Whatman filter paper (Sigma Aldrich).

Hydro-alcoholic (HE) (ethanol : water 1:1) extract: 50 g artichoke dried leaves were extracted two times with 500 ml ethanol – water (50:50) by stirring for 4h at 40 °C. This artichoke solution was centrifuged at 4000 rpm for 10 min at room temperature and moved the ethanol from the sample in a rotation vacuum evaporator.

Both types of samples were filtered through a 45 µm filter and stored at 4 °C until analysis.

#### x.4. HPLC-MS analysis

The UHPLC system (Dionex Ultimate 3000RS equipped with a Thermo Accucore C18 column, 100/2.1 with a particle size of 2.6 µm) was coupled to a Thermo Q Exactive Orbitrap mass spectrometer equipped with an electrospray ionization source (ESI). Eluent A (500 ml of water containing 10 ml of acetonitrile, 0.5 ml of formic acid and 2.5 mM of ammonium formate) and eluent B (500 ml of acetonitrile containing 10 ml of water, 0.5 ml of formic acid and 2.5 mM of ammonium formate) were used in the HPLC separation in positive ionization mode, and eluent A (500 ml of water containing 10 ml of acetonitrile and 2.5 mM of ammonium acetate) and eluent B (500 ml of acetonitrile containing 10 ml of water and 2.5 mM of ammonium acetate) were used in the HPLC separation in negative ionization mode. Flow rate was 200 µl/min. The following gradient elution program was used both positive and negative ionization mode: 0-1 min,

95% A, 1-22 min, 20% A; 22-24 min, 20% A; 24-26 min, 95% A; 26-40 min, 95% A. 5 µl of samples were injected in every run. The Q Exactive hybrid quadrupole-orbitrap mass spectrometer was operated with the following parameters: capillary temperature 320 °C, spray voltage 4.0 kV in positive mode and 3.8 kV in negative mode, the resolution was set to 35000 in the case of MS and to 17500 in the case of MS/MS. The mass range scanned was 100-1000 m/z. Collision energy was 40NCE in the MS/MS scans. The used UHPLC-ESI-MS measurement accuracy is within 5ppm. The difference between measured and calculated molecular ion masses were always below 5 ppm.

## ACKNOWLEDGMENTS

We would like to thank to the members of the Agricultural and Molecular Research Institute of University of Nyíregyháza for their helpful technical assistance. We are thankful to Dr. Neli Kinga Olah for her comments and suggestions regarding phytoconstituents of artichoke and manuscript preparations. The research expenses were covered by the "In vitro study of some plant extracts of natural origin with emphasis on their anti-tumor effects." HURO/0801 Hungarian-Romanian Cross Border Cooperation 2007-2013 grant.

## REFERENCES

1. R.E. J.Llorach, F. Tomás-Barberan, F. Ferreres, *Journal of Agricultural and Food Chemistry*, **2002**, *50*, 3458.
2. F. Fratianni, M. Tucci, M. De Palma, R. Pepe, F. Nazzaro, *Food Chemistry*, **2007**, *104*, 1282.
3. R. Ferracane, N. Pellegrini, A. Visconti, G. Graziani, E. Chiavaro, C. Miglio, V. Fogliano, *Journal of Agricultural and Food Chemistry*, **2008**, *56*, 8601.
4. F. Tomás-Barberán, J.C. Espín, *Journal of the Science of Food and Agriculture*, **2001**, *81*, 853.
5. M. Lutz, C. Henríquez, M. Escobar, *Journal of Food Composition and Analysis*, **2011**, *24*, 49.
6. X. Wu, G. Beecher, J. Holden, D. Haytowitz, S. Gebhardt, R. Prior, *Journal of Agricultural and Food Chemistry*, **2004**, *52*, 4026.
7. B.L. Halvorsen, Carlsen M.H., Phillips K. M., Bohn S.K., Jacobs D.R., Blomhoff R. *American Journal of Clinical Nutrition*, **2006**, *84*, 95.
8. M. Ben Salem, H. Affes, K. Ksouda, R. Dhouibi, Z. Sahnoun, S. Hammami, K.M. Zeghal, *Plant Food for Human Nutrition*, **2015**, *70(4)*,441.

9. M. Rondanelli, F. Monteferrario, S. Perna, M.A. Faliva, A. Opizzi, *Monaldi Archives of Chest Disease*, **2013**, 80 (1), 17.
10. B. Wider, M.H. Pittler, J. Thompson-Coon, E. Ernst, *The Cochrane Database of Systematic Reviews*, **2013**, (3):CD003335.
11. A.M. Mileo, D. Di Venere, C. Abbruzzese, S. Miccadei, *Oxidative Medicine and Cellular Longevity*, **2015**, 363827.
12. C. Pulito, F. Mori, A. Sacconi, L. Casadei, M. Ferraiuolo, M.C. Valerio, R. Santoro, F. Goeman, A. Maidecchi, L. Mattoli, C. Manetti, S. Di Agostino, P. Muti, G. Blandino, S. Strano, *Oncotarget*, **2015**, 6 (20), 18134.
13. E.N. Simsek, T. Uysal, *Asian Pacific Journal of Cancer Prevention*, **2013**, 14 (11), 6791.
14. S. Vigh, C. Pribac, M. Czapár, Z. Zsvér-Vadas, L. Moş, C. Mihali, L. Cziáky, S.T. Sinka, V. Turcuş, E. Máthé, *Studia Universitatis Vasile Goldiș*, **2016**, 26 (4), 423.
15. I.M. Abu-Reidah, D. Arráez-Román, A. Segura-Carretero, A. Fernández-Gutiérrez, *Food Chemistry*, **2013**, 141, 2269.
16. A. Moglia, S. Lanteri, C. Comino, A. Acquadro, R. de Vos, J. Beekwilder, *Journal of Agricultural and Food Chemistry*, **2008**, 56, 8641.
17. M.N. Clifford, W. Zheng, N. Kuhnert, *Phytochemical Analysis*, **2006**, 17, 384.
18. R. Coinu, S. Carta, P.P. Urgeghe, N. Mulinacci, P. Pinelli, F. Franconi, A. Romani, *Food Chemistry*, **2007**, 101, 524.
19. R. Ferracane, N. Pellegrini, A. Visconti, G. Graziani, E. Chiavaro, C. Miglio, V. Fogliano, *Journal of Agricultural and Food Chemistry*, **2008**, 56, 8601.
20. K. Schütz, E. Muks, R. Carle, A. Schieber, *Journal of Agricultural and Food Chemistry*, **2006**, 54, 8812.
21. E. Azzini, R. Bugianesi, F. Romano, D. Di Venere, S. Miccadei, A. Durazzo, *The British Journal of Nutrition*, **2007**, 97, 963.
22. S. Lombardo, G. Pandino, G. Mauromicale, M. Knödler, R. Carle, A. Schieber, *Food Chemistry*, **2010**, 119, 1175.
23. K. Schütz, D. Kammerer, R. Carle, A. Schieber, *Journal of Agricultural and Food Chemistry*, **2004**, 52, 4090.
24. N. Mulinacci, D. Prucher, M. Peruzzi, A. Romani, P. Pinelli, C. Giaccherini, F. F. Vincieri, *Journal of Pharmaceutical and Biomedical Analysis*, **2004**, 34, 349.
25. G. Pandino, F.L. Courts, S. Lombardo, G. Mauromicale, G. Williamson, *Journal of Agricultural and Food Chemistry*, **2009**, 58, 1026.
26. F. Piozzi, M. Paternostro, S. Passannanti, E. Gacs-Baitz, *Phytochemistry*, **1986**, 25, 539.
27. K. Sas, H. Robotka, J. Toldi, L. Vécsei, *Journal of the Neurological Sciences*, **2007**; 257 (1-2), 221.
28. A. Arlt, S. Sebens, S. Krebs, C. Geismann, M. Grossmann, M.L. Kruse, S. Schreiber, H. Schäfer, *Oncogene*, **2013**, 32 (40), 4825.
29. L. Servillo, N. D'Onofrio, L. Longobardi, I. Sirangelo, A. Giovane, D. Cautela, D. Castaldo, A. Giordano, M.L. Balestrieri, *Journal of Cellular Biochemistry*, **2013**, 114 (11), 2522.
30. R. Bernhard, *Lebensmittel-Wissenschaft & Technologie*, **1972**, 5, 185.

31. M. Kawase, H. Sakagami, N. Motohashi, H. Hauer, S.S. Chatterjee, G. Spengler, A.V. Vigyikanne, A. Molnár, J. Molnár, *In Vivo*, **2005**, 19 (4), 705.
32. H. Zhao, M. Zhang, F. Zhou, W. Cao, L. Bi, Y. Xie, Q. Yang, S. Wang, *Journal of Molecular and Cellular Cardiology*, **2016**, 101,11.
33. J. Hinou, C. Harvala, S. Philianos, *Annales Pharmaceutiques Francaises*, **1989**, 47 (2), 95.
34. M.V. Pereira Dos Santos Nascimento, F. Arruda-Silva, A.B. Gobbo Luz, B. Baratto, D. Venzke, B.G. Mendes, T.S. Fröde, M. Geraldo Pizzolatti, E.M. Dalmarco, *Immunopharmacology and Immunotoxicology*, **2016**, 38 (5), 344.
35. C. Pereira, L. Barros, A.M. Carvalho, C. Santos-Buelga, I.C. Ferreira, *Food and Function*, **2015**, 6 (1), 56.
36. D. Negro, V. Montesano, S. Grieco, P. Crupi, G. Sarli, A. De Lisi, G. Sonnante, *Journal of Food Science*, **2012**, 77(2), C244.
37. J. Magielse, A. Verlaet, A. Breynaert, B. M. Keenoy, S. Apers, L. Pieters, N. Hermans, *Molecular Nutrition and Food Research*, **2014**, 58 (1), 211.
38. M. Wang, J.E. Simon, I.F. Aviles, K. He, Q.Y. Zheng, Y. Tadmor, *Journal of Agricultural and Food Chemistry*, **2003**, 51 (3), 601.
39. K. Patel, M. Gadewar, V. Tahilyani, D.K. Patel, *Chinese Journal of Integrative Medicine*, **2013**, 19, 792.
40. J. Liu, X. Wen, B. Liu, Q. Zhang, J. Zhang, H. Miao, R. Zhu, *Molecular Medicine Reports*, **2016**, 13 (3), 2401.
41. S. Noori, Z. M. Hassan, B. Yaghmaei, M. Dolatkah, *Cellular Immunology*, **2013**, 286 (1-2),16.
42. H. Shi, H. Shi, F. Ren, D. Chen, Y. Chen, Z. Duan, *Journal of Cellular and Molecular Medicine*, **2016**, doi: 10.1111/jcmm.12994.
43. A. Yoshinaga, N. Kajiya, K. Oishi, Y. Kamada, A. Ikeda, P. K. Chigwechokha, T. Kibe, M. Kishida, S. Kishida, M. Komatsu, K. Shiozaki, *European Journal of Pharmacology*, **2016**, 782, 21.
44. S.K. Ku, J.S. Bae, *Canadian Journal of Physiology and Pharmacology*, **2016**, 94 (3), 287.
45. H. Kang, S.K. Ku, B. Jung, J.S. Bae, *Inflammation Research*, **2015**, 64(12), 1005.
46. M. Lutz, C. Henzíguez, M. Escobar, *Journal of Food Composition and Analysis*, **2011**, 24, 49.
47. W. Li, Y. Wang, X. Wang, H. Zhang, Z. He, W. Zhi, F. Liu, X. Niu, *Fundamental and Clinical Pharmacology*, **2016**, doi: 10.1111/fcp.12255.
48. I. Mokdad Bzeouich, N. Mustapha, M. Maatouk, K. Ghedira, M. Ghoul, L. Chekir-Ghedira, *Regulatory Toxicology and Pharmacology*, **2016**, 82, 48.
49. K.C. Choi, Y.O. Son, J.M. Hwang, B.T. Kim, M. Chae, J.C. Lee, *Pharmaceutical Biology*, **2016**, 55 (1), 611.
50. F.J. Lima, F. Cosker, T.S. Brito, H.V. Ribeiro-Filho, C.M. Silva, K.S. Aragão, S. Lahlou, M.H. Souza, A.A. Santos, P.J. Magalhães, *European Journal of Pharmacology*, **2014**, 740, 192.
51. Y.Y. Chen, M.H. Lee, C.C. Hsu, C.L. Wei, Y.C. Tsai, *Journal of Agricultural and Food Chemistry*, **2012**, 60 (4), 955.

52. R.S. Pawar, E. Grundel, *Drug Testing and Analysis*, **2016**, doi: 10.1002/dta. 1980.
53. P. Mucaji, D. Grancai, M. Nagy, M. Buděšínský, K. Ubik, *Ceska a Slovenska Farmacie*, **2001**, 50 (6), 277.
54. H. Ding, H. Wang, L. Zhu, W. Wei, *Neurochemical Research*, **2016**, doi:10.1007/s11064-016-2077-8.
55. W.T. Gai, D.P. Yu, X. S. Wang, P.T. Wang, *Oncology Letters*, **2016**, 12 (4), 2880.
56. J.L. Gao, Y.M. Shui, W. Jiang, E.Y. Huang, Q.Y. Shou, X. Ji, B.C. He, G.Y. Lv, T.C. He, *Oncotarget*. **2016**. 71802.
57. E. Serni, V. Audino, S. Del Carlo, C. Manera, G. Saccomanni, M. Macchia, *Natural Product Research*, **2013**, 27 (23), 2212.
58. T. Kroon, T. Baccega, A. Olsén, J. Gabrielsson, N.D. Oakes, *Journal of Lipid Research*, **2017**, 58 (1), 31.
59. S. Mocellin, M. Briarava, P. Pilati, *Journal of the National Cancer Institute*, **2016**, 109 (3), pii: djw230.
60. S.C. Gominak, *Medical Hypotheses*, **2016**, 94, 103.





*Dedicated to Professor Costel Sârbu on the  
Occasion of His 65<sup>th</sup> Anniversary*

## **ANALYSIS OF PHYTOCONSTITUENT PROFILE OF FENUGREEK –*TRIGONELLA FOENUEM-GRAECUM* L. - SEED EXTRACTS**

**SZABOLCS VÍGH<sup>a,b</sup>, ZOLTÁN CZIÁKY<sup>b</sup>, LÁSZLÓ TAMÁS SINKA<sup>b</sup>,  
CIPRIAN PRIBAC<sup>c</sup>, LIANA MOȘ<sup>c</sup>, VIOLETA TURCUȘ<sup>c</sup>,  
JUDIT REMENYIK<sup>d</sup> AND ENDRE MÁTHÉ<sup>b,c,d,\*</sup>**

**ABSTRACT.** Fenugreek (*Trigonella foenum-graecum* L.) is a well-known herb for its efficiency in the prevention/treatment of diabetes among other chronic diseases. The aim of present study was to analyse the phytoconstituent profile of aqueous and hydro-alcoholic extracts of fenugreek seeds produced in Hungary. The aqueous and hydro-aqueous extracts were analysed using a UHPLC-ESI-MS approach, and in the first 54, while in the second extract 67 phytoconstituents were identified that mostly corroborate the previously described health promoting effects of fenugreek. However, it remains a huge challenge to correlate the phytoconstituent composition of the two extracts with the generated dose dependent hormetic response and cytotoxic effects that were reported by us in case of some human breast cancerous cell lines.

**Keywords:** fenugreek, *Trigonella foenum-graecum*, phytoconstituents, UHPLC-ESI-MS

---

<sup>a</sup> University of Nyíregyháza, Institute of Agricultural Sciences, Sostói str. 31/B, H-4432, Nyíregyháza, Hungary (present address)

<sup>b</sup> University of Nyíregyháza, Agricultural and Molecular Research Institute, Sostói str. 31/B, H-4432, Nyíregyháza, Hungary

<sup>c</sup> “Vasile Goldiș” Western University of Arad, Faculty of Medicine, Liviu Rebreanu Str.91-93, RO-310414, Arad, Romania

<sup>d</sup> University of Debrecen, Faculty of Agriculture and Food Sciences and Environmental Management, Böszörményi str. 138, H-4032 Debrecen, Hungary

\* Corresponding author: endre.mathe64@gmail.com

## INTRODUCTION

The fenugreek (*Trigonella foenum-graecum* L.) has been grown in Asia, Africa and Europe from ancient times being utilized as a food (fresh shoots), spice (seed) and herbal remedy. Its popularity has ever been increasing so that recently, it is cultivated in countries like India, Pakistan, China, Russia, Greece, Turkey, Israel, Egypt, Sudan, Morocco, Tunisia, Germany, Austria, United Kingdom, Spain, Portugal, USA and Argentina. Due to its large cultivation areal, several fenugreek ecotypes and/or varieties were described upon taxonomical characters comprising morphological features like seed types. Furry (1950) was proposing six fenugreek seed types like Yemenese, Transcaucasian, African, Afghan, Chinese-Persian and Indian, while Petropoulos (1973) had been suggesting categories like the Fluorescent, Ethiopian, Indian and Mediterranean seed types [1,2].

Several beneficial biological and pharmacological properties are attributed to the fenugreek seeds such as anti-diabetic, hypocholesterolaemic, contraceptive and anti-fertility, gastric ulcer and wound healing, anti-cancer, anti-microbial, anthelmintic and anti-nociceptive effects, respectively [3].

The fenugreek seeds contain (per 100g of edible portion): 369 calories, 7.8% moisture, 28.2 g protein, 5.9 g fat, 54.5 g total carbohydrate, 8g fibre, 3.6 g ash [4]. Fenugreek seeds containing diosgenin are considered one of the few natural sources of steroid saponin that is used for the synthesis of sex hormones, oral contraceptives and medicinally useful steroids [5]. Several furostanol saponins called trigoneosides Ia, Ib, IIa, IIb, IIIa, IIIb, IVa, Va, Vb, VI, VIIb, VIIIb, IX were isolated from fenugreek seeds originating from India [6,7]. Trigoneosides like Xa, Xb, XIb, XIIa, XIIb and XIIIa were identified from fenugreek seeds of the Egyptian origin [8]. Graecunins H-N are glycosides of diosgenin have also been isolated from fenugreek seeds, and belong to the spirostanol saponins [9]. Fenugrin B is another saponin that was also identified in fenugreek seeds [10]. Among sterols campesterol, stigmasterol,  $\beta$ -sitosterol and cholesterol were shown in different parts of the plant including seeds [11]. The fenugreek saponins exhibited hypocholesterolemic activity in rats [12]. Triterpenoids like lupeol, botulin, betulinic acid and soyasaponin were also isolated from fenugreek seeds [13]. Another important compound found in fenugreek seeds is the trigonelline which is the methylbetaine derivate of nicotinic acid, and its hypoglycemic and antipellagra effects have been demonstrated [14-16]. The flavonoid content of fenugreek seeds had been intensively analysed, and it was suggested to confer antibacterial activity to seed extracts [17]. Quercetin, luteolin, vitexin, orientin, isoorientin, vicianin-1, vicianin-2, naringenin, kaempferol, 7,4'-dimethoxyflavanone were identified among flavonoids. Other phenolic compounds were detected in different parts of plants (root, shoot, and pod) like

scopoletin, trigocoumarin, chlorogenic, caffeic and coumaric acids [18]. Studies and estimations have shown that the 4-hydroxyisoleucine represents up to 30-80 percent of free amino acid pool in fenugreek seeds [19,20]. A non-protein amino acid (S)-canavanine, and other amino acids like lysine and tryptophane were identified in fenugreek seeds [21,22]. The protein content of fenugreek leaves and seeds reaches 25-30 percent, so that approximately equals to that of soybeans [20]. It was suggested that the hypocholesterolemic effects of fenugreek seeds could be related to the amino acid content or to the relatively high fibre content (54 percent) and saponins (5 percent), [23]. Among vitamins in fenugreek seeds had been identified thiamine, riboflavin, pyridoxine, cyanocobalamine, niacin, Ca-pantothenate and biotin, while vitamin C was present mostly in the vegetative organs of the plant [24,25]. The lipid content of dried fenugreek seeds had been shown to reach approximately 7.5 percent, and the lipid profile consisted of neutral lipids (triacylglycerol, diacylglycerols, monoacylglycerols, free fatty acids, and sterols), glycolipids and phospholipids [26].

In the current paper we are reporting the UHPLC-ESI-MS chemomapping of aqueous and hydro-alcoholic fenugreek seed extracts that were found by us to induce dose dependent hormetic response and cytotoxicity in case of human breast cancerous cell lines [27]. We were able to detect 54 and 67 phytoconstituents in the aqueous and hydro-alcoholic artichoke extracts, respectively. Some of the newly identified compounds were confirmed by standards, while other have been already described by others [27-33].

## RESULTS AND DISCUSSION

The aqueous and the hydro-alcoholic extracts of fenugreek seeds were investigated with the reversed phase UHPLC-ESI-MS in positive and negative ionisation modes as described in Materials and Methods. The gradient mobile phase was based on acetonitrile and water. There have been 54 phytoconstituents identified in the aqueous fenugreek seed extract as shown on Figure 1-2 and in Table 1.

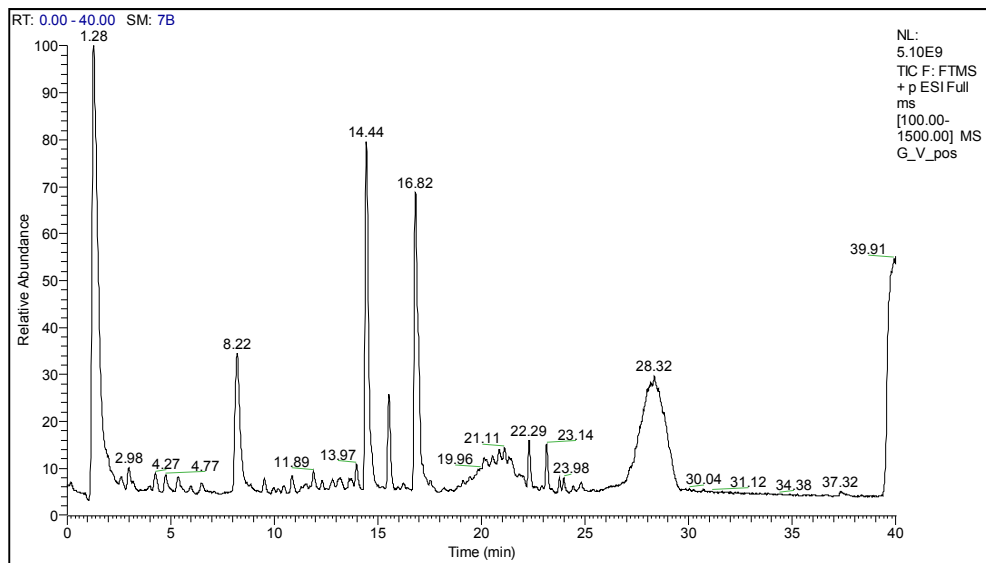


**Figure 1.** Total ion chromatogram of aqueous extract of fenugreek in positive ionisation mode.

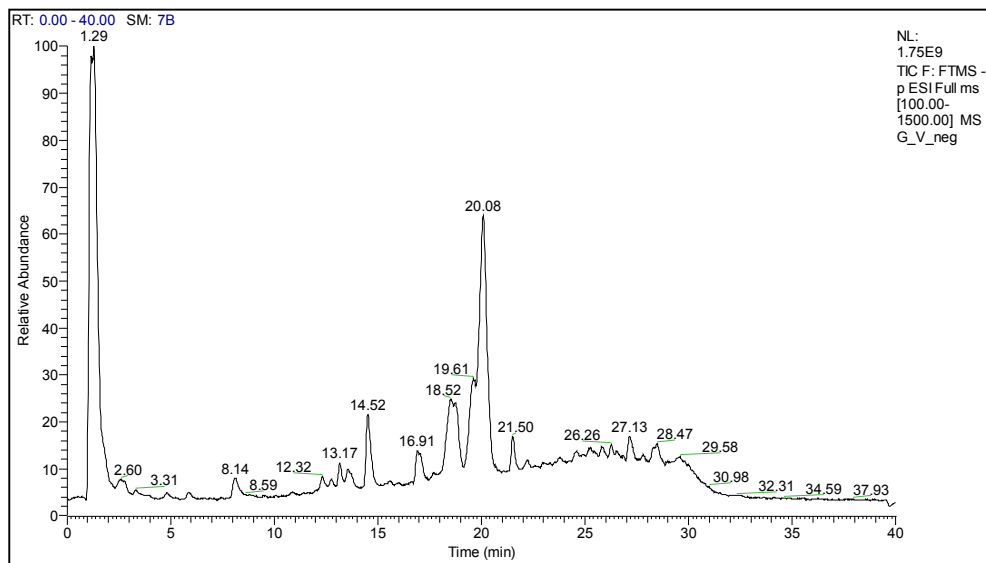


**Figure 2.** Total ion chromatogram of aqueous extract of fenugreek in negative ionisation mode.

**Table 1.** Phytoconstituents identified in the aqueous fenugreek seed extract. Rt –retention time; [M+H]<sup>+</sup> - molecular ion masses; [M+H]<sup>-</sup> - the found fragment ion mass; Ref- references; (\*) [M]<sup>+</sup>; (\*\*) confirmed by standards.

Peak	R <sub>t</sub>	[M+H] <sup>+</sup>	[M+H] <sup>-</sup>	Formula	Fragment s found	Assignment	Ref.
1	1.27	104.10754 <sup>*</sup>		C <sub>5</sub> H <sub>14</sub> NO	60.0814, 59.0735	Choline	27
2	1.30	138.05550 <sup>*</sup>		C <sub>7</sub> H <sub>8</sub> NO <sub>2</sub>	110.0601, 96.0450	Trigonelline	27
3	1.31	175.11951		C <sub>6</sub> H <sub>14</sub> N <sub>4</sub> O <sub>2</sub>	158.0922, 130.0975	Arginine <sup>**</sup>	27
4	1.31	148.06099		C <sub>5</sub> H <sub>9</sub> NO <sub>4</sub>	130.0863, 102.0553	Glutamic acid	27
5	1.31	118.08681		C <sub>5</sub> H <sub>11</sub> NO <sub>2</sub>	59.0736, 58.0657	Betaine	27
6	1.32	133.06132		C <sub>4</sub> H <sub>8</sub> N <sub>2</sub> O <sub>3</sub>	116.0342, 88.0397	Asparagine <sup>**</sup>	27
7	1.43	189.12392		C <sub>8</sub> H <sub>16</sub> N <sub>2</sub> O <sub>3</sub>	172.0961, 130.0863	N-α-Acetyl- lysine	
8	1.46	148.09737		C <sub>6</sub> H <sub>13</sub> NO <sub>3</sub>	130.0862, 113.0598	4-Hydroxyiso- leucine	27
9	1.49	324.05968		C <sub>9</sub> H <sub>13</sub> N <sub>3</sub> O <sub>5</sub>	112.0507, 95.0243	Cytidine <sup>**</sup>	
10	1.51	146.09296		C <sub>5</sub> H <sub>11</sub> N <sub>3</sub> O <sub>2</sub>	128.0821, 111.0555	4-Guanidino- butyric acid	
11	1.52	130.08681		C <sub>6</sub> H <sub>11</sub> NO <sub>2</sub>	84.0812, 67.0548	Pipecolic acid	
12	1.56	136.06233		C <sub>5</sub> H <sub>5</sub> N <sub>5</sub>	119.0352, 94.0406	Adenine	
13	1.66		283.06786	C <sub>10</sub> H <sub>12</sub> N <sub>4</sub> O <sub>6</sub>	151.0248, 108.0188	Xanthosine	
14	1.73		243.06171	C <sub>9</sub> H <sub>12</sub> N <sub>2</sub> O <sub>6</sub>	200.0558, 153.0293	Uridine	
15	1.75	170.08172		C <sub>8</sub> H <sub>11</sub> NO <sub>3</sub>	152.0704, 134.0600	Pyridoxine <sup>**</sup>	27
16	1.82	182.08172		C <sub>9</sub> H <sub>11</sub> NO <sub>3</sub>	165.0545, 147.0439	2- Hydroxyphenyl- alanine	
17	1.96	123.05584		C <sub>6</sub> H <sub>6</sub> N <sub>2</sub> O	106.0287, 96.0447	Nicotinamide <sup>**</sup>	27
18	2.01	330.06035		C <sub>10</sub> H <sub>12</sub> N <sub>5</sub> O <sub>6</sub> P	232.0828, 136.0617	Adenosine 3',5'- cyclic monophosphate	
19	2.10	277.13997		C <sub>11</sub> H <sub>20</sub> N <sub>2</sub> O <sub>6</sub>	259.1286, 213.1231	Saccharopine	
20	2.23	385.12942		C <sub>14</sub> H <sub>20</sub> N <sub>6</sub> O <sub>5</sub> S	136.0618, 134.0271	S-Adenosyl- homocysteine	
21	2.60	152.05724		C <sub>5</sub> H <sub>5</sub> N <sub>5</sub> O	135.0301, 128.0455	Guanine	

Peak	R <sub>t</sub>	[M+H] <sup>+</sup>	[M-H] <sup>-</sup>	Formula	Fragment s found	Assignment	Ref.
22	2.63		282.08385	C <sub>10</sub> H <sub>13</sub> N <sub>5</sub> O <sub>5</sub>	150.0407, 133.0142	Guanosine	
23	2.74		163.03952	C <sub>9</sub> H <sub>8</sub> O <sub>3</sub>	119.0487, 93.0329	p-Coumaric acid	
24	2.95	268.10458		C <sub>10</sub> H <sub>13</sub> N <sub>5</sub> O <sub>4</sub>	136.0617, 119.0358	Adenosine**	
25	3.10	252.10967		C <sub>10</sub> H <sub>13</sub> N <sub>5</sub> O <sub>3</sub>	136.0618, 117.0548	2'-Deoxyadenosine	
26	3.21	166.08681		C <sub>9</sub> H <sub>11</sub> NO <sub>2</sub>	149.0598, 131.0493	Phenylalanine**	27
27	4.86	220.11850		C <sub>9</sub> H <sub>17</sub> NO <sub>5</sub>	202.1073, 184.0967	Pantothenic acid**	27
28	6.49	205.09771		C <sub>11</sub> H <sub>12</sub> N <sub>2</sub> O <sub>2</sub>	188.0706, 170.0599	Tryptophan**	27
29	6.75	129.05517		C <sub>6</sub> H <sub>8</sub> O <sub>3</sub>	111.0443, 101.0600	Sotolone	27
30	8.31	190.05042		C <sub>10</sub> H <sub>7</sub> NO <sub>3</sub>	162.0547, 144.0435	Kynurenic acid	
31	9.53	295.12940		C <sub>14</sub> H <sub>18</sub> N <sub>2</sub> O <sub>5</sub>	278.1017, 232.0965	γ-Glutamylphenylalanine	
32	11.56	186.11302		C <sub>9</sub> H <sub>15</sub> NO <sub>3</sub>	168.1017, 150.0909	Ecgonine	
33	12.32		593.15065	C <sub>27</sub> H <sub>30</sub> O <sub>15</sub>	503.1202, 473.1087	Vicenin-2	28
34	12.75		593.15065	C <sub>27</sub> H <sub>30</sub> O <sub>15</sub>	503.1215, 473.1088	Apigenin-di-C-hexoside (Vicenin-2-isomer)	28
35	13.17		563.14009	C <sub>26</sub> H <sub>28</sub> O <sub>14</sub>	503.1187, 473.1091	Vicenin-3	28
36	13.74	449.10839		C <sub>21</sub> H <sub>20</sub> O <sub>11</sub>	395.0760, 377.0658	Isoorientin	27
37	13.75		563.14009	C <sub>26</sub> H <sub>28</sub> O <sub>14</sub>	503.1194, 473.1096	Vicenin-1	28
38	13.90	200.12867		C <sub>10</sub> H <sub>17</sub> NO <sub>3</sub>	182.1174, 100.0759	Ecgonine methyl ester	
39	14.43		577.15574	C <sub>27</sub> H <sub>30</sub> O <sub>14</sub>	503.1193, 473.1097	Apigenin-6-C-glucoside-8-C-rhamnoside	28
40	14.65	433.11348		C <sub>21</sub> H <sub>20</sub> O <sub>10</sub>	379.0805, 361.0709	Isovitexin	27
41	18.25		1195.57478	C <sub>56</sub> H <sub>92</sub> O <sub>27</sub>	705.3873, 609.3632	Trigofoenoside G	31
42	18.49		905.47461	C <sub>44</sub> H <sub>74</sub> O <sub>19</sub>	773.4326, 611.3798	Trigoneoside Ia	29
43	18.62		1063.53252	C <sub>51</sub> H <sub>84</sub> O <sub>23</sub>	609.3646, 447.3091	Protoyuccagenin-S4	31
44	18.83		919.49026	C <sub>45</sub> H <sub>76</sub> O <sub>19</sub>	773.4315, 611.3812	Trigoneoside Xa	30

Peak	R <sub>t</sub>	[M+H] <sup>+</sup>	[M-H] <sup>-</sup>	Formula	Fragment s found	Assignment	Ref.
45	18.84		905.47461	C <sub>44</sub> H <sub>74</sub> O <sub>19</sub>	773.4336, 611.3795	Trigoneoside Ib	29
46	19.61		919.49026	C <sub>45</sub> H <sub>76</sub> O <sub>19</sub>	773.4322, 611.3808	Trigoneoside Xb	30
47	19.73		887.46405	C <sub>44</sub> H <sub>72</sub> O <sub>18</sub>	593.3680, 431.3171	Trigoneoside VIII	30
48	19.78		1225.58534	C <sub>57</sub> H <sub>94</sub> O <sub>28</sub>	1077.2218 901.4799	Trigoneoside XIIIa	30
49	19.88		889.47970	C <sub>44</sub> H <sub>74</sub> O <sub>18</sub>	757.4387, 595.3850	Trigoneoside IIa	29
50	19.98		1063.53252	C <sub>51</sub> H <sub>84</sub> O <sub>23</sub>	755.4216, 593.3688	Trigoneoside IVa	29
51	20.00		1065.54817	C <sub>51</sub> H <sub>86</sub> O <sub>23</sub>	757.4368, 595.3844	Trigofoenoside C	29
52	20.10		1047.53760	C <sub>51</sub> H <sub>84</sub> O <sub>22</sub>	755.4216, 575.3581	Asparasaponin I (Protodioscin, Trigonelloside C)	31
53	20.30		901.47970	C <sub>45</sub> H <sub>74</sub> O <sub>18</sub>	755.4237, 593.3704	Trigoneoside XIIa	30
54	20.37		903.49535	C <sub>45</sub> H <sub>76</sub> O <sub>18</sub>	757.4390, 595.3836	Trigoneoside IIIa	29

There have been 67 phytoconstituents identified in the hydro-alcoholic fenugreek seed extract as shown in Table 2.

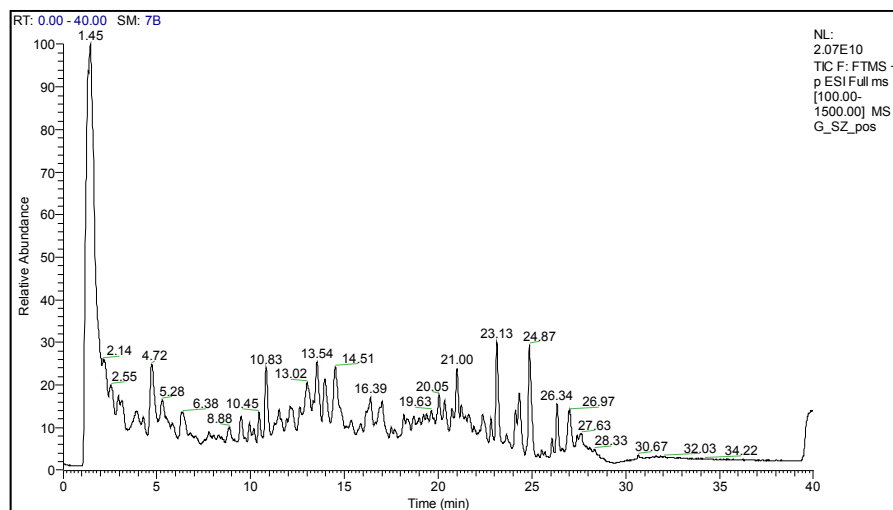


**Figure 3.** Total ion chromatogram of hydro-alcoholic extract of fenugreek in positive ionisation mode.



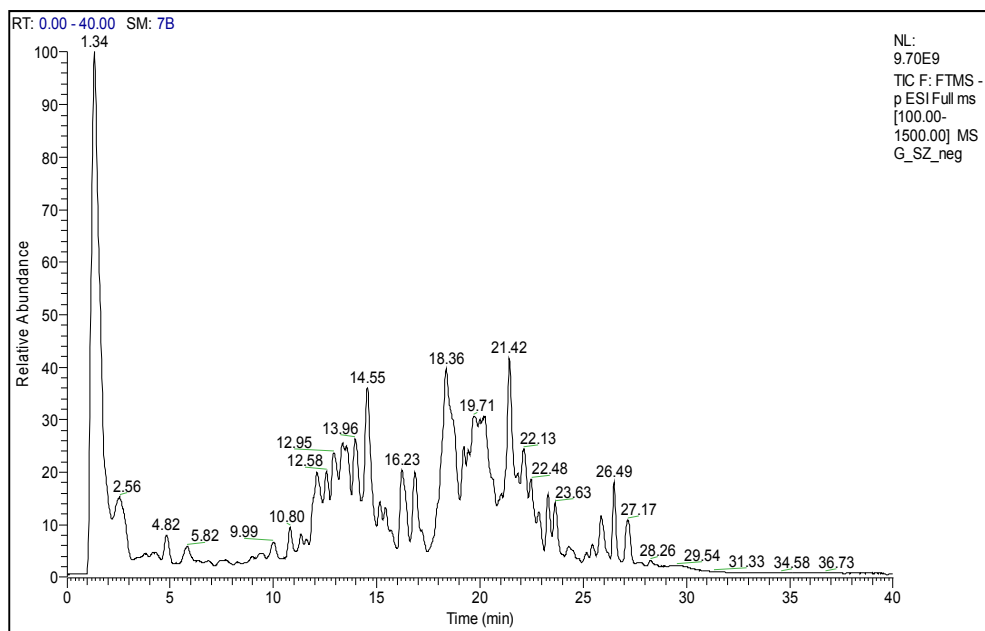


**Figure 4.** Total ion chromatogram of hydro-alcoholic extract of fenugreek in negative ionisation mode.

**Table 2.** Phytoconstituents identified in the hydro-alcoholic fenugreek seed extract. Rt –retention time; [M+H]<sup>+</sup> - molecular ion masses; [M+H]<sup>-</sup> - the found fragment ion mass; Ref- references; (\*) [M]<sup>+</sup>; (\*\*) confirmed by standards.

Peak	R <sub>t</sub>	[M+H] <sup>+</sup>	[M-H] <sup>-</sup>	Formula	Fragments found	Assignment	Ref.
1	1.22	104.10754 <sup>*</sup>		C <sub>5</sub> H <sub>14</sub> NO	60.0814, 59.0736	Choline	27
2	1.32	138.05550 <sup>*</sup>		C <sub>7</sub> H <sub>8</sub> NO <sub>2</sub>	110.0604, 96.0447	Trigonelline	27
3	1.31	175.11951		C <sub>6</sub> H <sub>14</sub> N <sub>4</sub> O <sub>2</sub>	158.0923, 130.0975	Arginine <sup>**</sup>	27
4	1.31	148.06099		C <sub>5</sub> H <sub>9</sub> NO <sub>4</sub>	130.0863, 102.0553	Glutamic acid	27
5	1.31	118.08681		C <sub>5</sub> H <sub>11</sub> NO <sub>2</sub>	59.0736, 58.0657	Betaine	27
6	1.40	189.12392		C <sub>8</sub> H <sub>16</sub> N <sub>2</sub> O <sub>3</sub>	172.0962, 130.0862	N-α-Acetyl-lysine	
7	1.42	146.09296		C <sub>5</sub> H <sub>11</sub> N <sub>3</sub> O <sub>2</sub>	128.0810, 111.0556	4-Guanidinobutyric acid	

Peak	R <sub>t</sub>	[M+H] <sup>+</sup>	[M-H] <sup>-</sup>	Formula	Fragments found	Assignment	Ref.
8	1.46	130.08681		C <sub>6</sub> H <sub>11</sub> NO <sub>2</sub>	84.0812, 67.0547	Pipecolic acid	
9	1.63	124.03986		C <sub>6</sub> H <sub>5</sub> NO <sub>2</sub>	96.0448, 80.0500	Nicotinic acid**	27
10	1.72		283.06786	C <sub>10</sub> H <sub>12</sub> N <sub>4</sub> O <sub>6</sub>	151.0248, 108.0188	Xanthosine	
11	1.73		243.06171	C <sub>9</sub> H <sub>12</sub> N <sub>2</sub> O <sub>6</sub>	200.0556, 153.0292	Uridine	
12	1.72	170.08172		C <sub>8</sub> H <sub>11</sub> NO <sub>3</sub>	152.0705, 134.0601	Pyridoxine**	27
13	1.79	182.08172		C <sub>9</sub> H <sub>11</sub> NO <sub>3</sub>	165.0545, 147.0440	2-Hydroxyphenyl- alanine	
14	1.93	123.05584		C <sub>6</sub> H <sub>6</sub> N <sub>2</sub> O	106.0288, 96.0448	Nicotinamide**	27
15	2.09	277.13997		C <sub>11</sub> H <sub>20</sub> N <sub>2</sub> O <sub>6</sub>	259.1282, 213.1233	Saccharopine	
16	2.20	385.12942		C <sub>14</sub> H <sub>20</sub> N <sub>6</sub> O <sub>5</sub> S	136.0617, 134.0270	S-Adenosyl- homocysteine	
17	2.62		282.08385	C <sub>10</sub> H <sub>13</sub> N <sub>5</sub> O <sub>5</sub>	150.0408, 133.0142	Guanosine	
18	2.66		163.03952	C <sub>9</sub> H <sub>8</sub> O <sub>3</sub>	119.0487, 93.0331	p-Coumaric acid	
19	2.95	268.10458		C <sub>10</sub> H <sub>13</sub> N <sub>5</sub> O <sub>4</sub>	136.0617, 119.0358	Adenosine**	
20	3.10	252.10967		C <sub>10</sub> H <sub>13</sub> N <sub>5</sub> O <sub>3</sub>	136.0617, 117.0547	2'- Deoxyadenosine	
21	3.17	166.08681		C <sub>9</sub> H <sub>11</sub> NO <sub>2</sub>	149.0600, 131.0492	Phenylalanine**	27
22	3.37	153.04126		C <sub>5</sub> H <sub>4</sub> N <sub>4</sub> O <sub>2</sub>	136.0142, 110.0351	Xanthine	
23	4.80	220.11850		C <sub>9</sub> H <sub>17</sub> NO <sub>5</sub>	202.1071, 184.0967	Pantothenic acid**	27
24	6.33	205.09771		C <sub>11</sub> H <sub>12</sub> N <sub>2</sub> O <sub>2</sub>	188.0705, 170.0597	Tryptophan**	27
25	6.75	129.05517		C <sub>6</sub> H <sub>8</sub> O <sub>3</sub>	111.0443, 101.0601	Sotolone	27
26	8.35	190.05042		C <sub>10</sub> H <sub>7</sub> NO <sub>3</sub>	162.0547, 144.0444	Kynurenic acid	
27	9.50	295.12940		C <sub>14</sub> H <sub>18</sub> N <sub>2</sub> O <sub>5</sub>	278.1019, 232.0964	γ-Glutamylphenyl- alanine	
28	9.94	134.04534		C <sub>4</sub> H <sub>7</sub> NO <sub>4</sub>	116.0344, 88.0397	Aspartic acid	
29	9.94	298.09739		C <sub>11</sub> H <sub>15</sub> N <sub>5</sub> O <sub>3</sub> S	163.0423, 145.0318	5'-S-Methyl-5'- thioadenosine	
30	10.92		455.09680	C <sub>17</sub> H <sub>21</sub> N <sub>4</sub> O <sub>9</sub> P	255.0886, 241.0725	Flavin mononucleotide	

Peak	R <sub>t</sub>	[M+H] <sup>+</sup>	[M-H] <sup>-</sup>	Formula	Fragments found	Assignment	Ref.
31	11.53	186.11302		C <sub>9</sub> H <sub>15</sub> NO <sub>3</sub>	168.1018, 150.0914	Ecgonine	
32	11.81	271.06065		C <sub>15</sub> H <sub>10</sub> O <sub>5</sub>	253.0483, 243.0648	Genistein	56
33	12.10		593.15065	C <sub>27</sub> H <sub>30</sub> O <sub>15</sub>	503.1193, 473.1087	Vicenin-2	28
34	12.58		593.15065	C <sub>27</sub> H <sub>30</sub> O <sub>15</sub>	503.1192, 473.1088	Apigenin-di-C-hexoside	28
35	12.81	193.05009		C <sub>10</sub> H <sub>8</sub> O <sub>4</sub>	178.0259, 165.0544	Scopoletin	27
36	13.10		563.14009	C <sub>26</sub> H <sub>28</sub> O <sub>14</sub>	503.1177, 473.1092	Vicenin-3	28
37	13.17	229.08647		C <sub>14</sub> H <sub>12</sub> O <sub>3</sub>	211.0754, 183.0804	Resveratrol	
38	13.52	449.10839		C <sub>21</sub> H <sub>20</sub> O <sub>11</sub>	395.0754, 377.0649	Isoorientin	27
39	13.70		563.14009	C <sub>26</sub> H <sub>28</sub> O <sub>14</sub>	503.1196, 473.1077	Vicenin-1	28
40	13.82	200.12867		C <sub>10</sub> H <sub>17</sub> NO <sub>3</sub>	182.1176, 100.0602	Ecgonine methyl ester	
41	13.96	433.11348		C <sub>21</sub> H <sub>20</sub> O <sub>10</sub>	415.1003, 397.0918	Vitexin	27
42	14.33		577.15574	C <sub>27</sub> H <sub>30</sub> O <sub>14</sub>	503.1193, 473.1084	Apigenin-6-C-glucoside-8-C-rhamnoside	28
43	14.51	433.11348		C <sub>21</sub> H <sub>20</sub> O <sub>10</sub>	379.0811, 361.0699	Isovitexin	27
44	14.77		461.10839	C <sub>22</sub> H <sub>22</sub> O <sub>11</sub>	371.0772, 353.0667	Scoparin	
45	15.69	493.13461		C <sub>23</sub> H <sub>25</sub> O <sub>12</sub>	331.0806, 316.0572	Tricin-7-O-glucoside	57
46	16.18	595.14517		C <sub>30</sub> H <sub>26</sub> O <sub>13</sub>	431.0971, 413.0861	Luteolin-8-C-(2"-O-(E)-p-coumaroyl-glycoside)	58
47	17.53		271.06065	C <sub>15</sub> H <sub>12</sub> O <sub>5</sub>	227.0709, 177.0181	Naringenin	
48	18.12		1195.57478	C <sub>56</sub> H <sub>92</sub> O <sub>27</sub>	705.3867, 609.3640	Trigofoenoside G	31
49	18.36		905.47461	C <sub>44</sub> H <sub>74</sub> O <sub>19</sub>	773.4312, 611.3799	Trigoneoside Ia	29
50	18.49		1063.53252	C <sub>51</sub> H <sub>84</sub> O <sub>23</sub>	609.3642, 447.3113	Protoyuccagenin-S4	31
51	18.75		919.49026	C <sub>45</sub> H <sub>76</sub> O <sub>19</sub>	773.4318, 611.3799	Trigoneoside Xa	30
52	18.91		905.47461	C <sub>44</sub> H <sub>74</sub> O <sub>19</sub>	773.4330, 611.3799	Trigoneoside Ib	29

Peak	R <sub>t</sub>	[M+H] <sup>+</sup>	[M-H] <sup>-</sup>	Formula	Fragments found	Assignment	Ref.
53	18.97	331.08178		C <sub>17</sub> H <sub>14</sub> O <sub>7</sub>	316.0573, 315.0494	Tricin	27
54	19.05		299.05556	C <sub>16</sub> H <sub>12</sub> O <sub>6</sub>	284.0326, 256.0375	Chrysoeriol	32
55	19.57		887.46405	C <sub>44</sub> H <sub>72</sub> O <sub>18</sub>	593.3685, 431.3164	Trigoneoside VIII	30
56	19.61		919.49026	C <sub>45</sub> H <sub>76</sub> O <sub>19</sub>	773.4322, 611.3808	Trigoneoside Xb	30
57	19.62		1225.58534	C <sub>57</sub> H <sub>94</sub> O <sub>28</sub>	1077.98729 01.4840	Trigoneoside XIIIa	30
58	19.87		271.09704	C <sub>16</sub> H <sub>14</sub> O <sub>4</sub>	243.1017, 161.0595	Medicarpin	27
59	19.67		889.47970	C <sub>44</sub> H <sub>74</sub> O <sub>18</sub>	757.4375, 595.3850	Trigoneoside IIa	29
60	19.69		935.48518	C <sub>45</sub> H <sub>76</sub> O <sub>20</sub>	757.4380, 595.3840	Protoneogitogenin -S5	31
61	19.79		1063.53252	C <sub>51</sub> H <sub>84</sub> O <sub>23</sub>	755.4224, 593.3696	Trigoneoside IVa	29
62	19.74		1065.54817	C <sub>51</sub> H <sub>86</sub> O <sub>23</sub>	757.4377, 595.3851	Trigofoenoside C	29
63	19.97		1047.53760	C <sub>51</sub> H <sub>84</sub> O <sub>22</sub>	755.4224, 575.3589	Asparasaponin I (Protodioscin, Trigonelloside C)	31
64	20.19		901.47970	C <sub>45</sub> H <sub>74</sub> O <sub>18</sub>	755.4287, 593.3687	Trigoneoside XIIa	30
65	20.29		903.49535	C <sub>45</sub> H <sub>76</sub> O <sub>18</sub>	757.4388, 595.3852	Trigoneoside IIIa	29
66	21.47		941.51100	C <sub>48</sub> H <sub>78</sub> O <sub>18</sub>	733.4561, 615.3893	Soyasaponin I	
67	27.22	457.36818		C <sub>30</sub> H <sub>48</sub> O <sub>3</sub>	411.3607, 393.3505	Ursolic acid	

The phytoconstituents were defined based on specific retention time, accurate mass, isotopic distribution and fragmentation pattern, and by screening MS databases like Metlin, mzCloud and Massbank. All together the detected compounds could be rendered into ten categories of phytoconstituents, while the aqueous and hydro-alcoholic fenugreek seed extracts were featuring both similarities and differences with respect to their content (Table 3).

**Table 3.** Phytoconstituents identified in the aqueous and hydro-alcoholic fenugreek seed extracts. Compounds to be found only in aqueous extract are shown in blue, while compounds found only in hydro-alcoholic extracts are high lightened in yellow.

Phytoconstituents		Aqueous fenugreek	Hydro-alcoholic fenugreek
<b>Alkaloids</b>	Ecgonine	+	+
	Ecgonine methyl ester	+	+
	Kynurenic acid	+	+
	Trigonelline	+	+
<b>Amino acids</b>	2-Hydroxyphenylalanine	+	+
	4-Guanidinobutyric acid	+	+
	Arginine	+	+
	Asparagine <sup>a</sup>	+	
	Betaine (Trimethylglycine)	+	+
	Glutamic acid	+	+
	Aspartic acid <sup>b</sup>		+
	Phenylalanine	+	+
	Pipecolic acid	+	+
	Tryptophan	+	+
	N- $\alpha$ -Acetyl-lysine	+	+
	4-Hydroxyisoleucin <sup>a</sup>	+	
	$\gamma$ -Glutamylphenylalanine	+	+
	<b>Coumarins</b>	Scopoletin <sup>b</sup>	
<b>Flavonoids</b>	Naringenin <sup>b</sup>		+
	Chrysoeriol <sup>b</sup>		+
	Tricin <sup>b</sup>		+
	Luteolin-8-C-(2''-O-(E)-p-coumaroylglycoside) <sup>b</sup>		+
	Tricin-7-O-glucoside <sup>b</sup>		+
	Genistein <sup>b</sup>		+
	Vitexin (Apigenin-8-C-glucoside) <sup>b</sup>		+
	Isovitexin (Apigenin-6-C-glucoside)	+	+
	Medicarpin <sup>b</sup>		+
	Scoparin (Chrysoeriol-8-C-glucoside) <sup>b</sup>		+
	Vicenin-2 (6,8-Di-C-glucosylapigenin)	+	+
	Apigenin-di-C-hexoside (Vicenin-2-isomer)	+	+
	Vicenin-3 (6-C-Glucosyl-8-C-xylosylapigenin)	+	+
	Isorientin (Homoorientin, Luteolin-6-C-glucoside)	+	+
	Vicenin-1 (6-C-Xylosyl-8-C-glucosylapigenin)	+	+
	Apigenin-6-C-glucoside-8-C-rhamnoside	+	+

Phytoconstituents		Aqueous fenugreek	Hydro-alcoholic fenugreek
<b>Other metabolites</b>	Sotolone(3-Hydroxy-4,5-dimethyl-2(5H)furanone)	+	+
	Choline	+	+
	Saccharopine	+	+
<b>Polyphenols</b>	Resveratrol <sup>b</sup>		+
	p-Coumaric acid	+	+
<b>Purines and pyrimidine</b>	5'-S-Methyl-5'-thioadenosine <sup>b</sup>		+
	2'-Deoxyadenosine	+	+
	Adenine <sup>a</sup>	+	
	Adenosine	+	+
	Adenosine 3',5'-cyclic monophosphate <sup>a</sup>	+	
	Cytidine <sup>a</sup>	+	
	Flavin mononucleotide (FMN) <sup>b</sup>		+
	Guanine <sup>a</sup>	+	
	Guanosine	+	+
	S-Adenosylhomocysteine	+	+
	Uridine	+	+
	Xanthine <sup>b</sup>		+
	Xanthosine	+	+
	<b>Saponins</b>	Soyasaponin I <sup>b</sup>	
Trigoneoside Ia		+	+
Trigoneoside Ib		+	+
Trigoneoside IIa		+	+
Trigoneoside IIIa		+	+
Trigoneoside IVa		+	+
Trigoneoside VIII		+	+
Trigoneoside Xa		+	+
Trigoneoside Xb		+	+
Trigoneoside XIIa		+	+
Trigoneoside XIIIa		+	+
Asparasaponin I (Protodisocin, Trigonelloside C)		+	+
Trigofoneoside C		+	+
Trigofoneoside G		+	+
Protoneogitogenin-S5 <sup>b</sup>			+
Protoyuccagenin-S4	+	+	
<b>Terpenoid</b>	Ursolic acid <sup>b</sup>		+
<b>Vitamines</b>	Nicotinamide	+	+
	Nicotinic acid (B3, niacin) <sup>b</sup>		+
	Pantothenic acid (B5)	+	+
	Pyridoxine (B6)	+	+

<sup>a</sup>Compounds to be found only in aqueous extract,

<sup>b</sup>Compounds found only in hydro-alcoholic extracts

According to our current knowledge, we are the first to identify among the **alkaloid** type of compounds the ecgonine methyl ester and ecognine in fenugreek seed extracts. In mice, ecgonine methyl ester was shown to protect against cocaine lethality. This effect is consistent with its vasodilatory effects [34]. Moreover, we are reporting for the first time in fenugreek extracts the presence of kynurenic acid that is produced via the kynurenine pathway of tryptophan amino acid catabolism, the latest to be found in our both fenugreek extracts [35]. The neuroprotective role of kynurenic acid has been demonstrated [36]. Our experiments confirm the presence of trigonelline in our both fenugreek seed extracts. Trigonelline was shown to inhibit Nrf2 together with blocking of Nrf2-dependent expression of proteasomal genes [37].

We were able to detect the 4-hydroxyisoleucin, the most abundant **amino acid** in fenugreek seeds together with asparagine both being only present in the aqueous extract. Aspartic acid was present only in the hydro-alcoholic fenugreek seed extract, while all the other amino acids listed in Table 3 could be found in both extracts.

Among **coumarins** we are reporting for the first time the identification of scopoletin in hydro-alcoholic extract of fenugreek seeds, a compound that has already described in fenugreek root, shoot, pod, stem and leaves [18, 38]. Scopoletin was suggested to have an important anti-inflammatory effect by inhibiting the phosphorylation of NF- $\kappa$ B and p38 MAPK in mice [39], and to inhibit human tumor vascularization in xenograft models [40].

**Flavonoids** like naringenin, vitexin (apigenin-8-C-glucoside), luteolin-8-C-(2''-O-(E)-p-coumaroyl)glycoside, isoorientin, vicienin-1, vicienin-2, vicienin-3 (6-C-glucosyl-8-C-xylosyl)apigenin), apigenin-6-C-glucoside-8-C-rhamnoside, chrysoeriol and triclin had been reported already in fenugreek seeds [5, 28-33]. However, flavonoids like, triclin-7-O-glucoside, genistein, isovitexin (apigenin-6-C-glucoside), medicarpin, scoparin and apigenin-6-C-glucoside-8-C-rhamnoside are revealed for the first time in fenugreek seed extracts.

The scoparin is a chrysoeriol glucoside and its biological effects are not known. In case of chrysoeriol was shown to partly inhibit adipogenesis by blocking the accumulation of triacylglycerol in the 3T3-L1 cells [41]. Moreover, it was demonstrated that chrysoeriol is a PI3K-AKT-mTOR pathway inhibitor with potent antitumor activity against human multiple myeloma cells in vitro [42].

The genistein is an estrogen agonist phytoestrogen, and when isolated from soy, it is reported to display neuroprotective effects against neuronal death in animal models [43]. Experimental data suggested that genistein may exhibit anticancer properties on HT29 colon cancer cells by modulating caspase-3 and p38 MAPK pathway at different transcriptional and protein levels [44].

The isovitexin (apigenin-6-C-glucoside), an isomer of vitexin, generally occurring together with vitexin, and together are exhibiting diverse biological

activities like anti-oxidant, anti-cancer, anti-inflammatory, anti-hyperalgesic, and neuroprotective effects [45].

The medicarpin was shown to have osteogenic activity promoting bone regeneration by activating Wnt and Notch signalling pathway [46]. Medicarpin it was suggested to have pro-apoptotic effects against drug-sensitive (P388) and multidrug resistant P388 leukemia cells [47].

The **polyphenol** content of fenugreek seeds was also analysed, and the presence of resveratrol had been demonstrated for the first time in our hydro-alcoholic extract. Resveratrol was shown to affect lipids and arachidonic acid metabolisms, and together with its antioxidant activity elicited a great research interest in fields such as cancer, neurodegenerative and cardiovascular diseases and metabolic disorders [48].

Trigocoumarin and caffeic acid seemed to be present at a low abundance in our aqueous fenugreek seed extract as suggested by the molecular mass corresponding peaks, and the structure confirming isotopic pattern, but no fragmentation profiles were generated hence they have not been included in the tables with phytoconstituents.

The quercetin, p-coumaric acid and chlorogenic acid were poorly detectable in both extracts, and again the fragmentation profile based evidences are missing, yet molecular masses and isotopic patterns are available. Nevertheless they have not been included into the tables with phytoconstituents.

Among **metabolites** we were able to identify sotolone (3-Hydroxy-4,5-dimethyl-2(5H)furanone), choline and saccharopine as new phytoconstituents in fenugreek seed extracts. We have to admit that sotolone was also detected in fenugreek hairy root cultures [49]. The sotolone is known to impart powerful Madeira-oxidized-curry-walnut notes to various hydro-alcoholic beverages. It has been much studied in oxidized Jura flor-sherry wines, dry white wines, aged Roussillon sweet wines, and old Port wines, in which it contributes to the characteristic "Madeira-oxidized" aroma of these beverages [50]. However, the sotolone biological effects are not known, though it was shown to interfere with the maple syrup urine disease, which is a rare autosomal-recessive metabolic disorder caused by a deficit of oxidative decarboxylation of branched-chain amino acids [51].

The choline is another phytoconstituent that we show to be present in both of our fenugreek seed extracts. It has been demonstrated that choline supplementation in insulin resistant (IR) mice would ameliorate muscle function by remodelling glucose and fatty acid (FA) metabolism [52]. This will be achieved by the reduction of glucose utilization for FA and triglyceride (TAG) synthesis, and increased muscle storage of glucose as glycogen. It was demonstrated that a choline rich diet would prevent non-alcoholic fatty liver.



We have identified for the first time the saccharopine in fenugreek seed extracts. Lysine is catabolized in developing plant tissues through the saccharopine pathway, and have been shown to be involved in the development of maize seed and stress responses [53]. In the case of mammalian myotubes, saccharopine was shown to stimulate Akt and mTOR signalling that has suppressed autophagic-proteolysis, and might reduce muscle wasting [54].

**Purines and pyrimidine** such as 5'-S-Methyl-5'-thioadenosine, 2'-deoxyadenosine, adenine, adenosine, adenosine 3',5'-cyclic monophosphate, cytidine, flavin mononucleotide (FMN), guanine, guanosine, S-adenosylhomocysteine, uridine and xanthine have been identified for the first time in fenugreek seed extracts. The presence of 5'-S-methyl-5'-thioadenosine in apples was correlated with the conversion of methionine related to ethylene biosynthesis [55]. S-adenosylhomocysteine is the by-product of all S-adenosylmethionine-dependent transmethylation reactions, and its presence seems to be related to cardiovascular disease, kidney disease, diabetes, and obesity [56].

The presence of **saponins** was extensively studied in the case of fenugreek including the vegetative organs and seeds of the plant [6-11]. The trigoneoside profile of our fenugreek seeds was different from that described for those originated from India and Egypt, respectively. Trigoneosides such as Ia, Ib, IIa, IIIa and IVa were present, while trigoneosides like IIb, IIIb, Va, Vb, VI, VIIb, VIIIb and IX were absent from our extracts as compared to the Indian fenugreek seed. On the other hand, trigoneosides like Xa, Xb, XIIa and XIIIa were identified, though trigoneosides like XIb and XIIb were missing from our fenugreek seed extracts as compared to the seeds of Egyptian origin. We were able to detect soyasaponin I in our fenugreek seed hydro-alcoholic extract. Soyasaponin I was shown to inhibit the Renin- Angiotensin- Aldosterone System, so it could be considered a potent native anti-hypertensive compound that has to be further tested [57]. However, diosgenin, gitogenin, tigogenin and betulin were poorly detectable in our hydro-alcoholic seed extract, while only traces of graecunin B, lupeol and betulinic acid were found in both of our seed extracts. We have to admit that due to the relatively low abundance of the above mentioned saponins in our extracts, we were unable to generate fragmentation profiles, so that their presence, was defined by the molecular mass corresponding peaks, and the structure confirming isotopic pattern. Neotigenin and fenugrin B were absent from our fenugreek seed extracts. It seems therefore likely that our fenugreek seed features a specific saponin profile, and that is clearly distinct from that were previously described. This it means that the hypocholesterolemic activity attributed to the saponin content of earlier described fenugreek seeds has to be carefully re-examined in the case of the fenugreek seed used in our experiments [12].

We were able to identify in our fenugreek seed extracts some of the already reported B group **vitamins** like niacin, pantothenic acid and pyridoxine, while nicotinamide was detected for the first time, but biotin was absent [24,25]. The thiamine, riboflavine, cyanocobalamin and vitamin C were hardly detectable in our fenugreek seed extracts, so in the absence of fragmentation profiles, their presence could only be confirmed by the molecular mass corresponding peaks, and the structure specific isotopic pattern. It has been suggested that some of the B vitamins act as cancer risk reduction agent [58], and having anti-inflammatory effects associated with atherosclerosis and autoimmunity [59].

We were also able to identify for the first time among terpenoids the ursolic acid that was present only in the hydro-alcoholic fenugreek seed extract. It has been demonstrated that the ursolic acid exerted anti-oxidative and anti-inflammatory effects on mouse brain injury model by activating the Nrf2-ARE pathway [60], while its anti-cancer and anti-metastatic effects were also proven [61,62].

## CONCLUSIONS

The comparative chemomapping of aqueous and hydro-alcoholic fenugreek seed extracts revealed already known and new phytoconstituents that further support the antidiabetic effects of fenugreek seeds. Originally, these antidiabetic effects were attributed mainly to galactomannan, 4-hydroxyisoleucin (4-OH-Ile), diosgenin and trigonelline [63]. It had been shown that these compounds featured direct antidiabetic properties in clinical studies by increasing insulin secretion (4-OH-Ile), decreasing insulin resistance and glucose resorption (galactomannan), and improvement in B-cells regeneration (trigonelline). Moreover, the presence of such phytoconstituents in our extracts is expected to improve blood lipid spectre (4-OH-Ile, diosgenin), and to show reno-protective (4-OH-Ile, trigonelline), neuroprotective (trigonelline) and antioxidant (diosgenin, trigonelline) properties. Other phytoconstituents identified in our seed extracts plead for a more substantial neuroprotective (kynurenine, genistein, vitexin, isovitexin), anti-inflammatory (trigonelline, scopoletin, ursolic acid, vitamins), hypocholesterolemic (saponins), muscle and/or hepatic insulin resistance reducing (choline) effects. However, when the phytoconstituent profile of saponins from Hungarian seeds was compared to the previously reported Indian and African seeds some differences were imminent. These differences were of qualitative nature but it seems logic to envision other dissimilarities at the quantitative level too. The ecological and cultivation conditions together with the genome based specificities are going to influence the qualitative and quantitative phytoconstituent profile of any fenugreek cultivated variety. This is the reason

why the careful assessment of chemical composition of fenugreek seeds from different sources is of great importance especially if they are intended for human consumption.

Given the large body of phytoconstituents found in fenugreek seed with effects that span across a wide health promoting spectrum, the future studies are expected to shed light on the quantitative parameters, and the cellular mechanisms attributed to such extracts. In this respect, remains to be elucidated whether such a multi phytoconstituent extract elicits an overcompensation to a disruption of homeostasis or a direct stimulatory response. It is expected that both overcompensation/disruption of homeostasis or stimulatory response will be below the toxic threshold, yet highly consistent with the hormetic concentration-response model [64]. This is exactly the case for our aqueous fenugreek seed extract that at very low concentrations increases the viability and division rate of human breast cancerous cells, while at high concentrations is exceedingly cytotoxic [27]. Moreover, our hydro-alcoholic fenugreek seed extract features only cytotoxicity and no evident dose-dependent hormetic response. Taken together our paper is one such an attempt that tries to correlate the phytoconstituent profile of fenugreek seed extracts with their corresponding biological effect seen in case of human breast cancerous cell lines. More system biology type of experiments are needed to unravel the complexity of beneficial effects of fenugreek.

## **EXPERIMENTAL SECTION**

### **x. Materials and methods**

#### ***x.1. Chemicals and reagents***

Acetonitrile, water and formic acid were procured from Fisher Scientific (Geel, Belgium), while ammonium acetate and ammonium formate were from Sigma-Aldrich (Munich, Germany).

#### ***x.2. Plant material***

The fenugreek seeds were obtained from TRIGONELLA MED. LTD., Mosonmagyaróvár, Hungary.

#### ***x.3. Sample preparation***

The aqueous extract was obtained by boiling 5g fenugreek dried seeds in 100 ml water for 5 minutes then left to cool down at room temperature and centrifuged for 10 minutes at 4000 rpm. The obtained

supernatant was filtered through Whatman filter paper, and aliquots stored in 15 ml Falcon tubes at -20°C freezer up until their use.

To obtain the hydro-alcoholic (ethanol : water 1:1) extract, 5 g dried fenugreek seeds were extracted two times with 500 ml ethanol–water (1:1) by stirring for 4h at 40 °C. The generated primary extract was centrifuged at 4000 rpm for 10 min at room temperature, and finally the ethanol was removed using a rotation vacuum evaporator. The ethanol free extract was filtered using a 45 µm Milipore filter unit and stored at 4°C until further studies.

#### ***x.4. UHPLC-ESI-MS analysis***

A Dionex Ultimate 3000RS UHPLC system equipped with a Thermo Accucore C18 column, 100/2.1 with a particle size of 2.6 µm was coupled to a Thermo Q Exactive Orbitrap mass spectrometer equipped with an electrospray ionization source (ESI), and the measurement accuracy was within 5ppm. The mass spectrometer was operated at 320°C capillary temperature, 4.0 kV in positive mode and 3.8 kV in negative mode of spray voltage, and a resolution of 35,000 in the case of MS, while 17,500 was for MS/MS. The 100-1000 m/z was the scanned mass interval. For MS/MS scans the collision energy was 40NCE. The difference between measured and calculated molecular ion masses were always below 5 ppm.

In case of positive ionization mode UHPLC separation, a specific eluent A (500 ml of water containing 10 ml of acetonitrile, 0.5 ml of formic acid and 2.5 mM of ammonium formate) and eluent B (500 ml of acetonitrile containing 10 ml of water, 0.5 ml of formic acid and 2.5 mM of ammonium formate) combination was used.

For the negative ionization mode UHPLC separation, another combination of eluent A (500 ml of water containing 10 ml of acetonitrile and 2.5 mM of ammonium acetate) and eluent B (500 ml of acetonitrile containing 10 ml of water and 2.5 mM of ammonium acetate) was applied.

The flow rate was set for 200 µl/min, and the same gradient elution program was used both positive and negative ionization mode type of determinations (0-1 min, 95% A, 1-22 min, 20% A; 22-24 min, 20% A; 24-26 min, 95% A; 26-40 min, 95% A). 5 µl of aqueous or hydro-alcoholic fenugreek seed extracts were injected at every run.

#### **ACKNOWLEDGMENTS**

The research was supported by the “In vitro study of some plant extracts of natural origin with emphasis on their anti-tumor effects.” HURO/ 0801 Hungarian-Romanian Cross Border Cooperation 2007-2013 grant.

## REFERENCES

1. Furry, *Les cahiers de la recherche agronomique*, **1950**, 3, 25.
2. G.A. Petropoulos, "Agronomic, genetic and chemical studies of *Trigonella foenum-graecum* L.", **1973**, PhD thesis, Bath University.
3. M. Al-Habori, A. Raman, "Pharmacological properties", Taylor & Francis, London UK. **2002**. 162.
4. J.A. Duke, "Handbook of medicinal herbs", **1986**, CRC Florida, p-490.
5. H. Skalta, "Fenugreek: The Genus *Trigonella*", Taylor & Francis, London, **2002**, chapter 9.
6. M. Yoshikawa, T. Murakami, H. Komatsu, J. Yamahara, H. Matsuda, *Chemical Pharmaceutical Bulletin (Tokyo)*, **1997**, 45 (1), 81.
7. M. Yoshikawa, T. Murakami, H. Komatsu, N. Murakami, J. Yamahara, H. Matsuda, *Heterocycles*, **1998**, 47 (1), 397.
8. T. Murakami, A. Kishi, H. Matsuda, M. Yoshikawa, *Chemical Pharmaceutical Bulletin*, **1997**, 48 (7), 994.
9. I.P. Varshney, M.F.A. Beg, *Indian Journal of Chemistry, Sect.B.* **1978**, 16 (12), 1134.
10. H. Grangrade, R. Kaushal, *Indian Drugs*. **1979**, 16 (7), 149.
11. P. Khanna, S.C. Jain, *Lloydia*, **1993**, 36, 96.
12. R. D.Sharma, *Nutrition Reports International*, **1986**, 33 (4), 669.
13. M. Shang, Y. Tezuka, S. Cai, J. Li, S. Kadota, W. Fan, T. Namba, *Zhongcaoyao*, **1998**, 29 (10), 655.
14. W. Karrer, "Konstitution und Vorkommen der organischen Pflanzenstoffe", Birkhäuser Verlag, Basel und Stuttgart. **1958**, p.997, 1009.
15. J. Shani, A. Goldschmied, B. Joseph, Z. Ahronson, F.G. Sulman, *Archive of International Pharmacodynamics and Therapeutics*, **1974**, 210 (10), 27.
16. M. Covello, *Bollettino Della Societa Italiana Di Biologia Sperimentale*, **1943**, 18, 159.
17. M.A. Bhatti, M.T.J. Khan, B. Ahmed, M. Jamshaid, W. Ahmad, *Fitoterapia*, **1996**, 67 (4), 372.
18. L. Reppel, D. Wagenbreth, *Flora*, **1958**, 146, 212.
19. L. Fowden, H. Pratt, A. Smith, *Phytochemistry*, **1973**, 12, 1707.
20. Y. Sauvaire, P. Girardon, J.C. Baccou, J. Ristérucchi, *Phytochemistry*, **1984**, 23 (3), 479.
21. H. Van Etten, R. W. Miller, I.A. Wolff, Q. Jones, *Journal of Agricultural and Food Chemistry*, **1961**, 9 (1), 79.
22. M. Hidvégi, A. El-Kady, R. Lásztity, F. Békés, L. Simon-Sarkadi, *Acta Alimentaria*, **1984**, 13, 315.
23. G. Valette, Y. Sauvaire, J.C. Baccou, G. Ribes, *Atherosclerosis*, **1984**, 50 (1), 105.
24. G. Picci, *Annali della Facoltà Agraria Università di Pisa*, **1959**, 20, 51.
25. K.S. Venkataramani, *Indian Acaemy of Science*, **1950**, 32B, 112.
26. J. Hemavathy, J.V. Prabhakar, *Food Chemistry*, **1989**, 31 (1), 1.

27. Sz. Vigh, Zs. Zsvér-Vadas, C. Pribac, L. Mos, Z. Cziáky, M. Czapár, C.V. Mihali, V. Turcus, E. Máthé, *Studia Universitatis "Vasile Goldis"*, **2016**, 26 (4), 435.
28. G.A. Petropoulos, "Fenugreek: The Genus *Trigonella*", Taylor & Francis, London, **2002**.
29. Z. Benayad, C. Gómez-Cordovés, N.E. Es-Safi, *International Journal of Molecular Sciences*, **2014**, 15, 20668.
30. M. Yoshikawa, T. Murakami, H. Komatsu, N. Murakami, J. Yamahara, H. Matsuda, *Chemical and Pharmaceutical Bulletin*, **1997**, 45, 81.
31. T. Murakami, A. Kishi, H. Matsuda, M. Yoshikawa, *Chemical and Pharmaceutical Bulletin*, **2000**, 48, 994.
32. L. Kang, Y. Zhao, X. Pang, H. Yu, C. Xiong, J. Zhang, Y. Gao, K. Yu, C. Liu, B. Ma, *Journal of Pharmaceutical and Biomedical Analysis*, **2013**, 74, 257.
33. V. Sattiraju, K. S. Chandrashekar, *International Journal of Pharmacognosy and Phytochemical Research*, **2014**, 6, 715.
34. R.S. Hoffman, J.L. Kaplan, O.L. Hung, L.R. Goldfrank, *Journal of Toxicology. Clinical Toxicology*. **2004**; 42 (4), 349.
35. K. Lim, F.J. Fernández-Gomez, N. Braidy, C. Estrada, C. Costa, S. Costa, A. Bessede, E. Fernandez-Villalba, A. Zinger, M.T. Herrero, G.J. Guillemín, *Progress in Neurobiology*, **2016**, pii: S0301-0082(15)30055-1.
36. K. Sas, H. Robotka, J. Toldi, L. Vécsei, *Journal of the Neurological Science*, **2007**, 257 (1-2), 221.
37. A. Arlt, S. Sebens, S. Krebs, C. Geismann, M. Grossmann, M.L. Kruse, S. Schreiber, H. Schäfer, *Oncogene*, **2013**, 32 (40), 4825.
38. Wang, H. Sun, Y. Han, X. Wang, C. Yuan, *Zhongguo Zhong Yao Za Zhi*, **1997**, 22 (8), 486.
39. M.V. Pereira Dos Santos Nascimento, F. Arruda-Silva, A.B. Gobbo Luz, B. Baratto, D. Venzke, B.G. Mendes, T.S. Fröde, M. Geraldo Pizzolatti, E.M. Dalmarco, *Immunopharmacology and Immunotoxicology*, **2016**, 38 (5), 344.
40. Y.M. Tabana, L.E. Hassan, M.B. Ahamed, S.S. Dahham, M.A. Iqbal, M.A. Saeed, M.S. Khan, D. Sandai, A.S. Majid, C.E. Oon, A.M. Majid, *Microvascular Research*, **2016**, 107, 17.
41. A. Nishina, M. Ukiya, M. Fukatsu, M. Koketsu, M. Ninomiya, D. Sato, J. Yamamoto, K. Kobayashi-Hattori, T. Okubo, H. Tokuoka, H. Kimura, *Biological and Pharmaceutical Bulletin*, **2015**, 38 (11), 1794.
42. Y. Yang, X. Zhou, M. Xiao, Z. Hong, Q. Gong, L. Jiang, J. Zhou, *Journal of Huazhong University of Science and Technology. Medical Sciences*, **2010**, 30 (6), 734.
43. Arbabi, G. Hamidi, S.A. Talaei, M. Salami, *Iranian Journal of Basic Medical Sciences*, **2016**, 19 (12), 1285.
44. Shafiee, M. Saidijam, H. Tavilani, N. Ghasemkhani, I. Khodadadi, *International Journal of Molecular and Cellular Medicine*, **2016**, 5 (3), 178.
45. M. He, J.W. Min, W.L. Kong, X.H. He, J.X. Li, B.W. Peng, *Fitoterapia*, **2016**, 115, 74.

46. M. Dixit, A. Raghuvanshi, C.P. Gupta, J. Kureel, M.N. Mansoori, P. Shukla, A.A. John, K. Singh, D. Purohit, P. Awasthi, D. Singh, A. Goel, *PLoS One*, **2015**, *10* (12), e0144541.
47. Gatouillat, A.A. Magid, E. Bertin, H. El btaouri, H. Morjani, C. Lavaud, C. Madoulet, *Phytomedicine*, **2015**, *22* (13), 1186.
48. C. Nguyen, J.F. Savouret, M. Widerak, M.T. Corvol, F. Rannou, *Nutrients*. **2017**, *9* (1), pii: E45.
49. F. Peraza-Luna, M. Rodríguez-Mendiola, C. Arias-Castro, J. M. Bessiere, G. Calva-Calva, *Journal of Agricultural and Food Chemistry*, **2001**, *49* (12), 6012.
50. C. Scholtes, S. Nizet, S. Collin, *Journal of Agricultural and Food Chemistry*, **2015**, *63* (11), 2886.
51. P. Haberstick, C.H. Kindler, M. Schürch, *Anaesthesist*, **2010**, *59* (10), 914.
52. A. Taylor, L.C. Schenkel, M. Yokich, M. Bakovic, *Biochemistry and Cell Biology*, **2016**, *6*, 1.
53. E. Kiyota, I.A. Pena, P. Arruda, *Plant, Cell and Environment*, **2015**, *38* (11), 2450.
54. T. Sato, Y. Ito, T. Nagasawa, *Molecular and Cellular Biochemistry*. **2015**, *410* (1-2), 93.
55. D.O. Adams, S.F. Yang, *Plant Physiology*, **1977**, *60* (6), 892.
56. Y. Xiao, X. Su, W. Huang, J. Zhang, C. Peng, H. Huang, X. Wu, H. Huang, M. Xia, W. Ling, *The International Journal of Biochemistry and Cell Biology*, **2015**, *67*, 158.
57. Z. Tavassoli, M. Taghdir, B. Ranjbar, *Journal of Biomolecular and Structure Dynamics*, **2017**, *19*, 1.
58. S. Mocellin, M. Briarava, P. Pilati *Journal of the National Cancer Institute*, **2016**, *109* (3), pii: djw230.
59. S.C. Gominak, *Medical Hypotheses*, **2016**, *94*, 103.
60. Ding, H. Wang, L. Zhu, W. Wei, *Neurochemical Research*, **2016**, doi: 10.1007/s11064-016-2077-8.
61. W.T. Gai, D.P. Yu, X.S. Wang, P.T. Wang, *Oncology Letters*, **2016**, *12* (4), 2880.
62. L. Gao, Y.M. Shui, W. Jiang, E.Y. Huang, Q.Y. Shou, X. Ji, B.C. He, G.Y. Lv, T.C. He, *Oncotarget*, **2016**, doi: 10.18632/oncotarget.12375.
63. D. Koupý, H. Kotolová, J. Rudá Kučerová, *Ceska a Slovenska Farmacie*, **2015**, *64* (3), 67.
64. E.J. Calabrese, L. A. Baldwin, *Human and Experimental Toxicology*, **2002**, *21*, 91.

*Dedicated to Professor Costel Sârbu on the  
Occasion of His 65<sup>th</sup> Anniversary*

## VALIDATED LC-MS/MS METHOD FOR THE CONCOMITANT DETERMINATION OF AMOXICILLIN AND CLAVULANIC ACID FROM HUMAN PLASMA

JÓZSEF BALÁZSI<sup>a</sup>, CSABA PAIZS<sup>b</sup>, FLORIN-DAN IRIMIE<sup>b</sup>,  
MONICA IOANA TOȘA<sup>b</sup>, LÁSZLÓ CSABA BENCZE<sup>b</sup>,  
RÓBERT TÓTÓŠ<sup>b\*</sup>

**ABSTRACT.** The purpose of this study was the development and validation of an LC-MS/MS method, for the concomitant and rapid determination amoxicillin and clavulanic acid from human plasma. The sample workup involved a simple protein precipitation procedure. A core/shell type analytical column (50×2,1 mm, 2.6 Å) was used with PFP stationary phase. A mobile phase with high aqueous composition provided satisfactory separation with good accuracy and precision (stable ionization). The mass spectrometer was operated in positive electrospray ionization mode for both analytes and internal standard. The following parameters were evaluated for validation purpose: Selectivity, sensitivity, matrix effect, anticoagulant effect, linearity, precision and accuracy, recovery, analyte/IS stability in solvent/matrix and carryover. The validated calibration range was 190-22222 ng/ml for amoxicillin, and 147-4908 ng/ml for clavulanic acid. The correlation coefficient  $R^2$  was at least 0.99 for both analytes. The validated method has been successfully used for the evaluation bioequivalence of generic amoxicillin/potassium clavulanate formulations.

**Keywords:** *amoxicillin, clavulanic acid, method validation, bioequivalence trial, LC-MS/MS*

---

<sup>a</sup> S.C. Kynetyx HT SRL, 34 Frunzișului street, RO-400664 Cluj-Napoca, Romania

<sup>b</sup> Babeș-Bolyai University, Faculty of Chemistry and Chemical Engineering, Biocatalysis and Biotransformation Research Centre, 11 Arany János str., RO-400028, Cluj-Napoca, Romania

\* Corresponding author: totosr@chem.ubbcluj.ro



## INTRODUCTION

Amoxicillin (2*S*,5*R*,6*R*)-6-[(*R*)-(-)-2-Amino-2-(*p*-hydroxyphenyl) acetamido]-3,3-dimethyl-7-oxo-4-thia-1-azabicyclo [3.2.0]-heptane-2-carboxylic acid trihydrate (C<sub>16</sub>H<sub>19</sub>N<sub>3</sub>O<sub>5</sub>S•3H<sub>2</sub>O) is a semisynthetic antibiotic, an analog of ampicillin derived from 6-aminopenicillanic acid is shown in Figure 1, with a broad spectrum of bactericidal activity against many gram-positive and gram-negative microorganisms [1].

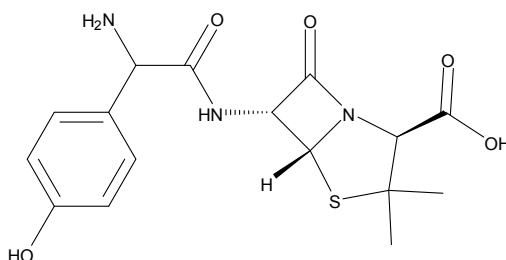


**Figure 1.** Structure of amoxicillin

Amoxicillin is susceptible to degradation by  $\beta$ -lactamases, and therefore, the activity spectrum does not include organisms which produce these enzymes [1].

Clavulanic acid (*Z*)-(2*R*,5*R*)-3-(2-hydroxyethylidene)-7-oxo-4-oxa-1-azabicyclo[3.2.0]-heptane-2-carboxylic acid (C<sub>8</sub>H<sub>8</sub>KNO<sub>5</sub> – potassium salt) is a  $\beta$ -lactam (Figure 2), produced by the fermentation of *Streptomyces clavuligerus* structurally related to the penicillins, which possesses the ability to inactivate a wide range of  $\beta$ -lactamase enzymes commonly found in microorganisms resistant to penicillins. In particular, it has good activity against the clinically important plasmid-mediated  $\beta$ -lactamases frequently responsible for transferred drug resistance [15].

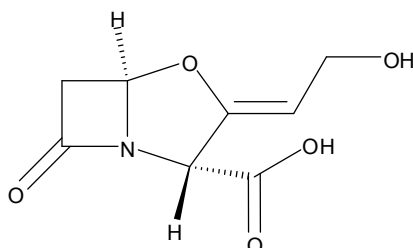


**Figure 2.** Structure of clavulanic acid

The formulation of amoxicillin and clavulanic acid (as potassium salt) protects amoxicillin from  $\beta$ -lactamase enzymes degradation and effectively extends the antibiotic spectrum of amoxicillin to many bacteria normally resistant to amoxicillin and other  $\beta$ -lactam antibiotics. Thus amoxicillin/clavulanic acid possesses the distinctive properties of a broad-spectrum antibiotic and a  $\beta$ -lactamase inhibitor [5].

## RESULTS AND DISCUSSION

### Determination of acquisition parameters

There are several methods known in the literature for the individual and/or simultaneous determination of amoxicillin and clavulanic acid in human plasma and other biological matrix using UV [2,6,11,13] and MS/MS methods [3-5,7-9,12]. All MS/MS methods involve polarity switching, for monitoring the clavulanic acid in negative electrospray ionization mode. The method developed in this study uses positive ionization mode for the detection of all entities. Even if the clavulanic acid prefers a negative ionization mode, the abundance in positive ionization mode was high enough to achieve a suitable LLOQ (Lower Limit of Quantitation).

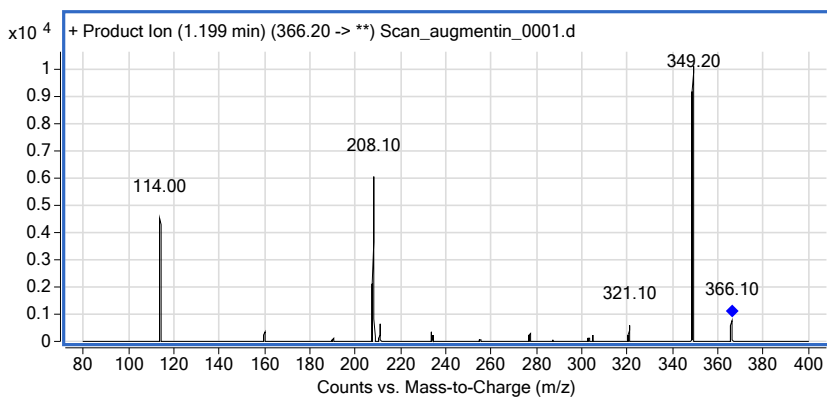
The  $m/z$  transitions used for multiple reaction monitoring (MRM) were chosen based on the spectra from Figures 3-5. The monitored transitions should not interfere in their  $m/z$  value, specific for a given analyte. Their intensity should be as high as possible for the qualifiers, and the qualifier/quantifier ratio should remain stable over the time. Taking into account the considerations above the following transitions were chosen for the quantitative assay method:

**Amoxicillin:**  $m/z$  366.2 $\rightarrow$ 349.2, (366.2 $\rightarrow$ 208.1 qualifier ion) CE 5V,

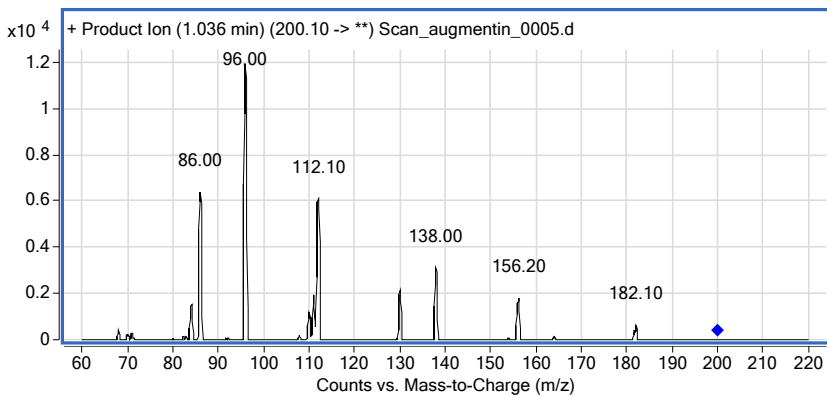
**Clavulanic acid:**  $m/z$  200.1 $\rightarrow$ 96.0 (200.1 $\rightarrow$ 112.1 qualifier ion) CE 7V,

**Ampicillin (IS):**  $m/z$  350.2 $\rightarrow$ 106.2 (350.2 $\rightarrow$ 160.0 qualifier ion) CE 10V.  
(CE – Collision Energy)

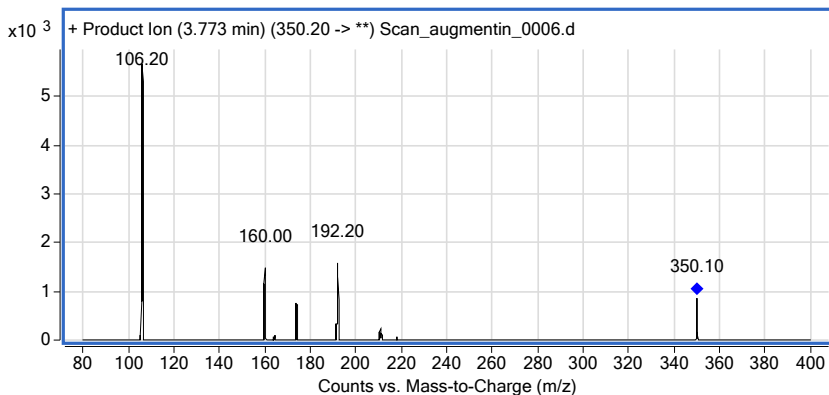
For each analyte/IS (Internal Standard) the single charged molecular ions were used as precursors.



**Figure 3.** ESI (+) Spectrum of Amoxicillin

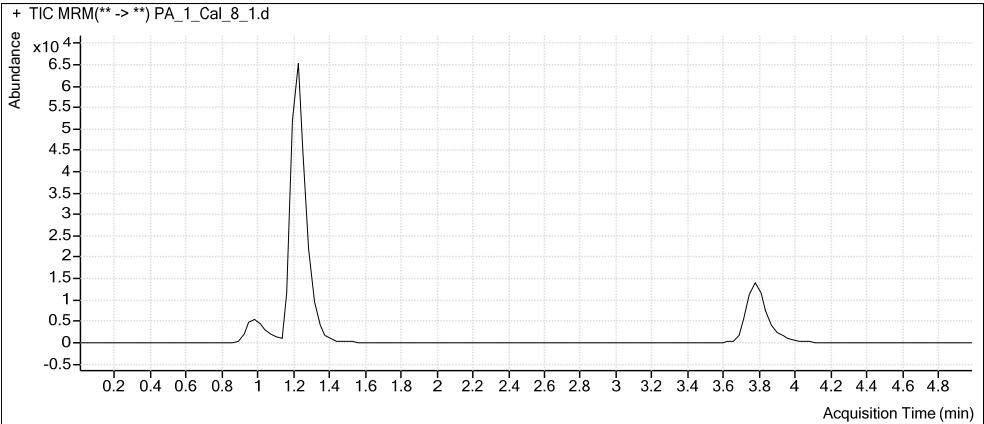


**Figure 4.** ESI (+) Spectrum of - Clavulanic acid



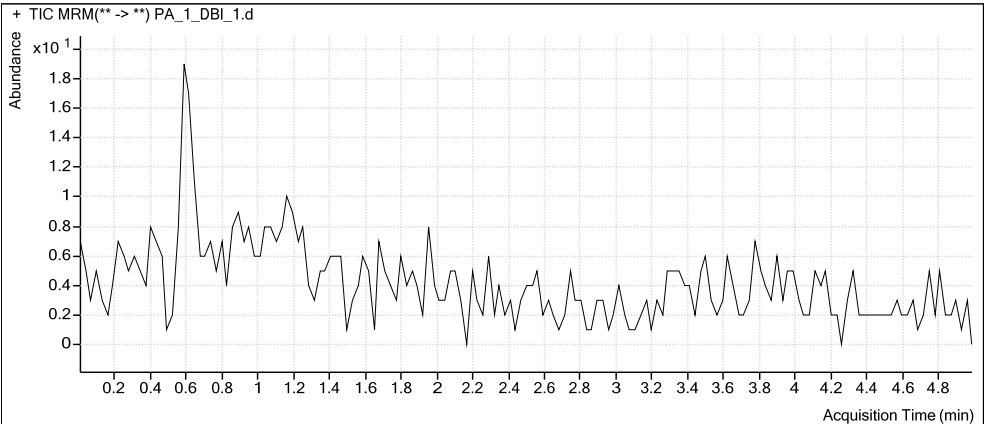
**Figure 5.** ESI (+) Spectrum Ampicillin (IS)

Figure 6 shows a typical MRM total ion chromatogram for an ULOQ (upper limit of calibration) sample. The elution order is: clavulanic acid, amoxicillin, ampicillin (IS) Values are back calculated concentrations for each analyte.



**Figure 6.** MRM chromatogram of Cal8 (clavulanic acid 4822.58 ng/ml, amoxicillin 22146.87 ng/ml, ampicillin 598.82 ng/ml)

It's noticeable, that no significant spectral response has been observed at the retention time of the analytes/IS in matrix blank samples (Figure 7).



**Figure 7.** MRM chromatogram of DBI1 (matrix blank 0 ng/ml each analyte)

## Bioanalytical method validation

The analytical method was validated according to the EMEA/CHMP/EWP/192217/2009 Guideline on validation of bioanalytical methods [14].

The tested parameters were: selectivity, sensitivity, matrix effect, anticoagulant effect, intra/interbatch precision and accuracy, recovery, short/long term stability of stock solutions of analytes, short term stability of working solutions of analytes, bench top stability in biological matrix, freeze thaw stability in biological matrix, injector/autosampler stability of the processed samples, stability during delayed processing, dilution integrity, carryover. All tests were performed using 6 replicates at the mentioned QC (Quality Control) levels.

The validated calibration range was 190-22222 ng/ml for amoxicillin, and 147-4908 ng/ml for clavulanic acid. The calibration curves were obtained using a quadratic weighted ( $1/x^2$ ) for Amoxicillin and quadratic weighted ( $1/x^2$ ) for Clavulanic Acid regression analysis of the peak area ratio (analyte/internal standard) versus the nominal concentration of the calibration standards. A summary of main results of validation batches is presented in Tables 1 and 2.

## Summary of method validation

**Table 1.** Bioanalytical method validation summary for amoxicillin

Calibration concentrations (Units)	190.48, 476.20, 1190.50, 2380.99, 4761.99, 9523.98, 15873.30, 22222.61 (ng/ml)
Lower limit of quantification (Units)	LLOQ, 190.48 ng/ml, Accuracy 113.22 %, RSD 0.86
QC Concentrations (Units)	LLOQ-QC, LQC, MQC, HQC 190.48, 476.20, 4761.99, 15873.30 (ng/ml)
Between-run accuracy (%)	LLOQ-QC, LQC, MQC, HQC 111.08, 94.84, 99.46, 104.46
Between-run precision (RSD)	LLOQ-QC, LQC, MQC, HQC 2.78, 2.38, 1.76, 1.42
Matrix factor (MF)	LQC 0.8385
RSD	3.97
Recovery (%)	LQC MQC HQC 73.64 75.94 77.34
Long term stability of stock solution and working solutions (Observed change %)	Confirmed up to 30 days at 4 °C LQC Stab. 95.21, change -4.79% HQC Stab. 93.81 change -7.19%
Short term stability in biological matrix at room temperature or at sample processing temperature. (Observed change %)	Confirmed up to 48.71(6) h LQC Stab. 100.85, change + 0.85% HQC Stab. 100.28 change +0.28%
Long term stability in biological matrix (Observed change %)	Confirmed up to 38 days at -50 °C LQC Stab. 107.60, change +7.60% HQC Stab. 105.00 change +5.00%

Autosampler storage stability (Observed change %)	Confirmed up to 72 h LQC Stab. 97.85, change -2.15% HQC Stab. 97.39 change -2.61%
Freeze and thaw stability (Observed change %)	-50 °C , 3 cycles LQC Stab. 100.23, change +0.23% HQC Stab. 98.99, change -1.01%
Dilution integrity	Concentration diluted (2-fold) 99.67 %; RSD 1.46 % Concentration diluted (4-fold) 99.55%; RSD 3.39 %

**Table 2.** Bioanalytical method validation summary for clavulanic acid

<b>Analyte – Clavulanic acid</b>	
Calibration concentrations (Units)	147.25, 267.73, 501.99, 1003.97, 1673.29, 2454.15, 3569.68, 4908.31 (ng/ml)
Lower limit of quantification (Units)	LLOQ, 147.25 ng/ml, Accuracy 105.98 %, RSD 5.22
QC Concentrations (Units)	LLOQ-QC, LQC, MQC, HQC 147.25, 267.73, 1673.29, 3569.68 (ng/ml)
Between-run accuracy (%)	LLOQ-QC, LQC, MQC, HQC 101.91, 100.73, 100.26, 101.74
Between-run precision (RSD)	LLOQ-QC, LQC, MQC, HQC 4.99, 3.09, 2.24, 1.79
Matrix factor (MF) RSD	LQC 0.7038 3.68
Recovery (%)	LQC MQC HQC 72.04 75.16 75.37
Long term stability of stock solutions (Observed change %)	Confirmed up to 14 days at 4 °C LQC Stab. 90.52, change -9.48% HQC Stab. 89.57 change -10.43%
Short term stability in biological matrix at room temperature or at sample processing temperature. (Observed change %)	Confirmed up to 48.71(6) h LQC Stab. 97.33 change -2.67% HQC Stab. 96.41 change -3.59%
Long term stability in biological matrix (Observed change %)	Confirmed up to 38 days at -50 °C LQC Stab. 102.05, change +2.05% HQC Stab. 107.86 change +7.86%
Autosampler storage stability (Observed change %)	Confirmed up to 72 h LQC Stab. 96.33, change -3.67% HQC Stab. 96.05 change -3.95%
Freeze and thaw stability (Observed change %)	-50 °C , 3 cycles LQC Stab. 103.66, change +3.66% HQC Stab. 99.12, change -0.88%
Dilution integrity	Concentration diluted (2-fold) 97.24 %; RSD 0.99% Concentration diluted (4-fold) 93.65 %; RSD 2.42 %

PA – Precision and Accuracy batch

LQC/MQC/HQC – Low/Medium/High Quality Control sample

**Table 3.** Linearity summary results for amoxicillin

Calibration level	Nominal conc. (ng/ml)	Mean conc.±S.D (ng/ml)	RSD %	Accuracy %
Cal_1_1	190.48	213.34±7.77	3.64	112.00
Cal_1_2	190.48	215.05±2.07	0.96	112.90
Cal_2	476.20	439.69±3.47	0.79	92.33
Cal_3	1190.50	1037.28±41.79	4.03	87.13
Cal_4	2380.99	2215.72±69.24	3.12	93.06
Cal_5	4761.99	4569.95±126.44	2.77	95.97
Cal_6	9523.98	10229.15±303.30	2.97	107.40
Cal_7	15873.30	15943.79±209.70	1.32	100.44
Cal_8_1	22222.61	22094.46±185.96	0.84	99.42
Cal_8_2	22222.61	22073.03±240.97	1.09	99.33

**Table 4.** Linearity summary results for clavulanic acid

Calibration level	Nominal conc. (ng/ml)	Mean conc.±S.D (ng/ml)	RSD %	Accuracy %
Cal_1_1	147.25	152.20±3.62	2.38	103.36
Cal_1_2	147.25	145.84±3.17	2.18	99.04
Cal_2	267.73	266.28±4.17	1.57	99.46
Cal_3	501.99	486.25±10.79	2.22	96.86
Cal_4	1003.97	1022.20±13.02	1.27	101.82
Cal_5	1673.29	1632.69±34.29	2.10	97.57
Cal_6	2454.15	2526.76±91.56	3.62	102.96
Cal_7	3569.68	3526.70±120.87	3.43	98.80
Cal_8_1	4908.31	4893.25±70.37	1.44	99.69
Cal_8_2	4908.31	4929.98±43.00	0.87	100.44

## CONCLUSIONS

A rapid and robust method has been developed and validated for the simultaneous determination of amoxicillin and clavulanic acid in human plasma. The quantitation was performed on an Agilent 1200 series HPLC system, coupled to an Agilent 6410 triple quadrupole mass spectrometer, using electrospray ionization technique. All components were detected in positive ionization mode. The method was successfully used for the evaluation of bioequivalence of a generic formulation of amoxicillin/ clavulanic acid in human subjects.

## EXPERIMENTAL SECTION

### Solvents and reference materials used

All used solvents are of HPLC grade. Dichloromethane (stabilized with amylene) was purchased from Riedel (Sigma), formic acid and acetonitrile from Merck KGaA, HPLC water was obtained using a Millipore Simplicity UV water purification system. Certified reference materials of amoxicillin trihydrate, potassium clavulanate and ampicillin trihydrate (internal standard-IS) were obtained from Sigma-Aldrich and are of analytical standard grade (Vetranal). Blank human plasma was obtained from the regional blood transfusion center (CRTS) Cluj.

### Instrumentation and working parameters

An Agilent 1200 series HPLC system with a Phenomenex Kinetex PFP column (50 × 2.10 mm) equipped with Phenomenex Security Guard (4 × 2.0 mm) was used for separation. The used mobile phase was an isocratic mixture of 8:92 acetonitrile:water (containing 0.25% formic acid). The used flow rate was 0.3 ml/min, the column temperature was set to 38 °C. An Agilent 6410 triple Quadrupole Mass Spectrometer (Agilent Technologies, USA), equipped with electrospray ion source was used for the LC-MS/MS analyses. The runtime was 5 min/sample. The data acquisition and processing was carried out using MassHunter software. The whole system (software and hardware) was validated. The mass spectrometer was operated in positive ionization mode for both analytes and IS. Nitrogen was used as nebulizing gas and collision cell gas. The temperature of the ESI source was set to 350 °C, and the needle voltage to 4000V.

The quantitation was performed using MRM (multiple reaction monitoring) of the transitions: m/z 366.2→349.2, (366.2→208.1 qualifier ion) collision energy 5V, for amoxicillin, 200.1→96.0 (200.1→112.1 qualifier ion) collision energy 7V, for clavulanic acid, and 350.2→106.2 (350.2→160.0 qualifier ion) collision energy 10V for ampicillin (IS).

The mass spectrometer was operated at unit resolution with a dwell time of 300 ms per transition.

### Stock and working solutions preparation

Stock solutions were prepared in ultrapure water dissolving accurately weighed amounts of reference materials, at 1.7 mg/ml – amoxicillin and 1 mg/ml K clavulanate and ampicillin. They were stored between 2-8 °C.



Working solutions of analytes and internal standard were prepared freshly before use by successive dilutions from stock solutions to appropriate levels, using water as solvent. They were used for spiking in human plasma used for calibrators and QC samples preparation.

### **Calibrators and QC samples preparation**

400  $\mu$ l of blank human plasma, 50  $\mu$ l of spiking solution of analyte and 50  $\mu$ l of spiking solution of internal standard were added in polypropylene tubes, to yield final concentrations of 190.48, 476.20, 1190.50, 2380.99, 4761.99, 9523.98, 15873.30, 22222.61 ng/ml for amoxicillin and 147.25, 267.73, 501.99, 1003.97, 1673.29, 2454.15, 3569.68, 4908.31 ng/ml for clavulanic acid.

### **Sample preparation (workup)**

To precipitate proteins, 1500  $\mu$ l of acetonitrile was added to the spiked samples, then vortexed for 20 minutes at 1500 rpm. Further the samples were centrifuged for 10 minutes at 4000 rpm. 1750  $\mu$ l of supernatant was transferred into a new test tube. 1500  $\mu$ l of ultrapure water and 5000  $\mu$ l of dichloromethane were added and the samples were vortexed for 5 minutes at 1500 rpm. To accelerate phase separation samples were centrifuged for 10 minutes at 4000 rpm. Finally 800  $\mu$ l of the resulting supernatant were transferred to HPLC autosampler vials and injected into the analytical system (15  $\mu$ l/sample).

The novelty of the method is the extraction of acetonitrile from the aqueous mixture with dichloromethane which was meant to reduce the organic content of the samples as much as possible without evaporation. In this way the organic content of the samples was close to the composition of the mobile phase, giving a better peakshape of the chromatograms. Furthermore, the presence of high amounts of acetonitrile in the samples acts inhibitory on the ionization of clavulanic acid in positive acquisition mode. The used dichloromethane was stabilized with amylene (ethanol stabilized dichloromethane should not be used, because alcohol promotes the decomposition/hydrolysis [10] of the  $\beta$ -lactam ring in penicillin class antibiotics).

### **Calibration curve parameters**

The linearity of the method was evaluated using spiked plasma samples in the concentration range mentioned above using the method of least squares. Three linearity curves were analyzed.

Each calibration batch (curve) consisted of: blank samples in duplicate, zero samples (blank with IS) in duplicate and eight non-zero concentration levels, of which the lower and upper limit of quantitation samples were in duplicate. The calibration curves were obtained by using a quadratic weighted ( $1/x^2$ ) for Amoxicillin and quadratic weighted ( $1/x^2$ ) for Clavulanic Acid regression analysis of the peak area ratio (analyte/internal standard) versus the nominal concentration of the calibration standards. Study samples concentrations were obtained by interpolation from the calibration curve.

The linearity results are summarized in Tables 3 and 4 in the 'Results and Discussion' section.

## ACKNOWLEDGMENTS

This work was performed using private funding of S.C KYNETYX HT SRL.

## REFERENCES

1. <http://www.rxlist.com/augmentin-drug.htm> (Augmentin (Amoxicillin Clavulanate): Side Effects, Interactions, Warning, Dosage & Uses; Viewed: 14.02.2017)
2. HU Guoxin, DAI Zongshun, LONG Lihong, HAN Ying, Hou Shuxian, WU Li, *Journal of Huazhong University of Science and Technology [Med Sci]*, **2002**, 22, 224.
3. B. Ćirić, D. Jandrić, V. Kilibarda, J. Jović-Stošić, V. Dragojević-Simić, S. Vučinić, *Vojnosanitetski Pregled*, **2010**, 67, 887.
4. M. Ashraf-Khorassani, L.T. Taylor, L.M. Koeth, J.A. Roush, *Chromatographia*, **2005**, 62, 459.
5. T.B. Vree1, E. Dammers, P.S. Exler, *Journal of Antimicrobial Chemotherapy*, **2003**, 51, 373.
6. K.M. Matar, E.M. Nazi, Y.M. El-Sayed, M.J. Al-Yamani, S.A. Al-Suwayeh, K.I. Al-Khamis, *Journal of Liquid Chromatography & Related Technologies*, **2005**, 28, 97.
7. K.-H. Yoon, S.-Y. Lee, W. Kim, J.-S. Park, H.-J. Kim, *Journal of Chromatography B*, **2004**, 813, 121.
8. T. Reins, S. De Boever, S. De Baere, P. De Backer, S. Croubels, *Analytica Chimica Acta*, **2007**, 597, 282.
9. W.Xi, L. He, C. Guo, Q. Cai, Z. Zeng, *Analytical Letters*, **2012**, 45, 1764.
10. V. Carvalho Santos, J.F. Brandão Pereira, R. Brandão Haga, C. O. Rangel-Yagui, J.A. Couto Teixeira, A. Converti, A. Pessoa Jr., *Biochemical Engineering Journal*, **2009**, 45, 89.

11. S.M. Foroutan, A. Zarghi, A. Shafaati, A. Khoddam, H. Mohaved, *Journal of Pharmaceutical and Biomedical Analysis*, **2007**, *45*, 531.
12. T. Reins, S. De Baere, S. Croubels, P. De Backer, *Journal of Mass Spectrometry*, **2006**, *41*, 1414.
13. L.R. Pires de Abreu, R.A. Mas Ortiz, S. Calafatti de Castro, J. Pedrazzoli Jr., *Journal of Pharmacy and Pharmaceutical Sciences*, **2003**, *6*, 223.
14. EMEA/CHMP/EWP/192217/2009 Rev. 1 Corr. 2\*\* Guideline on validation of bioanalytical method, 21 July 2011 (Updated 03/06/2015).
15. C. Reading, T. Farmer, *Biochemical Journal*, **1981**, *199*, 779.